



THE UNIVERSITY OF  
**WAIKATO**  
*Te Whare Wānanga o Waikato*

Research Commons

<http://waikato.researchgateway.ac.nz/>

## Research Commons at the University of Waikato

### Copyright Statement:

The digital copy of this thesis is protected by the Copyright Act 1994 (New Zealand).

The thesis may be consulted by you, provided you comply with the provisions of the Act and the following conditions of use:

- Any use you make of these documents or images must be for research or private study purposes only, and you may not make them available to any other person.
- Authors control the copyright of their thesis. You will recognise the author's right to be identified as the author of the thesis, and due acknowledgement will be made to the author where appropriate.
- You will obtain the author's permission before publishing any material from the thesis.

**SEDIMENTARY FACIES AND UNCONFORMITY  
ANALYSIS OF SOME PALEOCENE-EOCENE  
SECTIONS, MARLBOROUGH AND CAMPBELL  
ISLAND, NEW ZEALAND**

A thesis  
submitted in partial fulfilment  
of the requirements for the degree  
of  
**Master of Science in Earth Sciences**  
at  
**The University of Waikato**

By  
**BEN ANDREW**



THE UNIVERSITY OF  
**WAIKATO**  
*Te Whare Wānanga o Waikato*

The University of Waikato

2010

“Unlike fair-weather friends, the land does not desert us in times of greatest need, for it is indifferent yet different from day to day.”

- *Brian Turner*



The view looking towards Courejeles Point and Isle de Jeanette Marie from high above Northwest Bay, Campbell Island. A day of rare perfection in the midst of the Southern Ocean.

(Photo by Chris Mace, 2009)

# ABSTRACT

---

Throughout the Late Cretaceous to Eocene, sedimentation in gradually subsiding basins on the passive eastern margin of the micro-continent of Zealandia recorded climatic and paleoceanographic changes in a greenhouse world. One such fundamental change in Southern Ocean circulation is hypothesised to be recorded in a regionally extensive unconformity surface and short-lived lithofacies changes contained within Late Paleocene to Early Eocene sedimentary successions at key sections throughout New Zealand, and investigated here on Campbell Island and in southeastern Marlborough.

On Campbell Island, this oceanographic event is represented by an unconformity between the Late Cretaceous to Late Paleocene Garden Cove Formation and the Early Eocene to Oligocene Tucker Cove Limestone. This unconformity signifies a major lithofacies change from Garden Cove Formation which consists of siliceous mudstone containing fine sand to coarse silt sized siliciclastic grains, pelletal glaucony grains and rare quartz pebbles, to a nannofossil and foraminiferal limestone containing little to no siliciclastic grains comprising the Tucker Cove Limestone. Geochemically this lithofacies change is characterised by a dramatic decrease in terrigenous supply and a shift from siliceous to calcareous productivity, along with a significant concentration of Zr and rare earth elements. Lithofacies at this site are inferred to record possible episodes of ice rafting and eventual unconformity formation by invigorated intermediate depth ocean currents which resulted in winnowing of sea-floor sediments and concentration of heavy minerals.

At the distal Mead Stream site in southeastern Marlborough, deposition of bio-siliceous sediments of the Mead Hill Formation and Amuri Limestone was locally disrupted by deposition of the Waipawa Formation, the lateral equivalent of an important hydrocarbon source rock identified in several of New Zealand's sedimentary basins. In outcrop, the Waipawa Formation at Mead Stream is characterised by a very distinctive 'rusty' brown fissile appearance, while in thin section, though radiolarians and sponge spicules are common, the overall fine grained nature of the unit makes identification of other components difficult. Geochemical proxies show a significant increase in terrigenous supply in the Waipawa Formation, along with an increase in siliceous productivity concomitant with a decrease in oxygenation at the site. Lithofacies changes through the Late Paleocene at Mead Stream suggest the site lay under a zone of upwelling which resulted in an increase in siliceous productivity during the Late Paleocene.

At the more proximal sites of Muzzle Stream and Kaikoura wharf in southeastern Marlborough, Mead Hill Formation and Amuri Limestone are separated by an unconformity, overlain by Teredo Limestone. The Teredo Limestone is considered to be a lateral equivalent of the Waipawa Formation, but both the base and top of the Teredo Limestone are time-transgressive. This means that at Muzzle Stream the unit is contemporaneous with the Waipawa Formation (Late Paleocene), while at Kaikoura wharf the unit is entirely Early Eocene in age. At these sites, the Teredo Limestone Member of the Amuri Limestone is a calcareous greensand sometimes containing phosphatised limestone clasts and sharks teeth. In thin sections, the unit consists of well sorted, fine to very fine sand sized siliciclastic grains and fine sand sized pelletal and vermicular glaucony set in a calcareous matrix that shows evidence of secondary silicification. Unconformity formation and the subsequent deposition of the overlying Teredo Limestone record a period of invigorated intermediate depth ocean currents that resulted in the transport of siliciclastic grains and glaucony to these bathyal sites. This interpretation is supported by a palinspastic map of the Teredo Limestone that suggests the unit was deposited under different conditions than those responsible for the deposition of the bounding Mead Hill Formation and Amuri Limestone. This map also suggests the Teredo Limestone was deposited as a 'skin drift', here named the Clarence Drift, possibly under the influence of contour currents.

Based on similarities between unconformities and lithofacies changes in Late Paleocene to Early Eocene sedimentary sections and an earlier, well documented event at the Cretaceous/Tertiary boundary in southeastern Marlborough, evidence for a period of enhanced siliceous productivity, invigorated ocean currents and possible episodes of ice rafting is suggested to be consistent with a brief period of Antarctic ice sheet growth during a phase of global cooling in the Late Paleocene.

The possible identification of Antarctic ice sheets, ephemeral though they may have been, not only challenges long held beliefs that the Antarctic continent remained ice free during the early Paleogene greenhouse world but also questions the suggested mechanisms responsible for Antarctic ice sheet growth. The lack of ocean gateways in the Southern Ocean during this time effectively rules out thermal isolation of the Antarctic continent as a driver. Given that this period of ice sheet growth is contemporaneous with a documented period of enhanced global ocean productivity and terrestrial carbon accumulation and related draw down in atmospheric CO<sub>2</sub>, it is suggested this may represent the driver responsible for brief Antarctic glaciation during this period, though the postulated link requires further investigation.

# ACKNOWLEDGEMENTS

---

First and foremost, I would like to acknowledge my family and friends, the people who gave me so much time and support and asked very little in return, thank you. To Mum and Dad, thank you for your unwavering support and belief in me, I could not have done it without you, cheers. Cam, Matt and Loren, thank you for reminding me there is a world outside my cubicle and providing a couch to vegetate on every Friday night without fail. To Larry, Dirk and the rest of the Masters research group, thanks for your companionship through the last two years.

Secondly I would like to thank my supervisors Cam Nelson, Steve Hood and Chris Hollis. To Cam, I express my gratitude for the amount of time you have given me, whether it be discussing the project, providing much needed motivation or the laborious task of editing, thanks again. To Steve, thanks for being the first point of contact throughout much of this process, your assistance is greatly appreciated. To Chris, this task would have been much more difficult without your enthusiasm for, and knowledge, of the project, thanks.

I would like to acknowledge the assistance of members of the Global and Climate Change section, GNS, Lower Hutt. Particularly James Crampton, Poul Schiøler and Percy Strong for providing access to unpublished data as well as assistance with field work conducted in the Clarence Valley. Along with Huge Morgans, for supervising and providing tips on how to change four wheels on two separate vans in the car park of the Flaxbourne Tearooms while feeling less than ideal. I would also like to thank others who have helped me in the process of my field work, namely Rebecca Richards for assistance at Kaikoura and members of the University of Otago 2009 Campbell Island Expedition, Gary Wilson for organising the trip and allowing me a place on the boat, Bill and Phil, Steve, Julie-Anne (Mum), Rebecca, Hamish and Chris. Special thanks go to Pont Lurcock, Bob Dagg and Billy Wallace, cheers for sharing the raunchy Mills & Boon at Northwest Bay hut, toasted cheese and vegemite sandwiches and four days fighting sea lions and *Dracophyllum*, field work I will never forget. Special thanks to staff at the University of Waikato, Roger Briggs, Steve Cooke and Renat Radosinsky for their assistance with XRF analysis and interpretation and thin section preparation, as well as Jacinta Parenzee, Annette Rodgers and Ganqing Xu for their assistance with other lab work and general problems.

I would like to acknowledge the Murray and Nimo families for providing access to Bluff and Muzzle stations, respectively. With a specific thanks to the Murrays for their warm hospitality during the CBEP 2009 pre-conference field trip.

Finally, I acknowledge the University of Waikato, The Royal Society of New Zealand Marsden Fund and AusIMM for providing funding assistance for this study.



# TABLE OF CONTENTS

---

	<i>page</i>
Title Page	i
Fronticepiece	iii
Abstract	v
Acknowledgements	vii
Table of Contents	ix
List of Figures	xiii-xvii
List of Tables	xviii

## **CHAPTER 1 – Introduction**

1.1 THE PALEOGENE GREENHOUSE	1
1.2 CLIMATIC VARIATION AND DRIVERS	3
1.3 THE IMPORTANCE OF THE GREENHOUSE WORLD	5
1.4 RECORDS OF CLIMATIC AND OCEANOGRAPHIC CHANGE FROM ZEALANDIA	6
1.4.1 Passive Margin Records	6
1.4.2 Development of Passive Margin Sedimentation	8
1.4.3 The Importance of Paleogene Climatic Records from Zealandia	12
1.5 AIMS	14
1.6 THESIS STRUCTURE	16

## **CHAPTER 2 – Methods**

2.1 SAMPLING AND FIELD MEASUREMENTS	19
2.2 DEFINITIONS AND USAGE	19
2.3 ANALYTICAL METHODS	20
2.3.1 Sample Preparation	20
2.3.2 Petrographic Analysis	22
2.3.3 Mineralogical Determination	23
2.3.4 X-Ray Fluorescence	24
2.3.5 Carbonate Percentage	27
2.3.6 Stable Isotope Analysis	29
2.3.7 Micropaleontologic Analysis	31



### **CHAPTER 3 – Sedimentary Successions of Campbell Island**

3.1	PHYSICAL SETTING	33
3.2	LATE CRETACEOUS-OLIGOCENE LITHOSTRATIGRAPHY OF CAMPBELL ISLAND GROUP	36
3.2.1	Complex Point Group	37
3.2.2	Garden Cove Formation	38
3.2.3	Tucker Cove Limestone	40
3.3	LITHOFACIES AT CAMPBELL ISLAND	41
3.3.1	Site Description	41
3.3.2	Field Descriptions	45
3.3.3	Petrography and Mineralogy	49
3.3.4	Geochemistry	53

### **CHAPTER 4 – Sedimentary Successions of Southeastern Marlborough**

4.1	PHYSICAL SETTING	63
4.2	LATE CRETACEOUS-LATE EOCENE LITHOSTRATIGRAPHY OF MUZZLE GROUP	67
4.2.1	Mead Hill Formation	68
4.2.2	Waipawa Formation	70
4.2.3	Amuri Limestone	72
	<i>Teredo Limestone Member</i>	72
	<i>Amuri Limestone Lithotypes</i>	74
4.3	LITHOFACIES AT MEAD STREAM	75
4.3.1	Site Description	75
4.3.2	Field Descriptions	77
4.3.3	Petrography and Mineralogy	80
4.3.4	Geochemistry	84
4.4	LITHOFACIES AT MUZZLE STREAM	92
4.4.1	Site Description	92
4.4.2	Field Descriptions	93
4.4.3	Petrography and Mineralogy	96
4.4.4	Geochemistry	101
4.5	LITHOFACIES AT KAIKOURA WHARF	107
4.5.1	Site Description	107
4.5.2	Field Descriptions	112
4.5.3	Petrography and Mineralogy	118
4.5.4	Geochemistry	125

<b>CHAPTER 5 – Discussion</b>	
5.1 REVISION OF EARLY PALEOGENE STRATIGRAPHIC NOMENCLATURE OF SOUTHEASTERN MARLBOROUGH	133
5.1.1 Reinterpretation of Lithostratigraphy at Kaikoura Wharf	134
5.1.2 Suggested Future Stratigraphic Nomenclature	135
<i>Amuri Limestone</i>	135
<i>Teredo Limestone Member</i>	136
<i>Amuri Limestone Lithotypes</i>	139
5.2 PALEOENVIRONMENTAL SIGNIFICANCE OF LITHOFACIES	139
5.2.1 Siliceous Micrite and Chert Facies (F1)	139
5.2.2 Organic Mudstone Facies (F2)	142
5.2.3 Micrite Facies (F3)	145
5.2.4 Greensand Facies (F4)	147
5.2.5 Calcareous Glauconitic Mudstone Facies (F5)	151
5.2.6 Fine Sandy Mudstone Facies (F6)	152
5.2.7 Lithofacies Relationships	153
5.3 PALEODISTRIBUTION MAPS	155
5.3.1 Spatial Distribution of Late Cretaceous to Early Eocene Units, With Emphasis on the Teredo Limestone	159
<i>Urutawan-Motuan Sediments</i>	159
<i>Herring Formation</i>	159
<i>Mead Hill Formation</i>	160
<i>Amuri Limestone</i>	161
<i>Teredo Limestone</i>	162
<i>The Clarence Drift</i>	165
5.3.2 Temporal Lithofacies Changes	169
<i>Lower Teurian</i>	170
<i>Upper Teurian</i>	173
<i>Waipawan</i>	177
<i>Mangaorapan</i>	179
5.4 PALEOCENE-EOCENE OCEAN CIRCULATION PATTERNS	180
<b>CHAPTER 6 – Conclusions</b>	187
6.1 REVISED PALEOCENE-EOCENE LITHOSTRATIGRAPHY OF SOUTHEASTERN MARLBOROUGH	187
6.2 LITHOFACIES CHANGES IN SOUTHEASTERN MARLBOROUGH AND CAMPBELL ISLAND	188

6.3	ICE IN THE GREENHOUSE	190
6.4	SUGGESTIONS FOR FUTURE STUDY	191
	<b>REFERENCES</b>	193
	<b>APPENDIX A – Geological Timescales</b>	209
	<b>APPENDIX B – Sample Catalogue</b>	211 & CD
	<b>APPENDIX C – Petrographic Data</b>	215
	<b>APPENDIX D – Bulk Geochemical Data</b>	221 & CD
	<b>APPENDIX E – Stratigraphic Data for Paleodistribution Maps</b>	CD
	<b>DIGITAL APPENDICES CD</b>	Front Pocket
	<b>ENCLOSURE 1</b>	Back Pocket

# ***LIST OF FIGURES***

---

## **CHAPTER 1 – Introduction**

- Figure 1.1** Global temperature record for the last 80 Myrs in comparison to the present situation. 2
- Figure 1.2** Primary orbital components controlling the amount and distribution of incoming solar radiation on Earth. 4
- Figure 1.3** The four main factors controlling sedimentation on passive margins. 7
- Figure 1.4** Schematic diagram showing 1<sup>st</sup> and 2<sup>nd</sup> order depositional cycles recognised in Cretaceous-Cenozoic sedimentary successions from New Zealand 10
- Figure 1.5** (A) Outline of the micro-continent of Zealandia during the Late Paleocene. (B) Map of modern-day New Zealand showing the location key Paleocene sedimentary successions. 13

## **CHAPTER 2 – Methods**

- Figure 2.1** Flow diagram showing experimental pathways. 21
- Figure 2.2** Calibration curve for determining carbonate percentage. 28

## **CHAPTER 3 – Sedimentary Successions of Campbell Island**

- Figure 3.1** Map of Campbell Island. 34
- Figure 3.2** Composite stratigraphic columns for (A) the Garden Cove Formation and (B) the Tucker Cove Limestone. 37
- Figure 3.3** Map of the central portion of Campbell Island. 42
- Figure 3.4** Composite stratigraphic column for the Paleocene and bounding strata on Campbell Island. 43
- Figure 3.5** Logged sections from Campbell Island containing the contact between Garden Cove Formation and Tucker Cove Limestone. 44
- Figure 3.6** Subangular quartz pebble at Limestone Point. 46
- Figure 3.7** Fissile, highly weathered, jarositic fine sandy mudstone facies (F6). 46
- Figure 3.8** Highly weathered calcareous glauconitic mudstone facies (F5). 48
- Figure 3.9** Characteristic features of the Tucker Cove Limestone. 48

<b>Figure 3.10</b>	Photomicrographs of the fine sandy mudstone facies (F6) and calcareous glauconitic mudstone facies (F5).	50
<b>Figure 3.11</b>	Scanning electron microscope image and photomicrograph of the micrite facies (F3d).	52
<b>Figure 3.12</b>	Al normalised major element concentrations for the three facies identified on Campbell Island.	54
<b>Figure 3.13</b>	Al normalised trace element concentrations for the three facies identified on Campbell Island.	56
<b>Figure 3.14</b>	The relationship between valency and ionic radius in geochemically important species.	57
<b>Figure 3.15</b>	Chondrite normalised Rare Earth Element patterns for the three facies identified on Campbell Island.	58
<b>Figure 3.16</b>	Relationship between Al <sub>2</sub> O <sub>3</sub> and TiO <sub>2</sub> in the Garden Cove Formation and Tucker Cove Limestone.	59
<b>Figure 3.17</b>	Ternary diagram of relative proportions of Al <sub>2</sub> O <sub>3</sub> , SiO <sub>2</sub> and CaCO <sub>3</sub> in the three facies identified on Campbell Island.	60
<b>Figure 3.18</b>	Variations in geochemical proxies from Campbell Island sections.	61

#### **CHAPTER 4 - Sedimentary Successions of Southeastern Marlborough**

<b>Figure 4.1</b>	Map of southeastern Marlborough.	64
<b>Figure 4.2</b>	Schematic cross section across the Inland and Seaward Kaikoura Ranges.	65
<b>Figure 4.3</b>	Geological map and cross section of Kaikoura Peninsula.	66
<b>Figure 4.4</b>	Late Cretaceous to Early Miocene lithostratigraphy of southeastern Marlborough.	68
<b>Figure 4.5</b>	Logged section from Mead Stream.	76
<b>Figure 4.6</b>	Stratigraphic column for Late Paleocene strata at Mead Stream.	77
<b>Figure 4.7</b>	Irregular, coalescing chert nodules in the siliceous micrite and chert facies (F1a).	78
<b>Figure 4.8</b>	Bioturbation in the siliceous micrite and chert facies (F1a).	79
<b>Figure 4.9</b>	Siliceous mudstone and argillaceous mudstone interbeds of the organic mudstone facies (F2).	80
<b>Figure 4.10</b>	Photomicrographs of the siliceous micrite and chert facies (F1a) and organic mudstone facies (F2).	81

<b>Figure 4.11</b>	Scanning electron microscope images and elemental maps from the siliceous micrite and chert facie (F1a).	82
<b>Figure 4.12</b>	Al normalised major element concentrations for the two facies identified at Mead Stream.	85
<b>Figure 4.13</b>	Al normalised trace element concentrations for the two facies identified at Mead Stream.	87
<b>Figure 4.14</b>	Ternary diagram of relative proportions of Al <sub>2</sub> O <sub>3</sub> , SiO <sub>2</sub> and CaCO <sub>3</sub> in the two facies identified at Mead Stream.	89
<b>Figure 4.15</b>	Variations in geochemical proxies at Mead Stream.	90
<b>Figure 4.16</b>	Logged section from Muzzle Stream.	92
<b>Figure 4.17</b>	Stratigraphic column for Late Cretaceous-Late Paleocene strata at Muzzle Stream.	93
<b>Figure 4.18</b>	<i>Thalassinoides</i> burrow in the siliceous micrite and chert facies (F1b).	94
<b>Figure 4.19</b>	Raised irregular ring structure in the micrite facies (F3a).	96
<b>Figure 4.20</b>	Photomicrographs of the three facies identified at Muzzle Stream.	99
<b>Figure 4.21</b>	Al normalised major element concentrations for the three facies identified at Muzzle Stream.	102
<b>Figure 4.22</b>	Al normalised trace element concentrations for the three facies identified at Muzzle Stream.	103
<b>Figure 4.23</b>	Ternary diagram of relative proportions of Al <sub>2</sub> O <sub>3</sub> , SiO <sub>2</sub> and CaCO <sub>3</sub> in the three facies identified at Muzzle Stream.	105
<b>Figure 4.24</b>	Variations in geochemical proxies at Muzzle Stream.	106
<b>Figure 4.25</b>	Geological sketch map of Kaikoura wharf.	109
<b>Figure 4.26</b>	Low angle to bedding thrust fault identified at the Kaikoura wharf section.	111
<b>Figure 4.27</b>	Sedimentary dykes intersecting the sedimentary succession at Kaikoura wharf.	112
<b>Figure 4.28</b>	Stratigraphic column for Late Cretaceous-Early Eocene strata at Kaikoura wharf.	113
<b>Figure 4.29</b>	Siliceous micrite and chert facies (F1c) at the Kaikoura wharf section.	114
<b>Figure 4.30</b>	<i>Scolicia</i> burrows in the greensand facies (F4b).	115
<b>Figure 4.31</b>	Characteristic features of the Teredo Limestone at Kaikoura wharf.	116
<b>Figure 4.32</b>	Micrite facies (F3b) at Kaikoura wharf.	118

<b>Figure 4.33</b>	Photomicrographs of the siliceous micrite and chert facies (F1c).	119
<b>Figure 4.34</b>	Photomicrographs of the lower greensand facies (F4b) unit at Kaikoura wharf.	120
<b>Figure 4.35</b>	Photomicrographs of the upper greensand facies (F4b) unit at Kaikoura wharf.	122
<b>Figure 4.36</b>	Photomicrographs of the micrite facies (F3b).	123
<b>Figure 4.37</b>	Photomicrographs of chert samples under cathodeluminescent light.	124
<b>Figure 4.38</b>	Al normalised major element concentrations for the three facies identified at Kaikoura wharf.	125
<b>Figure 4.39</b>	Al normalised trace element concentrations for the three facies identified at Kaikoura wharf.	127
<b>Figure 4.40</b>	Relationship between $Al_2O_3$ and $TiO_2$ in the Mead Hill Formation and Amuri Limestone.	129
<b>Figure 4.41</b>	Ternary diagram of relative proportions of $Al_2O_3$ , $SiO_2$ and $CaCO_3$ in the two facies identified at Mead Stream.	130
<b>Figure 4.42</b>	Variations in geochemical proxies at Kaikoura wharf.	131

## CHAPTER 5 – Discussion

<b>Figure 5.1</b>	Palinspastic reconstruction of central New Zealand at about the K/T boundary.	134
<b>Figure 5.2</b>	Calcitic tubes on the uppermost contact of the Teredo Limestone at Haumuri Bluff.	137
<b>Figure 5.3</b>	Schematic diagram of inferred provenance relations for the siliciclastic fraction of the Teredo Limestone.	149
<b>Figure 5.4</b>	Relationship between lithofacies in the study sites of this investigation.	154
<b>Figure 5.5</b>	The major structural boundaries and blocks used in the retro-deformation of southeastern Marlborough.	156
<b>Figure 5.6</b>	Retro-deformed configuration of southeastern Marlborough.	157
<b>Figure 5.7</b>	Palinspastic map for the Urutawan-Motuan sediments.	160
<b>Figure 5.8</b>	Palinspastic map for the Herring Formation.	161
<b>Figure 5.9</b>	Palinspastic map for the (A) Mead Hill Formation, (B) Lower Limestone lithotype of the Amuri Limestone and (C) Teredo Limestone Member of the Amuri Limestone.	163

- Figure 5.10** Sediment drifts of southern and eastern New Zealand at the present day. 166
- Figure 5.11** Transect through the middle Clarence Valley showing the changing abundance of the major components within the Teredo Limestone. 168
- Figure 5.12** Lithofacies map of southeastern Marlborough during the lower Teurian (c. 64 Ma). 171
- Figure 5.13** Lithofacies map of southeastern Marlborough during the upper Teurian (c. 58 Ma). 173
- Figure 5.14** Graph showing the relationship between Si[exc], Ba[exc] and TRG at Mead Stream. 175
- Figure 5.15** Schematic diagram showing the range of average current speeds at which sediment particles of different sizes are eroded, transported, and deposited. 176
- Figure 5.16** Lithofacies map of southeastern Marlborough during the Waipawan (c. 55 Ma). 178
- Figure 5.17** Lithofacies map of southeastern Marlborough during the Mangaorapan (c. 52 Ma). 180
- Figure 5.18** Ocean structure of the present day New Zealand sector of the Southern Ocean. 183
- Figure 5.19** Paleogeographic reconstruction for New Zealand during the Late Paleocene (56 Ma). 185
- ENCLOSURE 1** Lithostratigraphic panel for Late Cretaceous to Miocene rocks of southeastern Marlborough and Campbell Island and geochemical proxies alongside stratigraphic columns from Mead Stream, Muzzle Stream, Kaikoura wharf and Campbell Island. Back Pocket



# ***LIST OF TABLES***

---

<b>Table 2.1</b>	Semi-quantitative abundance limits used during petrographic analysis.	23
<b>Table 2.2</b>	Estimated background concentrations of Al <sub>2</sub> O <sub>3</sub> , TiO <sub>2</sub> , CaCO <sub>3</sub> , SiO <sub>2</sub> , and Ba for samples from Marlborough and Campbell Island.	25
<b>Table 2.3</b>	Comparison of carbonate contents determined using three different methods.	28
<b>Table 3.1</b>	Lithologic characteristics of units from the Garden Cove Formation.	38
<b>Table 3.2</b>	Lithologic characteristics of units from the Tucker Cove Limestone.	40
<b>Table 5.1</b>	Comparison between previously published and reinterpreted lithostratigraphy for Kaikoura wharf.	135
<b>Table 5.2</b>	Current and suggested future lithostratigraphic nomenclature in southeastern Marlborough for Paleocene to Middle Eocene rocks.	138
<b>Table 5.3</b>	Key characteristics of the six lithofacies identified in southeastern Marlborough and at Campbell Island.	140
<b>Table 5.4</b>	Deformations and adopted retro-deformations used in the retro-deformation models of southeastern Marlborough.	155
<b>Table 5.5</b>	Stratigraphic data localities used for the late Early Cretaceous to Early Eocene palinspastic reconstructions.	158

# **CHAPTER 1**

## **INTRODUCTION**

---

### **1.1 THE PALEOGENE GREENHOUSE**

The Paleogene is a period of time between 65 and 23.8 Ma which encompasses the Paleocene, Eocene and Oligocene epochs. On the broadest scale, the Paleogene can be divided into two separate climatic periods termed the 'greenhouse world' that transitioned into the 'icehouse world' (Figure 1.1). The 'greenhouse world' is a term given by Fischer (1984) to periods of time in the Earth's history when global temperatures were much warmer than present and it is presumed that the poles remained ice free (Miller et al. 2005). The early Paleogene (65 – 40 Ma) is considered to be one of these times and it is generally accepted that this period was characterised by much warmer temperatures when compared to present day conditions. Deep-sea temperatures ranged between 10 and 12°C during the early Paleogene (Wing et al. 2003), while sea-surface temperatures in high latitudes reached ~30°C (Bijl et al. 2009; Hollis et al. 2009a) and as high as ~40°C in the tropics (Pearson et al. 2007; Huber 2008). Long held beliefs suggested that along with high temperatures, the Paleogene (outside the Oligocene) was characterised by low latitudinal temperature gradients and stable temperature, however recent studies have shown this may not be the case in all regions (Crouch et al. 2009). For example, based on Mg/Ca ratios of planktic foraminifera and archeal membrane lipids in bathyal sediments from Canterbury, New Zealand, Hollis et al. (2009b) demonstrated a dramatic shift in both sea-floor and sea-surface temperatures during the Late Paleocene to Early Eocene. To explain such high temperatures, modellers invoke CO<sub>2</sub> concentrations >2-4 times present day levels (Miller et al. 2005). It is some New Zealand deposits that formed during the early Paleogene 'greenhouse world' that are the focus of this study.

The textbook history of Cenozoic climate has Antarctic ice sheets forming around the Eocene/Oligocene boundary (Zachos et al. 2001; Coxhall & Pearson 2007) and an Arctic ice sheet forming much later in the Neogene

(Shackleton et al. 1984). However, recent sedimentologic and geochemical evidence suggests that Arctic ice sheets may have formed as early as the Eocene (Spielhagen & Tripathi 2009), while evidence of Milankovitch scale sea level oscillations from the New Jersey and Russian platforms suggest glacio-eustatically driven sea level change as far back as the Late Cretaceous (Miller et al. 2005). Climatic and oceanographic events that occurred within the early Paleogene 'greenhouse world' are the focus of this study.

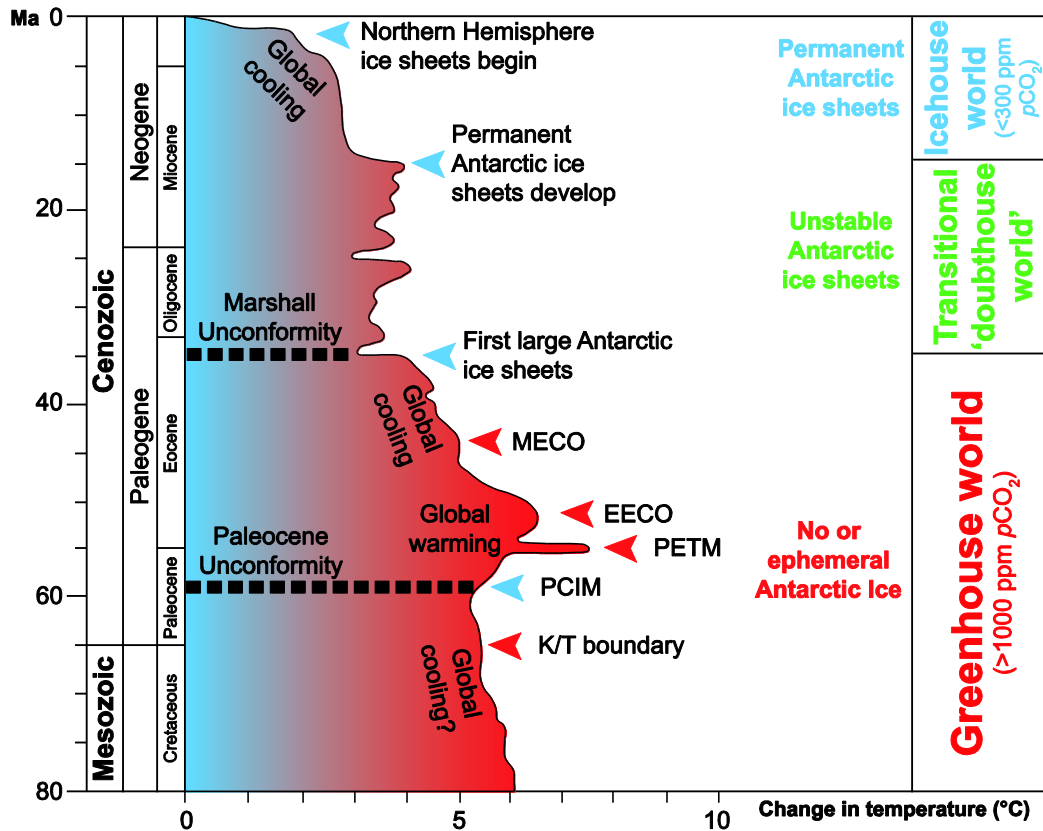


**Figure 1.1** Global temperature record for the last 80 Myrs (after Barrett 2003) in comparison to the present situation showing some major Cenozoic climatic events (after Zachos et al. 2001). K/T boundary: Cretaceous-Tertiary boundary; PCIM: Paleocene carbon isotope maximum; PETM: Paleocene-Eocene thermal maximum; EECO: early Eocene climatic optimum; MECO: middle Eocene climatic optimum.

Though the late Paleogene (Oligocene) can be considered to be an 'icehouse world' under the definition of Fischer (1984), it realistically represents a period of transition between the early Paleogene 'greenhouse' and true 'icehouse' that formed in the Neogene (Figure 1.1). The period saw a general decrease in temperatures and atmospheric CO<sub>2</sub> concentrations associated with major rapid and oscillatory glaciation on

Antarctica (Barrett 2003; DeConto & Pollard 2003; Pagani et al. 2005). While this period is important globally, it is not considered within this study.

## **1.2 CLIMATIC VARIATION AND DRIVERS**

Evidence from sedimentary records has long shown the continuously changing nature of the Earth's climate through the Cenozoic, which at the broadest scale, is characterised by the shift from greenhouse to icehouse conditions. However, the greater availability of high quality sediment cores recovered by scientific drilling programs, such as the Ocean Drilling Program (ODP) and Deep Sea Drilling Project (DSDP), has led to the identification of superimposed geologically abrupt and transient climatic events punctuating this Cenozoic climate record (Figure 1.1). Zachos et al. (2001) suggest that shifts and trends in global climate throughout the Cenozoic can be attributed to a combination of two driving forces which operate over differing time scales. The first driver, plate tectonics, is considered to be responsible for the long term global mean climate over periods from  $10^5 - 10^7$  years. These processes affect global climate by driving gradual but continual changes in the Earth's boundary conditions which include geography, topography, ocean gateway locations, bathymetry and concentrations of atmospheric greenhouse gases. Examples of major changes in the Earth's boundary conditions during the Paleogene include the opening the Tasmanian Gateway between Tasmania and Antarctic and Drake Passage between South America and Antarctica during the late Eocene to Oligocene, emplacement of the North Atlantic Igneous Province around the Paleocene-Eocene boundary and the collision of India with Asia during the Eocene (Zachos et al. 2001).

The second driver is considered to be changes in the Earth's orbital parameters of eccentricity, obliquity and precession (Figure 1.2), which tend to act over shorter time periods between  $10^4$  and  $10^6$  years. Eccentricity, the longest of these cycles, has a periodicity of 400 and 100 k.y. and is a measure of the departure of the Earth's orbit from a perfect circle to a more elliptical shape. Changes in the eccentricity of the Earth's orbit are driven by torques exerted on the Earth-Sun system by other planets, specifically Jupiter and Venus due to their size and proximity,

respectively (Muller & MacDonald 2000). Obliquity is the angle of tilt of the Earth's axis of rotation with respect to the plane of the elliptic. The angle of obliquity varies between  $22.1^\circ$  and  $24.5^\circ$  with a periodicity of about 40 k.y. (Zachos et al. 2001). Precession is the wobble of the Earth's axis of rotation due to the torque of the Sun and Moon on the Earth's equatorial bulge. This wobble can be compared to a tilted spinning top which wobbles due to the torque of gravity (Muller & MacDonald 2000; Zachos et al. 2001). Though the axis of Earth's rotation precesses with a period of 26 k.y., the modulating affect of orbital eccentricity means that the period of the precessional signal observed in the geological record is actually 19 and 23 k.y.

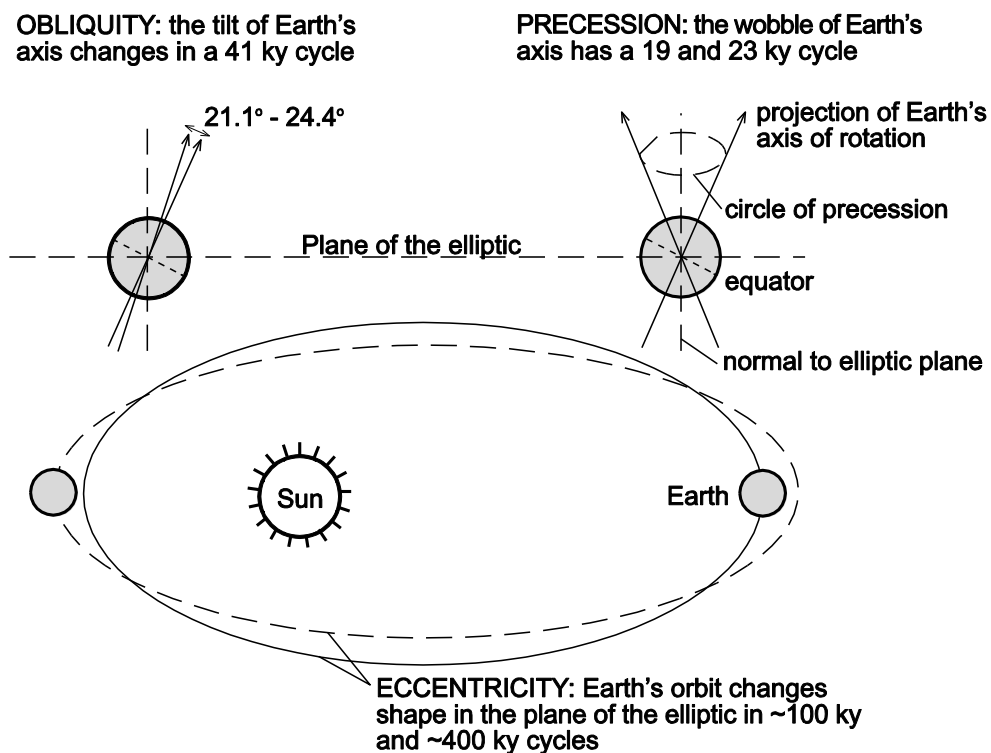


**Figure 1.2** Primary orbital components controlling the amount and distribution of incoming solar radiation on Earth (Muller & MacDonald 2000).

Milankovitch theory states that changes in these orbital parameters will affect the amount of solar radiation that reaches the Earth's surface, referred to as insolation, at various times and therefore have a direct affect on global climate. Though eccentricity is important in determining total insolation, it plays only an indirect role in determining the global distribution. It is for this reason that Zachos et al. (2001) state that eccentricity alone cannot account for changes in the Earth's climate in the

past. It does, however, as stated previously, modulate precession by affecting movement of the perihelion, the point at which the Earth passes closest to the sun. The perihelion moves most rapidly when eccentricity is greatest (Muller & MacDonald 2000). Precession affects global climate by determining where in the orbit around the sun seasons occur with respect to perihelion and aphelion (Zachos et al. 2001). Presently, perihelion occurs on the 4<sup>th</sup> of January, meaning the Earth is closest to the sun during the Northern winter, limiting the development of large scale northern ice sheets (Muller & MacDonald 2000). Obliquity is suggested by Muller and MacDonald (2000) to be the only orbital parameter to affect total yearly insolation at the poles. Increased obliquity means more insolation at the poles and leads to higher seasonal contrast with colder winters and hotter summers in both hemispheres.

### **1.3 THE IMPORTANCE OF THE GREENHOUSE WORLD**

Zachos et al. (2008) state that if fossil-fuel emissions continue unabated, as they have since the beginning of the industrial revolution, 5000 gt of carbon will be released by the year 2400. Prior to the eventual sequestration of this anthropogenic carbon to the geosphere through deposition of calcium carbonate and organic carbon, most of this will be accumulated in the atmosphere and oceans. Zachos et al. (2008) suggest that if only 60% of this carbon is accumulated in the atmosphere, this will result in an increase in  $p\text{CO}_2$  to 1800 ppm. Similar  $p\text{CO}_2$  values to these have not been present on Earth for ~50 m.y. during the early Paleogene greenhouse, when boron-isotope ratios suggest  $p\text{CO}_2$  was greater than 2000 ppm (Pearson & Palmer 2000; Pagani et al. 2005).

As a realisation of this problem, a large proportion of research from the last 20 years has focussed on relationships and possible tipping points leading to extreme climates (Williams et al. 2007), especially focussing on hyperthermals of which the Paleocene-Eocene Thermal Maximum, abridged to PETM, is the most prominent and best studied. However, very few studies have investigated periods of comparative cooling that appear to be more anomalous in the early Paleogene, given the general characteristics of the greenhouse world.

One example of this is a ~2-3 m.y period of cooling that occurred in the Late Paleocene associated with the highest  $\delta^{13}\text{C}$  values of the entire Cenozoic carbon isotope record, known as the 'Paleocene carbon isotope maximum', or PCIM (Thompson & Schmitz 1997; Zachos et al. 2001; Kurtz et al. 2003; Hollis et al. 2005b). This excursion is interpreted to reflect a period of increased rates of organic carbon ( $\text{C}_{\text{org}}$ ) burial, either as a result of enhanced surface ocean productivity (Schmitz et al. 1997; Thompson & Schmitz 1997) and/or accumulation of terrestrial carbon (Kurtz et al. 2003).

## **1.4 RECORDS OF CLIMATIC AND OCEANOGRAPHIC CHANGE FROM ZEALANDIA**

### **1.4.1 Passive Margin Records**

Continental margins can broadly be divided into active or passive margins. Active margins lie converging along plate boundaries and are affected to varying degrees by plate tectonic movements. Passive continental margins are divergent ones, within the interior of a lithospheric plate and are generally 'rafted' away from active margins as a result of sea-floor spreading (Pratson et al. 2007).

Passive margins accumulate large volumes of sediment, in typically tectonically stable but continuously subsiding environments (Kennett 1982). Initially, subsidence of passive margins is driven by thermal subsidence as a result of cooling of the adjacent oceanic lithosphere following rifting (Pratson et al. 2007). Thermal subsidence tapers off over time according to the relationship  $1/\sqrt{\text{age}}$  (Parson & Sclater 1977), meaning subsidence in young margins ranges between 40 and 100 m/m.y., while in mature margins, rates are generally  $<3$  m/m.y. (Pratson et al. 2007). As sediment accumulates on passive margins, isostatic subsidence and sediment compaction as a result of sediment loading begin to also influence subsidence rates (Pratson et al. 2007).

The distribution of depositional paleoenvironments and their lithofacies is controlled by sediment supply, climate, eustacy, and subsidence, and

more importantly the complex interrelations between these factors (Figure 1.3) (Mountain et al. 2007). If the complex interactions can be understood and interpreted, passive margin records have the ability to provide long term records of paleoenvironmental change. The long term nature of passive margin records is important for a number of reasons (Mountain et al. 2007). First, they record the complex behaviour of the Earth system under boundary conditions greatly different to those of the present today. Second, they provide a good chance to evaluate numerical models over longer time-scales. And third, the fundamental processes that drive the Earth system act on time-scales far longer than the short term (~20 k.y.).

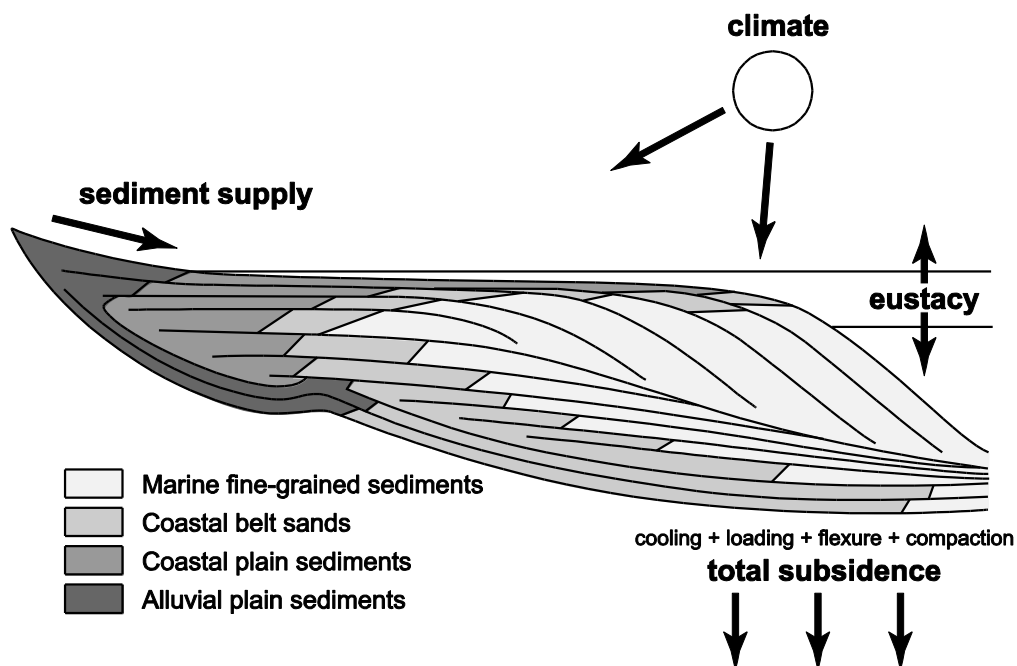


**Figure 1.3** The four main factors controlling sedimentation on passive margins, namely sediment supply, climate, eustacy and subsidence (Vail & Sangree 1988).

The New Jersey margin on the eastern coast of North America is an example of a classical long-lived passive margin, with initiation of rifting occurring in the Late Triassic, followed by sea-floor spreading by the Middle Jurassic. This plate setting has not changed to the present (Mountain et al. 2007). The long-lived nature, combined with a relatively simple tectonic history dominated by thermal subsidence, sediment loading and flexure, has meant that the New Jersey margin sequences have played a critical role in our understanding of Late Cretaceous to Recent global eustatic and climatic changes (e.g. Miller et al. 1998, 2005; Van Sickel et al. 2004; John et al. 2008).



### 1.4.2 Development of Passive Margin Sedimentation

In New Zealand, a passive margin was developed within a 1<sup>st</sup> order tectonic megacycle represented by supra-basement Cretaceous-Cenozoic sedimentary successions (Figure 1.4) (King et al. 1999). This ~100 m.y transgressive-regressive megasequence is divided into seven 2<sup>nd</sup> order depositional cycles, of which those deposited within the transgressive phase of this megasequence will be discussed here.

Deposition of the 1<sup>st</sup> order tectonic megasequence was initiated ~100 Ma with the deposition of Cycle 1 (Figure 1.4) during cessation of subduction of the Phoenix plate beneath the eastern margin of Gondwana and an abrupt shift from a convergent to extensional tectonic setting (Laird & Bradshaw 2004; Mortimer 2004). Until this period, the eastern margin of Gondwana had undergone progressive Pacific-ward growth by terrane accretion and batholith intrusion through the Late Paleozoic to Mesozoic (Mortimer 2004). This rapid shift in tectonic regimes was initially proposed by Bradshaw (1989) to have occurred as a result of oblique subduction of the Phoenix-Pacific spreading ridge eliminating the subduction zone. Luyendyk (1995) modified this by suggesting the shift occurred as a result of subducted slab capture, whereby the Phoenix plate became too small to subduct beneath the eastern margin of Gondwana as the Phoenix-Pacific spreading ridge approached the subduction zone. As subduction ceased, the spreading ridge stalled and areas of New Zealand, the Chatham Rise, Campbell Plateau and Lord Howe Rise, collectively referred to as Zealandia by Luyendyk (1995) (Figure 1.5A), and Marie Byrd Land were captured by the northward moving Pacific plate. In what is presently the northeastern portions of the North Island and South Island, New Zealand (i.e. Raukumara and Marlborough regions, respectively) compressional tectonics continued through to the late Early Cretaceous before the onset of extension (King et al. 1999; Crampton et al. 2003). Crustal thickening and regional uplift as a consequence of a number of events, such as prolonged convergence along the eastern margin of Zealandia, meant that as the micro-continent rifted from Gondwana it was subject to rapid erosion, accompanied by spectacular crustal thinning and thermal

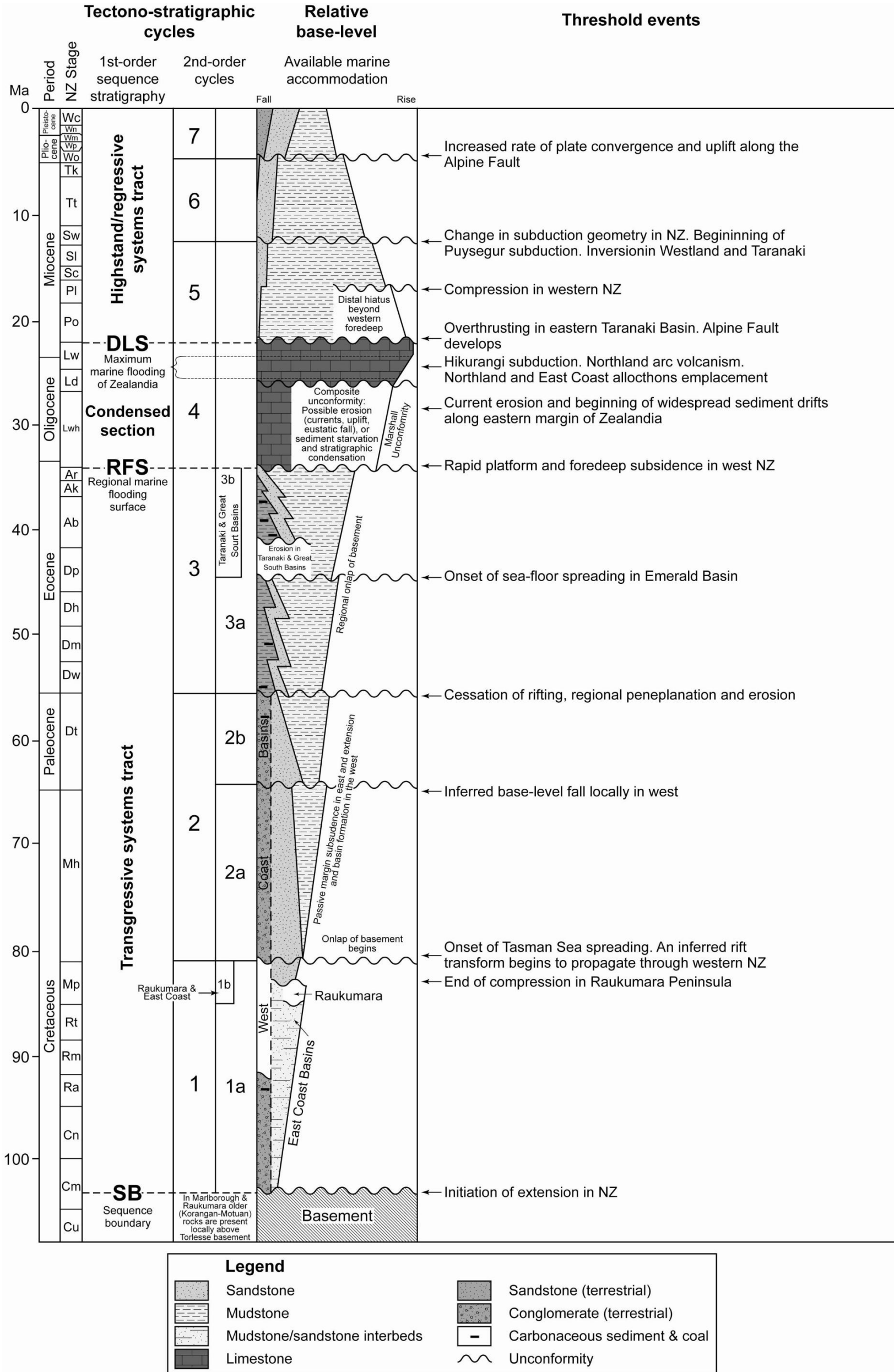


**Figure 1.4** Schematic diagram showing generalised depositional patterns, unconformities and important tectonic and oceanographic events set within the broad framework of the 1<sup>st</sup> order tectonic megacycle represented by supra-basement Cretaceous-Cenozoic sedimentary successions from New Zealand (from King et al. 1999). New Zealand stages are defined in Appendix A.



relaxation (Ballance 1993). During this initial period of crustal extension prior to Tasman Sea spreading, sedimentation was generally within normal fault controlled grabens, where Early to Late Cretaceous syn-rift deposits were widely developed throughout many sedimentary basins.

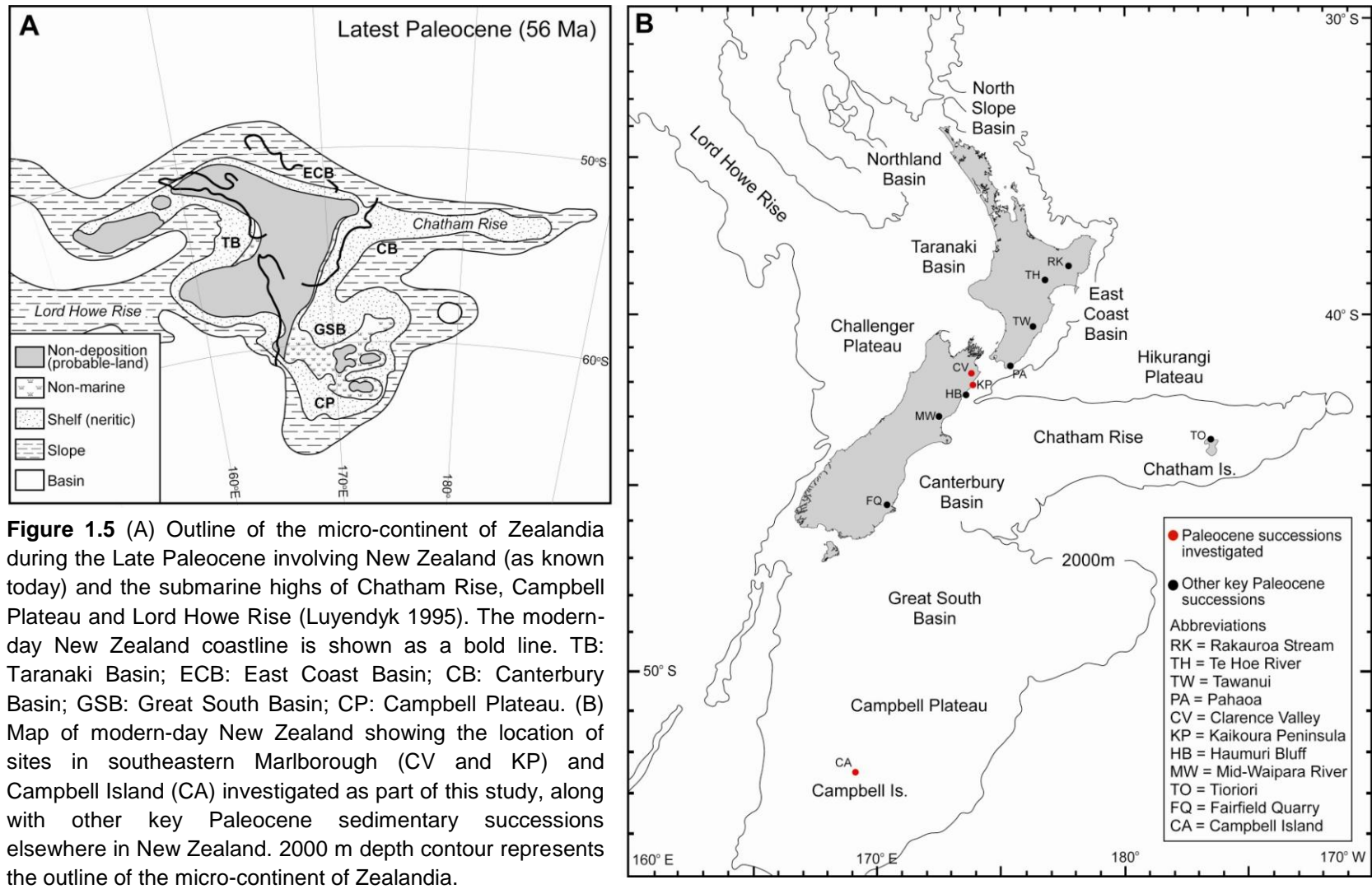
The onset of Tasman Sea spreading demarcating the western side of Zealandia during the Late Cretaceous was concomitant with initiation of passive margin thermal subsidence and marine transgression in the eastern basins (Field et al. 1997; Cook et al. 1999; King et al. 1999; Crampton et al. 2003). This period corresponds to Cycle 2 of King et al. (1999) (Figure 1.4) and is generally characterised by fining upward sequences of the Taratu Formation (Great South Basin), Broken River Formation (Canterbury Basin) and Paton Formation (Marlborough) which were deposited in coastal plains and transgressive shallow marine sedimentary environments. Sedimentation in the East Coast Basin during this period was characterised by shallow marine to bathyal sandstones, flysch and shales of the Tahora and Glenburn Formations. By the latest Cretaceous, deposition of siliceous mudstone of the Whangai Formation and correlatives (Conway Formation and Ngatuturi Claystone) occurred throughout the East Coast Basin in a region extending from New Caledonia to the Great South Basin (Beggs 1976, 1978; Crampton 1988; Field et al. 1989; Ballance 1993; Field et al. 1997; Cook et al. 1999). The widespread nature of the Whangai facies is interpreted by Moore (1988) to reflect increased siliceous productivity and a decrease in coarse terrigenous material, expressed not only by a decrease in grain size but also the amount of sediment, as a result of continued thermal subsidence. In the Marlborough region of northeastern South Island, the decrease in terrigenous supply was rapid in comparison to other basins, leading to deposition of micro-bioclastic sediments of the Muzzle Group by the latest Cretaceous. Given that the base of the Muzzle Group was deposited in inner-mid shelf depth waters (Strong et al. 1995), Crampton et al. (2003) interpreted the paucity of siliciclastics as reflecting negligible subaerial or submarine erosion on, or transport from, the crest of the Chatham Rise as a result of low relief (Figure 1.5A). Extension continued in western basins through this period (King et al. 1999).

The boundary between Cycles 2 and 3 corresponds to the cessation of Tasman Sea spreading and by this time the entire region of Zealandia was tectonically quiescent. Within Cycle 3, Eocene sedimentation throughout Zealandia occurred on a gently subsiding continental margin characterised by subdued topography and broad coastal plains. Continued post-rift cooling and passive margin subsidence in the east led to the widespread development of calcilutites of the Amuri carbonate megafacies (Nelson 1978; Hood & Nelson 1996). Towards the end of Cycle 3, spreading began in the Emerald Basin to the south of New Zealand, resulting in the propagation of continental rifting through southwestern New Zealand (King et al. 1999).

Passive margin thermal subsidence culminated in the Oligocene, corresponding to Cycle 4 of King et al. (1999), with development of the maximum marine flooding surface of the 1<sup>st</sup> order tectonic megacycle, as evidenced by carbonate dominated, condensed sections in almost all basins (Figure 1.4). It has been recently suggested that the continent of Zealandia may have been entirely submerged during this period (Landis et al. 2008). This cycle also signals the cessation of passive margin subsidence in eastern regions and extension in western regions and a shift to transpression followed by the initiation of subduction at the Hikurangi and Puysegur margins to the north and south, respectively, by ~20-25 Ma (King et al. 1999; Furlong & Kamp 2009). The end of Cycle 4 represents the end of the transgressive phase of the 1<sup>st</sup> order tectonic megasequence and a transition to highstand/regressive systems tracts (King et al. 1999).

#### **1.4.3 The Importance of Paleogene Climatic Records from Zealandia**

Strata of importance to this study were deposited within Cycles 2 and 3 of the 2<sup>nd</sup> order depositional cycles of King et al. (1999). During the Late Cretaceous to early Paleogene period of relative tectonic quiescence along the eastern margin of Zealandia, the micro-continent lay at a paleolatitude of 55-60°S (Crampton et al. 2003). Hollis et al. (2005b) state that Paleogene circulation models show that the continent of Zealandia lay



in a transition zone between a cool cyclonic gyre to the south and a warm anticyclonic gyre to the north. This is supported by Nelson & Cooke (2001) who showed a similar transition between cool and warm subtropical water masses based on lithological, paleontological and geochemical data from Deep Sea Drilling Project (DSDP) cores in the southwest Pacific. During this period, the Marlborough region of northeastern South Island was ideally located to record the latitudinal migration of this transition zone through lithologic changes in micro-bioclastic sediments of the Muzzle Group (Killops et al. 2000; Hollis et al. 2005b).

Hollis et al. (2005b) considered high latitude Pacific climate records from the passive margin of Zealandia crucial for the establishment of temperature gradients and the identification of areas of deep-water formation and other water mass and climatic features. However, the majority of climatic records for the early Paleogene are from the Atlantic and Indian Oceans, leaving the climate evolution of the Pacific Ocean poorly resolved during this period (Hollis et al. 2005b; Bijl et al. 2009). This matter is important to address because Eocene circulation models show that 80% of ocean heat transport occurred in the Pacific (Huber & Sloan 2001).

## **1.5 AIMS**

Records of extreme climatic events under greenhouse conditions experienced during the early Paleogene are seen to be critical to furthering our understanding of climatic responses to changes in atmospheric CO<sub>2</sub> concentrations. In 2008 a project titled 'Ice in the Greenhouse: a Paleocene record of Antarctic deep-water flow' led by GNS Science and supported by the Royal Society of New Zealand Marsden Fund, began in earnest to investigate New Zealand records. The project involves collaboration with other research institutions, including the University of Waikato, the University of Otago and the University of Bristol. The central hypothesis of this project is that a significant Paleocene unconformity (or unconformities) in sedimentary successions from around New Zealand record a prolonged episode of deep-sea erosion that is linked to Antarctic cooling and ice-sheet growth, intensification of a

southern-sourced deep-water flow, and a fall in global sea level. This hypothesis is critical in evaluating the validity of two suggested models for Antarctic ice sheet growth. The previously accepted view is that the presence of Antarctic ice sheets is dependent on thermal isolation of the continent by the Antarctic Circumpolar Current (ACC). This is based on oxygen isotope records (Miller et al. 1987; Zachos et al. 2001) and sedimentological evidence (Zachos et al. 1992) which suggested that a marked increase in Antarctic ice volume and a decrease in ocean temperatures during the Oligocene was coincident with the opening of the Tasmanian Gateway. However, recent climate models (DeConto & Pollard 2003; DeConto et al. 2008) suggest that Antarctic glaciation occurs when atmospheric CO<sub>2</sub> falls below a certain threshold. Identification of unconformity surfaces related to an episode of Antarctic deep-water flow during the Paleocene, prior to the opening of either the Drake Passage or the Tasmanian Gateway, would imply that the latter model was more appropriate and that the stability of Antarctic ice sheets was primarily dependent on atmospheric CO<sub>2</sub> concentrations.

The collaborative nature of this project was brought about by the need for an integrated approach to the problem, making it necessary to bring together biostratigraphic, sedimentologic, seismic, geochemical and paleomagnetic studies. The University of Waikato is responsible for reporting the sedimentology and selective geochemistry of several key Paleocene sections in eastern New Zealand (Figure 1.5B). This thesis study investigates sites at Clarence Valley and Kaikoura Peninsula in southeastern Marlborough, as well as sections from Campbell Island south of the New Zealand mainland. A companion thesis (Michael Tayler, in prep.) is underway studying some of the key sections in eastern North Island.

The main aims of the present study are:

- i) Undertake a detailed sedimentologic investigation of key Paleocene sections containing unconformities in southeastern Marlborough and on Campbell Island (Figure 1.5B).



- ii) Undertake detailed petrographic and mineralogical studies to characterise lithofacies identified at key section in southeastern Marlborough and on Campbell Island.
- iii) Document trends in both the stable oxygen and carbon isotope and inorganic elemental composition through these sections.
- iv) Determine the origin and paleoenvironmental significance of lithofacies changes and unconformities recorded in the Late Cretaceous to Early Eocene sedimentary strata at the study sites.

## **1.6 THESIS STRUCTURE**

### **CHAPTER 1 - Introduction**

This chapter provides brief background on the Paleogene greenhouse world and the development and importance of New Zealand's passive margin during the Late Cretaceous to Oligocene, as well as noting the main study aims.

### **CHAPTER 2 – Methods**

This chapter outlines both field and laboratory techniques used throughout this study, as well as defining certain terms regarded to be of importance.

### **CHAPTER 3 – Sedimentary Successions of Campbell Island**

Chapter 3 first provides a physical description of Campbell Island and a review of the lithostratigraphy of the Late Cretaceous to Oligocene Campbell Island Group. The field and petrographic characteristics of the lithofacies identified on Campbell Island are documented. The chapter then presents geochemical results, including major and minor trace element concentrations characterising the various lithofacies, compositional plots, inorganic geochemical proxies and stable isotopes.

## **CHAPTER 4 – Sedimentary Successions of Southeastern Marlborough**

Chapter 4 follows a similar format to the preceding chapter, discussing the physical setting of southeastern Marlborough and the lithostratigraphy of the Late Cretaceous to Middle Eocene Muzzle Group. Subsequently, field and petrographic descriptions, as well as geochemical results are discussed for the three main study sites from this region, Mead Stream, Muzzle Stream and Kaikoura wharf.

## **CHAPTER 5 – Discussion**

This chapter begins by suggesting some future revisions for the early Paleogene lithostratigraphic nomenclature in southeastern Marlborough. This is followed by a discussion of the origin, significance and relationship between the various lithofacies identified in the course of this study. A series of isopach and paleolithofacies maps are also presented in this chapter to aid in the discussion of the spatial and temporal evolution of sedimentation in southeastern Marlborough through the Late Cretaceous to Early Eocene. Finally, this chapter discusses the sedimentary/oceanographic/climatic conditions occurring in the Late Paleocene that gave rise to the lithologic successions observed in outcrop in southeastern Marlborough and on Campbell Island.

## **CHAPTER 6 – Conclusions**

This chapter enumerates the main outcomes of this study and links them back to the original aims set out in Chapter 1.

## **APPENDIX A – Geological Timescales**

## **APPENDIX B – Sample Catalogue**

## **APPENDIX C – Petrographic Data**

## **APPENDIX D – Geochemical Data**

## **APPENDIX E – Stratigraphic Data for Paleodistribution Maps**

## **ENCLOSURE 1 – Stratigraphic columns and geochemical proxies from Mead Stream, Muzzle Stream, Kaikoura wharf and Campbell Island**

# CHAPTER 2

## METHODS

---

### 2.1 SAMPLING AND FIELD MEASUREMENTS

Field data and samples were collected from sections shown in Figure 1.5. Collection of field data was carried out following procedures described by Andrews (1982). Firstly, a brief site description was recorded, including aspects such as a field sketch, noting the location of the logged section with respect to important features at the site, as well as determining the exact location of logged sections using GPS. Co-ordinates for logged sections in southeastern Marlborough were recorded in terms of the New Zealand Map Grid (NZMG), while co-ordinates for logged sections from Campbell Island are recorded in terms of latitude and longitude. Following this, descriptions of attributes such as stratification, colour, weathering, hardness, texture, lithology, sedimentary structures and fossils were made, aiding in the establishment of a number of lithofacies. Broad characteristics were used to define lithofacies, allowing for identification of similar facies at different sites and comparison not only between sites, but also regions.

Stratigraphic thicknesses were then determined using a tape measure held perpendicular to bedding or a tape and compass survey where this was not possible. At this stage, samples were collected using a small sledge hammer and cold chisel and sample positions were recorded with respect to their location within the stratigraphic column. Samples were then placed in two, labelled, air tight sample bags. Labels consist of a location prefix followed by a sample number (e.g. MD01 for the first sample collected from Mead Stream).

### 2.2 DEFINITIONS AND USAGE

*Micrite* is used as a non-genetic description for very fine grained, highly calcareous rock observed in the field. Micrites with abundant silica that commonly show a high degree of induration and conchoidal fracture are termed *siliceous micrites* following Lawrence (1989). *Chert* is used as

defined by Lawrence (1989) and is “dense hard, vitreous rock, with conchoidal fracture, which consists of one or several forms of microcrystalline or cryptocrystalline authigenic silica.” The term *glaucony* is used as the name for the facies of green grains following Odin & Matter (1981). The term is preferred here due to the lack of geochemical data required to confidently identify the grains as the minerals *glauconitic smectite* or *glauconitic mica*. In many cases in this study, glaucony is closely associated with the term *perigenic*, which is used here following Lewis (1964). Lewis (1964) proposed the term *perigenic* to fill a gap between allogenic and authigenic, implying an origin of constituents contemporaneous with the sediment, followed by short transport and final incorporation in the sediment. Lewis (1964) states that the connotation of short transport is important to the definition of the term, meaning that perigenic grains are not transported into an environment significantly different to that in which they were formed.

Ages of all New Zealand stages mentioned in this study along with their correlation to international ages, foraminiferal and calcareous nannoplankton zonations, as well as the South Pacific radiolarian zonation are defined within the Paleogene and Cretaceous geological timescales in Appendix A.

## **2.3 ANALYTICAL METHODS**

The experimental pathways used in this study are shown as a logic flow chart in Figure 2.1.

### **2.3.1 Sample Preparation**

All rock samples were initially photographed and catalogued and then brushed with a wire brush to remove any contaminants such as moss, lichen or barnacles. Following this, samples were cut into slabs and unpolished, damp slabs scans were made using a flat bed scanner to capture large scale features within samples. At this stage, areas considered to be representative of the facies described in the field, as well as features of particular interest, were identified; petrographic thin sections were marked out and re-scanned as a record of where thin sections were

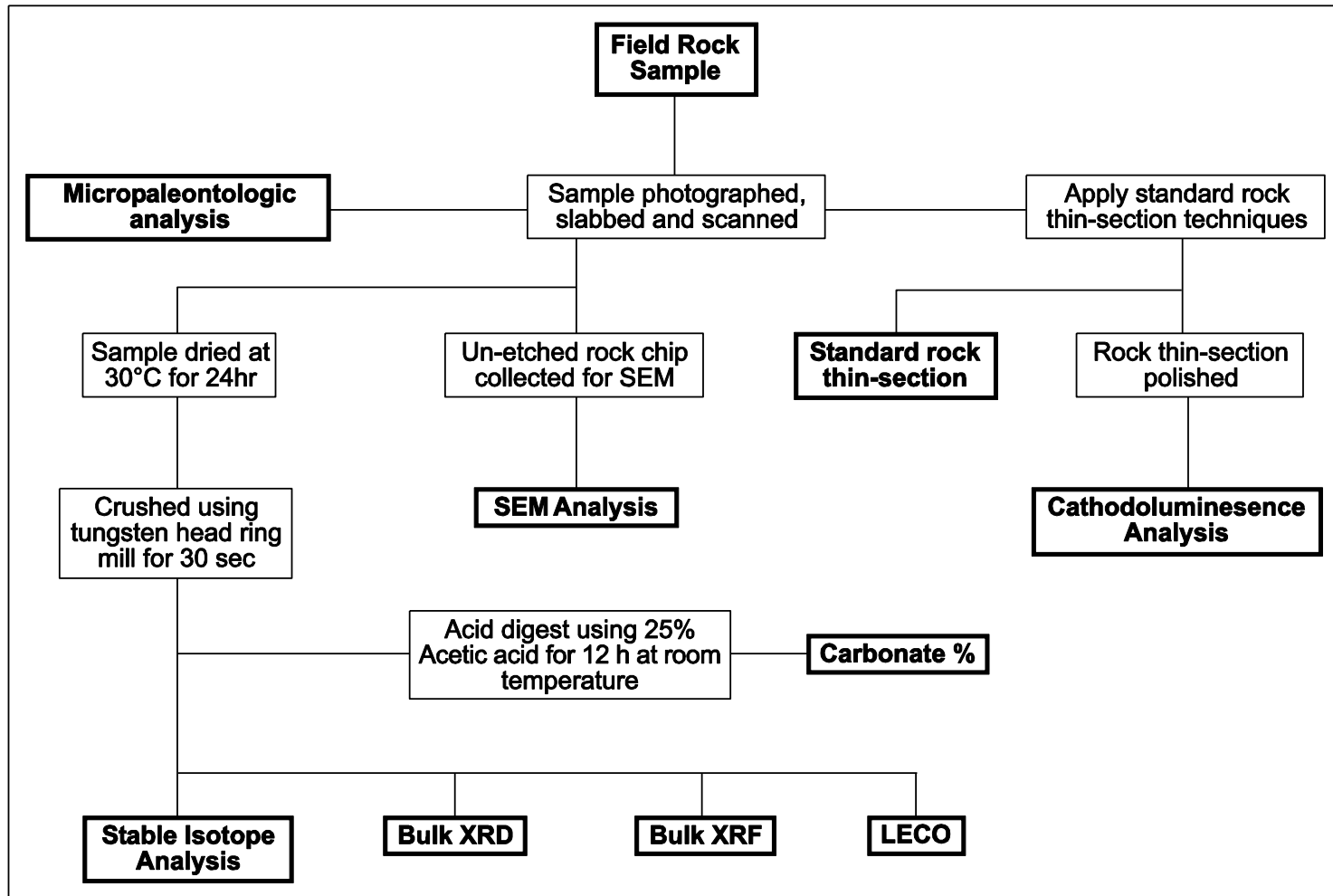


Figure 2.1 Flow diagram showing experimental pathways. Bold boxes denote end product analysis.

taken. Subsequently, blocks were cut and petrographic thin sections were made.

Samples collected from sites in Marlborough were prepared using standard petrographic thin section techniques. However, due to their relatively poor induration, samples collected from sites on Campbell Island required surface impregnation with araldite K142 prior to mounting on glass slides as part of the petrographic thin section making process. From the thin sections made, 25 were selected for cathodoluminescence (CL) petrography which required slides to be polished. Polishing was carried out initially with 500 grit polishing paper on a lap wheel. As the polishing process progresses, the texture of the paper is naturally reduced which negates the need to change to a finer grit paper. Final thin section polishing was conducted using polishing a cloth with fine alumina powder to produce the desired surface for further analysis. During this process, the condition of the sample surface is continually checked using a reflective light microscope to ensure damage is not being done to the sample.

Slabs that were not selected for petrographic analysis, as well as samples that had not been slabbed, were subject to sledge hammer pounding and the subsequent rock fragments were dried in an oven at 40°C for 24 hours. Once dry, these rock fragments were then placed in a tungsten head ring mill for 30 seconds, producing a fine powder. Powders were then placed in labelled plastic bags using a stainless steel spatula. To minimise cross-contamination, all contact surfaces were thoroughly cleaned between samples. As elemental analysis of Fe concentrations was carried out, the use of a tungsten head for the ring mill was seen to be of critical importance to minimise contamination from the usual iron head.

### **2.3.2 Petrographic Analysis**

Petrographic analysis was carried out using an Olympus AX70 petrographic microscope, with digital images being captured by a Nikon Digital Camera DXM1200 used in conjunction with Nikon ACT-1 Version

2.63 software. Descriptions of grain size, sorting and roundness were based on descriptions and comparison charts from Andrews (1982). Percentage abundance of siliciclastic and bioclastic components was determined with reference to comparison charts from Terry and Chilingar (1955) and recorded in petrographic data sheets using the semi-quantitative abundance limits shown in Table 2.1.

**Table 2.1** Semi-quantitative abundance limits used during petrographic analysis.

<b>Abbreviation</b>	<b>Term</b>	<b>% Abundance</b>
VA	Very abundant	>75
A	Abundant	50-75
VC	Very common	25-50
C	Common	15-25
M	Many	5-15
S	Some	1-5
R	Rare	<1
-	Absent	0

CL petrography was carried using a Nikon Eclipse E400 microscope with a CITL Cathodoluminescence MK5-1 unit. The electron gun was fired using a voltage of 16-18 kV and a current of 400  $\mu$ A. Photomicrographs of both plane polarised light and CL images were captured using a Nikon Digital Camera DXM1200, used in conjunction with Nikon NIS Elements Version 3.03 digital image software.

### **2.3.3 Mineralogical Determination**

Mineralogical determination was carried out using a Philips (XPERT) X-ray diffraction (XRD) machine using nickel-filtered copper radiation.

Bulk mineralogy was determined for all samples using unorientated samples which were back-packed into sample holders to avoid direct pressure or handling of the powder face (Hume & Nelson 1982). These samples were scanned between 1° and 42° 2 $\theta$ .

Data were initially interpreted using the computer software program XPertHighscore. This was used to process data files, identify and label x-ray diffraction peaks and identify common minerals such as calcite and quartz. For peaks that could not be associated with common rock forming minerals by the software, the mineral powder diffraction data book (JCPDS

1980) was used, while peaks for opal C/T were identified based on the description of Hesse (1990).

Scanning electron microscopy (SEM) was carried out on un-etched chips of fresh sample that had simply been cleaned using distilled water. Once cleaned and dried, samples were coated in platinum using a Hitachi E-1030 Ion Sputter Coater prior to viewing using a Hitachi S-4700 Field Emission SEM. Elemental maps of SEM images were created using Noran System Six Electron Dispersive Spectroscopy (EDS), which assisted in fine mineral identification. Images were saved as jpeg files for later use.

#### **2.3.4 X-Ray Fluorescence**

Bulk elemental geochemistry of all samples was determined using a Spectro X-Lab 2000 fully automated X-ray Fluorescence (XRF) spectrometer on pressed briquettes. Briquettes were prepared using ~5 g of sample and ~15 drops of PVA binder which was pressed in aluminium cups. The use of pressed briquettes for determining major element abundances is less precise than fused glass beads, leading to over estimation of major elements and weight percentages that sum to greater than 100% (Appendix D). However, this method is a better one for determining trace element contents.

As biogenic, authigenic and diagenetic components such as carbonate, silica and pyrite are common in samples analysed as part of this study, the variations in elemental concentrations are inherently tied to these components. Normalisation of elemental concentrations to some element that is only associated with the aluminosilicate component of a sample is a simple method of negating the dilution effects of both biogenic and authigenic components, without having to remove these fractions by methods such as acid leaching (Schmitz et al. 1991). This process allows for the investigation of significant variations in the chemistry of the clay fraction of sediments using bulk analytical techniques. Elements commonly associated with the aluminosilicate component of sediments



include Al, Sc (Schmitz et al. 1991) and Ti (Schroeder et al. 1997). All have been commonly employed in numerous studies of sediments from different environments (Schmitz 1987b; Thompson & Schmitz 1997; Hollis et al. 2003c; Turgeon & Brumsack 2006).

Three forms of normalising equations were used in the interpretation of bulk element data. Al normalised values were calculated using the equation adapted by Hollis et al. (2003a) from Schmitz et al. (1991), shown below.

$$\text{Element}^* = \text{Element}_{[\text{sample}]} / \text{Al}_2\text{O}_3_{[\text{sample}]} \times \text{Al}_2\text{O}_3_{[\text{background}]}$$

'Element\*' represents the concentration of selected element in the sample if Al<sub>2</sub>O<sub>3</sub> is equal to an average background level calculated for each region (Table 2.2) and allows for comparison of elemental data between different geological materials (Schmitz et al. 1991).

**Table 2.2** Estimated background concentrations of Al<sub>2</sub>O<sub>3</sub>, TiO<sub>2</sub>, CaCO<sub>3</sub>, SiO<sub>2</sub>, and Ba for samples from Marlborough and Campbell Island (after Hollis et al. 2003a, b).

Element	Background Concentrations <sup>†</sup>	
	Marlborough	Campbell Island
Al <sub>2</sub> O <sub>3</sub>	12	16.7 <sup>‡</sup>
TiO <sub>2</sub>	0.70	0.88
CaCO <sub>3</sub>	0.2	0.2
SiO <sub>2</sub>	70	75.41
Ba	550	205.2

<sup>†</sup>Oxides are reported in wt%, while Ba is reported in ppm, <sup>‡</sup>Al<sub>2</sub>O<sub>3</sub> value for Campbell Island is AS value from Wedepohl (1971).

Enrichment factors (EF) relative to average shale (AS) of Wedepohl (1971) were calculated using the equation described by Turgeon and Brumsack (2006), shown below.

$$\text{EF}_{\text{element}} = (\text{element}/\text{Al})_{\text{sample}} \div (\text{element}/\text{Al})_{\text{AS}}$$

Elements having a similar Al normalised ratio to AS will have an EF of one, while Turgeon and Brumsack (2006) consider an element to be 'enriched' when  $EF_{\text{element}} \geq 5$  and 'depleted' when  $EF_{\text{element}} \leq 0.5$ .

Terrigenous sediment (TRG), excess silica (Si[exc]), calcium carbonate (Ca[exc]) and barium (Ba[exc]) were calculated using equations adapted from Hollis et al. (2003b), shown below. Excess values represent elemental concentrations above 'normal' detrital background and can therefore be seen as proxies for biogenic productivity.

$$TRG = TiO_2[\text{sample}] / TiO_2[\text{Background}] \times 100$$

$$Ca[\text{exc}] = CaO_{[\text{sample}]} \times 100/56 - (TiO_2[\text{sample}] \times (CaCO_3[\text{Background}]/TiO_2[\text{Background}])))$$

$$Si[\text{exc}] = SiO_2[\text{sample}] - (TiO_2^{[\text{sample}]} \times (SiO_2[\text{Background}]/TiO_2[\text{Background}])))$$

$$Ba[\text{exc}] = Ba_{[\text{sample}]} - (TiO_2[\text{sample}] \times (Ba_{[\text{Background}]} / TiO_2[\text{Background}])))$$

Background values for Marlborough are taken from Hollis et al. (2003). While these values represent detrital background levels for the Marlborough paleo-embayment (MPE) around the K/T boundary, it was decided to use these values as opposed to developing new values for the Late Paleocene for three reasons. Firstly, Hollis et al. (2003b) state that terrigenous source sediments for the southeastern Marlborough around the K/T boundary are higher in  $TiO_2$  and  $SiO_2$ , and lower in  $CaCO_3$  in comparison to regional or global averages used in other studies. This means that the use of average shale (AS) values of Wedepohl (1971) or average crustal values as suggested by Schmitz (1987a), would lead to overestimation of normalised values. Secondly, it is assumed in this study that terrigenous sources within the MPE would not have changed greatly over the period of the Paleocene due to the passive margin tectonic setting of the area at the time. Thirdly, this allows for direct comparison between the two studies.

Background values for Campbell Island were calculated on a CaCO<sub>3</sub>-free basis using the methods of Hollis et al (2003b).

### **2.3.5 Carbonate Percentage**

The carbonate percentage for samples was calculated from CaO values using the oxide conversion factor of 1.786 after Hollis et al. (2003).

To gauge to the accuracy of this method, carbonate percentages from 10 samples of varying lithologies were determined using other two different methods (Table 2.3).

The first method used a LECO TruSpec CN Carbon/Nitrogen Determinator to measure the total carbon (TC) within the sample, which is used to approximate the percentage of carbonate. This approximation of carbonate percentage is based on the assumption that Total Organic Carbon (TOC) makes up <0.1 wt% of TC in pelagic limestones, and that the remaining carbon is held as Total Inorganic Carbon (TIC) in the form of carbonate.

250 mg of dried, powdered sample was measured into tinfoil cups before being placed in a loading head. Samples are then combusted at 950°C in a temporary oxygen enriched atmosphere to convert carbon in the solid sample to gas form CO<sub>2</sub>. The combustion gases are passed through a secondary furnace at 850°C for further oxidation and particulate removal before then being passed through an additional furnace filter and two-stage thermoelectric cooler, removing moisture, into a collection vessel known as the ballast. Carbon is then measured in the combustion gases as carbon dioxide by the CO<sub>2</sub> infrared detector.

Five reference standards were run at the same time to allow the preparation of a calibration curve (Figure 2.2) to calculate the carbonate percentage based on TC of the sample.

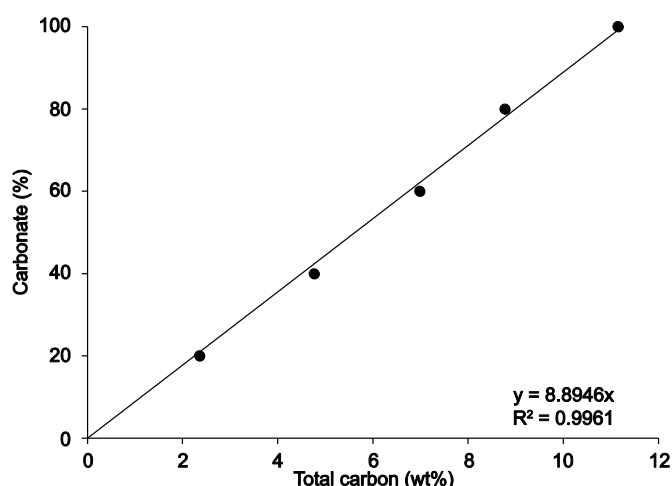


**Figure 2.2** Calibration curve for determining carbonate percentage based on total carbon values, determined using the LECO TruSpec CN Carbon/Nitrogen Determinator.

Acid digestion was the other method used to determine the carbonate percentage of the 10 selected samples. The method of acid digestion used is adapted from Barber (1974), treating 5 g of sample with 50 ml of 25% v/v acetic acid at room temperature for 12 hours. The insoluble residue is then washed into a Whatman No. 42 size 150 mm filter paper which has been dried at 40°C and weighed. The insoluble residue and filter paper are then dried at 40° C for 24 hours before re-weighing. The percentage carbonate is determined by calculating the percentage difference between the total sample and the insoluble fraction.

**Table 2.3** Comparison of carbonate percentage results from 10 samples, determined using three methods, X-ray Fluorescence (XRF), LECO TruSpec CN Carbon/Nitrogen Determinator (LECO) and acid digestion.

	XRF	CaCO <sub>3</sub> (wt.%)	
		LECO	Acid digestion
MD01	36.7	34.0	28.2
MD24	59.7	56.2	47.5
MZ04	39.5	24.4	22.8
MZ08	85.5	74.3	63.9
KK01	30.6	26.7	23.9
KK14	2.5	1.9	4.3
KK27	76.2	72.4	54.0
CC02	78.2	72.0	53.4
LP02	77.2	74.0	57.2
SB01	83.4	77.9	62.0

Carbonate values calculated based on CaO determined by XRF are consistently higher than values determined using the other two methods

described, suggesting a possible over estimation using this method. However, close agreement between values determined using this method and LECO would suggest XRF values provide a reasonable estimate of carbonate percentage. Consistently lower carbonate percentages determined using the acid digestion method may result from incomplete digestion, even though this method followed that set out by Barber (1974).

### **2.3.6 Stable Isotope Analysis**

$\delta^{13}\text{C}$  and  $\delta^{18}\text{O}$  analysis was carried out at the University of Waikato. Samples containing sufficient carbonate are loaded into individual reaction vessels, which in turn are placed in a 24-position carousel housed in an oven kept at 70°C. Samples are then reacted using a predetermined dose of 105% orthophosphoric acid for 10 minutes in a Europa CAPS (Carbonate Automatic Preparation System) using an acid dosing or 'drip' method. As the sample is reacting, water is removed by passing the  $\text{CO}_2$  through a loop that is maintained at -90°C, before it is frozen in a dedicated cold finger positioned close to the inlet to the mass spectrometer to minimise transfer time.

Once the reaction is complete,  $\text{CO}_2$  is introduced into the Europa Geo 20/20 isotope ratio mass spectrometer where gas pressures are balanced and sample gas is run against an internal reference gas. This reference gas is calibrated daily by running it against an internal standard, WCS. WCS was calibrated against NBS-19, and cross-checked against NBS-20. External precision for replicate analyses of WCS is better than 0.05 ‰ for both carbon and oxygen.

Carbon and oxygen isotope values are presented in the usual delta ( $\delta$ ) notation, normalised, and expressed in per mille (‰) relative to Vienna Peedee belemnite, VPDB (Coplen 1988, 1994).

$\delta^{13}\text{C}_{\text{org}}$  was analysed using a Dumas elemental analyser (Europa Scientific ANCA-SL) interfaced to an isotope mass spectrometer Europa Scientific 20-20 Stable Isotope Analyser. 10-70 mg of sample was weighed into tin

foil capsules, depending on Total Organic Carbon (TOC) of the sample. These cups were then closed and pressed into a spherical shape. Weighed samples were loaded into the carousel of the autosampler attached to the Europa Scientific ANCA-SL. Samples were combusted at 1020°C in a temporary oxygen enriched atmosphere to convert carbon in the solid sample to gas form CO<sub>2</sub>. The resulting combustion gases were swept through a reduction reactor, a water filter and onto a gas chromatograph (GC) column using helium as a carrier gas. As CO<sub>2</sub> was separated from other gases in the gas chromatograph column, a sub-sample of CO<sub>2</sub> was transformed into the mass spectrometer ion source for the measurement of <sup>13</sup>C abundance.

Samples were analysed against a laboratory sucrose standard which has a  $\delta^{13}\text{C}_{\text{org}}$  value of -10.80 ‰. The sucrose had been standardised against a certified standard (calibrated relative to PDB) from CSIRO, Canberra, Australia. When analysing samples, sucrose standards are analysed after every 12 samples. Internal reference checks are also done at these regular intervals. Instrument error is about  $\pm 0.3$  ‰.

Carbon isotope values are presented in the usual delta ( $\delta$ ) notation, normalised, and expressed in per mille (‰), relative to Peedee belemnite, PDB.

Limestones investigated as part of this study are part of the Amuri Mega Facies which is considered part of Diagenetic Class IV within Hood and Nelson's (1996) diagenetic classification scheme for New Zealand limestones. Deep burial is a key characteristic of class IV limestones, and leads to a negative shift in  $\delta^{18}\text{O}$  as a result of temperature-dependant fractionations accompanying burial pressures and tectonic stresses (Nelson & Smith 1996).  $\delta^{18}\text{O}$  values measured as part of this study ranging between -6.9 and -1.5 ‰ are consistent with values for New Zealand micrites (mean, -4.08) as the result of alteration of carbonate oozes (0-2 ‰) by burial diagenesis (Nelson & Smith 1996).

Diagenetic alteration of the  $\delta^{18}\text{O}$  signal in bulk carbonate samples is shown significant covariance between  $\delta^{18}\text{O}$  and  $\delta^{13}\text{C}$  in samples from all sites. For this reason,  $\delta^{18}\text{O}$  is not considered to provide a guide to paleotemperature in this study.

Hollis et al. (2003b) suggests that  $\delta^{13}\text{C}$  is less prone to diagenetic alteration than  $\delta^{18}\text{O}$  and are considered to be reliable when the source of carbon is in sufficient abundance to counter diagenetic effects.

### **2.3.7 Micropaleontologic Analysis**

Micropaleontologic analysis was carried out by GNS Science. Samples were processed for radiolarians and dinoflagellate cysts (referred to as dinoflagellates herein) in order to develop an integrated biostratigraphy for measured sections, as well as carrying out paleoenvironmental analysis.

Radiolarian microfossil extraction was carried out using standard acid-leaching and chemical cleaning procedures set out in Hollis (2006). This process involved treatment of crushed chips, 5-10 mm in size, with 15% hydrochloric acid (HCl) until the reaction has ceased. For siliceous samples which show weak reactions with HCl, samples are rinsed then reacted in 5% hydrofluoric acid (HF) for 2-4 hours. Samples are subsequently washed through a 63  $\mu\text{m}$  screen, with residues finally being cleaned by gently heating in a 1:1 solution of 10% hydrogen peroxide and calgon ( $\text{NaPO}_3$ )<sub>6</sub> (Hollis 2006).

Samples were processed for dinoflagellates using HF digestion, followed by brief oxidation and sieving over a 6  $\mu\text{m}$  screen (Hollis et al. 2005c).

# **CHAPTER 3**

## **SEDIMENTARY SUCCESSIONS OF CAMPBELL ISLAND**

---

### **3.1 PHYSICAL SETTING**

Campbell Island is the southernmost of New Zealand's subantarctic islands and therefore New Zealand's southernmost sovereign territory. It is situated approximately 700 km south of the South Island at latitude 52° 30' S, in the vast Southern Ocean (Dingwall & Gregory 2004) (Figure 1.5). Campbell Island has an area of 114 km<sup>2</sup>, being up to 14 km wide and 14 km long, with an average breadth of about 6.5 km. The island lies at the southern margin of the Campbell Plateau, a prominent structural feature of the New Zealand region composed of continental crust, about 20 km thick, that lies 500 to 2000 m below sea level (Adams 1962).

A period of Miocene alkali basaltic volcanism (7.5-6.6 Ma) (Hoernle et al. 2006) led to doming of basement schist and Cretaceous-Paleogene cover rocks (Oliver et al. 1950), as well as the development of a large composite volcanic cone, with the edifice being centred in the area that is now Northwest Bay (Figure 3.1). Subsequent subsidence and coastal erosion of the northwest sector of this complex, combined with further coastal and glacial erosion, has led to the development of the island's present day shape (Figure 3.1). The southern and western coastlines are dominated by cliffs, some rising to 300 m in height, and here there is no safe anchorage except in Northwest Bay and Monument and Southeast Harbours in good weather (Kerr 1976). The eastern coast is less rugged, with two large, glacially carved inlets, Perseverance and Northeast Harbours, both providing safe anchorage. Perseverance Harbour, the southernmost and largest of the two, is of comparable size to Otago Harbour and extends westward ~6.5 km from its entrance. Garden, Camp and Tucker Coves are situated at the head of the harbour and have been the centre for much of the habitation since the island was discovered in 1810.



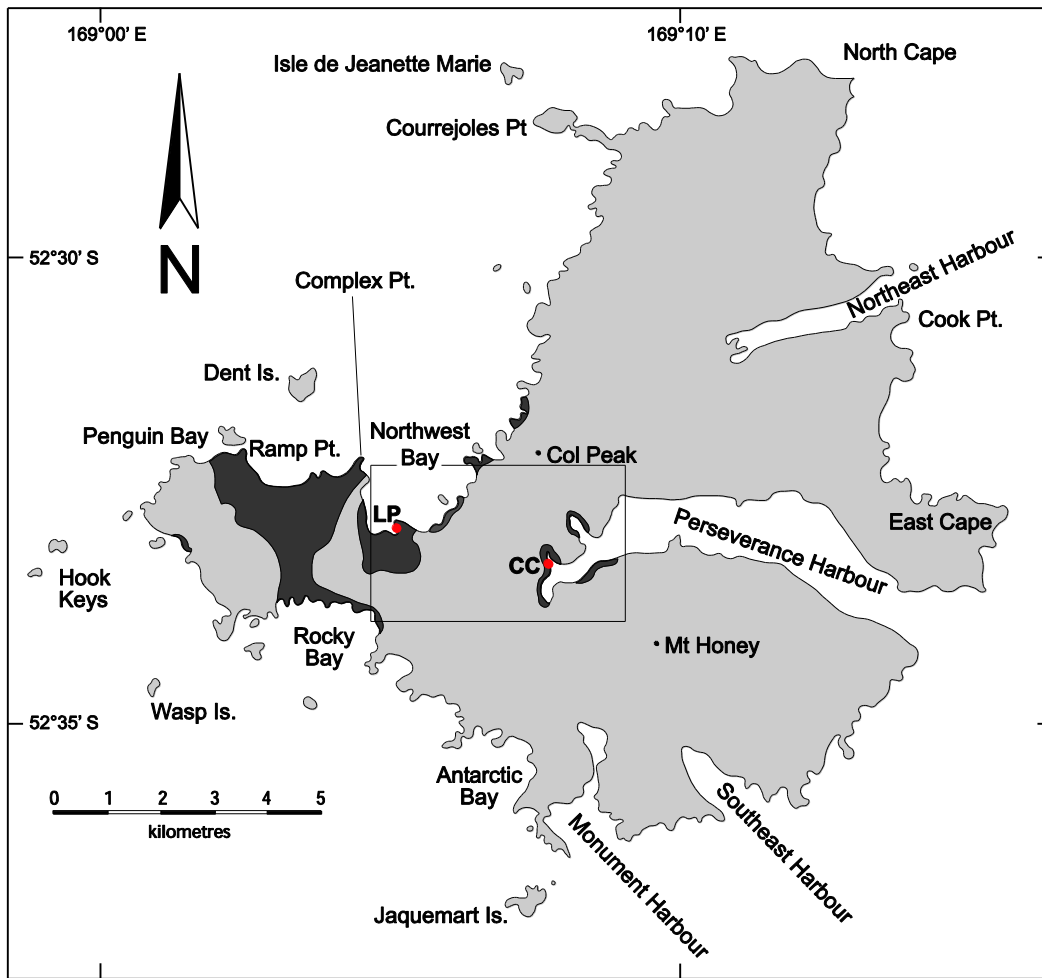


**Figure 3.1** Map of Campbell Island showing the distribution of the Late Cretaceous-Paleogene Campbell Island Group (black) (adapted from Oliver et al. 1950). Boxed area is enlarged in Figure 3.3 and shows the main sites (red dots) where work was conducted in this study. LP: Limestone Point; CC: Camp Cove (adapted from Fell 2002).

The latitude of Campbell Island is south of the forest zone, so that tussock, shrubland and herbfields dominate the landscape (Moore 2004). The monotony of brown tussock is broken in places by areas of head height *Dracophyllum* and low *Coprosma* which make for difficulty when traversing the island. The most notable flora are the mega-herbs such as the lily, *Chrysobactron rossi*, and the famous ‘blue sunflower’, *Pleurophyllum speciosum*. The island supports small breeding populations of the three main seal species in the New Zealand region – New Zealand fur seal, southern elephant seal and the New Zealand (Hooker’s) sea lion (Moore 2004). The latter resides in large numbers in the area surrounding the meteorological station at the foot of Beeman Hill and on the sandy beach to the east of Complex Point (Figure 3.1), making foot passage hazardous

at times. Campbell Island is world renowned for its bird life, leading to recognition of the area as a UNESCO world heritage area in 1998 as part of New Zealand's subantarctic islands. The island is not only the breeding ground for no less than six species of albatross and the rare yellow-eyed penguin (Moore 2004), but also home to seabirds such as giant petrels, skua gulls and Antarctic turns (Kerr 1976), as well as important endemic species such as the Campbell Island Shag and the Campbell Island Teal.

Campbell Island's geographical location in the high latitude Southern Ocean is the major control on the climate of the island, which is typically cloudy, wet and windy. The maritime effect of the surrounding oceans means that air arriving at Campbell Island is moisture laden and when it is forced to rise over the island leads to the formation of an overcast cloud cap. This cloud cover is so persistent that the island receives only 659 hours of sunshine each year on average, equating to 16% of the total sunlight hours available if Campbell Island were cloud free (Brenstrum 2004). To emphasise this point, a comparison may be drawn with Auckland which receives 2101 hours of sunshine, or 50% of the possible sunshine. On average, 130 sunless days occur per year, with June 1970 receiving the unenviable record of one and a half hours of sunshine for the entire month.

Precipitation is common, with rain being recorded 320 days per year. However, it is generally never heavy, with the mean annual rainfall being 1425 mm (Brenstrum 2004), a little less than New Plymouth (Kerr 1976). This can be compared to Hokitika which receives 2874 mm of rainfall spread over only 208 days.

Campbell Island's location also places it within the 'Furious Fifties', a zone of persistent and often strong westerly winds. This occurs as a result of strong pressure gradients between mobile anticyclones that pass mostly to the north of Campbell Island and depressions moving eastwards in the circumpolar trough near the edge of the Antarctic continent (Brenstrum 2004). Meteorological records from the island show that winds gusts of gale force or stronger are experienced 280 times a year on average, with

the wind blowing from the northwest, west or southwest approximately 70% of year. As wind speeds are measured from a location in Tucker Cove at the head of Perseverance Harbour (Figure 3.1), they are not considered to be representative of the island as a whole. Benstrum (2004) suggested that limited measurements from surrounding higher terrain, such as Beeman Hill and Col Peak (Figure 3.3), are typically twice those observed at sea-level.

Although Campbell Island's location means it has a wet, windy climate, it also means that there is little variation in temperature, both diurnally and seasonally. Average daily temperatures range from 9.3°C in January to 4.7°C in July in comparison to the rest of New Zealand where average daily temperatures tend to vary by more than 10°C between February and July (Brenstrum 2004).

### **3.2 LATE CRETACEOUS-OLIGOCENE LITHOSTRATIGRAPHY OF CAMPBELL ISLAND GROUP**

While the first observations of the geology of Campbell Island were made during the late nineteenth century, it was not until 1944 that the first detailed geological investigation was undertaken. This was carried out by R. L. Oliver (Oliver et al. 1950) while he was stationed on the island as a "coast-watcher" during World War II, and included production of a geological map (Hollis et al. 1997). Oliver et al. (1950) established four formations, the Complex Point Formation, Garden Cove Formation, Tucker Cove Limestone and Shoal Point Formation, along with a number of igneous units. Beggs (1978) modified the stratigraphy of Oliver et al. (1950) by elevating the Complex Point Formation to group level, establishing the Campbell Island Group to include the Garden Cove Formation and Tucker Cove Limestone and retaining the Shoal Point Formation. Beggs' (1978) study was the last detailed investigation of the Cretaceous-Paleogene sedimentary deposits on Campbell Island prior to work by Hollis et al. (1997) who carried out a comprehensive biostratigraphic investigation of samples made available from previous work, retaining the stratigraphic subdivisions developed by Oliver et al. (1950) and Beggs (1978) (Figure 3.2). While the Campbell Island Group

is the of main focus of the present study, the importance of the underlying Complex Point Group as a sediment source for the Garden Cove Formation means it will also be discussed briefly.

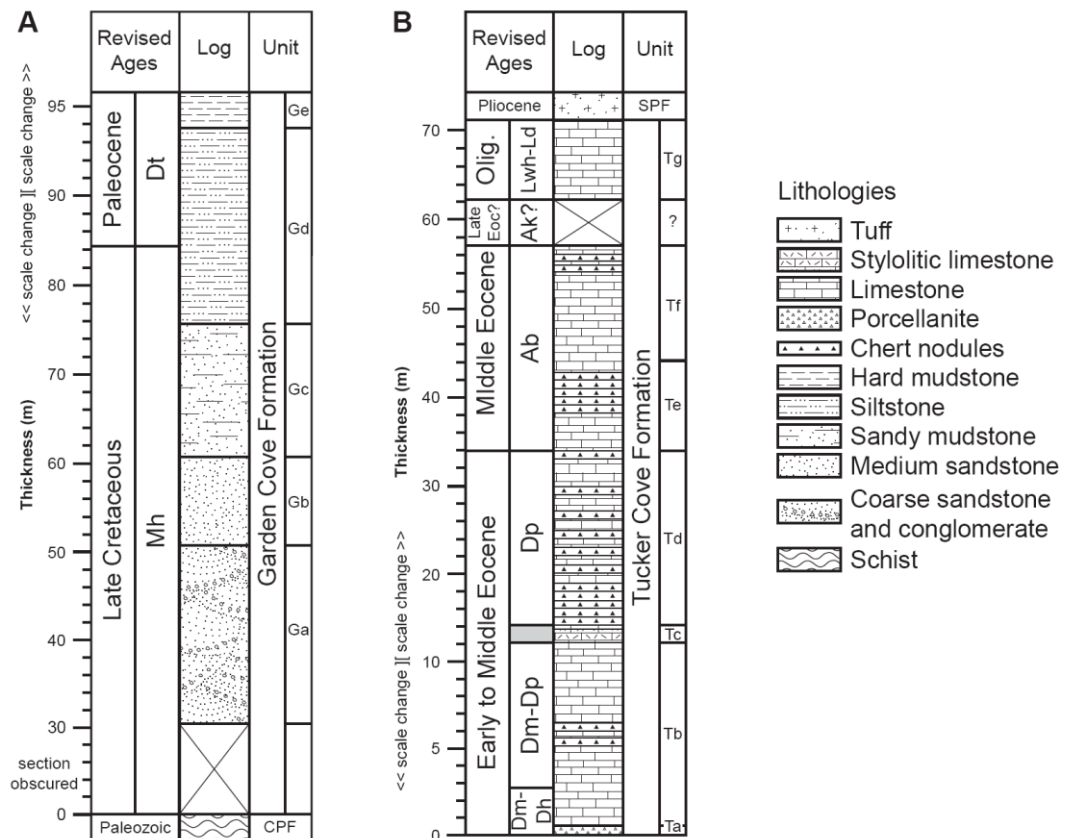


**Figure 3.2** Composite stratigraphic columns for (A) the Garden Cove Formation from the head of Perseverance Harbour and (B) the Tucker Cove Limestone from the western side of Campbell Island (adapted from Hollis et al. 1997). Units are defined in Tables 3.1 and 3.2. CPF: Complex Point Formation; SPF: Shoal Point Formation. New Zealand Stages are defined in Appendix A.

### 3.2.1 Complex Point Group

Low grade metamorphic rocks of the Complex Point Group make up the basement rock exposed on Campbell Island (Oliver et al. 1950). These strata vary in lithology from grey pelitic semischist to dark brown metagreywacke (Cook et al. 1999). Petrographically, the Complex Point Group is dominated by subrounded detrital quartz grains showing undulose extinction and minor granulation, with much less common plagioclase and rare microcline (Beggs 1978). The matrix shows strongfoliation of very fine authigenic muscovite and minor chlorite. Beggs (1978) states that along with pale brown biotite and white mica, sphene

and siderite, heavy minerals include tourmaline, clinozoisite, rutile, apatite, zircon and brookite.

With the exception of K-feldspar, the Complex Point Group appears to be mineralogically similar to the Greenland Group of the South Island (Cook et al. 1999). This affinity with the Western Province tectonic terranes is further supported by geochronologic evidence from a sample of schist collected at Complex Point which has a K/Ar total-rock age of 443 Ma (Adams et al. 1979). Though this can only be considered a minimum age due to possible overprinting as a result of later intrusions on the island, it is nonetheless similar to K/Ar total-ages of slates from the Greenland Group (300-438 Ma) and K/Ar total-rock ages of the Swanson Group (410-450 Ma) in Marie Byrd Land, West Antarctica (Cook et al. 1999).

### **3.2.2 Garden Cove Formation**

The Garden Cove Formation, the lower formation of the Campbell Island Group, was initially described by Oliver et al. (1950) as consisting of approximately 15 m of “quartz sandstone and conglomerate, and carbonaceous mudstone...”. Quartz pebbles and rare schist fragments are concentrated at the base of the formation, being overlain by quartz sandstone which fines upwards into carbonaceous mudstone (Oliver et al. 1950). Beggs (1978) further subdivided this formation into five units based on lithology and environmental significance (Table 3.1). These units were subsequently used by Hollis et al. (1997).

**Table 3.1** Lithologic characteristics of units in stratigraphic order from the Garden Cove Formation established by Beggs (1978) (after Hollis et al. 1997).

Ge	Hard dark fissile siliceous mudstone
Gd	Hard dark massive bioturbated mudstone
Gc	Fine to medium sandstone with carbonaceous laminae
Gb	Poorly-sorted coarse sandstone
Ga	Cross-bedded coarse sandstone and basal conglomerate

Beggs' (1978) descriptions are based on observations made from a measured section west of Complex Point which is stated to be 30 m thick. Though the lithostratigraphic units observed in Camp and Garden Coves at the head of Perseverance Harbour are similar, their thickness is greatly increased. Measurements by Dr Ian Turnbull (Hollis et al. 1997) suggested a thickness of ~70 m, which is comparable to that measured during this study. Hollis et al. (1997) suggested that some of this increase may be related to inflation as a result of igneous intrusions, resulting in as much as a 20% increase around Duris Point where there is a high concentration of basaltic dykes (Figure 3.3).

The Garden Cove Formation is interpreted by Beggs (1978) as representing a transgressive sedimentary sequence. At the base of the sequence, Unit Ga is considered to represent non-marine, fluvial channel or point-bar deposits. Unit Gb was interpreted as being coastal flood plain deposits, in turn overlain by estuarine channel and mud deposits of Units Gc and Gd. Unit Ge was suggested to be fully marine due to the presence of planktic microfauna and a high proportion of clay-size material. These paleoenvironmental interpretations were supported by the micropaleontologic analyses carried out by Hollis et al. (1997). Both foraminifera and radiolarians are absent in the lower units of the Garden Cove Formation due to the non to marginal-marine nature of the formation. Palynomorph assemblages show strong terrestrial influences to within ~5 m of the contact with the overlying Tucker Cove Limestone, with plant cuticles and pollen being abundant in lower units but decreasing upsection in accordance with Beggs' (1978) interpretation. Deposition of the upper units of the Garden Cove Formation is considered to have occurred in an inner shelf to brackish setting based on limited foraminiferal evidence from one sample collected from the top of Unit Gd and dinoflagellates which suggest a fully marine setting (Hollis et al. 1997).

Due to the paucity of foraminifera and radiolarians in samples processed, dinoflagellate biostratigraphy provides the best opportunity for a relatively complete subdivision of the Cretaceous-Paleogene sedimentary strata on Campbell Island (Hollis et al. 1997). Based on dinoflagellates in samples

collected from Unit Ga, the base of the Garden Cove Formation is latest Cretaceous (Maastrichtian, late Haumurian, *Alterbidinium acutululum* dinoflagellate zone) in age. The top of the Garden Cove Formation is Paleocene (Teurian, *Paleoecocystodinium glozowense* dinoflagellate zone). Palynomorph assemblages suggest that the K/T boundary lies ~9 m below the contact with the overlying Tucker Cove Limestone at Camp Cove.

### **3.2.3 Tucker Cove Limestone**

The Garden Cove Formation is unconformably overlain by the Tucker Cove Limestone (Hollis et al. 1997). Oliver et al. (1950) described the Tucker Cove Limestone as 90-150 m of "... white, fine grained, foraminiferal limestone..." containing common "... flint concretionary nodules ..." which average ~100 mm in size. Beggs (1978) goes further to describe the lowest few centimetres of the formation as consisting of cream to pale yellow, glauconite bearing porcellanite. The rest of the formation was described as "... monotonous, moderately to well lithified, white fine-grained limestone ..." with the "flint concretionary nodules" of Oliver et al. (1950) being identified as chert nodules. Hollis et al. (1997) further subdivided the Tucker Cove Limestone into seven units based on the descriptions by Beggs (1976) from a number of sections (Table 3.2).

**Table 3.2** Lithologic characteristics of units in stratigraphic order from the Tucker Cove Limestone (Hollis et al. 1997).

Tg	White micritic limestone
Tf	Scaly white micritic limestone with isolated horizons of small chert nodules in upper part
Te	White micritic limestone with horizons of large chert nodules in lower part and scattered small chert nodules in upper part
Td	White micritic limestone with numerous large chert nodules near the base, numerous small nodules below an angular uniformity with unit Te
Tc	Light grey stylolitized micritic limestone
Tb	White massive micritic limestone with occasional chert horizons
Ta	Yellow-cream glauconitic porcellanite

Based on these descriptions, the Tucker Cove Limestone can be considered to be part of the Amuri carbonate megafacies of Hood & Nelson (1996) which was widely deposited within eastern basins of Zealandia during the late Cretaceous to Eocene.

Beggs (1978) suggested the Tucker Cove Limestone was deposited as a pelagic ooze, remote from sources of siliciclastic material. A depositional depth of from 250-4000 m was initially suggested based on comparisons with European chalk and the present day depth of the carbonate compensation depth in the southwest Pacific (Beggs 1976). This initial interpretation is supported by palynomorph assemblages showing a fully marine environment with relatively little terrestrial influences at the base of the Tucker Cove Limestone (Hollis et al. 1997). Both foraminifera and radiolarian assemblages reflect the high latitude nature of the location during the period of deposition. Evidence provided by benthic foraminifera suggest the Tucker Cove Limestone was deposited at lower bathyal depths (>1500 m) under fully oceanic conditions (Hollis et al. 1997). This is not suggested to have changed greatly throughout the period of deposition.

The basal unit (Ta) of the Tucker Cove Limestone has been dated as Early to Middle Eocene, definitely of Mangaorapan (Dm) age at Camp Cove based on nannofossils and Mangaorapan to Heretaungan (Dm-Dh) based on foraminifera at Complex Point (Hollis et al. 1997). The Tucker Cove Limestone is suggested to contain relatively complete Mangaorapan to Porangan (Dm-Dp) and Bortonian to Duntroonian (Ab-Ld) intervals which are separated by an angular unconformity.

### **3.3 LITHOFACIES AT CAMPBELL ISLAND**

#### **3.3.1 Site Description**

The present study is based on field work carried out by myself and others as part of the University of Otago 2009 Campbell Island Expedition. The expedition travelled to Campbell Island aboard the University of Otago research vessel *RV Polaris II*, leaving Bluff on 16 February, 2009 and returning to Bluff on 1 March, 2009. Work conducted as part of the



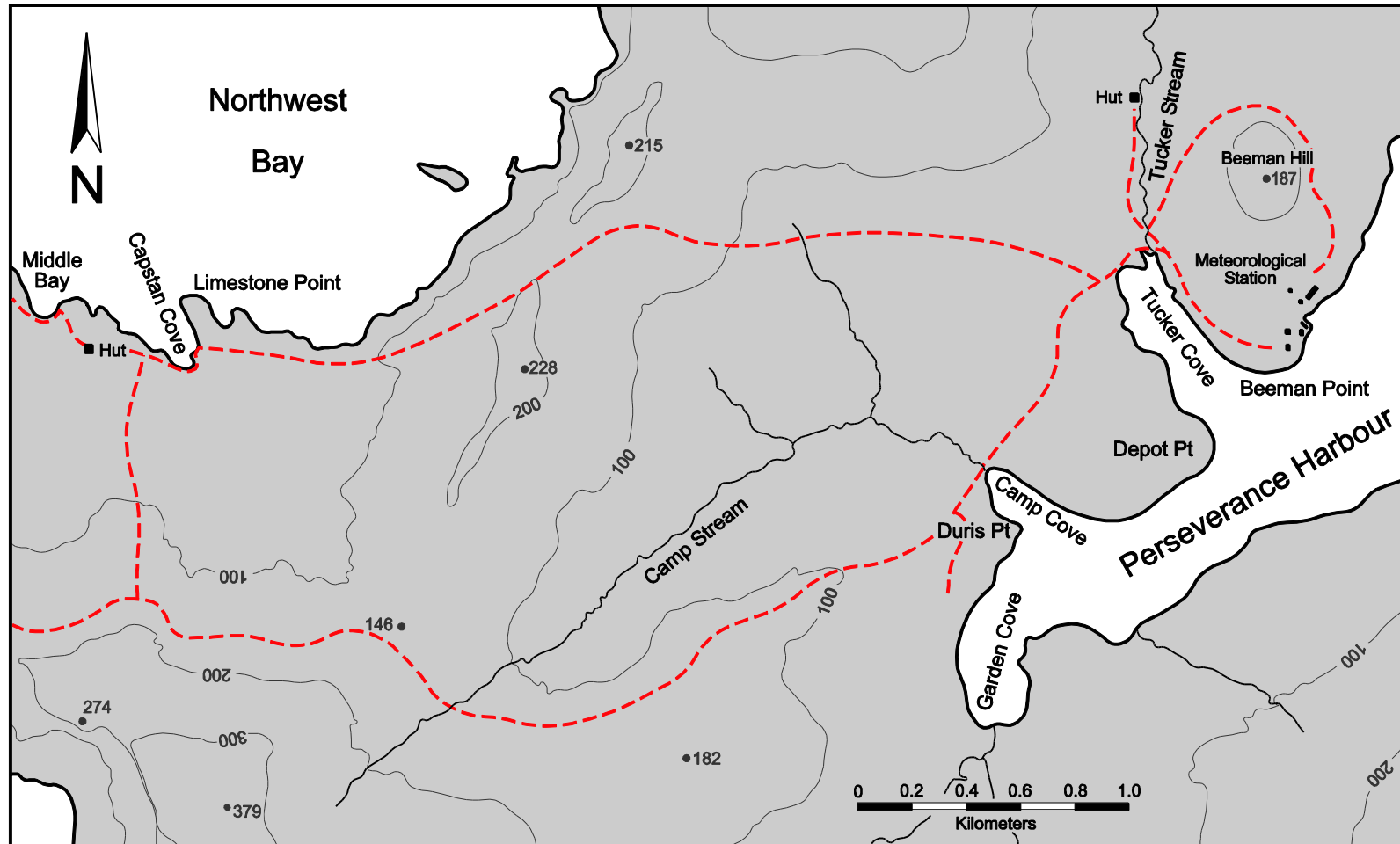


**Figure 3.3** Map of the central portion of Campbell Island showing the main study locations at Capstan Cove (Limestone Point) and the head of Perseverance Harbour. Contours and spots heights in metres. Red dotted line denotes walking track.

expedition included a seafloor survey utilising sidescan and multibeam sonar, seafloor sampling including dredging and piston coring, kelp sampling and, relevant to this study, land based geological section logging and sampling.

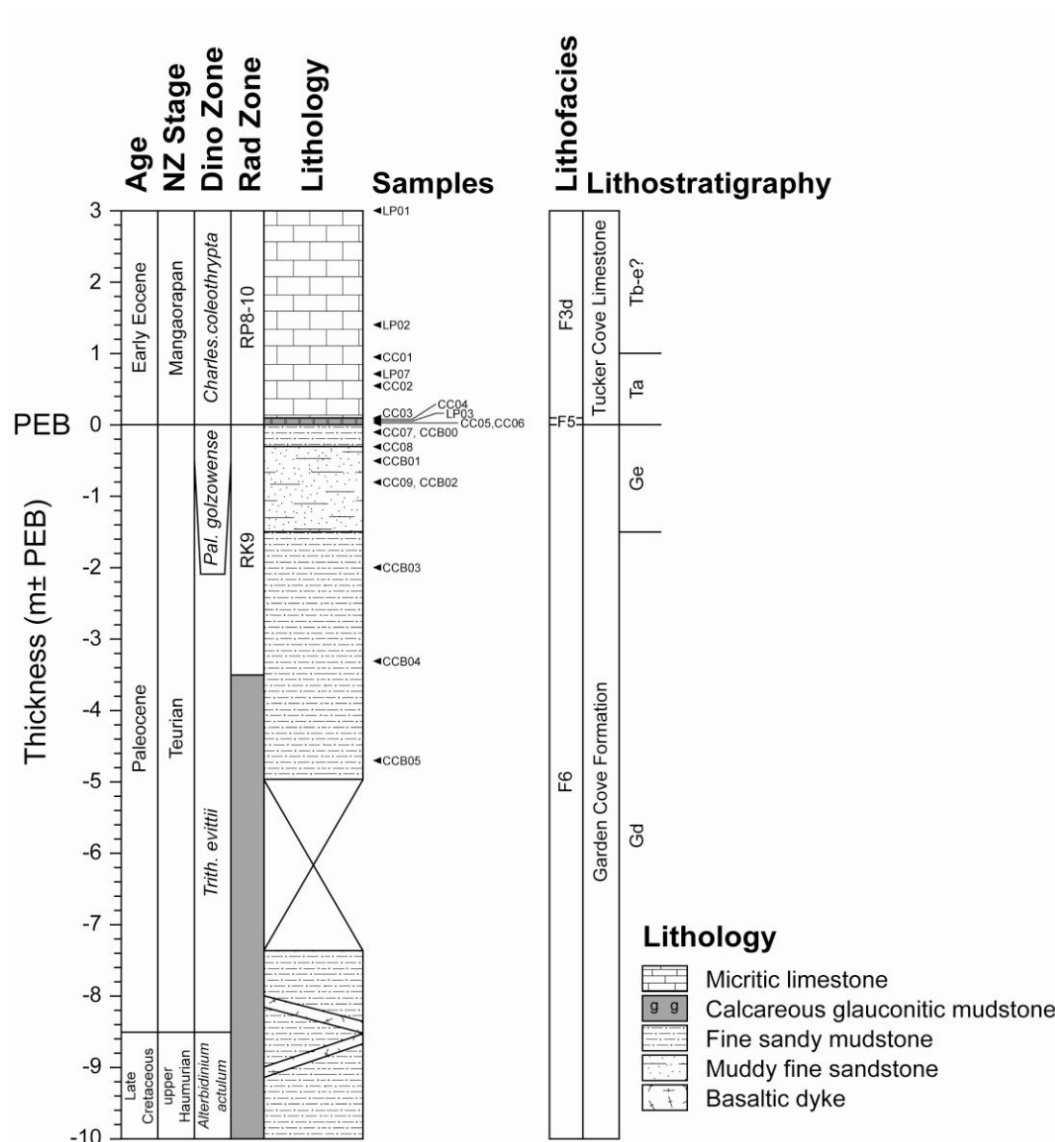


**Figure 3.4** Composite stratigraphic column for the Paleocene and bounding strata on Campbell Island in relation to the Paleocene-Eocene boundary (PEB). Age control after Hollis et al. (1997). Lithostratigraphy after Beggs (1976, 1978). Lithology, lithofacies and samples (this study).

Samples and descriptions of the contact between the Garden Cove Formation and Tucker Cove Limestone were collected from two sites on Campbell Island, at Capstan Cove on Limestone Point (LP) and at Camp Cove (CC) (Figure 3.3). Due to lithologic similarities of the contact

between the Garden Cove Formation and Tucker Cove Limestone at both sites, the information obtained is combined to create a composite stratigraphic column (Figure 3.4).

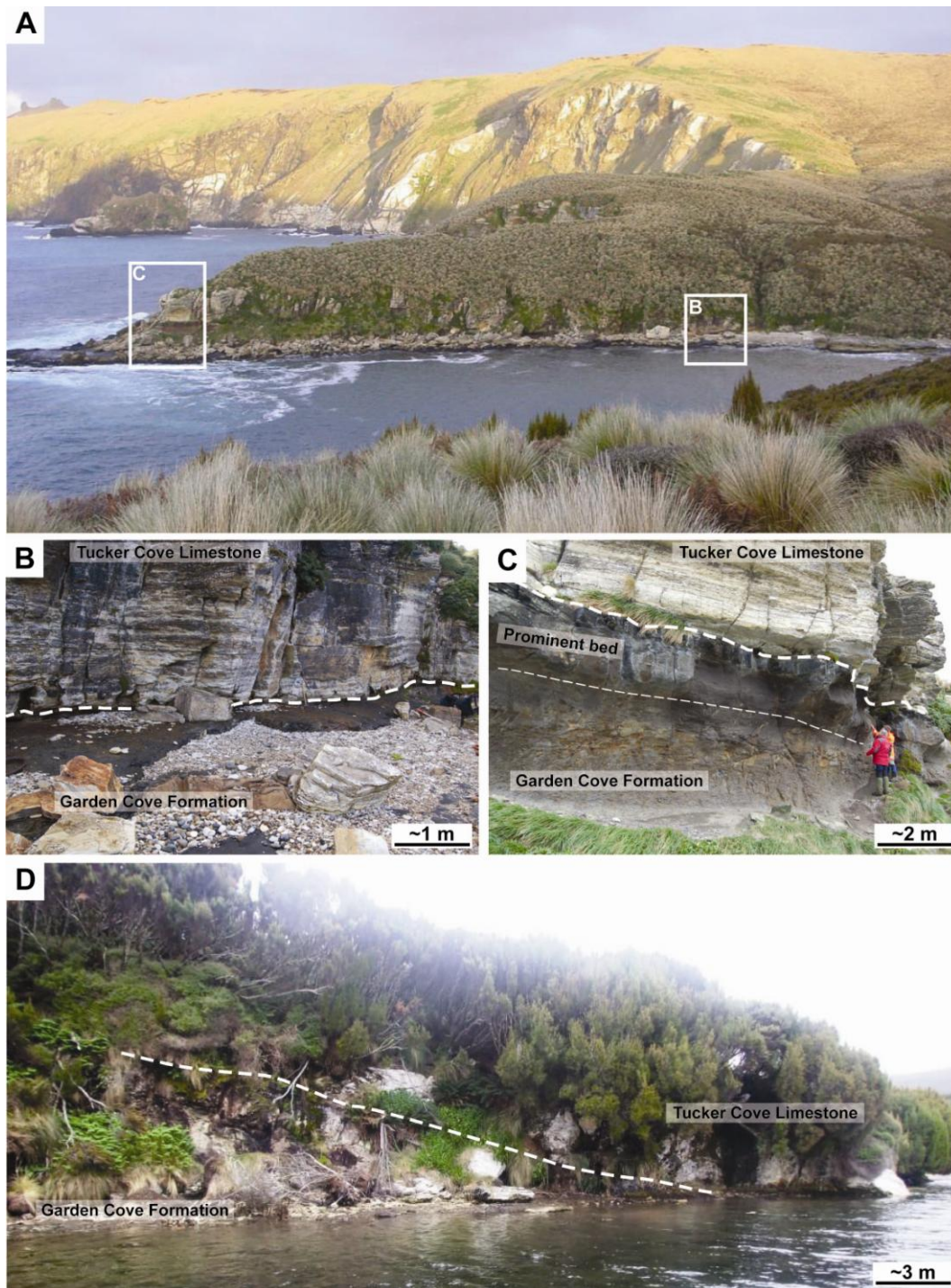


**Figure 3.5** Logged sections from Campbell Island containing the contact between Garden Cove Formation and Tucker Cove Limestone, (A) eastern shoreline of Capstan Cove and Limestone Point with locations (B) and (C) marked; (B) contact at Capstan Cove (Photo: J. Crampton); (C) contact at Limestone Point; (D) contact in Camp Cove.

The low angle nature of the contact between the Garden Cove Formation and Tucker Cove Limestone at Capstan Cove (177/08° NW) means that it crops out in low cliffs along the entirety of the eastern shoreline where not obscured (Figure 3.5A). The location of the stratigraphic column from Capstan Cove is S 52°33'02.5", E 169°05'30.1" (Figure 3.5B), where the majority of samples were also collected. However, due to accessibility, a sample from directly below the contact was also collected from Limestone Point (S 52°32'54.8", E 169°05'27.2") (Figure 3.5C).

The contact between the Garden Cove Formation and Tucker Cove Limestone in Camp Cove is exposed in low cliffs near the head of the inlet (Figure 3.5D) at S 52°33'24.5", E 169°08'04.9". The dip of beds within the Tucker Cove Limestone (059/14° NW) meant a tape and compass survey could be undertaken along the length of the southwestern shoreline from the head of Camp Cove to Duris Point. This stratigraphic section is intersected by a number of basaltic dykes, which are particularly concentrated around Duris Point.

### **3.3.2 Field Descriptions**

Within the Garden Cove Formation and Tucker Cove Limestone, three lithofacies have been identified as part of the wider study, namely: fine sandy mudstone facies (F6), calcareous glauconitic mudstone facies (F5) and micrite facies (F3d) (Figure 3.4).

#### *Fine sandy mudstone facies (F6)*

The fine sandy mudstone facies can generally be described as a dark brown, micaceous, non-calcareous, fine sandy mudstone. Within 1.4 m of the overlying contact, this facies has a more massive, sandy character and is moderately weathered with greater induration than the lower portion, resulting in the prominent unit shown in Figure 3.5c. Even though this interval of F6 is sandier in nature, it is correlated with unit Ge, the hard dark fissile siliceous mudstone of Beggs (1976). It contains conspicuous dark green, subangular to subrounded, fine to medium sand sized glaucony grains which reach a maximum concentration of ~5% directly

below the overlying contact. The glaucony grains are disseminated throughout the unit but are more concentrated within burrows. Rare subangular to rounded quartz pebbles occur 'floating' within the uppermost 30 cm of the unit (Figure 3.6) along with white, non-calcareous, elliptical burrow structures.



**Figure 3.6** Subangular quartz pebble set within F6 at Limestone Point (S 52°33'02.5", E 169°05'30.1").

1.4 m below the contact between the Garden Cove Formation and the Tucker Cove Limestone, F6 can be considered a true fine sandy mudstone with extensive bioturbation. This interval is moderately to highly weathered with limonite staining of joint surfaces and a jarositic appearance (Figure 3.7). It is correlated with unit Gd, the hard dark massive bioturbated mudstone of Beggs (1976).



**Figure 3.7** Fissile, highly weathered, jarositic lower interval of F6 at Camp Cove (S 52°33'24.5", E 169°08'04.9").

Sulphide nodules, <50 mm in size, are common throughout the upper 10 m of F6. Weathering results in limonite staining around the nodules. When exposed the centre of the nodules reveals brassy yellow pyrite. Bioturbation by an unidentified ichnotaxa is also common throughout F6 as well as possible rare *Zoophycus* and *Chondrites* trace fossils lower in F6 (James Crampton pers. commun. 2009). If this is the case, this would bring into question the validity of the Beggs' (1976) initial 'estuarine' paleoenvironmental interpretation.

#### *Calcareous glauconitic mudstone facies (F5)*

F5 sits directly above the boundary between the Garden Cove Formation and Tucker Cove Limestone and consists of 80 mm of light to dark greyish green, calcareous, glauconitic mudstone (Figure 3.4). This facies is highly weathered, preserving little to no original structure and is soft to very soft. This weathered nature means that F5 forms a thin recessive unit atop the Garden Cove Formation wherever the contact between the two formations is preserved. Glaucony, making up ~7% of the facies in hand sample, consists of dark green to black, subangular to rounded, fine to medium sand sized grains.

F5 can be divided into three separate sub-facies on the basis of a number of key characteristics such as weathering, and colour and the sharpness of boundaries observed between the three sub-facies in the field (Figure 3.8). F5a is dark greenish grey, highly weathered and very soft. Weathering of this sub-facies has occurred to such a degree that no original structure is preserved, including glaucony grains. The underlying contact with the Garden Cove Formation also shows extensive limonite staining, suggesting weathering of Fe rich glaucony has occurred. F5b is less weathered, being greenish grey with identifiable glaucony grains which constitute 7-10% of the total sub-facies, while the light greyish cream, F5c, is less weathered again with <5% glaucony. The upper two sub-facies of F5 are sandier than F5a and induration increases rapidly away from the contact with the underlying F6. It is likely that the extreme weathering of this facies has occurred as a result of development of a preferential groundwater flow path between the more highly indurated, low

porosity units bounding the F5 unit. The similarities between both the Limestone Point and Camp Cove sections, ~3 km apart, would suggest that such a process has not been restricted to one location but has occurred wherever this stratigraphy occurs on Campbell Island.

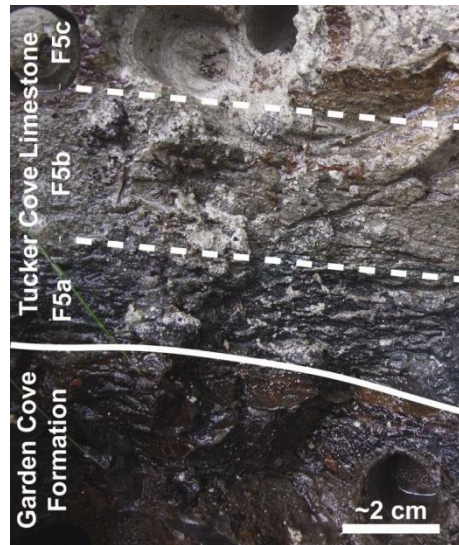


**Figure 3.8** Sub-facies identified within F5 on the basis of colour, glaucony content and degree of weathering at Camp Cove (S 52°33'24.5", E 169°08'04.9").

#### *Micrite facies (F3d)*

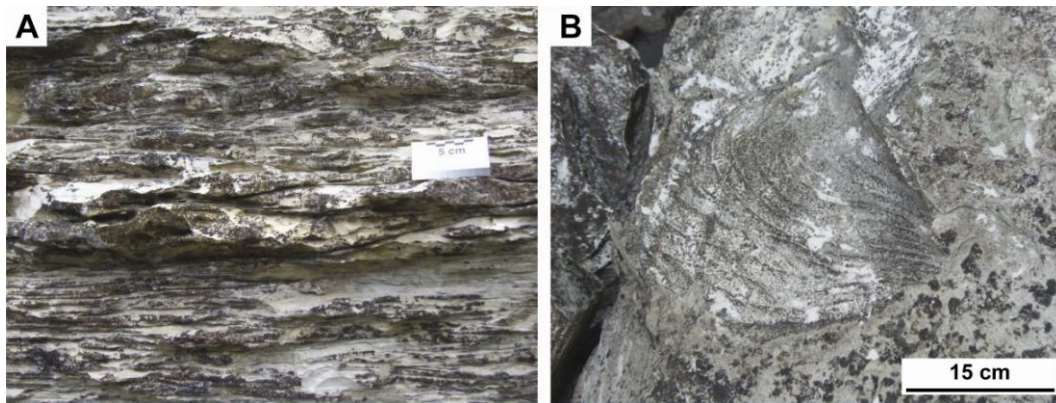


**Figure 3.9** Characteristic features of the Tucker Cove Limestone. (A) Wavy discontinuous stylolitic beds. (B) *Zoophycus* trace fossil in the bedding plane of a fallen block at Limestone Point (S 52°33'02.5", E 169°05'30.1").

The micrite facies on Campbell Island consists of 30-50 mm thick, strongly developed stylolitic beds of light grey micrite (Figure 3.9a). These beds are wavy in places and can only be traced ~3 m laterally before beds pinch. F3d is slightly to moderately weathered which is reflected in the induration of the facies. Glaucony consist of dark green to black, subangular to rounded, fine sand size grains and decreases from ~5% at

the underlying contact with F5 to 0% 1.5 m above the base of the facies. F3d contains abundant *Zoophycus* and *Chondrites* trace fossils, visible both in cross-section and along the surface of bedding planes (Figure 3.9b).

### **3.3.3 Petrography and Mineralogy**

#### *Fine sandy mudstone facies (F6)*

In thin section, F6 is characterised by very fine sand to coarse silt sized quartz grains with less common K feldspar set in a siliceous/argillaceous and carbonaceous matrix which makes up to 50-65% of the total rock. Cathodoluminescence light was used to differentiate quartz grains from K feldspar, with quartz exhibiting characteristic dull dark blue and rare reddish brown luminescence, while K feldspars show bright pale blue luminescence under the same excitation conditions (Figure 3.10A, B). Quartz grains are generally angular to subangular and moderately to poorly sorted and include rare, coarse to very coarse sand sized grains (Figure 3.10A, B). Quartz grains commonly show a 'shattered' internal structure (possibly an artefact of resin impregnation for thin section preparation) with rare grains showing undulose extinction. F6 contains some authigenic pyrite as well as muscovite and rare zircon.

As with field observations of lithofacies characteristics, the petrographic characteristics within F6 also change upsection. Thin sections from the uppermost two samples (CC07, CC08) contain the quartz and feldspar grains and appear petrographically similar. Burrows identified in the field contain concentrations of clean, very fine sand to silt sized quartz grains and glaucony. Glaucony within these two samples is dominated by bright green, pelletal, very fine sand sized grains with a microcrystalline internal structure. Rare grains show brownish green to reddish brown oxidation rims, along with dehydration cracks. A small number of glauconitised biotite grains were identified on the basis of well developed cleavage, pleochroism in plane polarised light and high order interference colours under cross polarised light. Glaucony grains are poorly sorted, suggesting possible fragmentation. The upper two samples also contain rounded brownish orange phosphatic grains that exhibit near isotropic extinction



behaviour under cross polarised light, making up ~3% of the sample in thin section.

CC09 from Camp Cove is the muddiest of the thin sections examined from F6, with the matrix making up ~65% of the total sample. This includes up to 5% muscovite and appears extensively bioturbated which has concentrated siliciclasts separated into discontinuous bands. Glaucony is dominated by brownish green, well rounded, very fine sand size, microcrystalline pelletal grains with less common vermicular grains of glauconitised biotite. These grains exhibit subtle, light to dark green pleochroism under plane polarised light and 3<sup>rd</sup> to 4<sup>th</sup> order interference colours under cross polarised light. Brownish orange, phosphatic grains are far less common in CC09, making up less than 1% of the total sample.

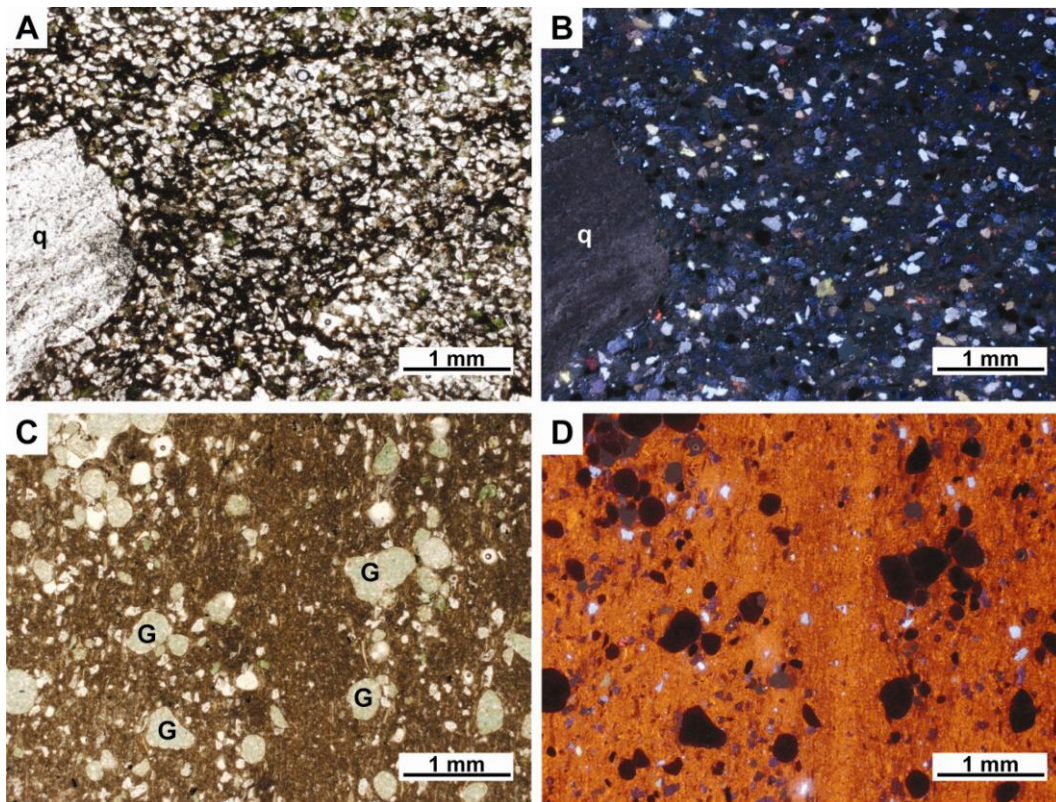


**Figure 3.10** Photomicrograph pairs under plane polarised light (left) and cathodoluminescence light (right) of selected thin sections from Campbell Island. (a) & (b) Characteristic image of the fine sandy mudstone facies of the Garden Cove Formation (CC08). Note the abundance of bright blue K feldspar grains in (b) and the subrounded quartz granule, q, in both images. (c) & (d) Medium sand sized microcrystalline glaucony grains, G, and coarse silt sized siliciclastics of the calcareous glauconitic mudstone facies (F5) set in a calcareous matrix (LP03).

Rare radiolarians were observed in thin sections of samples collected from near the top of the Garden Cove Formation. This appears to be inconsistent with observations made by Beggs (1976, 1978), who noted a large number of radiolarian tests as well as silicified foraminifera at a similar stratigraphic horizon. However, it supports observations made by Hollis et al. (1997), who stated that of the 23 samples examined as part of their investigation into the Cretaceous to Paleogene strata of Campbell Island, only one sample from the Garden Cove Formation yielded radiolarians.

An XRD trace for a bulk, unoriented sample mount of CC09 shows a doublet peak around 4.1 - 4.2 Å corresponding to quartz and opal C/T, suggesting that even though radiolarians are rare, biogenic silica may be an important source of SiO<sub>2</sub> near the top of F6 (Appendix C).

#### *Calcareous glauconitic mudstone facies (F5)*

Due to the highly weathered nature of this facies, only one sample collected from this facies was suitable for the making of a petrographic thin section, LP03. The sample consists of subrounded to rounded, very fine sand to silt sized quartz and K feldspar grains and fine to medium sand sized, well rounded, pelletal glaucony (Figure 3.10C, D). Quartz grains show a similar 'shattered' internal structure as well as undulose extinction. Glaucony grains are light green with a microcrystalline internal structure. LP03 also contains common phosphatised grains that, unlike the underlying facies, are generally not rounded but lath shaped. These grains are set in an argillaceous matrix which also contains rare muscovite. Lamination in this sample is shown by parallel seams of opaque limonite, concentration of glaucony grains in discontinuous lenses and alignment of muscovite and phosphatic grains.

Unoriented bulk XRD traces show quartz and low-Mg calcite are present in F5. This facies also contains phyllosilicates identified by a non-basal peak around 4.5 Å as well as a peak at 14.65 Å representing smectite clays (Appendix C).

### *Micrite facies (F3d)*

In thin section, F3d is characterised by foraminifera supported in a clotted micrite matrix. SEM analysis shows that the micrite facies from Campbell Island is dominated by detrital carbonate grains in the form of coccolith debris and secondary recrystallised calcite spar (Figure 3.11a). Grain sizes ranges from 0.1 – 5  $\mu\text{m}$ .

Microfossils in F3d are dominated by planktic forams, making up ~90% of the visible microfossils identified, while less numbers of benthic forams and rare radiolarians were also observed. Foraminiferal tests are poorly preserved, showing extensive calcite recrystallisation and in some cases replacement by silica (Figure 3.11b). Tests are mainly infilled with microcrystalline, spary calcite cement.

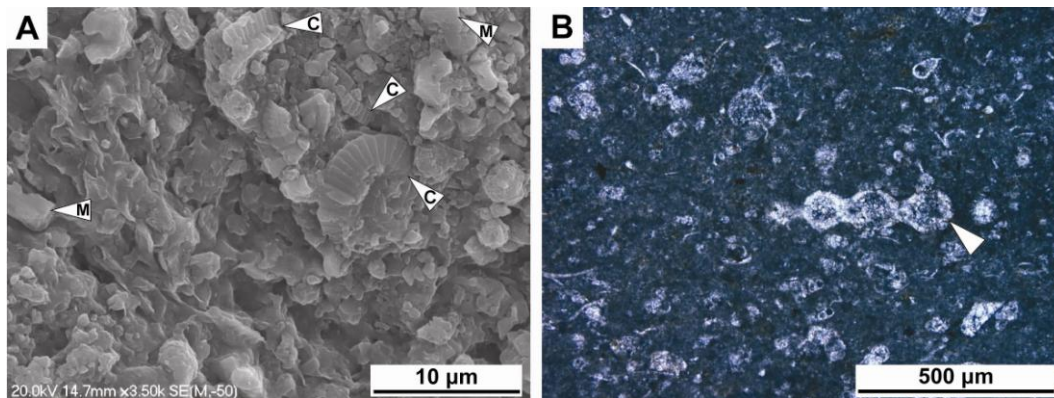


**Figure 3.11** (A) SEM image of the micrite facies (F3d) from Campbell Island (CC02). C: Coccolith debris; M: Recrystallised microcrystalline spar. (B) Highly recrystallised and fragmented foraminifera set in a micritic matrix (LP01). Note uniserial benthic foraminifera (arrowed) (XPL). Interference colours suggest foraminiferal tests have been replaced with silica.

F3d contains rare authigenic pyrite identified by the brassy yellow colour under reflected light. Bright green to brownish yellow green, very fine sand to coarse silt sized, microcrystalline pelletal glaucony is also present near the base of F3d, but decreases to <1% between CC01 and LP01. Rare grains have reddish brown, limonitised rims.

The mineralogy of F3d is dominated by low-Mg calcite along with varying amounts of silica which decreases upsection. This silica is assumed to be biogenic in origin due to the lack of detrital quartz in thin section and the

presence of radiolarians (Hollis et al. 1997) and silicified foraminiferal tests.

### **3.3.4 Geochemistry**

#### ***Inorganic Geochemistry***

Ernst (1970) suggested that the geochemical composition of a facies is influenced by a number of factors including climate, sediment origin and type and tectonic and diagenetic processes. With this in mind, this section discusses the major and trace element abundances for the facies described for Section 3.3.2, as well as discussing the composition of samples collected from the Campbell Island Group as a whole. Elemental abundances will be compared with average shale values (AS) of Wedepohl (1971) which will allow comparison of similar facies between different geographic regions (Campbell Island and Marlborough). As the underlying Complex Point Group can be considered an important source of terrigenous sediment which would greatly affect the geochemical characteristics of the overlying Campbell Island Group deposits, it is relevant to compare elemental concentrations from the three facies identified in the field with values representative of the elemental concentrations in the basement rocks. However, there is a lack of geochemical data for the Complex Point Group and so instead it was decided to use average values from the Greenland Group, West Coast, South Island (Roser et al. 1996) based on age correlations between the two groups made by Adams (1979) as well as petrographic similarities described by Beggs (1976) and Beggs et al. (1990). The influence of grain size on geochemical composition is recognised here by comparing Facies 6 with average elemental values of sandstone units from the Greenland Group and Facies 5 and 3d with average elemental values of argillaceous units from the Greenland Group. Bulk geochemical data are recorded in Appendix D.

## Major Elements

### *Fine sandy mudstone facies (F6)*

Major elemental concentrations for average shale (Wedepohl 1971) and average sandstone of the Greenland Group (Roser et al. 1996) consistently fall within the range of the Al normalised major elemental concentration for samples from F6 (Figure 3.12A). Given this, the average Al normalised concentration for CaO is considerably lower than both average shale concentrations and average sandstone concentrations from the Greenland Group and Na<sub>2</sub>O shows a very large range.

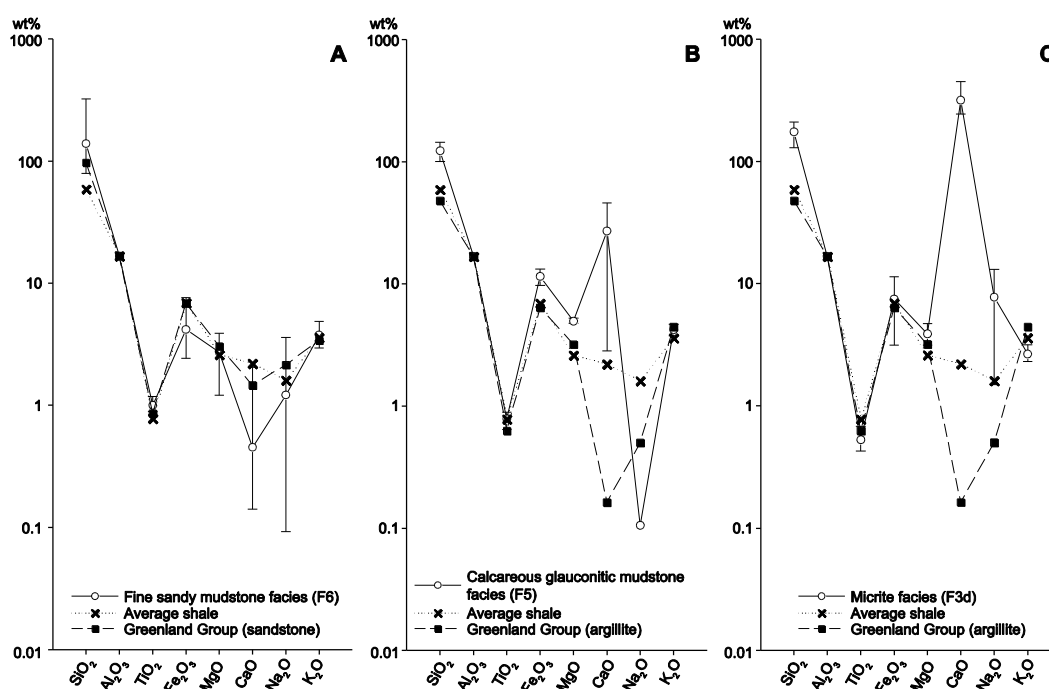


**Figure 3.12** Al normalised major element concentrations (range and mean values) for the three facies identified during field work on Campbell Island compared against average shale (Wedepohl 1971) and average sandstone of the Greenland Group, West Coast, South Island (Roser et al. 1996). (a) Fine sandy mudstone facies (F6); (b) Calcareous glauconitic mudstone facies (F5); (c) Micrite facies (F3d). Vertical bar indicates range of values.

### *Calcareous glauconitic mudstone facies (F5)*

Al normalised major elemental concentrations from samples of F5 show significant enrichment in SiO<sub>2</sub>, TiO<sub>2</sub>, Fe<sub>2</sub>O<sub>3</sub>, MgO and CaO (Figure 3.12B). Na<sub>2</sub>O is the only major element that is depleted in F5, with three of four samples from this facies having Na<sub>2</sub>O concentrations below detectable limits. TiO<sub>2</sub> and K<sub>2</sub>O are normal with respect to concentrations of both average argillite of the Greenland Group and average shale.

### *Micrite facies (F3d)*

Samples from the micrite facies on Campbell Island show significantly higher concentrations of SiO<sub>2</sub> and CaO with respect to both average major elemental concentrations in argillite of the Greenland Group and average shale, while K<sub>2</sub>O is lower (Figure 3.12C). Other Al normalised major elemental concentration in samples from this facies are 'normal', with average argillite and average shale values falling within the range of measured values for these elements.

### *Discussion*

High Al normalised values for SiO<sub>2</sub> and CaO (>100 wt%) in F5 and F3d reflect the large biogenic component of the primary sediments. Low CaO and Na<sub>2</sub>O values in F6 possibly reflect the absence of feldspar and calcite in the Complex Point Group with respect to the Greenland Group (Beggs et al. 1990). Enrichment of Fe<sub>2</sub>O<sub>3</sub> and MgO in the calcareous glauconitic mudstone facies with respect to average argillite concentrations of the Greenland Group and average shale concentration is inferred here to be related to the presence of glaucony in the facies. This is supported by the significant positive correlation between these elements and the geochemical proxy for clays in the sample, TRG (Appendix D).

### ***Trace Elements***

#### *Fine sandy mudstone facies (F6)*

As with major elemental concentrations for F6, the majority of Al normalised trace elemental concentrations are 'normal' with respect to trace elemental concentrations in average argillite of the Greenland Group and average shale (Figure 3.13A). Only U and Co have ranges that fall above both average shale and average argillite, while the range of measured values for Cu in samples from F6 is lower.

#### *Calcareous glauconitic mudstone facies (F5)*

Al normalised trace elemental concentrations in samples from F5 are consistently higher than both concentrations in average argillite of the Greenland Group and average shale (Figure 3.13B). Nb, Pb, Cu, Rb and

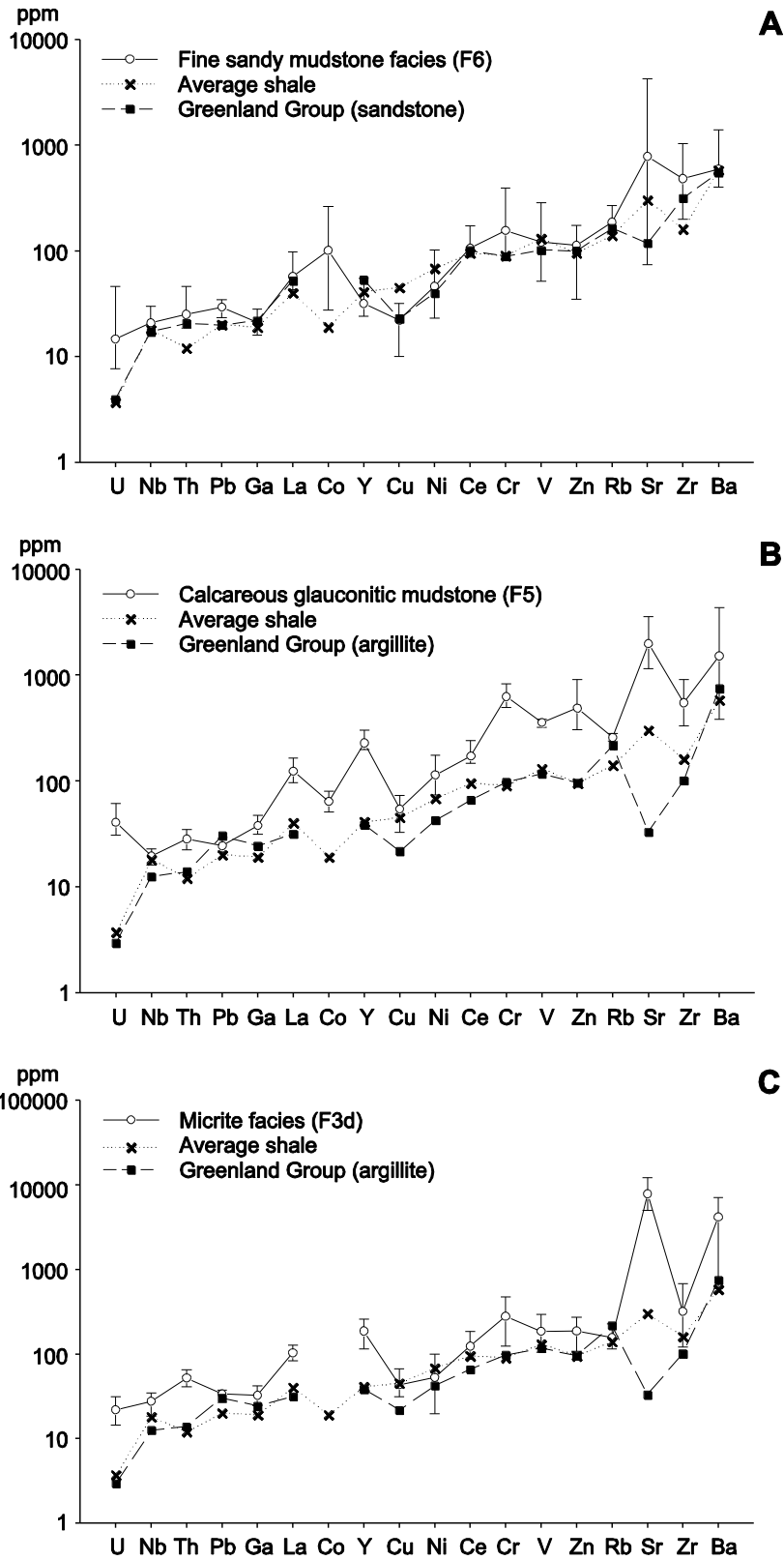


**Figure 3.13** Trace element concentrations (range and mean values) for the three facies identified during field work on Campbell Island compared against average shale (Wedepohl 1971) and average sandstone of the Greenland Group, West Coast, South Island (Roser et al. 1996). (A) Fine sandy mudstone facies (F6); (B) Calcareous glauconitic mudstone facies (F5); (C) Micrite facies (F3d). Vertical bar indicates range of values.

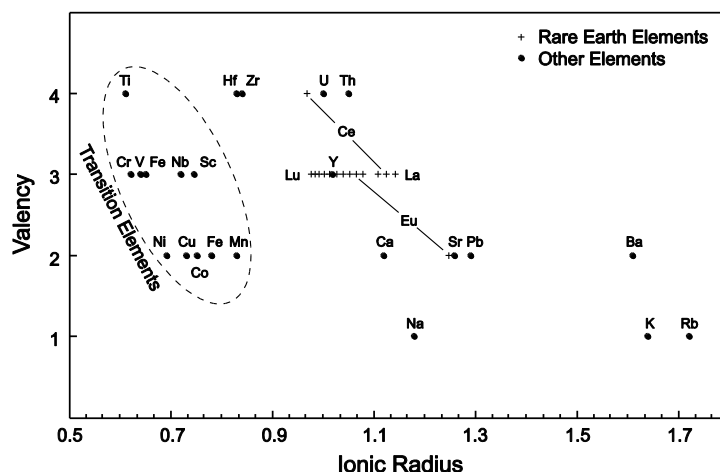
Ba are the only elements that are 'normal', with average shale and average argillite trace elemental concentrations falling within the range of measured values, while all other elements are higher.

#### *Micrite facies (F3d)*

F3d shows similar trends to F6, with the majority of Al normalised trace elemental concentrations considered 'normal' with respect to concentrations in average argillite of the Greenland Group and average shale (Figure 3.13C). U, Th, La, Y, and Cr are all enriched, with the range of measured values higher than average argillite and average shale concentration. Sr is significantly enriched in samples from F3d, with Al normalised concentrations almost two orders of magnitude higher than those observed in average argillite of the Greenland Group of Westland.

#### *Discussion*

Enrichment of U in F6 may be associated with organic matter (Moore 1988), while enrichment of Co could be attributed to the presence of pyrite (Ernst 1970), which is common in F6 and even occurs in large nodules in outcrop. Co, along with Cr, is also associated with clay minerals (Moore 1988).



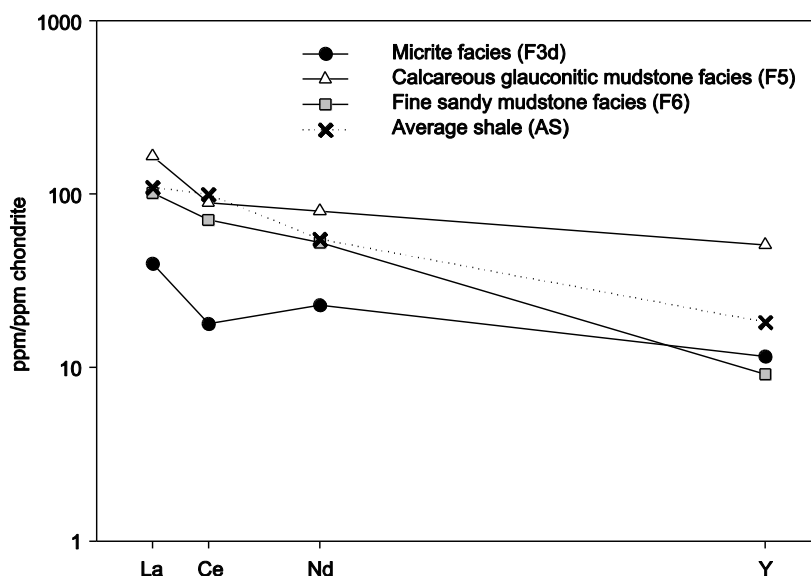
**Figure 3.14** The relationship between valency and ionic radius in Rare Earth Elements and a number of other geochemically important species (Taylor & McLennan 1988).

Figure 3.14 aids in an initial explanation of the enrichment pattern observed in F5. Enrichment of the transition elements, Cr, V and Zn, can be attributed to replacement of  $Fe^{3+}$ ,  $Fe^{2+}$  and  $Mg^{2+}$  at octahedral sites in



the glaucony lattice due to similarities in ionic radius and charge (McConchie 1978).

Taylor and McLennan (1988) suggest that elemental properties such as ionic radius frequently override traditional behaviour expected on the basis of valency in geochemical processes. Based on this suggestion and the difference in ionic radius shown in Figure 3.14, the enrichment pattern of REEs (La, Y and Ce) in F5 (Figure 3.15) cannot be attributed to the same processes responsible for the enrichment of transition elements described above. For this reason, sediment transport and weathering processes are considered here to be two possible mechanisms explaining the REE enrichment pattern in F5.



**Figure 3.15** Chondrite normalised Rare Earth Element patterns from F3d, F5 and F6 showing enrichment of REEs in F5 and depletion of Ce in F3d. Average shale (AS) values from Wedepohl (1971).

Nesbitt (1979) documented progressive enrichment of up to twice the parent rock values in the weathering profile of the Torrongo granodiorite in southeastern Australia. It is suggested that mobilisation of REEs occurs as a result of changes in groundwater pH (Nesbitt 1979). This assumption is supported by the highly weathered nature of F5 observed in the field.

However this does not explain the enrichment of Zr in this facies, which is an immobile element and is concentrated in heavy minerals, especially zircon (Moore 1988). Sediment transport can lead to the physical

separation of heavy minerals, especially zircon, resulting in the enrichment of heavy REEs (Taylor & McLennan 1988).

Enrichment of Sr in F5 and F3d is associated with  $\text{CaCO}_3$  in the facies as Sr tends to substitute for Ca in the crystal lattice due to their similar ionic charge and radius (Figure 3.14).

### **Compositional Plots**

The strong correlation between  $\text{TiO}_2$  and  $\text{Al}_2\text{O}_3$  in Figure 3.16 suggests that the majority of  $\text{TiO}_2$  is associated with clay minerals, supporting the assumption that  $\text{TiO}_2$  can be used as a proxy for terrigenous supply. This would also suggest that the source of terrigenous material remained relatively constant across the contact between the Garden Cove Formation and Tucker Cove Limestone.

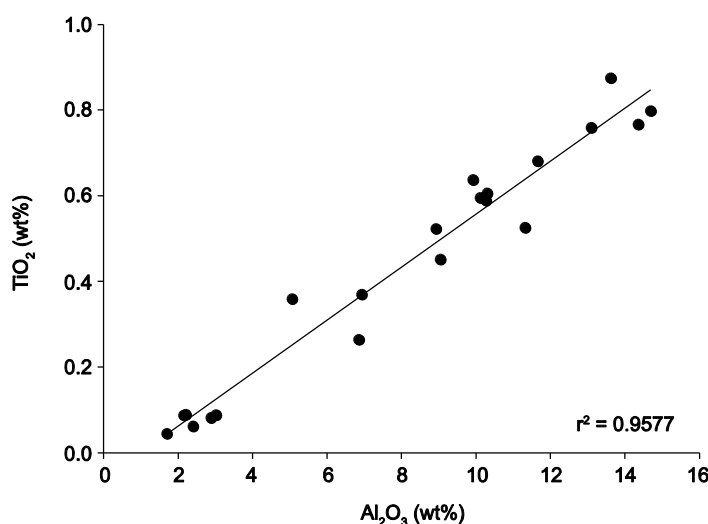


**Figure 3.16** Relationship between  $\text{Al}_2\text{O}_3$  and  $\text{TiO}_2$  in the Garden Cove Formation and Tucker Cove Limestone.

In Figure 3.17, the three axes are considered to represent the three major chemical components of sedimentary rocks,  $\text{Al}_2\text{O}_3$ ,  $\text{SiO}_2$  and  $\text{CaCO}_3$ , representing clays, quartz and/or biogenic silica and calcium carbonate, respectively (Moore 1988; Turgeon & Brumsack 2006). When plotted on this ternary diagram, it is clear that the three facies identified in the field on Campbell Island possess distinct geochemical compositions.

Samples from F6 plot along the axis between  $\text{Al}_2\text{O}_3$  and  $\text{SiO}_2$  poles, suggesting simple, two component mixing between end members, with little or no carbonate. One of these end members would have had a similar composition to argillites of the Greenland Group, while the other would have higher concentrations of quartz and lower clay concentrations. Both F5 and F3d contain decreasing concentrations of  $\text{Al}_2\text{O}_3$  and  $\text{SiO}_2$ , while  $\text{CaCO}_3$  increases. These facies appear to be distributed along a carbonate dilution line, once again suggesting a continued source of terrigenous sediment similar to that which supplied F5, with increasing dilution by carbonates.

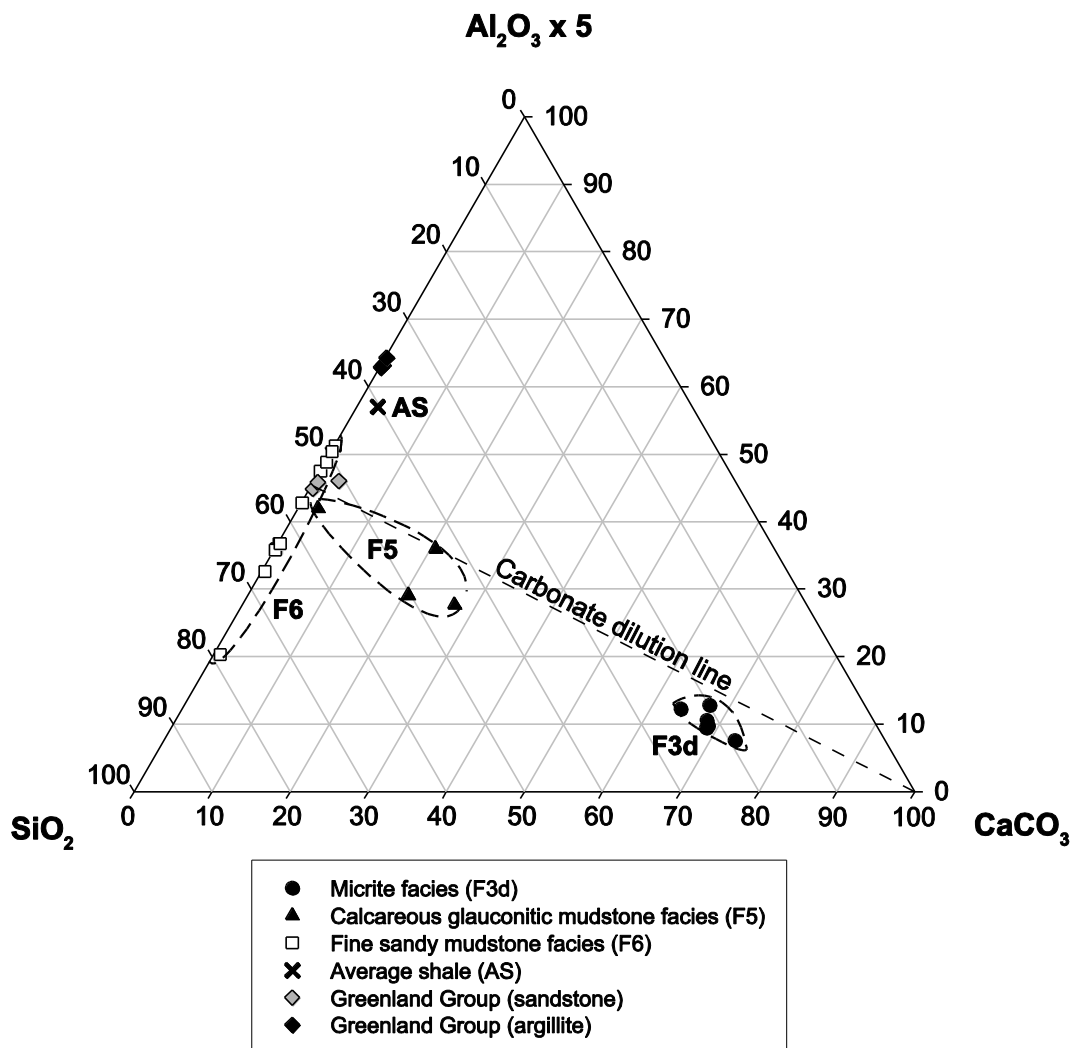


**Figure 3.17** Ternary diagram of relative proportions of  $\text{Al}_2\text{O}_3$  ( $\times 5$ ),  $\text{SiO}_2$  and  $\text{CaCO}_3$  in the fine sandy mudstone facies (F6), calcareous glauconitic greensand facies (F5) and micrite facies (F3d) at Campbell Island. An arbitrary multiplier of 5 is used for  $\text{Al}_2\text{O}_3$  in order to better distribute the data points within the graph (after Turgeon & Brumsack 2006). 'Average shale' (AS) (Wedepohl 1971) and Greenland Group sandstone and argillite compositions (Roser et al. 1996) are also shown.

## Proxies

Geochemical proxies show distinct trends throughout the measured sections from Capstan Cove and Camp Cove (Figure 3.18). Terrigenous sediment input (TRG), a proxy for clays based on the concentration of  $\text{TiO}_2$  in the sample, remains relatively high,  $\sim 70$  wt%, throughout the majority of F6 but drops to  $\sim 40$  wt% directly below the contact with the overlying Tucker Cove Limestone (Figure 3.18D). TRG spikes through the lowest 8 cm of the Tucker Cove Limestone, corresponding to F5, then drops to 10 wt% by the beginning of F3d. From 10 cm above the contact with the Garden Cove Formation, TRG values remain stable at  $\sim 10$  wt% for the rest of the measured section. TRG shows a significant negative correlation with both  $\text{Ca}[\text{exc}]$  and  $\text{Ba}[\text{exc}]$  (Appendix D).

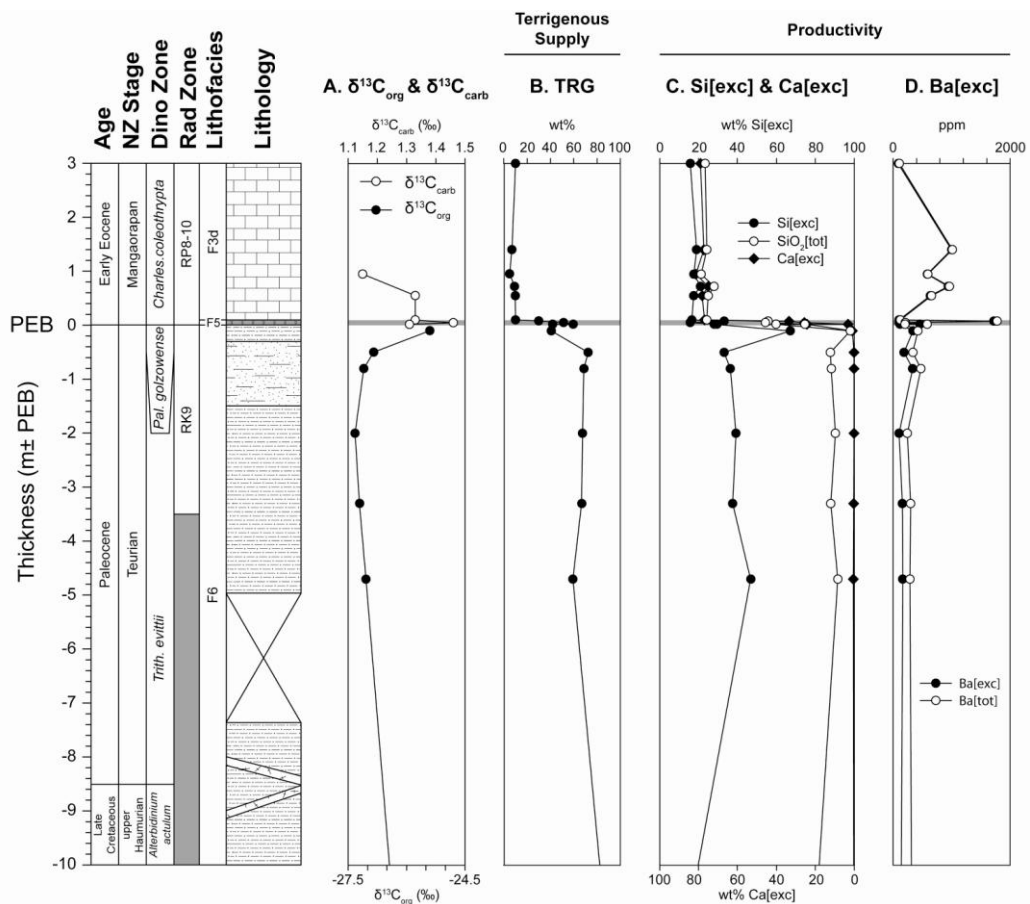


**Figure 3.18** Variations in (A)  $\delta^{13}\text{C}_{\text{org}}$  and  $\delta^{13}\text{C}_{\text{carb}}$ , (B) terrigenous sediment (TRG), (C) excess silica and excess carbonate ( $\text{Si}[\text{exc}]$ ,  $\text{Ca}[\text{exc}]$ ), and (D) barium (total and excess Ba,  $\text{Ba}[\text{exc}]$ ) in Campbell Island sections.

Proxies for paleoproductivity also show dramatic shifts across the contact between the Garden Cove Formation and Tucker Cove Limestone. Both excess silica ( $\text{Si}[\text{exc}]$ ) and total silica ( $\text{SiO}_2[\text{tot}]$ ) remain relatively stable

throughout most of the F6, at ~30 and ~90 wt% respectively, only increasing markedly in the sample collected directly below the contact (Figure 3.18C). The separation between SiO<sub>2</sub>[tot] and Si[exc] is related to the large input of terrigenous material. Values for SiO<sub>2</sub>[tot] decrease by as much as 70 wt% across the contact between the Garden Cove Formation and the Tucker Cove Limestone. Si[exc] and SiO<sub>2</sub>[tot] remain relatively stable through F3d and show far less separation in comparison to F6. Excess calcium (Ca[exc]) is low throughout F6, generally below 1 wt%, but increases rapidly through F5. Throughout F3d, Ca[exc] values remain relatively stable and high at ~80 wt%. Values for excess barium (Ba[exc]) from F6 remain similar between 136 and 367 ppm throughout the measured section and show separation between Ba[exc] and total barium (Ba[tot]). Ba[exc] and Ba[tot] become far more variable throughout the Tucker Cove Limestone (Figure 3.18D). Values reach as high as 1731 ppm near the base of F3d before decreasing to 92 ppm at the top of the measured section.

### ***Stable Isotope Geochemistry***

Even though it is stated by Hollis et al. (2003c) that  $\delta^{13}\text{C}$  is less prone to diagenetic alteration than  $\delta^{18}\text{O}$ , an average offset of ~0.5‰ is also observed in  $\delta^{13}\text{C}$  between Capstan Cove and Camp Cove. For this reason the  $\delta^{13}\text{C}$  values will not be considered within a composite stratigraphic column like the other inorganic geochemical data.  $\delta^{13}\text{C}_{\text{org}}$  values (Figure 13.18A) range between -27.3 and -25.4‰, falling within values suggested for sedimentary organic carbon by Nelson & Smith (1996).  $\delta^{13}\text{C}_{\text{org}}$  remains relatively stable through the majority of the Garden Cove Formation with a 1.5‰ positive shift occurring at the top of the section.  $\delta^{13}\text{C}$  of bulk carbonate from the Tucker Cove Limestone shows a 0.1‰ positive shift within the first 8 cm of the underlying contact with the Garden Cove Formation, before dropping by ~0.3‰ over the rest of the sampled interval (Figure 13.18A).

# **CHAPTER 4**

## **SEDIMENTARY SUCCESSIONS OF SOUTHEASTERN MARLBOROUGH**

---

### **4.1 PHYSICAL SETTING**

Southeastern Marlborough is situated in the northeast corner of the South Island of New Zealand (Figure 4.1). The study area lies between Cape Campbell in the north and Haumuri Bluff to the south and is bordered to the southwest by the Inland Kaikoura Range. The area lies at the southern end of the East Coast Deformed Belt of Spörli (1980) and within the Marlborough Fault System (MFS) of Van Dissen & Yeats (1991). The MFS consists of four major northeast-striking, dextral strike-slip faults: the Wairau, Awatere, Clarence and Hope Faults, as well as numerous subsidiary faults, and represents the transition zone between oblique subduction along the Hikurangi margin to the north and oblique, continent-continent collision along the Alpine Fault to the south (Crampton et al. 2003). From 16-35 km of dextral strike-slip displacement is inferred along the Clarence fault by Crampton et al. (2003) with current right-lateral strike-slip rates of c. 5 mm/yr (Hollis et al. 2005a), while Jordan Stream Thrust/Kekerengu Fault and Hope Faults are shown to accommodate 5-15 km and 20 km of dextral strike-slip displacement, respectively. Through a complex interplay of major dextral strike-slip faults, minor thrust faults and folds (Ota et al. 1996), the MFS is responsible for the major topographic features which dominate the region, such as the Inland and Seaward Kaikoura Ranges, Clarence Valley and the Kaikoura Peninsula, as well as the present day distribution of Late Cretaceous-Cenozoic cover rocks.

The Clarence Valley is an asymmetric, northeast trending valley which is structurally controlled by the MFS and bordered on either side by the Inland and Seaward Kaikoura Ranges. These ranges rise to their greatest elevation in Tapuae-o-Uenuku (2885 m) and Manakau (2608 m), respectively (Rattenbury et al. 2006). Elevation and tilting of two major fault blocks within the MFS are responsible for uplift of both ranges and means that the geology of the Clarence Valley is dominated by Mesozoic

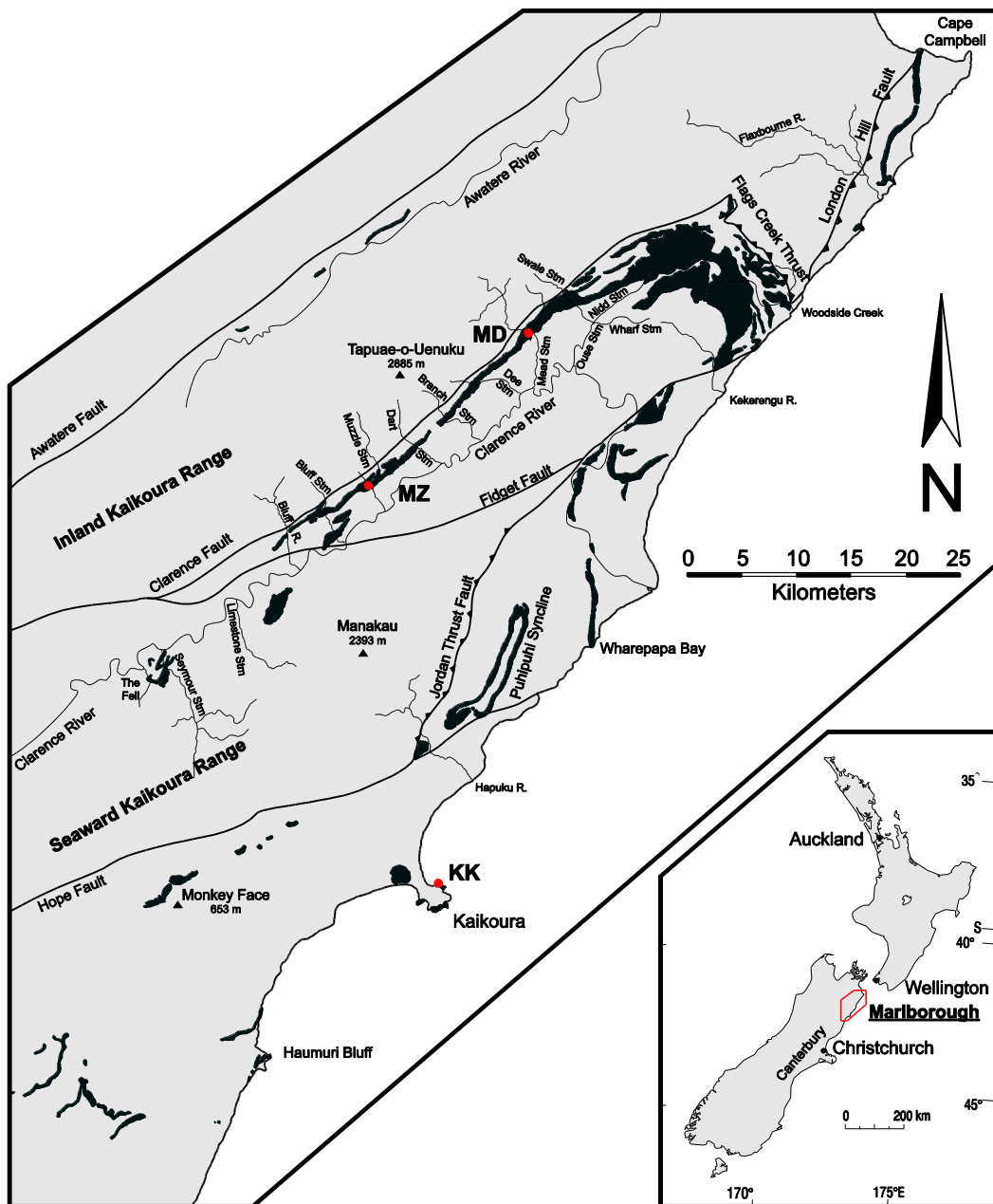


**Figure 4.1** Map of southeastern Marlborough showing the distribution of the Late Cretaceous-Paleogene Muzzle Group (dark grey) and main sites (red dots) where work was carried out in this study: MD, Mead Stream; MZ, Muzzle Stream; KK, Kaikoura Wharf (adapted from Rattenbury et al. 2006). *Inset.* Map showing the location of southeastern Marlborough within New Zealand.

basement rocks of the Pahau Terrane (Reay 1993). Late Cretaceous to Cenozoic sedimentary rocks are typically only preserved in narrow, down faulted and deformed belts to the southeast of each fault, excluding the Wairau Valley (Figure 4.2) (Reay 1993; Rattenbury et al. 2006). In the Clarence Valley this Neogene deformation means that the down-faulted Late Cretaceous to Cenozoic sedimentary succession to the southeast of

the Clarence Fault forms a 35 km strike ridge along the northwestern side of the valley (Strong et al. 1995). A number of tributary streams cut across this ridge, providing world renowned exposures of Late Cretaceous to Miocene strata, of which two, Mead Stream and Muzzle Stream, have been investigated as part of this study.

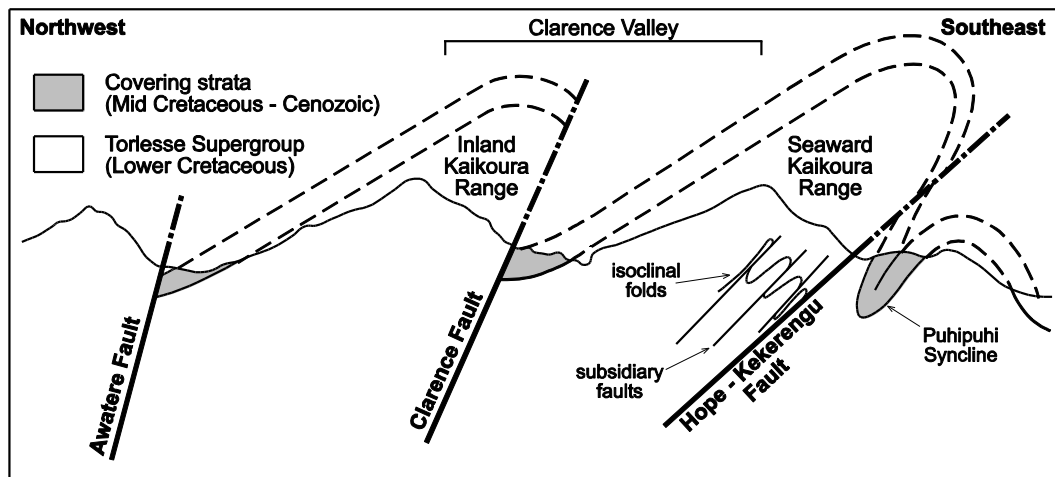


**Figure 4.2** Schematic cross section across the Inland and Seaward Kaikoura Ranges (from Reay 1993).

Ota et al. (1996) suggest that the Kaikoura Peninsula is recently emergent, with uplift occurring at a rate of 1.1 m/ka, based on ages determined for coastal terraces. Uplift has occurred as a result of block tilting towards the northwest, related to a west dipping reverse fault, situated 5 km southeast of the peninsula (Ota et al. 1996). The distribution of the Late Cretaceous-Miocene sediments on the Kaikoura Peninsula has been influenced by a period of compressional tectonics in the early Neogene (Rattenbury et al. 2006). This period resulted in gentle folding of strata and the formation of a series of anticlinal and synclinal structures perpendicular to the long axis of the Kaikoura Peninsula (Figure 4.3).

North of the Kaikoura Peninsula, the continental shelf is broad, being up to 50 km wide, but decreases to 10 km in width near Kaikoura. Directly south of the peninsula, the spectacular Kaikoura Canyon at the southern end of the Hikurangi Trench, approaches within ~500 m of the shoreline, with water depths at the head of the canyon reaching ~1000 m only 4 km offshore. Offshore southeast Marlborough, the continental shelf and slope



are incised by numerous canyons and small basins, one of which is the Conway Trough, a steep walled tributary on the south side of the Kaikoura Canyon. The geological history of the area has been strongly influenced by the initial development of mid and Late Cenozoic precursors of these fault controlled structures.

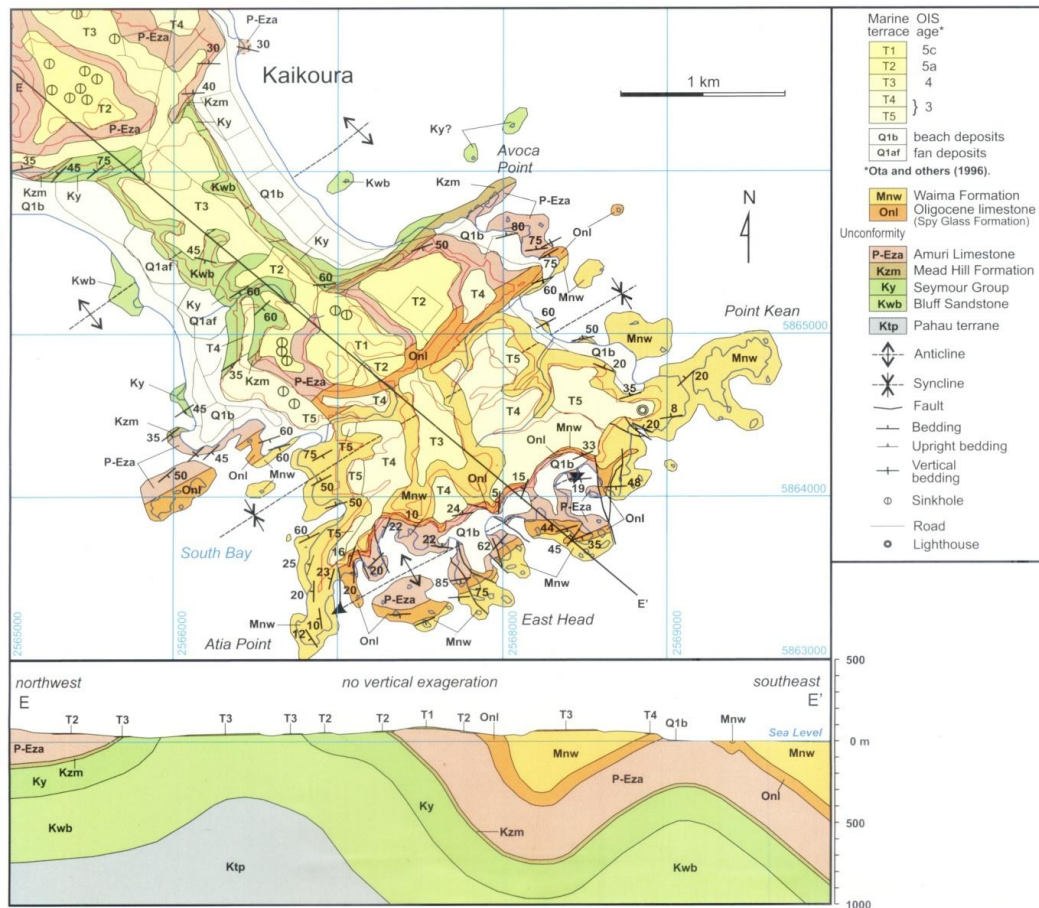


**Figure 4.3** Geological map and cross section of the Kaikoura Peninsula. The area has been uplifted and gently folded (from Rattenbury et al. 2006).

Nearly all the unforested area in the southeastern Marlborough region is now grazed by sheep or cattle in gentler country (Warren 1995). Within the Clarence Valley, introduced grasses such as Cock's Foot (*Dactylis glomerata*), rye-grass (*Lolium perenne*) and sterile bromes (*Bromus sterilis* & *B. tectorum*) dominate, however native tussock *Festuca novae-zealandia* and *Poa cita* ["caespitose"] and Kanuka (*Kunzea* [*Leptospermum*] *ericoides*) persist in areas throughout the valley. At higher altitudes Matagouri (*Discaria toumatou*), mountain flax (*Phorium cookianum*), Spaniards (*Achiphylia* spp.) and a species of snow grass (*Chionochloa* spp.) are common (Reay 1993). Both the native

Marlborough Daisy (*Pachystegia insignis*) and Marlborough Lilac (*Hebe hulkeana*) are common on rock faces (Reay 1993). Sweet briar rose poses a problem on river terraces and lower slopes, smothering grazing land, along with widespread and abundant Black Medick (*Medicago falcate*), Blue Borage (*Echium vulgare*) and the invasive Mouse-ear Hawkweed (*Hieracium pilosella*) (Reay 1993).

The climate of southeastern Marlborough can generally be characterised as sunny and mild. The area is well known for its long sunny days, with the town of Blenheim in the north receiving 2,470 sunshine hours per year, the highest of any main centre in New Zealand (New Zealand - A regional profile: Marlborough 1999). The region can be considered dry, receiving an annual mean rainfall of 650-700 mm, with summer or autumn drought being not uncommon (Warren 1995). This is typical of conditions experienced on the east coast of both islands. Orographic effects of the Inland and Seaward Kaikoura Ranges mean that the Clarence Valley is protected from moisture bearing winds, resulting in a dry climate and low rainfall (Reay 1993), leading to one area in the Clarence Valley being given the name 'The Desert'. Maximum daily average temperatures in summer range from 20°C-23°C (New Zealand - A regional report: Canterbury 1999), with a diurnal range of 12.1°C (Reay 1993). Jordan, in the Awatere Valley (along with Rangiora) holds the record for the highest recorded temperature in New Zealand, 42°C on 7 February 1973. The minimum mid-winter daily average temperature is 1.6°C with a diurnal range of 9.7°C, with deep and persistent snow cover in the Clarence Valley and the surrounding ranges (Reay 1993).

#### **4.2 LATE CRETACEOUS-LATE EOCENE LITHOSTRATIGRAPHY OF MUZZLE GROUP**

Micritic limestone of the Amuri carbonate megafacies (Hood & Nelson 1996) is conspicuous within sedimentary successions throughout the South Island's east coast. Description of these limestones from the Marlborough region was initially made by Hutton (1874) at Haumuri Bluff. Warren and Speden (1978) and Morris (1987) made important contributions to the stratigraphy of these Late Cretaceous to Cenozoic

sedimentary successions. However, the currently accepted stratigraphic nomenclature was developed by Reay (1993) (Figure 4.4) who established the Muzzle Group for the “sequence of calcareous, glauconitic, clastic and igneous lithologies which overlie the Seymour Group.” The Muzzle Group was initially divided into three formations - the Mead Hill Formation, Amuri Limestone Formation and Grass Seed Volcanics. Reay (1993) further recognised two members and four informal lithotypes within the Amuri Limestone - Teredo Limestone Member, Fells Greensand Member and the Lower Limestone, Lower Marl, Upper Limestone and Upper Marl lithotypes. Work by Killops et al. (2000) and Hollis et al. (2000) led Hollis et al. (2005b) to emend this by including the Waipawa Formation, a correlative of the Teredo Limestone, at the base of the Amuri Limestone, as well as establishing the Dee Marl Member.

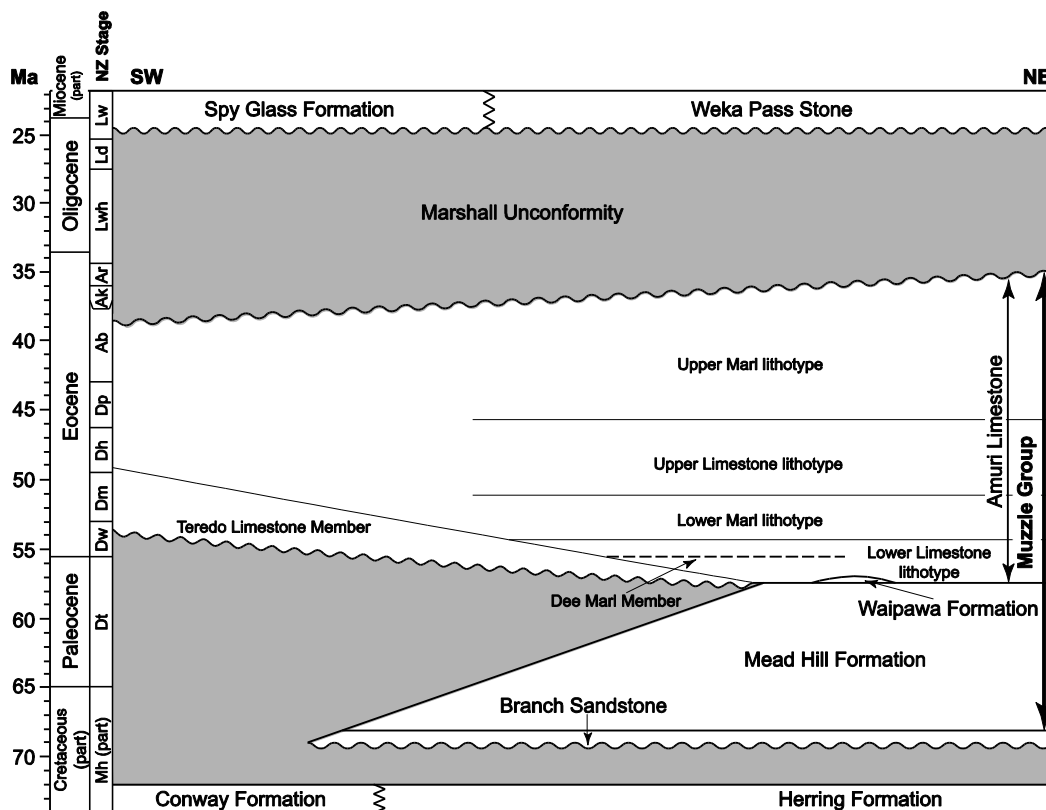


**Figure 4.4** Simplified lithostratigraphy for Late Cretaceous and Paleogene units of southeastern Marlborough (after Reay 1993; Browne 1995; Strong et al. 1995; Warren 1995; Hollis et al. 2005b).

#### **4.2.1 Mead Hill Formation**

Reay (1993) states that the first published reference to the Mead Hill Formation was by Webb (1966) who introduced the term for “greensands,

interbedded greensand and flint, bedded flint and flint and thin interbedded limestone". Reay (1993) suggests this description arose from the misidentification of dolomite, which is common within the Mead Hill Formation. He noted that before this the formation was known by numerous names including "flint-beds" (McKay 1886), "Chert Member (of the) Amuri Limestone Group" (MacPherson 1948) and "chert beds" (Kingma 1960). Reay (1993) describes the Mead Hill Formation as consisting of dm-bedded, greenish grey, muddy foraminiferal limestone interbedded with mm-bedded, medium to dark grey, calcareous, smectite mudstone or calcareous mudstone. While not considered to be a defining characteristic by Reay (1993), chert is present in varying quantities (5-95%) and is commonly associated with dolomite rhombs <1 mm in size (Lawrence 1993). Chert occurs as dark grey to black, small, circular (in plan), elliptical nodules that lead to a hummocky appearance on bedding surfaces. At several horizons, the superficial appearance of ribbon chert is observed as a result of coalescence of chert nodules (Reay 1993).

The Mead Hill Formation sits conformably either on Branch Sandstone or on Herring Formation (Figure 4.4). The basal contact is typically sharp, though locally gradational over several metres as a result of chertification extending down from the base of the Mead Hill Formation (Reay 1993). Although the contact between the Mead Hill Formation and underlying units is upper Haumurian throughout eastern Marlborough, Reay (1993) suggests that time transgressive relationships (younging southwards) can be inferred. As the Mead Hill Formation is overlain by an unconformity throughout much of eastern Marlborough, the top of the formation is also time transgressive, though in contrast to the base this youngs toward the northeast. At Mead Stream where the formation is thickest (~250 m), the top of the formation is upper Teurian (Strong et al. 1995) and is conformably overlain by the Amuri Limestone, as is common in northern sites. At Branch Stream in the middle Clarence Valley, the Mead Hill Formation is 120 m thick (Reay 1993) with the upper contact being upper Haumurian in age (Hollis et al. 2005c), while the formation is not preserved at Seymour Stream. Crampton et al. (2003) show that Paleocene aged Mead Hill Formation is only preserved in the northern

Clarence Valley and coastal sections north of Kaikoura Peninsula. Differences in thickness are attributed to both truncation beneath a low-angle unconformity and primary depositional thinning (Crampton et al. 2003).

The Mead Hill Formation was deposited as a hemipelagic siliceous-carbonate ooze on a terrigenous sediment-starved continental margin (Hollis et al. 2003c; 2005c). Foraminiferal and radiolarian evidence shows that the Mead Hill Formation was deposited in outer shelf to mid bathyal water depths (Strong et al. 1995; Hollis et al. 2005c) and that both water depth and oceanicity increased throughout the deposition of the formation with continuing subsidence of the Marlborough paleo-platform (Crampton et al. 2003). This is supported by consistently small amounts of terrestrially derived palynomorphs and organic matter found in the Mead Stream section (Strong et al. 1995), indicating the site was distant from a shoreline at the time and that no part of the section can be considered to represent a marginal marine environment.

#### **4.2.2 Waipawa Formation**

Named the Upper Chert Member of the Lower Limestone Formation by Morris (1987), Strong et al. (1995) drew comparisons with the Waipawa Formation from the North Island based on biostratigraphic and lithologic similarities, but did not go so far as to give the unit the same name. Instead, the Black Siltstone was established as an informal unit at the base of the Amuri Limestone. Killops et al. (2000) and Hollis et al. (2000) both make reference to the Waipawa Formation at Mead Stream, considering it a correlative of similar units distributed throughout many of New Zealand's Late Cretaceous-Cenozoic sedimentary basins. However, this was not formalised until the Muzzle Group was emended by Hollis et al. (2005b) to include the Waipawa Formation at the base of the Amuri Limestone at Mead Stream. The Waipawa Formation at Mead Stream consists of a thin pair of dark grey, siliceous mudstone units, which show rusty weathering and are separated by 4.8 m of siliceous limestone (Strong et al. 1995; Hollis et al. 2005b). These two units are 2.4 m and 0.3 m thick and termed Mudstone A and Mudstone B respectively, with

Mudstone A the lower of the two representing the 'Black Siltstone' of Strong et al. (1995).

Strong et al. (1995) suggested a possible unconformable contact between the Mead Hill and Waipawa Formations on the basis of the sharp lithologic change. However, it was also stated that the break is so small that it appears paleontologically irresolvable. Hollis et al. (2005b, c) consider the Waipawa Formation to sit conformably on Mead Hill Formation at Mead Stream. In Marlborough, the Waipawa Formation has only been described at Mead Stream, as the formation has either not been confidently located elsewhere (Hancock et al. 2003) or is not present due to the unconformity underlying the Amuri Limestone, as is the case in southern sites (Hollis et al. 2005b). Given this, Strong et al. (1995) state that paleontological evidence indicates the Waipawa Formation can be considered a lateral (more basinward) equivalent of the Teredo Limestone Member of the Amuri Limestone. Biostratigraphic evidence shows that the Waipawa Formation at Mead Stream was deposited during the upper Teurian, later than the base of nannofossil zone NP6 (58.4 Ma) but earlier than the base of zone NP8 (57.3 Ma) (Hollis et al. 2000), leading to the inference that the formation was deposited over ~500 k.y. between 58 and 57.5 Ma.

Strong et al. (1995) showed that the Waipawa Formation was deposited at bathyal depths at Mead Stream and that throughout the Teurian any paleobathymetric changes had relative minor effects in this environment.

Microfaunal assemblages, dominated by the agglutinated benthic foraminifera *Haplophragmoides*, are interpreted by Strong et al. (1995) to indicate environmental stress such as low oxygen/high organic matter during deposition of the Waipawa Formation at Mead Stream. This was supported by Killips et al. (2000), who inferred strong positive correlations between  $\delta^{13}\text{C}_{\text{kerogen}}$  values, total organic carbon (TOC) content and 24-*n*-propylcholestane abundance to be consistent with enhanced productivity resulting in an expanded oxygen minimum zone during the period of deposition of the Waipawa Formation throughout New Zealand.

### **4.2.3 Amuri Limestone**

Hutton (1874) used the name Amuri Limestone for “white to pale grey, argillaceous limestone always in thin beds, which are often broken up” at Haumuri Bluff (Reay 1993). Since then, the name has become synonymous with calcilutites deposited in eastern basins of Zealandia during the Late Cretaceous-Paleogene (e.g. Nelson 1978; Browne 1987; Field et al. 1989; Field et al. 1997). To the south of the Kaikoura Peninsula, the Amuri Limestone is part of the Eyre Group (Rattenbury et al. 2006) and youngs into the Canterbury Basin. At the Waipara River, the formation is entirely Oligocene (Field et al. 1989). While to the north, the Amuri Limestone is not recognised in coastal sections between Woodside Creek and Cape Campbell (Hollis et al. 2005a).

The Amuri Limestone in southeastern Marlborough contains three members: Teredo Limestone, Dee Marl and Fell Greensand, as well as four informal lithotypes: Lower Limestone, Lower Marl, Upper Limestone and Upper Marl (Reay 1993; Hollis et al. 2005b). Following the convention of Strong et al. (1995), the first letters of the lithotype names are capitalised to distinguish them from generic lithologies. In the following section, only the Teredo Limestone and informal lithotypes will be discussed, with the major focus on the Teredo Limestone. Full descriptions of members and lithotypes are covered in Reay (1993) and Hollis et al. (2005b).

#### ***Teredo Limestone Member***

Teredo Limestone was first introduced by Hector (1874) and redefined by Warren and Speden (1978) as the uppermost calcareous member of the Claverley Sandstone at Haumuri Bluff. Morris (1987) stated that Teredo Limestone be given separate formation rank in its own right due to stratigraphic significance, regional extent and lack of lithologic affinity. However, this was not accepted by Reay (1993), who suggested that as a result of the major unconformity underlying the Teredo Limestone and the fact that the Claverley Sandstone is not present in the Clarence Valley, the unit should be reassigned to the Amuri Limestone because of greater stratigraphic and lithologic affinities. This stratigraphic nomenclature has

been accepted by subsequent authors (e.g. Strong et al. 1995; Hollis et al. 2005b, c; Rattenbury et al. 2006). Reay (1993) defines the Teredo Limestone as containing two informal lithotypes, a basal unit consisting of “cream to grey, massive, slightly calcareous sandstone” and an upper unit consisting of “green, glauconitic, highly calcareous sandstone” considered to be the Teredo Limestone *sensu stricto*. The Teredo Limestone is distributed widely throughout eastern Marlborough and North Canterbury, extending from Dart Stream in the middle Clarence Valley, as far south as the mouth of the Waiau River (~70 km) (Reay 1993; Warren 1995). The erosional unconformity underlying the Teredo Limestone means that the member overlies progressively younger strata towards the northeast (Reay 1993). In the north of the middle Clarence Valley, the Teredo Limestone overlies Mead Hill Formation. Further south, around Seymour Stream, the unit overlies Herring Formation (Reay 1993), while at Haumuri Bluff and the Conway River mouth the unit overlies Claverley Sandstone (Warren 1995).

The unit thickens towards the southwest, ranging from 27 cm at Dart Stream to ~25 m at Seymour Stream (Morris 1987; Reay 1993). In the middle Clarence Valley, the age of the Teredo Limestone is upper Haumurian to Waipawan, while further south the top of the unit is as young as Mangaorapan (Reay 1993). These age ranges can only be considered maximum age constraints as they are inferred from the age of the overlying and underlying sediments (Morris 1987). Hollis et al. (2005c) confirmed evidence of a southwestward increase in the time gap represented by the sub-Teredo unconformity presented by Reay (1993) by showing that the Teredo Limestone at Muzzle Stream is Teurian while at Bluff Stream the unit is earliest Waipawan.

Reay (1993) suggested a shallow marine, inner shelf environment for deposition of the Teredo Limestone based on microfaunal ecology. However, Warren (1995) inferred a bathyal to near bathyal depth of deposition based on foraminiferal evidence, despite the sandy texture and glauconite content. This is supported by Hollis et al. (2005c) who stated that both Muzzle and Bluff Streams lay at mid-bathyal depths (800-1200)



during the deposition of the Teredo Limestone. All authors (e.g. Reay 1993; Warren 1995; Hollis et al. 2005c) agree that abundant glaucony, extensive bioturbation and the local presence of phosphatic nodules suggest slow, or at time nil, sedimentation rates.

### ***Amuri Limestone Lithotypes***

At the type area of Haumuri Bluff, the Amuri Limestone consists of ~100 m of hard white, micritic limestone interbedded with thin pale grey marly interbeds (Warren 1995). In the Clarence Valley where the Amuri Limestone reaches its greatest thickness of ~400 m at Mead Stream, four lithotypes are identified. The Lower Limestone consists of “dm bedded, light greenish grey, well indurated, foraminiferal micritic limestone and interbedded calcareous mudstone”, with an average CaCO<sub>3</sub> content of ~78% (Reay 1993). The distribution of this unit is very similar to the Mead Hill Formation. However, Reay (1993) suggests that the lithotype does not occur southeast of the Clarence River. The Lower Limestone conformably overlies the Mead Hill and Waipawa Formations in the northern Clarence Valley (Hancock et al. 2003; Hollis et al. 2005b), while the unit conformably overlies the Teredo Limestone through the middle Clarence Valley (Reay 1993; Hollis et al. 2005b,c). Sandy detritus persists from the Teredo Limestone into the basal part of the Lower Limestone above the generally sharp contact (Reay et al. 1993).

The Lower Marl is characterised by a dominance of cm-m thick, moderately indurated smectitic calcareous mudstone, interbedded with subordinate cm, well indurated, micritic limestone beds (Reay 1993). CaCO<sub>3</sub> concentrations in the Lower Marl decrease in comparison to the Lower Limestone, with values ranging from 42-73% and 68-75% in calcareous mudstone and limestone beds, respectively, the lowest values occurring near the middle of the unit (Reay 1993). The Lower Marl occurs throughout southeastern Marlborough wherever the Amuri Limestone is preserved, conformably overlying Lower Limestone in the northern and middle Clarence Valley and Teredo Limestone to the southeast, including on Kaikoura Peninsula (Reay 1993; Browne et al. 2005a).

The Upper Limestone is generally considered to be similar to the Lower Limestone, the major distinguishing features between it and the rest of the Amuri Limestone being the presence of stylobedding and the rarity of interbedded calcareous mudstone (Reay 1993). The Upper Limestone conformably overlies the Lower Marl and is preserved everywhere Cenozoic rocks are preserved (Reay 1993), reaching a maximum thickness of ~140 m at Dart Stream from where it thins rapidly to the southeast.

The Upper Marl consists of “massive or fissile, light greenish or bluish-grey, moderately indurated, smectitic, calcareous mudstone containing subordinate cm to dm-bedded, light grey or greenish cream, well indurated, micrite” (Reay 1993). The Upper Marl conformably overlies the Upper Limestone where Cenozoic rocks are preserved. The lower contact is gradational, with Reay (1993) arbitrarily setting the base of the Upper Marl at the “highest intercalated calcareous mudstone” in the Upper Limestone.

At Mead Stream, the Lower Limestone, Lower Marl, Upper Limestone and Upper Marl were deposited during the upper Teurian to Bortonian (Strong et al. 1995), while at Haumuri Bluff in the south the Amuri Limestone was deposited during the Waipawan and Runangan (Warren 1995).

Decreases in  $\text{CaCO}_3$  and dominance of calcareous mud beds within the Lower Marl and Upper Marl are suggested to be the result of increased influxes of terrigenous mud related to weathering during periods of global warming (Hollis et al. 2005a, b).

### **4.3 LITHOFACIES AT MEAD STREAM**

#### **4.3.1 Site Description**

Field work at Mead Stream in the northern Clarence Valley was carried out from 15/1/2008 to 18/1/2008. Access to the Mead Stream section is by private 4WD track through Bluff Station via Kekerengu and Coverham.

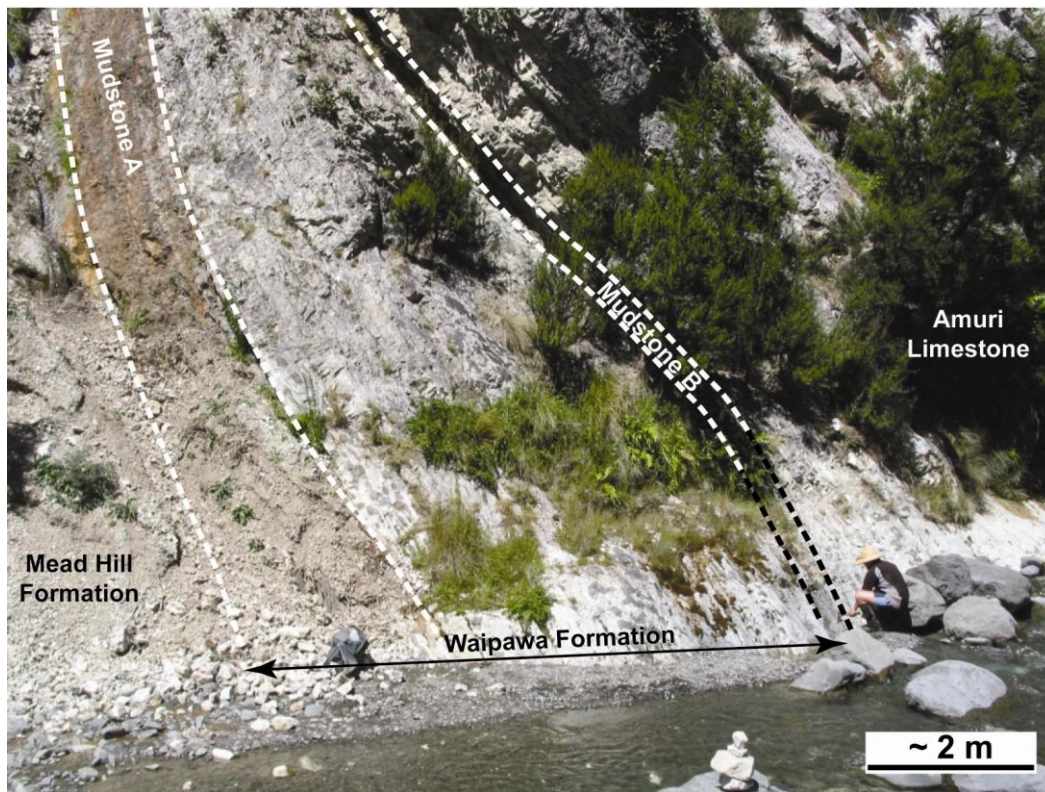


**Figure 4.5** Logged section from Mead Stream (NZMS 260 P30 758160).

Beds dip steeply ( $202/52^{\circ}\text{NW}$ ), allowing a stratigraphic column to be constructed from the true right of the stream at NZMS 260 P30 758160. The particular interval of interest in this study was the Waipawa Formation, as well as the Mead Hill Formation and Lower Limestone lithotype of the Amuri Limestone immediately adjacent to the Waipawa Formation. This interval occurs at approximately  $\sim 108$  m stratigraphically above the Cretaceous-Tertiary (K/T) boundary at Mead Stream.

Due to an accumulation of debris at the base of the Waipawa Formation (Figure 4.5), measurements through the unit were made  $\sim 3$  m above the stream bed. The presence or absence of this debris is dependent on rainfall and stream condition at the time, as on a return visit to the site in January 2009, the formation could be observed down to the stream bed. This is important because the thickness of Mudstone A measured during this study was 30 cm greater than measurements for the same unit by Hollis et al. (2005b). Based on measurements from a laterally continuous marker bed within Mudstone A, thickness variations occur mainly within the lower part of this unit, suggesting a possible degree of unconformity.

### 4.3.2 Field Description

Two lithofacies have been identified at Mead Stream, the siliceous micrite and chert facies (F1a) and the organic mudstone facies (F2) (Figure 4.6).

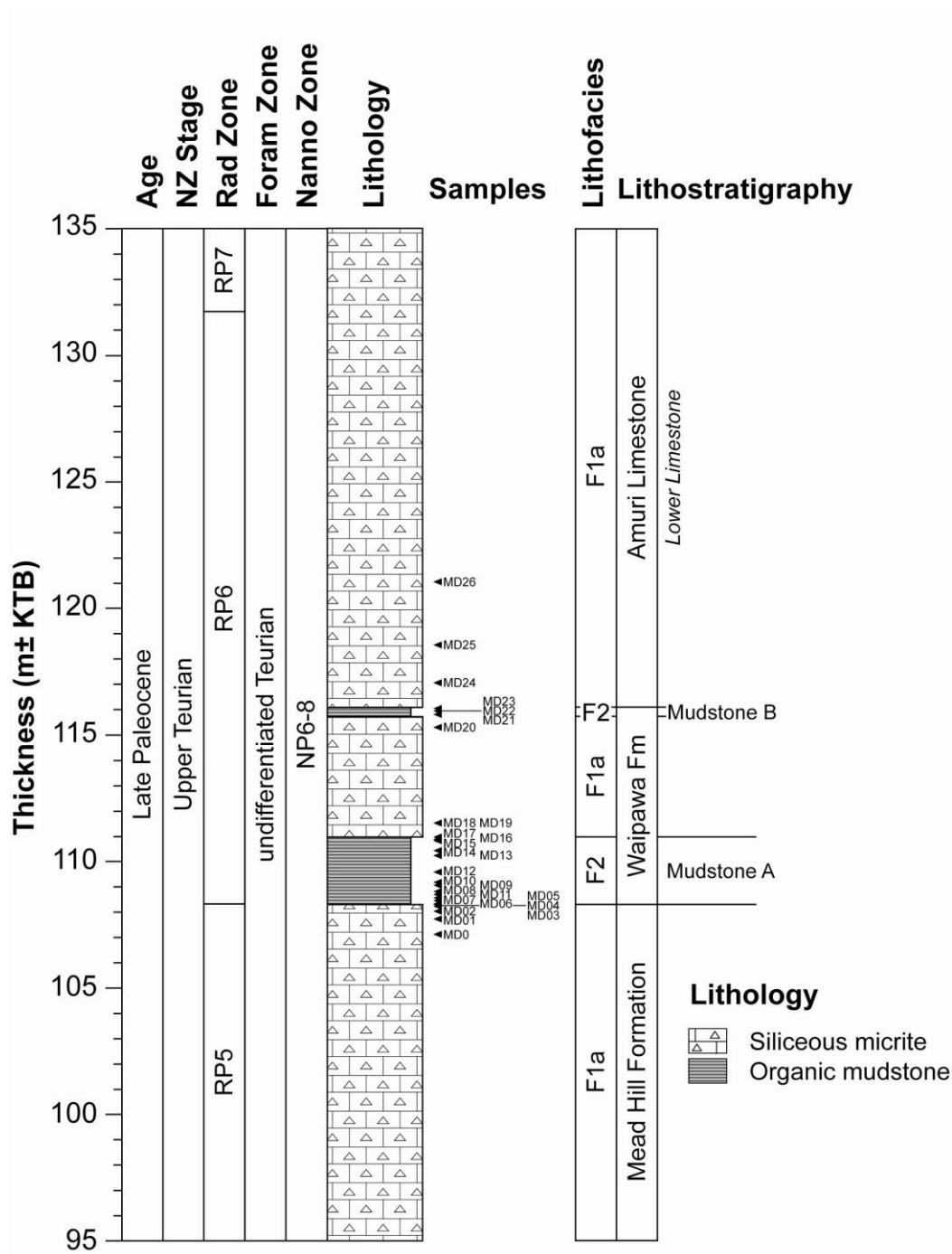


**Figure 4.6** Stratigraphic column for Late Paleocene strata at Mead Stream in relation to the Cretaceous/Tertiary boundary (KTB). Age control after Hollis et al. (2005). Lithostratigraphy after Reay (1993) and Hollis et al. (2005b), italics denotes informal lithotype. Lithology, lithofacies and samples (this study).

### *Siliceous micrite and chert facies (F1a)*

F1a consists of pale grey to cream, siliceous micrite containing dark grey to black, vitreous, elongate, generally oval chert nodules (Figure 4.7). Slight weathering commonly results in colour changes from light grey to cream that is most pronounced around chert nodules (Figure 4.7). F1a is hard to very hard and displays conchoidal fracturing as a result of the high silica content. The facies shows wavy bedding, with bed thicknesses from 10-30 cm, due to the distortion of beds by chert nodules. Bed thicknesses in F1a above Mudstone B decrease to more commonly <20 cm.

Chert nodules generally form elongate, oval shapes running parallel within beds. However, some are irregular, appearing to branch into adjacent beds and coalesce with surrounding nodules (Figure 4.7). Chert makes up less than 40% of F1a and decreases in abundance above the upper contact with Mudstone B.



**Figure 4.7** Irregular, coalescing chert nodules in F1a of the Waipawa Formation from Mead Stream (NZMS 260 P30 758160). Note zones of cream weathering around chert nodules. Geological hammer rests at the upper contact of Mudstone A.

Bioturbation is ubiquitous throughout F1a, with trace fossils being dominated by *Zoophycus* and *Chondrites* (Figure 4.8). The facies also

contains numerous fine, calcite healed joints, up to 8 mm in thick, running perpendicular to bedding.



**Figure 4.8** Bioturbation in the siliceous micrite and chert facies (F1a) at Mead Stream (NZMS 260 P30 758160). C: *Chondrites*; P: *Planolites*; Z: *Zoophycus*.

#### *Organic mudstone facies (F2)*

The organic mudstone facies at Mead Stream consists of cm bedded, weakly laminated, grey, siliceous mudstone interbedded with fissile, laminated, dark grey to dark brown, argillaceous mudstone (Figure 4.9). F2 is soft to moderately hard and moderately weathered, resulting in a jarositic appearance and limonite staining of joint surfaces. Beds generally tend to be continuous along the length of the outcrop but variable in thickness, with some beds bifurcating, resulting in a boudinage appearance in localised areas.

F2 forms two distinct units, 2.7 m and 0.26 m thick, corresponding to Mudstone A and Mudstone B of Hollis et al. (2005b) respectively, separated by 4.8 m of F1a. The basal contact of both units with the underlying F1a is sharp, with irregular relief as the result of wavy bedding within F1a. Pyritised burrows were identified extending from the base of Mudstone A into underlying F1a of the Mead Hill Formation.

The fissile nature of much of F2 meant that few large, coherent samples were collected. Given this, those that were able to be slabbed showed extensive bioturbation structures (see Figure 4.10d). Fine, calcite healed veins perpendicular to bedding are also common throughout F2.

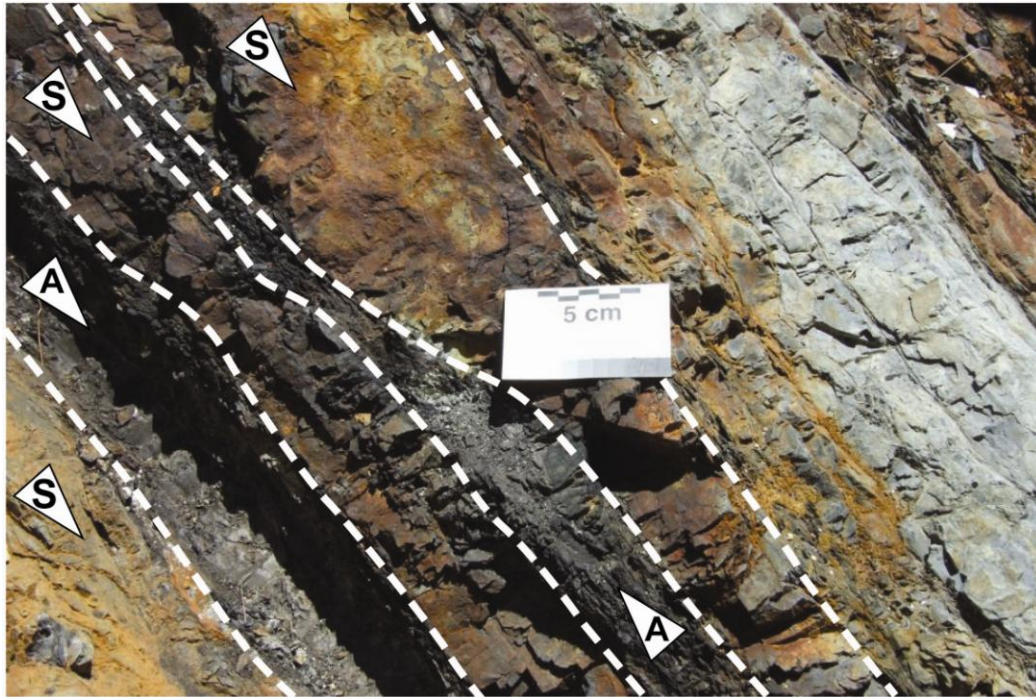


**Figure 4.9** Siliceous mudstone and argillaceous mudstone interbeds of the organic mudstone facies (F2) in the Waipawa Formation at Mead Stream showing characteristic brownish orange limonite staining of joint surfaces. A, argillaceous mudstone; S, siliceous mudstone.

### **4.3.3 Petrography and Mineralogy**

#### *Siliceous micrite and chert facies (F1a)*

In thin section, F1a is characterised by light grey, clotted micrite and light brown chert consisting of microcrystalline silica. The boundary between these two components is generally very sharp (Figure 4.10a). Under CL, a clear distinction is evident between the chert and micrite, the latter showing an orange colour characteristic of calcite and the former a dark reddish brown (Figure 4.10b). Scanning electron microscope (SEM) studies of F1a show that the micrite is primarily composed of detrital carbonate grains in the form of coccolith debris (Figure 4.11a) along with secondary microcrystalline carbonate cement and authigenic silica (Figure 4.10). Grain size ranges from 0.5  $\mu\text{m}$  to 5  $\mu\text{m}$ . These components were

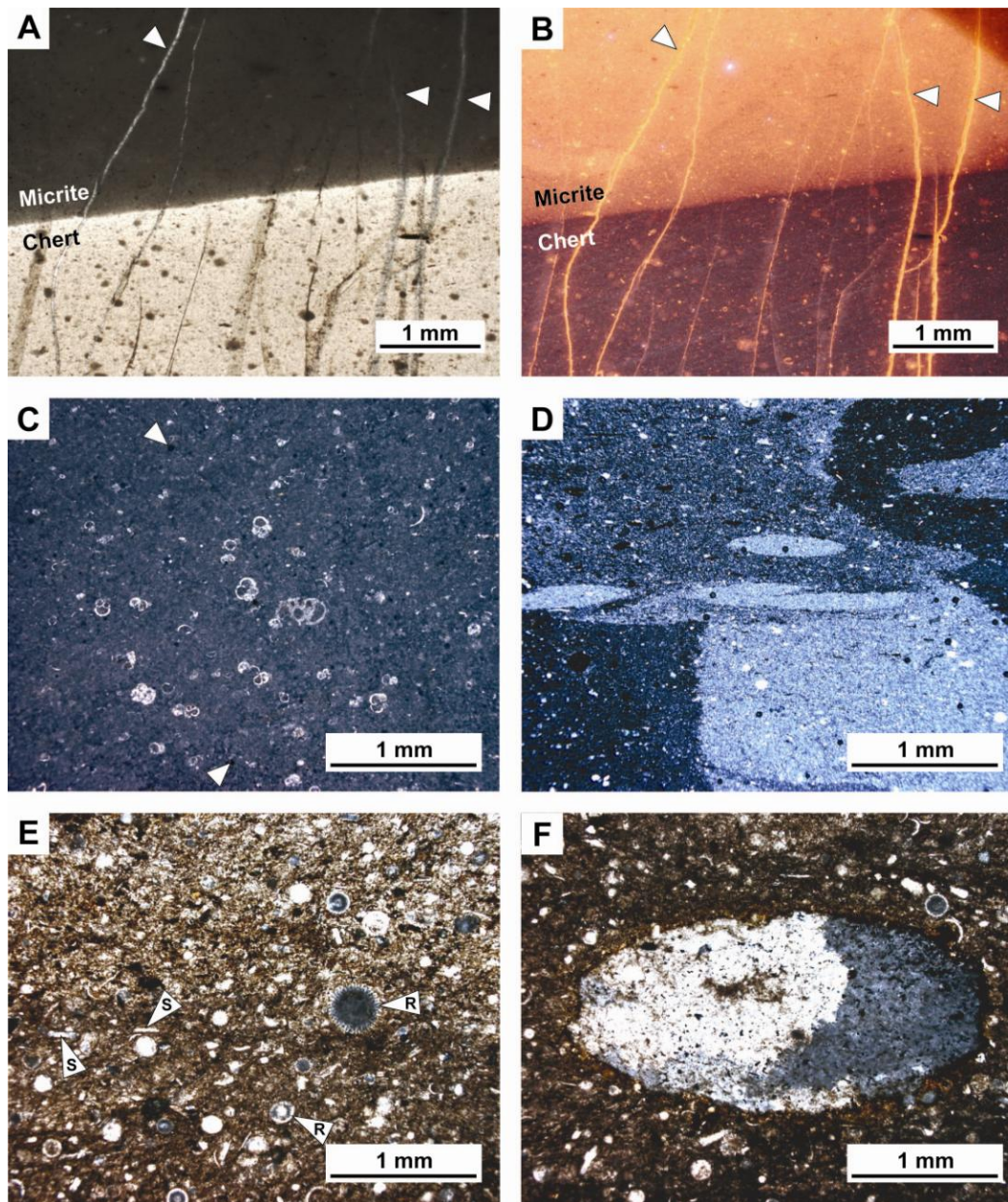


**Figure 4.10** Photomicrograph pairs under plane polarised light (A) and cathodoluminescence light (B) of the siliceous micrite and chert facies (F1a) (MD18). Distinct boundary between micrite and chert with late stage calcite veins (arrowed). Micrite shows the characteristic orange colour of calcite under CL light while chert shows a dark reddish brown. (C) Siliceous micrite and chert facies from above the Waipawa Formation (MD24) containing planktic foraminifera and authigenic pyrite (arrowed) (PPL). (D) Organic mudstone facies from Mudstone B (MD23) which is much finer than Mudstone A in (E) (XPL). Note the prominent colour contrasts due to bioturbation, possible compressed *Planolites*. (E) Organic mudstone facies from Mudstone A (MD13). R: Recrystallised spumellarian radiolarians; S: sponge spicules. (F) Burrow containing large blocky, pleochroic, calcite crystals rich in pyrite in organic mudstone facies (MD13) (PPL).



identified using energy dispersive spectroscopy (EDS) to create elemental maps of SEM images (Figure 4.11b, c, d). Ca is attributed to calcite, Si is attributed to silica and Al is attributed to clays.

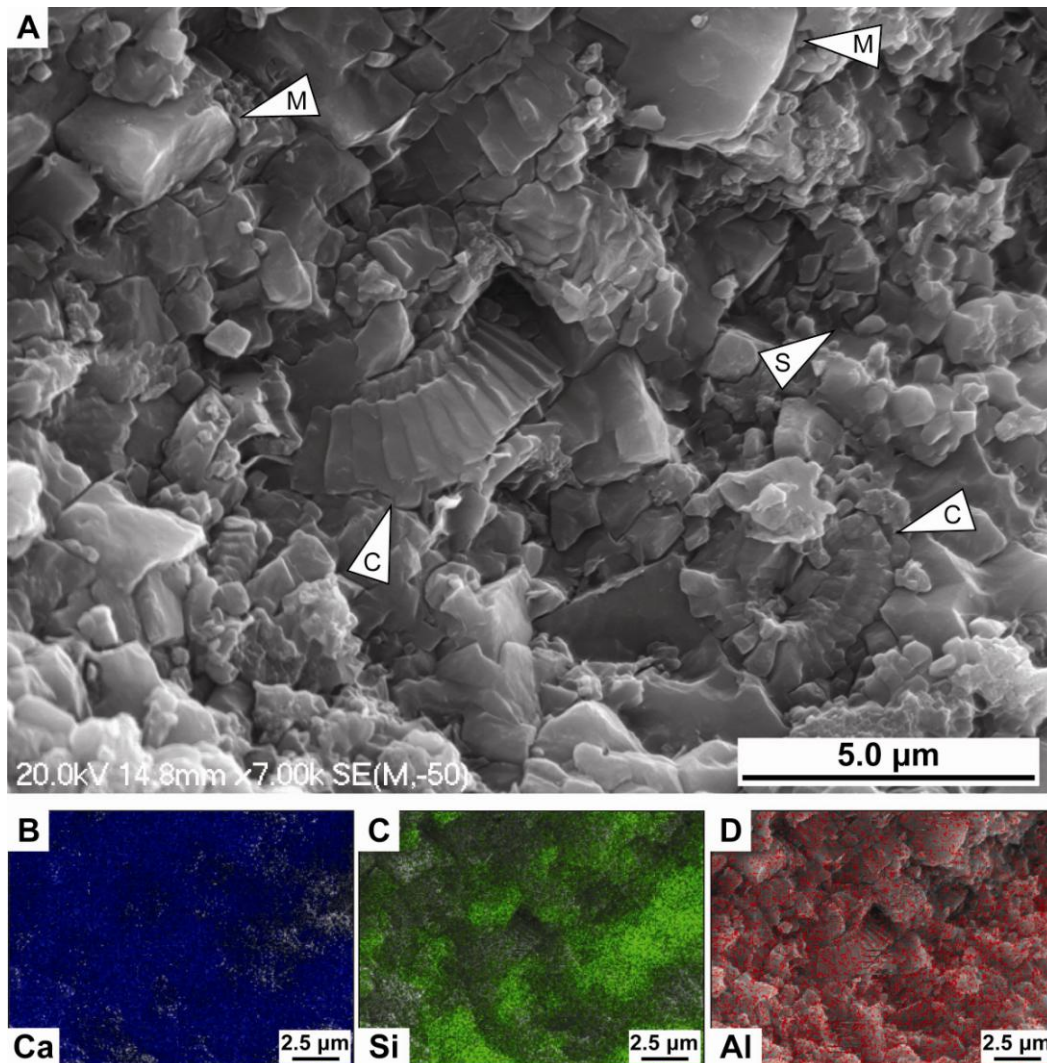


**Figure 4.11** (A) SEM image of siliceous micrite and chert facies (MD24). C: coccolith debris; M: microcrystalline carbonate cement; S: authigenic silica. Zones of calcium carbonate and authigenic silica are identified by producing elemental maps of calcium (B), silica (C) and aluminium (D) overlaid over the original SEM image. Intensity of colour denotes concentration of element. Note that Al is ubiquitous throughout the image and not concentrated in any one location, unlike Ca and Si.

Rare siliciclastics, visibly making up <1%, occur in F1a, and include subrounded silt sized quartz grains as well as mica grains. However, any argillaceous (clay) component is impossible to clearly resolve.

Microfossils identified in thin sections of samples from F1a of the Mead Hill Formation were mainly spumellarian radiolarians (~3%), with rare

nassellarian radiolarians and sponge spicules. Only rare, poorly preserved benthic foraminifera were observed in samples collected from below the Waipawa Formation, as well as in the F1a unit between Mudstone A and B. Above the Waipawa Formation, planktic foraminifera dominate, making up 5-10% of the total sample, with spumellarian radiolarians and sponge spicules being less common (~1%) (Figure 4.10C). Microfossil preservation in F1a is moderate to poor, with radiolarians tending to show recrystallised textures that obscure structural features, as well as infilling of the surface pores of their test with microcrystalline silica. The planktic foraminiferal tests in samples of F1a from the Amuri Limestone are infilled with micritic cement.

Veins identified in the field consist of dusty calcite spar crystals up to 3 mm across in thin section. Vein thickness varies considerably but is generally <100 µm, with veins running parallel to each other and cutting both chert and micrite. Under CL, these veins show very bright yellow-orange colours (Figure 4.10b)

XRD of bulk, unoriented powdered samples indicates that the micrite consists of low-Mg calcite and that the silica in chert nodules consists of quartz (Appendix C).

#### *Organic mudstone facies (F2)*

In thin section, F2 is generally characterised by fine grained, brown (probably organic matter) matrix containing siliciclastics, perigenic glaucony and phosphatic grains as well as abundant authigenic pyrite identified in thin section by its pale gold colour under reflected light.

This facies also contains some medium silt sized, subrounded quartz grains (~2%) as well as rare glaucony, phosphatised grains and plagioclase feldspar. Glaucony grains are dominated by bright green, microcrystalline, pelletal forms but also include rare vermicular grains of glauconitised biotite which show pleochroism and high order interference colours under cross polarised light. Phosphatic grains are generally subrounded to rounded, and identified by their yellow-brown colour and

nearly isotropic extinction behaviour under cross polarised light. Mudstone B differs from Mudstone A in being finer grained (cf. Figure 4.10d, e) and containing conspicuous muscovite (~5%). These grains are generally aligned with each other and are parallel to laminations observed in thin section.

Microfossils in Mudstone A are dominated by spumellarian radiolarians (~20%) (Figure 4.10e). Preservation of these microfossils varies, with some tests only preserved as fragments, while others remain whole, with varying degrees of cementation within pores on the surface of the test. In contrast to this, Mudstone B is poor in microfossils as a whole, containing only rare radiolarians which are highly recrystallised and infilled with microcrystalline silica as well as silicified benthic foraminifera.

Bioturbation is common throughout F2, resulting in some significant variations in the concentrations of organic matter and siliciclastic grains in samples (Figure 4.10d). One unusual burrow observed in MD13 appears to have been infilled with large blocky, pleochroic, calcite crystals rich in pyrite (Figure 4.10f).

#### **4.3.4 Geochemistry**

##### ***Inorganic Geochemistry***

The elemental concentrations in F1a and F2 are compared with average shale values of Wedepohl (1971) for both major and trace elements to allow for comparability between sites. The major elemental concentrations for F2 are also compared with values from the Waipawa Formation of Moore (1988). Compositional plots and geochemical proxies were created using an expanded dataset including unpublished geochemical data made available by Dr Chris Hollis (GNS, Lower Hutt) (Appendix D).

##### ***Major Elements***

###### ***Siliceous micrite and chert (F1a)***

Excluding SiO<sub>2</sub>, CaO and Na<sub>2</sub>O, all Al normalised major elemental concentrations in samples from the siliceous micrite and chert facies (F1a) are 'normal' with respect to concentrations observed in average shale

(Wedepohl 1971) (Figure 4.12A).  $\text{SiO}_2$  and  $\text{CaO}$  are significantly higher than values for average shale, while concentrations of  $\text{Na}_2\text{O}$  are lower.

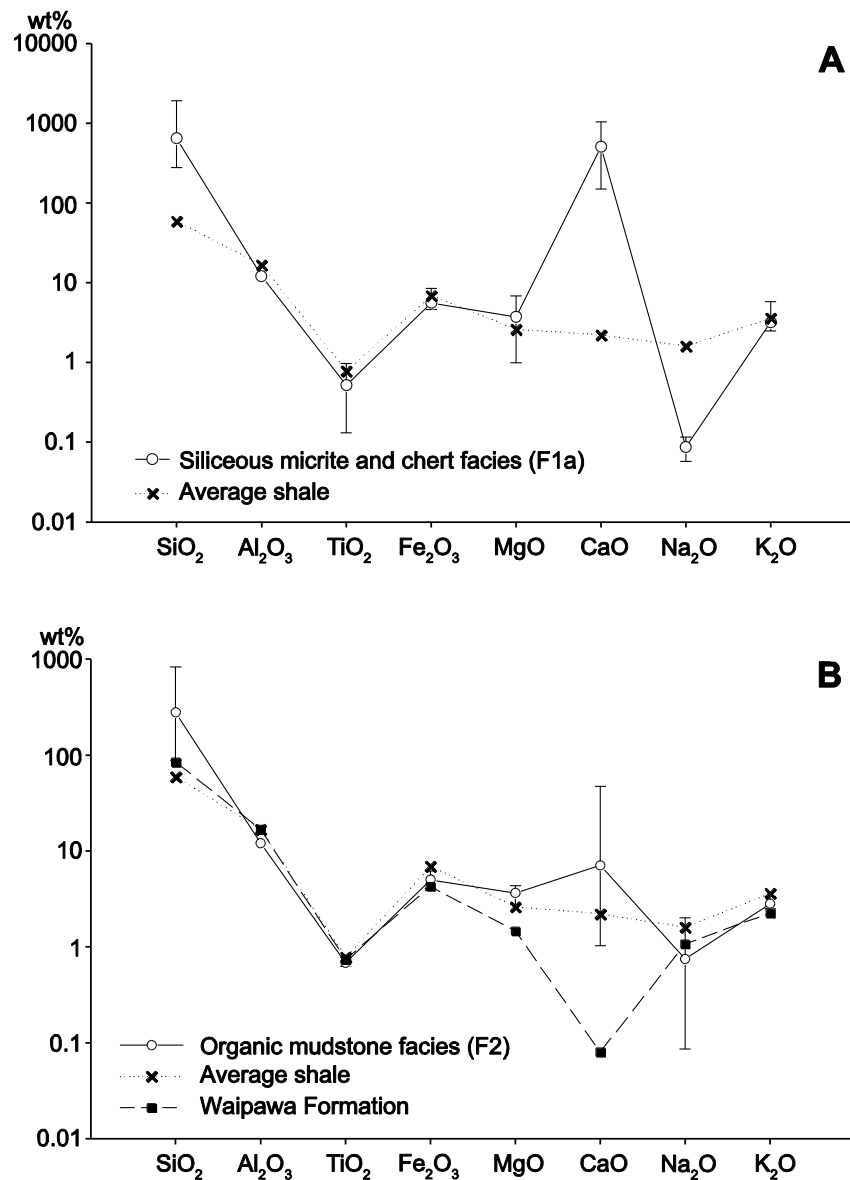


**Figure 4.12** Al normalised major element concentrations (range and mean values) for the two facies identified during field work at Mead Stream compared against average shale (Wedepohl 1971) and Waipawa Formation concentrations (Moore 1988). (A) Siliceous micrite and chert facies (F1a); (B) Organic mudstone facies (F2). Vertical bars indicate range of values.

#### *Organic mudstone facies (F2)*

Al normalised major elemental concentrations in samples from the organic mudstone facies (F2) at Mead Stream are 'normal' with respect to average shale concentrations (Figure 4.12B). However, samples of F2 at Mead Stream have significantly enriched Al normalised  $\text{CaO}$  concentrations

when compared with average values from the Waipawa Formation from the east coast of the North Island (Moore 1988).

### *Discussion*

Consistently high Al normalised values for SiO<sub>2</sub> and CaO (>100 wt%) in the siliceous micrite and chert facies (F1a) at Mead Stream reflect the large biogenic component of the primary sediments. High CaO concentrations in the organic mudstone facies (F2) can be considered a characteristic feature of the Waipawa Formation at Mead Stream (Killops et al. 2000).

### **Trace Elements**

#### *Siliceous micrite and chert facies (F1a)*

Al normalised trace elemental concentrations of samples from the siliceous micrite and chert facies (F1a) are consistently higher than values from average shale, with Sr and Ba being enriched by over two orders of magnitude (Figure 4.13A). Only Rb and Zr can be considered 'normal'.

#### *Organic mudstone facies (F2)*

Al normalised trace elemental concentrations in samples of the organic mudstone facies (F2) are also consistently higher than values of the average shale (Figure 4.13B). This pattern is similar to that observed in F1a, but occurs to a lesser degree, with only U, Th, La, Y, Cr, Sr, and Ba having ranges above average shale values, while the range of concentration for Nb and Rb are both lower than average shale.

### *Discussion*

Samples from both F1a and F2 show almost identical trends their Al normalised elemental concentrations. This would suggest that the source of terrigenous material for both the siliceous micrite and chert facies (F1a) and the organic mudstone facies (F2) at Mead Stream remained constant through the deposition of both facies. It is possible that the consistently high trace elemental concentrations observed in F1a are the result of Al normalisation. Overestimation of all trace elements could have occurred

as a result of overestimation of background  $\text{Al}_2\text{O}_3$  values (12% after Hollis et al. 2003b) used in the normalising equation.

Low  $\text{Al}_2\text{O}_3$  concentrations in this facies, combined with the affect of assuming an average background  $\text{Al}_2\text{O}_3$  of 12% (after Hollis et al. 2003c) could have lead to consistent over estimation of all trace elements.

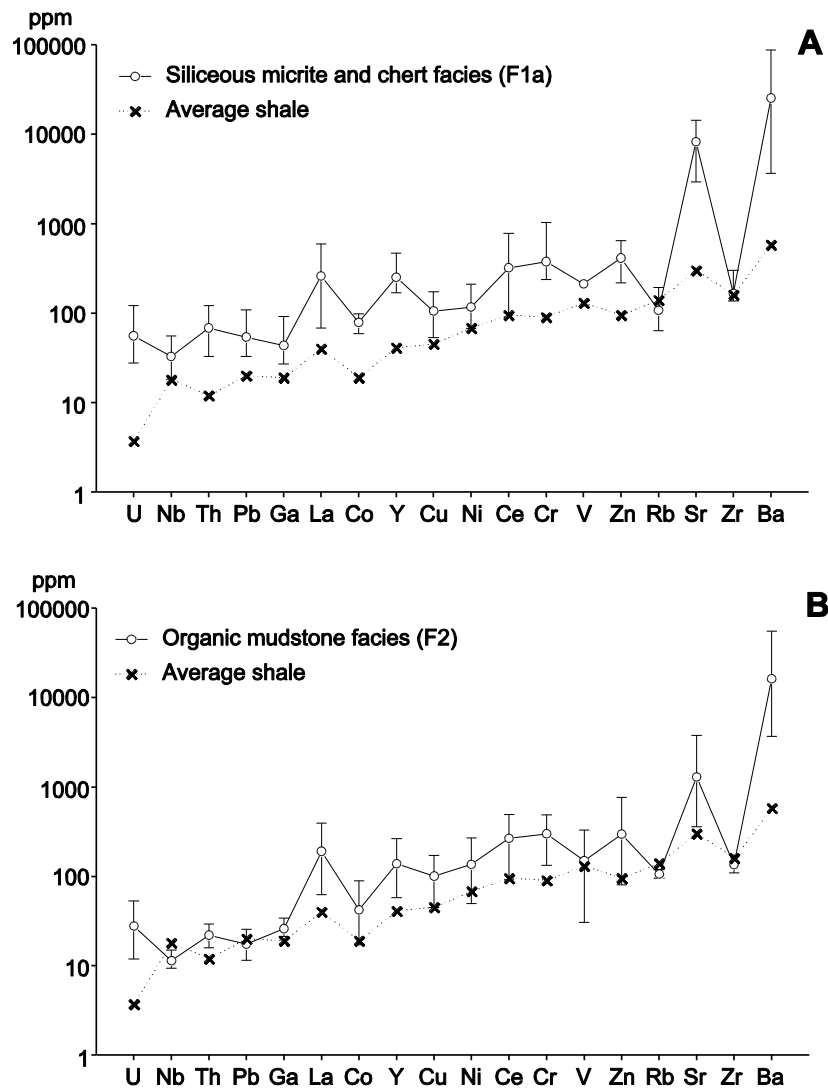


**Figure 4.13** Al normalised trace element concentrations (range and mean values) for the two facies identified during field work at Mead Stream compared against average shale concentrations (Wedepohl 1971). (A) Siliceous micrite and chert facies (F1a); (B) Organic mudstone facies (F2). Vertical bars indicate range of values.

### Compositional Plots

On a ternary plot of the three major chemical components of sedimentary rocks,  $\text{Al}_2\text{O}_3$ ,  $\text{SiO}_2$  and  $\text{CaCO}_3$ , representing clays, quartz and/or biogenic

silica and calcium carbonate, it is clear that the two facies identified at Mead Stream possess distinct geochemical compositions (Figure 4.14A).

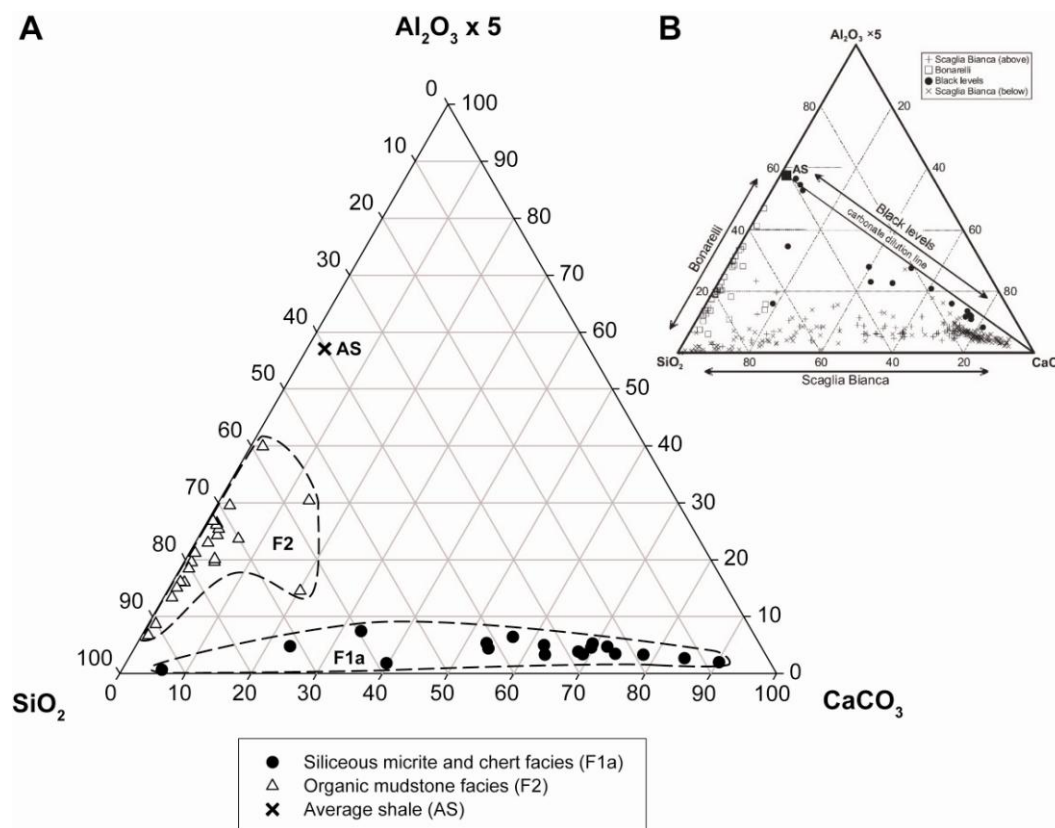


**Figure 4.14** (A) Ternary diagram of relative proportions of  $\text{Al}_2\text{O}_3$  ( $\times 5$ ),  $\text{SiO}_2$  and  $\text{CaCO}_3$  in the siliceous micrite and chert facies (F1a) and organic mudstone facies (F2) from Mead Stream. An arbitrary multiplier of 5 is used for  $\text{Al}_2\text{O}_3$  in order to better distribute the data points within the graph (after Turgeon & Brumsack 2006). (B) Comparative ternary diagram of relative proportions of  $\text{Al}_2\text{O}_3$  ( $\times 5$ ),  $\text{SiO}_2$  and  $\text{CaO}$  from the Furlo section, Umbria-Marche Basin, Italy (Turgeon & Brumsack 2006). Average shale plot (Wedepohl 1971) is shown.

F1a falls in an arching trend along the axis between the  $\text{SiO}_2$  and  $\text{CaCO}_3$  poles. This ternary plot shows that F1a ranges between highly siliceous and highly calcareous sediments. F2 falls along the axis between  $\text{Al}_2\text{O}_3$  and  $\text{SiO}_2$  below the composition of average shale. Rare samples are more calcareous in nature; however the majority of samples are siliceous with varying quantities of clay.

Turgeon & Brumsack (2006) described similar compositional trends from the Furlo section in the Umbria-Marche Basin of central Italy (Figure 4.14B). The Scaglia Bianca is a siliceous carbonate unit and is

comparable to the siliceous micrite and chert facies identified at Mead Stream. The Livello Bonarelli is a  $C_{org}$  rich black shale comparable to the Waipawa Formation, deposited during an ocean anoxic event at the Cenomanian/Turonian boundary (OAE2) during the Late Cretaceous (Turgeon & Brumsack 2006).

### **Proxies**

Geochemical proxies show distinct trends throughout the measured section from Mead Stream (Figure 4.15). Terrigenous sediment input (TRG), a proxy for clay content of the sample based on  $TiO_2$  concentration, is low (~5%) throughout F1a, both below and above the Waipawa Formation (Figure 4.15B). TRG increases markedly through both units of F2, with values fluctuating from a maximum of ~75% to as low as ~20%. Elevated TRG is associated with argillaceous mudstone interbeds while siliceous mudstone beds tend to have lower TRG values.

Paleoproductivity proxies ( $Si[exc]$ ,  $Ca[exc]$  and  $Ba[exc]$ ) show dramatic shifts through the Waipawa Formation (Figure 4.15C, D, E). Excess silica ( $Si[exc]$ ) and total silica ( $SiO_2[tot]$ ) start at ~10 wt% and increase through the basal F1a unit.  $Si[exc]$  and  $SiO_2[tot]$  remain very close to one another, a trend that is consistent throughout F1a, suggesting that silica in this facies is mostly biogenic in origin. Both  $SiO_2[tot]$  and  $Si[exc]$  decrease to ~30 wt% in the period separating Mudstone A and B before increasing to ~90 wt% in Mudstone B.  $Si[exc]$  increases through both F2 units, signifying an increase in siliceous productivity during the deposition of these units. Divergence between  $Si[exc]$  and  $SiO_2[tot]$  signifies that high  $SiO_2$  values in F2 are a result of influx of both biogenic and detrital silica.

Excess calcium ( $Ca[exc]$ ), a proxy for calcareous productivity (Hollis et al. 2003c), shows that throughout the deposition of the siliceous micrite and chert facies (F1a), calcareous productivity was high and remained relatively constant (~80 wt%), only decreasing in the metre of sediment underlying the base of the Waipawa Formation. However, throughout the



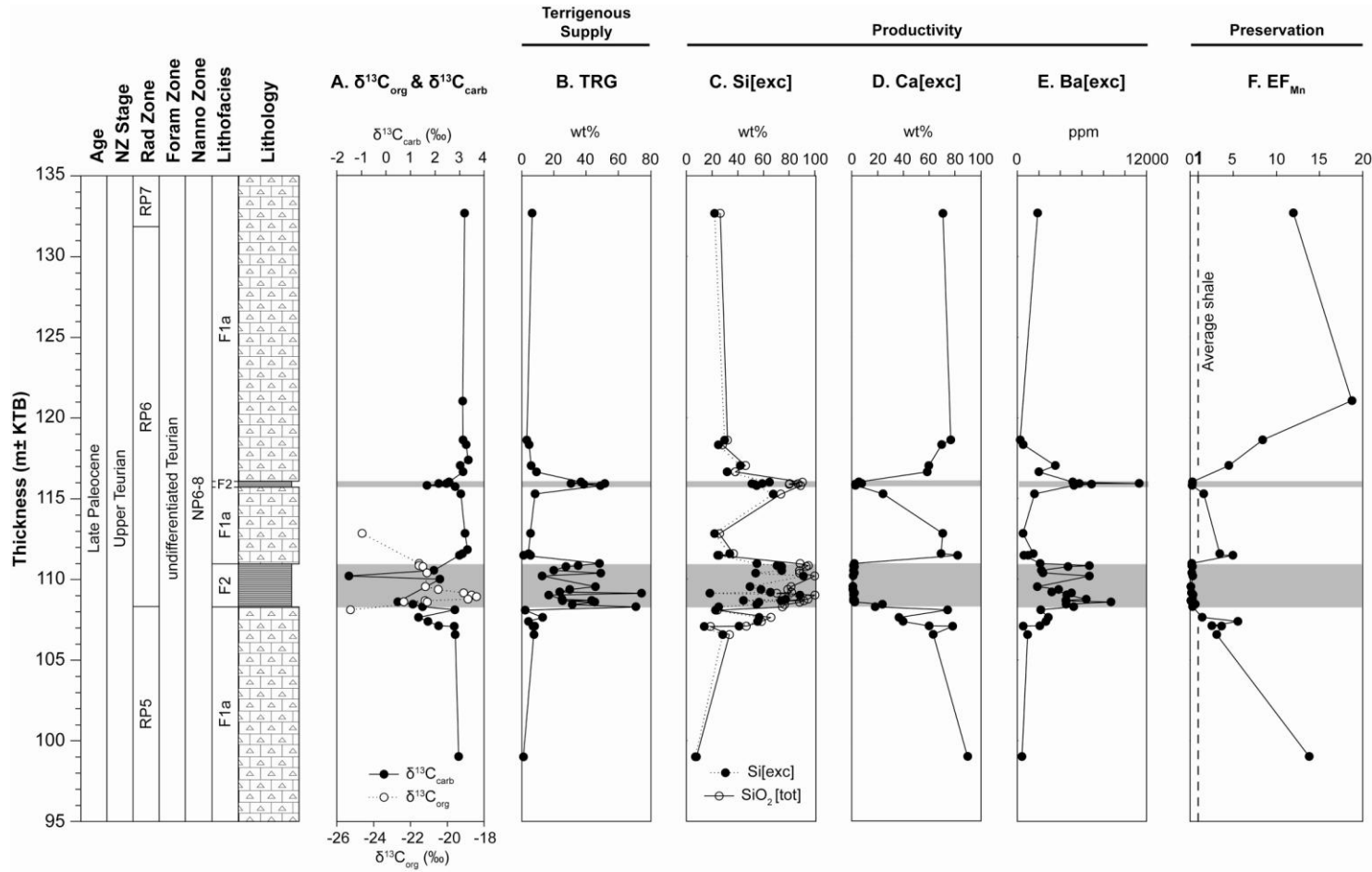


**Figure 4.15** Variations in (A)  $\delta^{13}\text{C}_{\text{org}}$  and  $\delta^{13}\text{C}_{\text{carb}}$ , (B) terrigenous sediment (TRG), (C) excess silica (Si[exc]), (D) excess calcium carbonate (Ca[exc]), (E) excess barium (Ba[exc]), and (F) enrichment factor of manganese ( $\text{EF}_{\text{Mn}}$ ) at Mead Stream.

deposition of F2, Ca[exc] is very low, ~1 wt%, indicating a dramatic decrease in calcareous productivity through this period.

The siliceous micrite and chert facies (F1a) shows relatively constant excess barium (Ba[exc]) concentrations, between ~1000 ppm and ~2000 ppm (Figure 4.15E). Ba[exc] increases markedly through both F2 units, reaching a maximum of ~12000 ppm in Mudstone B, but generally fluctuating between ~4000 ppm and ~6000 ppm. Ba[exc] is significantly correlated with SiO<sub>2</sub>, further supporting the suggestion of increased siliceous productivity through the Waipawa Formation.

Enrichment factor of manganese (EF<sub>Mn</sub>) is used here as a proxy for paleo-redox conditions. Soluble Mn<sup>2+</sup> will diffuse from sediments into oxygen-depleted bottom waters under reducing conditions at the sediment/water interface, leading to depletion of Mn with respect to concentrations observed in average shale (Turgeon & Brumsack 2006) (discussed Chapter 5). Therefore, sediments significantly depleted in Mn (EF<sub>Mn</sub> < 0.5) are inferred to be deposited under dysoxic or anoxic conditions.

Figure 4.15F shows that EF<sub>Mn</sub> in F1a is consistently above 1, with samples from the Mead Hill Formation and Amuri Limestone both showing EF<sub>Mn</sub> above 5. F2 shows depletion of Mn below a level of 0.5.

### ***Stable Isotope Geochemistry***

The δ<sup>13</sup>C of bulk carbonate through the measured section at Mead Stream is consistently high (~3‰) in F1a, with two negative carbon isotope excursions occurring within the organic mudstone facies (F2) units. The first carbon isotope excursion starts ~1 m below the base of Mudstone A, with δ<sup>13</sup>C values within Mudstone A ranging between 2.20‰ and -1.51‰. δ<sup>13</sup>C values from Mudstone B range between 1.67‰ and 2.57‰.

δ<sup>13</sup>C<sub>org</sub> values at Mead Stream were only determined for Mudstone A with values at the top of the Mead Hill Formation and siliceous micrite unit separating Mudstone A and B being -25.3‰ and -24.6‰ respectively. δ<sup>13</sup>C<sub>org</sub> values from -21.5 to -18.4‰ are consistent with values reported

from the Tartan Formation, a Waipawa Formation equivalent from the Great South Basin (Schjøler et al. 2010 and references there in). This positive carbon isotope excursion of ~7‰ through Mudstone A agrees with the results of Killops et al. (2000) and Schjøler et al. (2010).

#### 4.4 LITHOFACIES AT MUZZLE STREAM

##### 4.4.1 Site Description

Field work at Muzzle Stream in the middle Clarence Valley was carried out on 16/1/2008. Access to Muzzle Stream is by private 4WD track through Bluff and Muzzle stations via Kekerengu and Coverham.

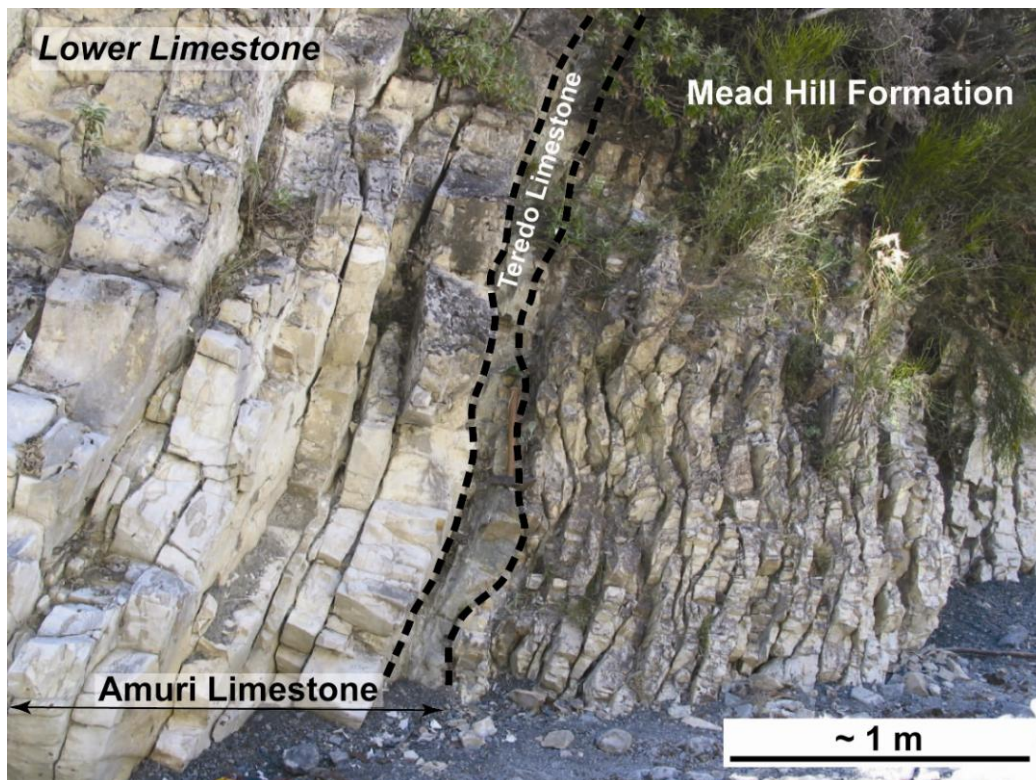


**Figure 4.16** Logged section from Muzzle Stream showing the relationship between the Mead Hill Formation and overlying Amuri Limestone (NZMS 260 O30 613025).

Isoclinal folding related to strike-slip faults results in three or more repeated sections at Muzzle Stream (Reay 1993; Hollis et al. 2005c). The section studied was the second repeated section in the west branch of Muzzle Stream (NZMS 260 O30 613025), above the confluence with Muzzle Stream proper. Beds at this location dip steeply ( $212/64^{\circ}$  NW) and although the interval of interest crops out on both sides of the stream, it was chosen to log and collect samples from the true left bank only (Figure 4.16).

#### 4.4.2 Field Descriptions

Two formations are identified in the Muzzle Stream section, the Mead Hill Formation and the Amuri Limestone which contains the Teredo Limestone Member and Lower Limestone lithotype. Within these formations, three lithofacies have been identified as part of this study: the siliceous micrite and chert facies (F1b), greensand facies (F4a) and micrite facies (F3a) (Figure 4.17).

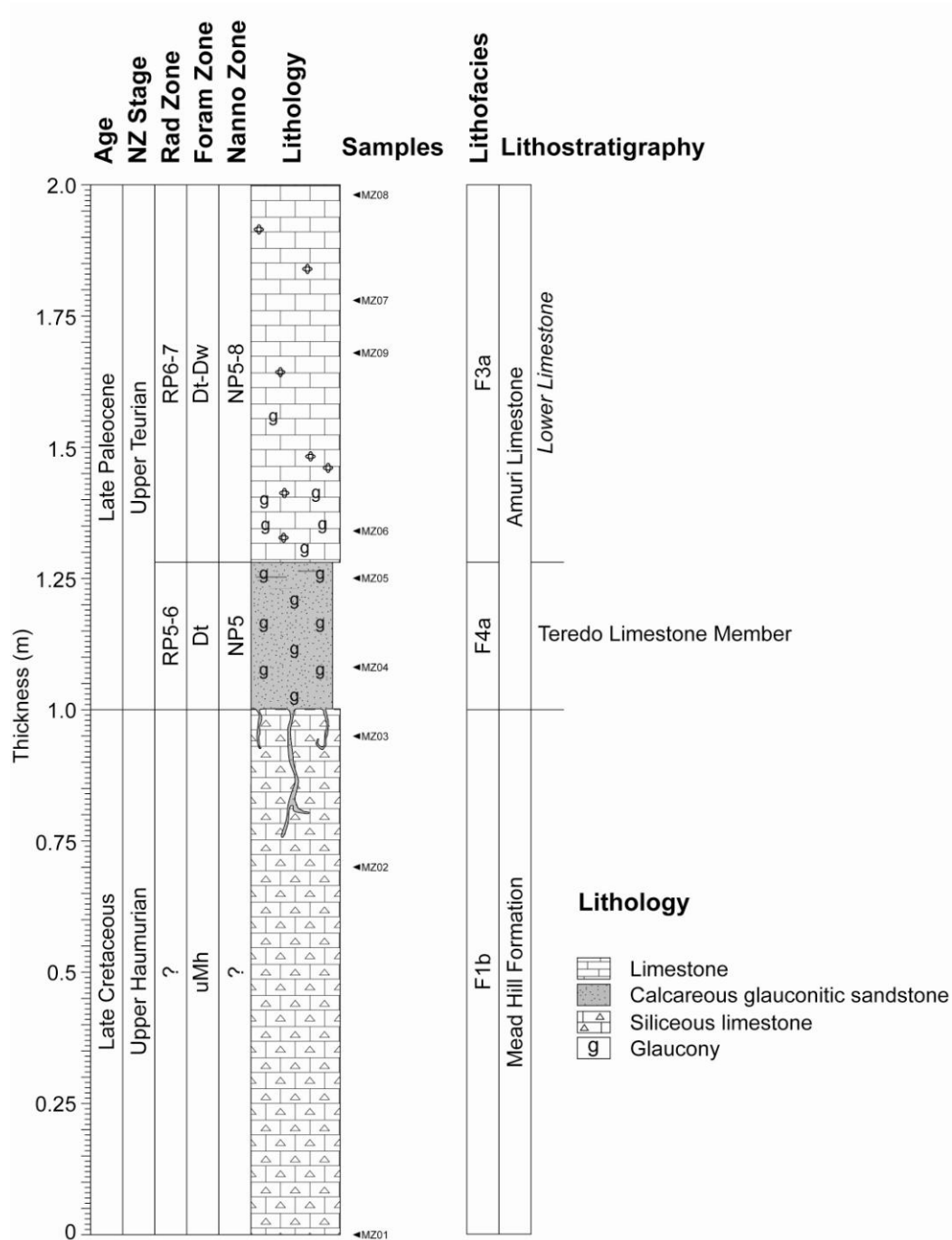


**Figure 4.17** Stratigraphic column of Late Cretaceous-Late Paleocene strata at Muzzle Stream. Age control after Hollis et al. (2005). Lithostratigraphy after Reay (1993), italics denotes informal lithotype. Lithology, lithofacies and samples (this study).

*Siliceous micrite and chert facies (F1b)*

F1b at Muzzle Stream consists of cream siliceous micrite interbedded with mm argillaceous beds. This facies is wavy bedded, leading to a lozenge-like or pinch-and-swell appearance of beds, with maximum bed thicknesses between 8 and 18 cm thick (Figure 4.16). F1b is slightly weathered but, because of its silica content as shown by a conchoidal fracture, results in F1b being hard to very hard.

F1b at Muzzle Stream contains some chert nodules which are dark grey to black in colour and generally possess an elliptical shape in cross section.

Bioturbation is common throughout F1b. *Zoophycus* trace fossils are ubiquitous; while *Thalassinoides* burrows extend down into the uppermost siliceous micrite and chert facies from the overlying greensand facies (Figure 4.18). F1b also contains prominent joints and calcite healed veins running perpendicular to bedding.



**Figure 4.18** *Thalassinoides* burrows infilled with greensand facies in a hand sample (MZ03) of the siliceous micrite and chert facies (F1b) from Muzzle Stream.

### *Greensand facies (F4a)*

F4a consists of grey green, calcareous, glauconitic, massive sandstone. The majority of the facies is sandy, but F4a becomes more argillaceous in its uppermost 5 cm (Figure 4.17). F4a is slightly to moderately weathered and hard to moderately hard, although in the argillaceous layer the induration decreases resulting in a recessive appearance. At Muzzle Stream, the greensand facies is 15-28 cm thick, the large variation in thickness resulting from the wavy nature of the topmost beds of the underlying siliceous micrite and chert facies. Glaucony consists of green to dark green, subangular to rounded, fine to medium sand grains. Glaucony is concentrated (~10%) in the sandy basal zone and decreases upsection to ~5% in the upper argillaceous layer.

As stated above, *Thalassinoides* burrows, up to 5 cm in diameter, extend down ~25 cm from the base of the greensand facies into the underlying siliceous micrite and chert facies. Burrows run both perpendicular and parallel to bedding and are infilled with F4a from the overlying unit (Figure 4.18).

It is suggested here that this unit represents a significant unconformity, based on the identification of extensive *Thalassinoides* burrowing at the base of the unit, the thickness variations of the unit and the presence of glaucony. This is consistent with previous interpretations made by Reay (1993) and Hollis et al. (2005c).

### *Micrite facies (F3a)*

The micrite facies at Muzzle Stream consists of cream, indurated micrite beds, 15 to 30 cm thick interbedded with thin (2-10 mm) marl beds. F3a beds generally show a more tabular geometry and increased bed thickness in comparison to the siliceous micrite facies (Figure 4.16). F3a is slightly weathered and hard to moderately hard. Brownish green to dark green, subangular to rounded, fine sand sized glaucony is present within the basal 40 cm of the facies, making up <2% of the total rock. Glaucony is concentrated along bioturbation structures. 40 cm above the lower contact with F4a, glaucony appears to absent.

Bioturbation is widespread throughout F3a, *Zoophycus* and *Chondrites* being the most commonly identified trace fossils. This facies also contains raised, ring like structures (Figure 4.19). These structures were originally suggested to be related to bioturbation, however in thin section they are light brown and are similar in appearance to chert nodules. The possibility that these ring structures represent the early stages of chert formation is supported by their non-luminescence observed under CL light, a characteristic of authigenic silica, as well as the concentration of silica measured by energy dispersive spectroscopy (EDS).



**Figure 4.19** Raised irregular, ring structures in the micrite facies (F3a) at Muzzle Stream.

#### **4.4.3 Petrography and Mineralogy**

##### *Siliceous micrite and chert facies (F1b)*

The siliceous micrite and chert facies at Muzzle Stream consists of light grey to brownish grey, clotted micrite (Figure 4.20A). It includes some siliciclastic grains (~5%), dominated by coarse silt sized, subrounded to subangular quartz grains. Rare authigenic pyrite, identified by the pale

bronze colour under reflected light, is present both as grains and as infills within radiolarian tests throughout F1b.

Visible microfossils are not abundant (~5%) and poorly preserved, showing recrystallised textures that obscure structural features, with tests tending to be silicified and infilled with microcrystalline silica so that identification is difficult. Overall, F1b appears to predominantly contain radiolarians and siliceous sponge spicules as well as less common planktic foraminifera and fragmented tests. Sponge spicules in MZ03 exhibit parallel alignment, suggesting the influence of bottom currents (Flügel 2004).

Veins identified in the field are generally infilled with dusty, calcite spar cement in thin section. Veins are variable in thickness, ranging from ~0.01 mm to ~1.0 mm, and generally run parallel to each other. Occasionally the veins have multiple stages of vein infill, with an initial siliceous infill followed by a subsequent period of calcite cement infill (Figure 4.20A, B).

#### *Greensand facies (F4a)*

In thin section, the greensand facies is characterised by a mixture of detrital, perigenic and biogenic grains set in a matrix of microcrystalline carbonate. Matrix makes up ~45% of the total sample in the majority of the facies resulting in a grain supported fabric. In the upper, more argillaceous portion of the greensand facies at Muzzle Stream, the proportion of matrix in the sample increases to 60% and grains appear to be mud supported.

Visible siliciclastics are dominated by well sorted, subangular to subrounded, fine to very fine sand sized quartz grains (~25%), along with some K feldspar (~5%) and rare plagioclase feldspar and muscovite. Differentiation between quartz and feldspar grains was difficult due to a lack of distinctive optical features. Morris (1987) encountered similar problems and therefore relied on the degree of alteration of feldspar grains to distinguish feldspar grains from quartz. In this study, feldspars were identified under CL light, with K feldspars and plagioclase tending to

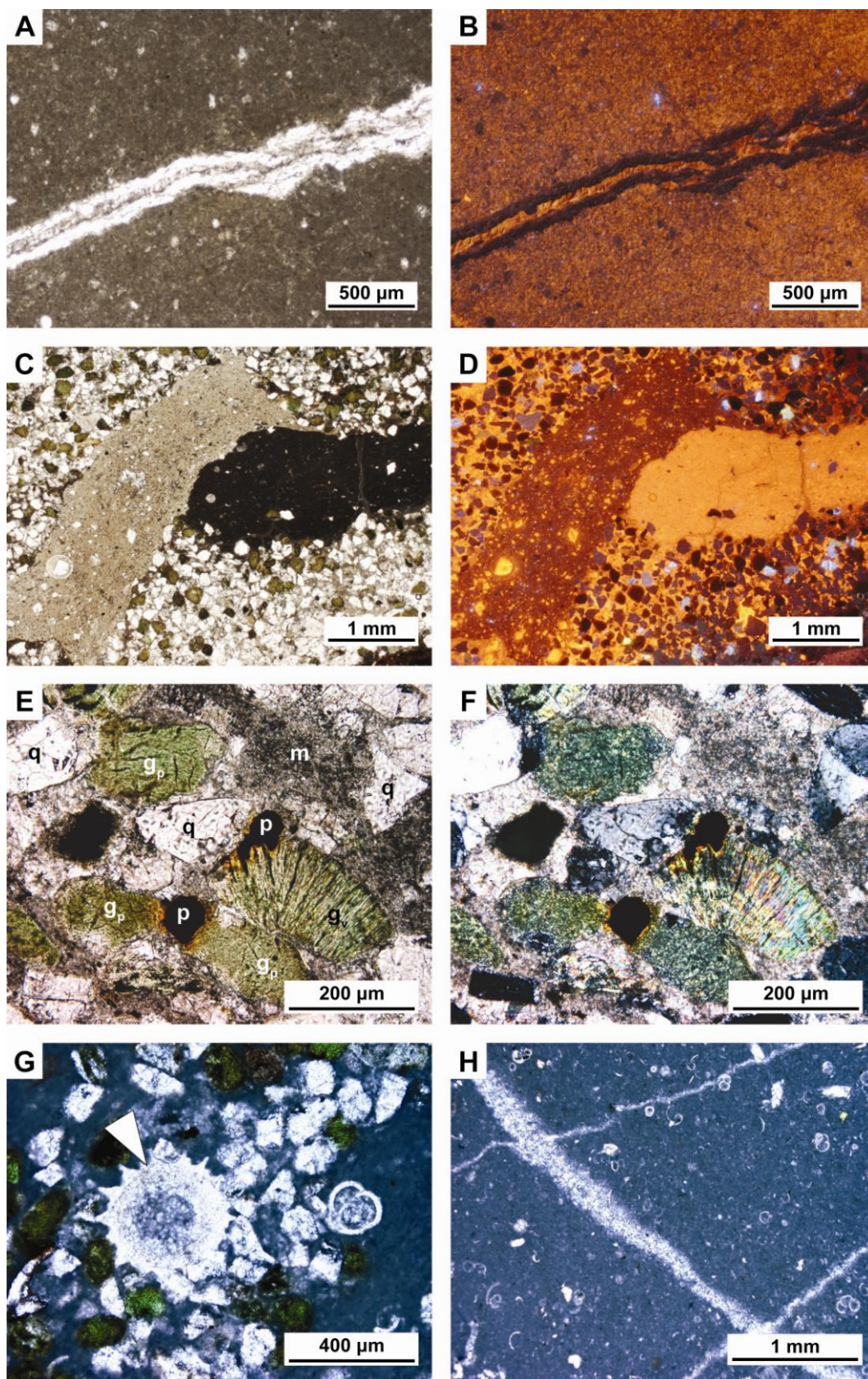


exhibit bright blue and yellowish green luminescence, respectively, while detrital quartz tends to exhibit dull blue colours for the same excitation conditions (Marshall 1988) (Figure 4.20D). Authigenic pyrite is rare but ubiquitous in F4a and is identified by the brassy yellow colour under reflected light. Rare lithics identified in thin section of the uppermost sample collected from the greensand facies consist of well rounded microcrystalline chert fragments.

Perigenic grains observed in the greensand facies from Muzzle Stream consist of glaucony and phosphatic grains. Glaucony grains are dominated by bright green, microcrystalline, pelletal forms inferred to represent glauconitised faecal pellets. Some grains have brownish red rims as a result of limonite staining, with the majority of glaucony grains exhibiting dehydration fractures. Vermicular grains of glauconitised biotite are relatively common (3-5%), identified by light to dark green pleochroism and high order interference colours under cross polarised light (Figure 4.20E, F). Glaucony grains are moderately to well sorted, with a modal

---

**Figure 4.20** Photomicrograph pairs under plane polarised light (left) and cathodoluminescence light (right) of selected samples from Muzzle Stream. (A) & (B) Vein cutting siliceous micrite from Muzzle Stream (F1c) (MZ01). Outer edges of vein shows dark reddish brown colours characteristic of authigenic silica while infill of the vein is orange, characteristic of calcite. (C) & (D) Multiple phases of burrow infill recorded in the greensand facies (F4a) from Muzzle Stream (MZ04). Note that the brown siliceous burrow running from the top middle of the image to bottom left of image, shows dark reddish brown luminescence characteristic of authigenic silica, while the dark brown micrite filled burrow in the middle right of the image shows bright orange luminescence characteristic of calcite. Siliciclastic grains are dominated by dull brownish red and blue quartz grains with some bright blue K feldspar grains. Photomicrograph pairs under plane polarised light (E) and cross polarised light (F) of the greensand facies (F4a) (MZ04). Characteristic grains of the greensand facies (F4a) from Muzzle Stream. q: detrital quartz; m: microcrystalline carbonate cement; p: pyrite; g<sub>p</sub>: microcrystalline pelletal glaucony; g<sub>v</sub>: vermicular glauconitised biotite grain. Note the 3<sup>rd</sup> and 4<sup>th</sup> order interference colours of the vermicular glaucony grain, retaining optical properties of parent the biotite crystal. (G) A radiolarian with well preserved ornate structural features (arrowed) surrounded by siliciclastic grains from the base of the micrite facies (F3a) at Muzzle Stream (MZ06) (PPL). (H) Intersecting calcitic veins in the micrite facies from Muzzle Stream (MZ06) (PPL). Note the low proportion of visible foraminiferal tests and micro-shell fragments.



size of 0.2 mm. Phosphatic grains are generally subangular to rounded, make up approximately 2% of the total sample in thin section, and range in size from 0.025 mm to 0.3 mm. These grains are identified by their orange-brown colour and nearly isotropic extinction behaviour under cross polarised light.

Microfossils observed in F4a include rare planktic foraminifera, spumellarian radiolarians and sponge spicules, making up less than 1% of the total sample in thin section. Microfossils are concentrated in micritic burrows with few or no siliciclastics and their tests are generally infilled with micrite or rarely sparry calcite cement, showing better preservation than those observed in the underlying siliceous micrite and chert facies.

Bioturbation is common throughout, resulting in the relative concentration or depletion of siliciclastic grains in certain areas. Multiple phases of burrow infill are preserved, possibly recording lithologies present prior to mixing as a result of bioturbation (Figure 4.20C, D). A large, elliptical pyritised burrow containing a small number of angular to subrounded siliciclastic grains was also observed in MZ04.

#### *Micrite facies (F3a)*

In thin section, F3a is generally characterised by light grey, clotted micrite containing up to 10% planktic foraminifera. SEM analysis of F3a shows that this facies is dominated by recrystallised microcrystalline spar with less commonly identifiable detrital carbonate grains in the form of coccolith debris. Grain size ranges from 0.5 to ~3  $\mu\text{m}$ .

Siliciclastic grains in the form of moderately sorted, subangular to subrounded, very fine sand to silt sized, detrital quartz, feldspar and muscovite, along with authigenic pyrite, perigenic glaucony and phosphatised grains, make up to 5% of the lowermost sample collected from the base of F3a (Figure 4.20G). Grains are concentrated within bioturbation structures. The abundance of these grains decreases rapidly away from the contact with the underlying greensand facies, making up

less than 1% in the three uppermost samples collected from this section (MZ07, MZ08 and MZ09).

Microfossils identified in thin sections from F3a are dominated by planktic foraminifera, with a few benthic foraminifera, radiolarians and other micro-shell fragments (Figure 4.20G, H). These increase from 10% at the base of the facies to 15% at the top of the measured section. Preservation of microfossil tests varies, although the majority of tests and shell fragments show significant recrystallisation with tests being predominantly infilled with micrite, while rare tests are infilled with sparry calcite cement or microcrystalline silica.

Veins identified in the field range in thickness from 0.025 mm to 30 mm and are infilled with dusty calcite spar cement, with crystals reaching 1.25 mm in size (Figure 4.20H).

#### **4.4.4 Geochemistry**

##### ***Inorganic Geochemistry***

The elemental concentrations of F1b, F4a and F3a are compared with average shale values of Wedepohl (1971) for both major and trace elemental concentrations so as to allow for comparisons between sites. The bulk geochemical data are recorded in Appendix D.

##### ***Major Elements***

###### ***Siliceous micrite and chert facies (F1b)***

The siliceous micrite and chert facies (F1b) at Muzzle Stream have 'normal' concentrations of  $\text{TiO}_2$  and  $\text{K}_2\text{O}$  with respect to average shale (Figure 4.21A).  $\text{SiO}_2$ ,  $\text{MgO}$  and  $\text{CaO}$  are all significantly higher than average shale concentrations while  $\text{Fe}_2\text{O}_3$  and  $\text{Na}_2\text{O}$  are lower. Depletion of  $\text{Na}_2\text{O}$  is so great that no samples from this facies had concentrations above detectable limits.

### Greensand facies (F4a)

The greensand facies (F4a) at Muzzle Stream is characterised by high Al normalised concentrations of SiO<sub>2</sub>, Fe<sub>2</sub>O<sub>3</sub>, MgO, CaO and K<sub>2</sub>O and low concentrations of TiO<sub>2</sub> (Figure 4.21B).

### Micrite facies (F3a)

Excluding SiO<sub>2</sub>, TiO<sub>2</sub>, CaO and Na<sub>2</sub>O, Al normalised major elemental concentrations in samples from the micrite facies at Muzzle Stream can be considered 'normal' with respect to average shale values (Figure 4.21C). SiO<sub>2</sub> and CaO are significantly higher while TiO<sub>2</sub> and Na<sub>2</sub>O are lower. As with F1b, Na<sub>2</sub>O concentrations are consistently below detectable limits.

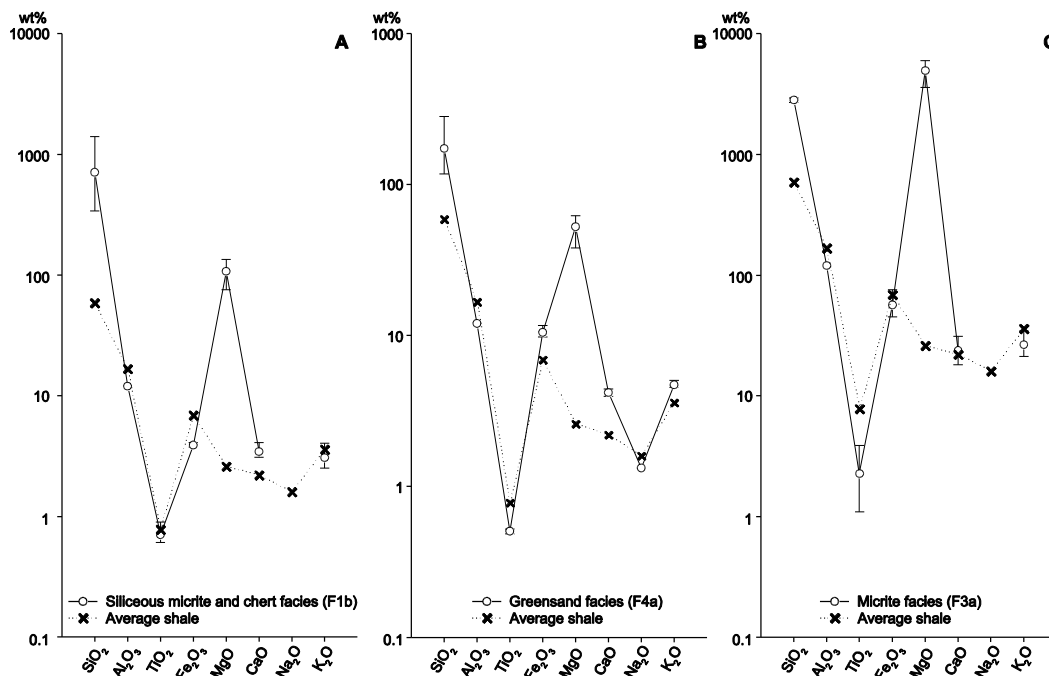


**Figure 4.21** Al normalised major element concentrations (range and mean values) for the three facies identified during field work at Muzzle Stream compared against average shale (Wedepohl 1971). (A) Siliceous micrite and chert facies (F1b); (B) Greensand facies (F4a); (C) Micrite facies (F3a). Vertical bars indicate range of values.

### Discussion

Consistently high Al normalised values for SiO<sub>2</sub> and CaO (>100 wt%) in samples from F1b and F3a at Muzzle Stream reflect the large biogenic component of the primary sediments. High concentrations of Fe<sub>2</sub>O<sub>3</sub>, MgO and K<sub>2</sub>O in the greensand facies (F4a) are likely to be related to the glaucony within this facies.

## Trace Elements

### *Siliceous micrite and chert facies (F1b)*

Samples from the siliceous micrite and chert facies (F1b) are characterised by high Al normalised trace elemental concentrations with respect to values in average shale (Figure 4.22A). U, Co, Y, Sr and Ba are significantly higher than average shale, while no trace elements are depleted with respect to average shale concentrations.

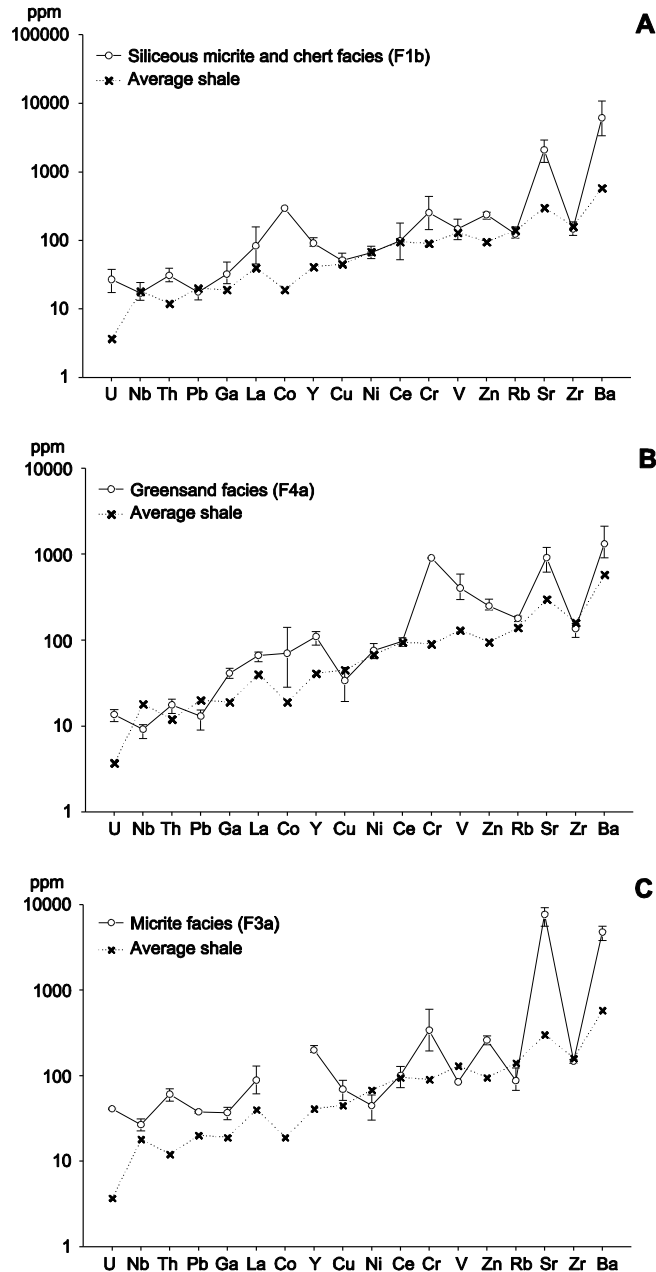


**Figure 4.22** Al normalised trace element concentrations (range and mean values) for the three facies identified during field work at Muzzle Stream compared against average shale concentrations (Wedepohl 1971). (A) Siliceous micrite and chert facies (F1b); (B) Greensand facies (F4a); (C) Micrite facies (F3a). Vertical bars indicate range of values.

### *Greensand facies (F4a)*

The greensand facies (F4a) at Muzzle Stream is characterised by consistently high Al normalised trace elemental concentrations, as only Cu, Ni, Ce and Zr can be considered 'normal' with respect to concentrations in average shale (Figure 4.22B). Excluding Nb and Pb, all other trace elements are high, with the range of measured values falling above their concentration in average shale.

### *Micrite facies (F3a)*

Al normalised trace elemental concentrations in samples from the micrite facies (F3a) at Muzzle Stream are consistently high with respect to trace elemental concentrations in average shale (Figure 4.22C). Only the range of measured values for Cu, V and Rb fall below values for average shale.

### *Discussion*

Trends in trace elemental concentrations in F3a are similar to those observed in F1b, but tend to be exaggerated suggesting a similar source of terrigenous sediment throughout the deposition of both facies. These trends are almost identical to those observed at Mead Stream (Figure 4.13), further supporting a continuous source of terrigenous sediment throughout Late Cretaceous to Late Paleocene in southeastern Marlborough.

Enrichment of the transition elements Cr, V and Zn can be attributed to replacement of  $\text{Fe}^{3+}$ ,  $\text{Fe}^{2+}$  and  $\text{Mg}^{2+}$  at octahedral sites in the glaucony lattice due to similarities in ionic radius and charge (McConchie 1978). This is consistent with enrichment of  $\text{Fe}_2\text{O}_3$ , MgO and  $\text{K}_2\text{O}$  in this facies (Figure 4.21B).

### ***Compositional Plots***

On a ternary plot of the three major chemical components of sedimentary rocks,  $\text{Al}_2\text{O}_3$ ,  $\text{SiO}_2$  and  $\text{CaCO}_3$ , representing clays, quartz and/or biogenic silica and calcium carbonate, it appears that the three facies identified at Muzzle Stream possess rather similar geochemical compositions (Figure 4.23).

Both F1b and F3a fall along the axis between the  $\text{SiO}_2$  and  $\text{CaCO}_3$ , with the siliceous micrite and chert facies plotting towards the  $\text{SiO}_2$  pole, the micrite facies plotting near the  $\text{CaCO}_3$  pole and both facies having low  $\text{Al}_2\text{O}_3$  values. This compositional distribution is similar to that observed for the siliceous micrite and chert facies at Mead Stream (F1a), supporting the observation of similarities between the two sites (Figure 4.14). F4a has a similar composition to F1b, with one sample in particular having very high silica values.

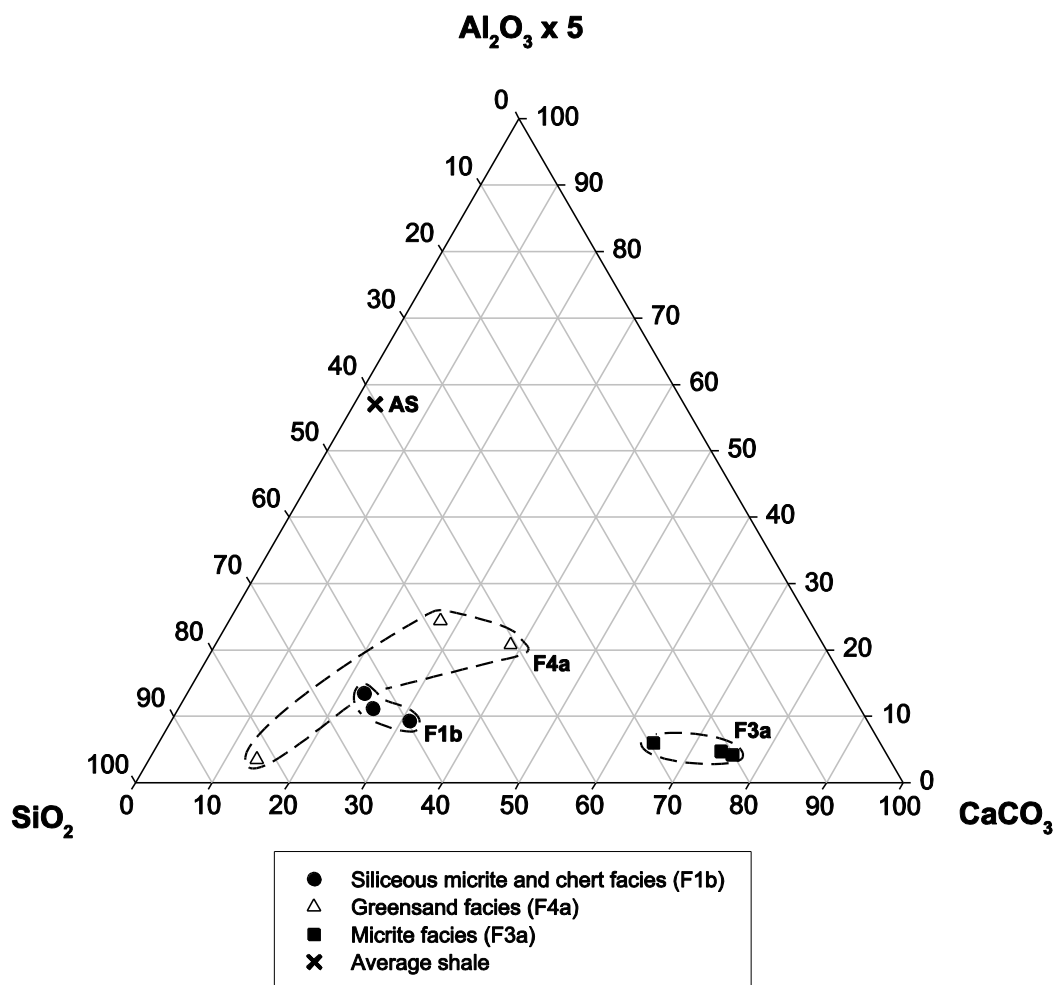


**Figure 4.23** Ternary diagram of relative proportions of  $\text{Al}_2\text{O}_3$  (x5),  $\text{SiO}_2$  and  $\text{CaCO}_3$  in the siliceous micrite and chert facies (F1b), greensand facies (F4a) and micrite facies (F3a) from Muzzle Stream. An arbitrary multiplier of 5 is used for  $\text{Al}_2\text{O}_3$  in order to better distribute the data points within the graph (after Turgeon & Brumsack 2006). “Average shale” (AS) (Wedepohl 1971) is also shown.



## Proxies

Geochemical proxies show distinct trends throughout the measured section from Muzzle Stream (Figure 4.24). Terrigenous sediment input (TRG), a proxy for clay content of the sample based on  $\text{TiO}_2$  concentration, is relatively constant, between 8.5% and 19.6% throughout F1b (Figure 4.24B). TRG then increases to ~30 wt% through the greensand facies, before decreasing steadily through F3a to almost 0 wt% at the top of the measured section.

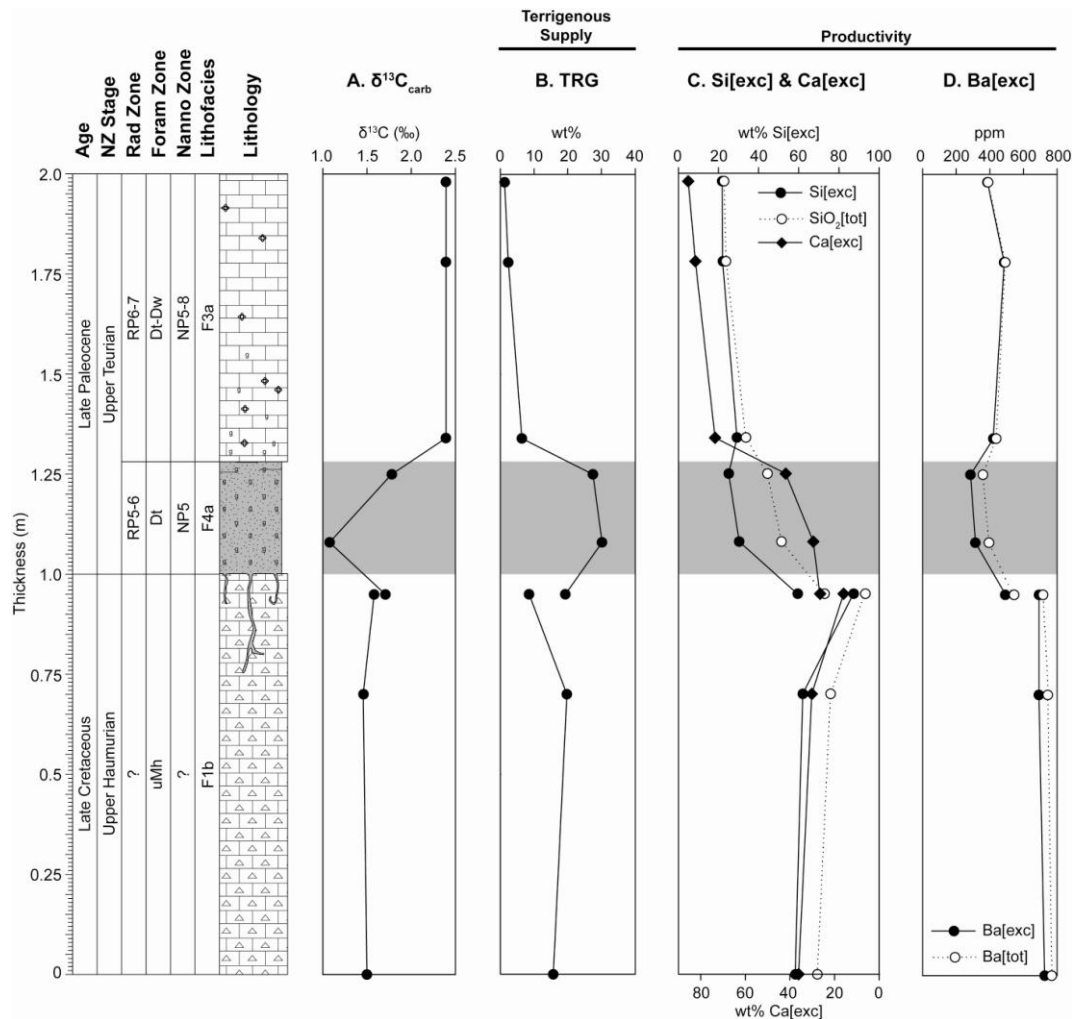


**Figure 4.24** Variations in (A)  $\delta^{13}\text{C}_{\text{carb}}$ , (B) terrigenous sediment (TRG), (C) excess silica and excess carbonate (Si[exc], Ca[exc]), and (d.) barium (total and excess Ba, Ba[exc]) at Muzzle Stream.

Paleoproductivity proxies (Si[exc] and Ca[exc]) show a shift from siliceous to calcareous productivity through the Late Cretaceous to Late Paleocene at Muzzle Stream (Figure 4.24C). Both total silica ( $\text{SiO}_2[\text{tot}]$ ) and excess silica (Si[exc]) are high throughout the siliceous micrite and chert facies (F1b), reaching a maximum of 93.2 wt% and 87.3 wt% in the uppermost

sample, respectively. Si[exc] is highest (59.4 wt%) in a sample of a burrow infilled with F4a collected from the top of F1b and decreases rapidly to remain constant around ~25 wt% throughout both the greensand facies and micrite facies.

Excess calcium (Ca[exc]) decreases through the siliceous micrite and chert facies (F1b), reaching a minimum for the section of 15.9 wt% in the uppermost sample collected from the facies (Figure 4.24C). Ca[exc] then increases steadily through both F4a and F3a from 26.5 wt% in burrows at the top of F1b, through to 85.5 wt% at the top of measured section.

Total barium (Ba[tot]) and excess barium (Ba[exc]) are relatively constant at ~700 ppm throughout the siliceous micrite and chert facies (F1b) at Muzzle Stream (Figure 4.24D). Ba[exc] decreases to ~300 ppm through the greensand facies (F4a), before increasing to between 386 ppm and 485 ppm for the remaining micrite facies (F3a).

### ***Stable Isotopes***

$\delta^{13}\text{C}$  of bulk carbonate from the siliceous micrite and chert facies (F1a) at Muzzle Stream is constant throughout the measured section, remaining at ~1.5‰ (Figure 4.24A). Bulk carbonate  $\delta^{13}\text{C}$  decreases through the greensand facies (F4a), from 1.71‰ in a burrow infilled with F4a in the underlying siliceous micrite facies to 1.08‰ at the base of F4a before returning to 1.78‰ near the upper contact of this facies.  $\delta^{13}\text{C}$  continues to become more enriched in heavy  $^{13}\text{C}$  into the base of F3a, reaching 2.39‰ and remaining constant throughout the rest of the measured section.

## **4.5 LITHOFACIES AT KAIKOURA WHARF**

### **4.5.1 Site Description**

Field work at Kaikoura wharf on the northern side of the Kaikoura Peninsula was carried out between 19/12/2008 and 21/12/2008. The site is located on the southeastern side of the Kaikoura wharf, on the Esplanade (NZMS 260 O30 678657). The rock outcrops are accessible throughout the tide, but best access is between half and low tide.



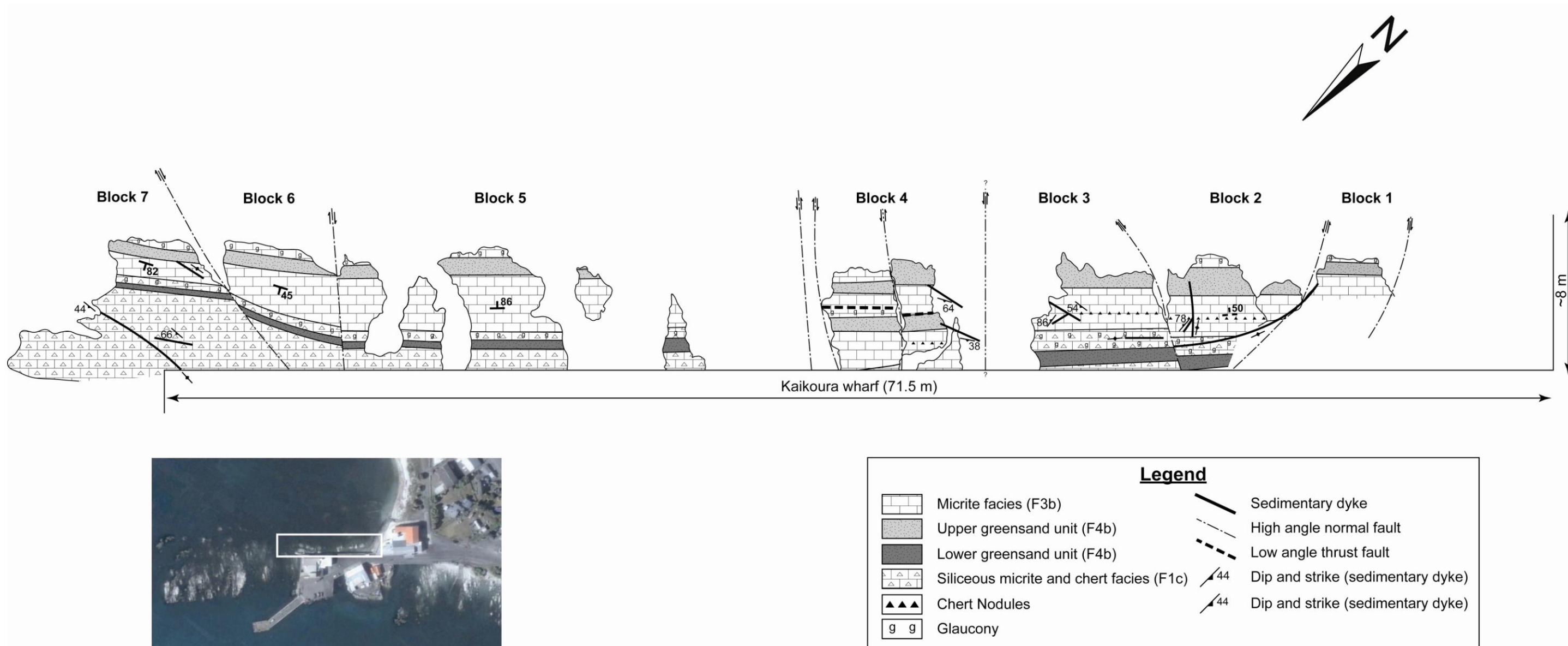


**Figure 4.25** Geological sketch map of the Kaikoura wharf section identifying major lithologic and structural features. Location of maps is identified by white box on aerial photograph.



The contact between the Mead Hill Formation and Amuri Limestone is exposed in an ~80 m (along strike) section along the side of the wharf (Figure 4.25). The length of the exposure allows for observation and description of some significant lateral variations in the deposits. Two distinct levels of bioturbated greensand beds can be used as easily identified marker beds to show that beds are not continuous along the length of the outcrop. Browne et al. (2005a) suggested that the upper greensand unit is complex and that in places (e.g. block 4, Figure 4.25) it is represented by several distinct bioturbated intervals. However, investigation of this site in this study has shown that there are not two burrowed surfaces, but repetition of the same burrowed surface as a result of low angle thrust faulting that strikes parallel to bedding (Figure 4.26). Directly above block 4, beds within the Lower Limestone lithotype of the Amuri Limestone appear to be continuous, placing some constraint on the timing of this deformation. The section is intersected by a number of minor normal faults with offsets of 0.2-0.5 m that cut the section at a high angle to bedding. These faults generally can be traced through the stratigraphy from the base of the wharf and be seen offsetting beds in the overlying Lower Limestone and Lower Marl when the tide is low.

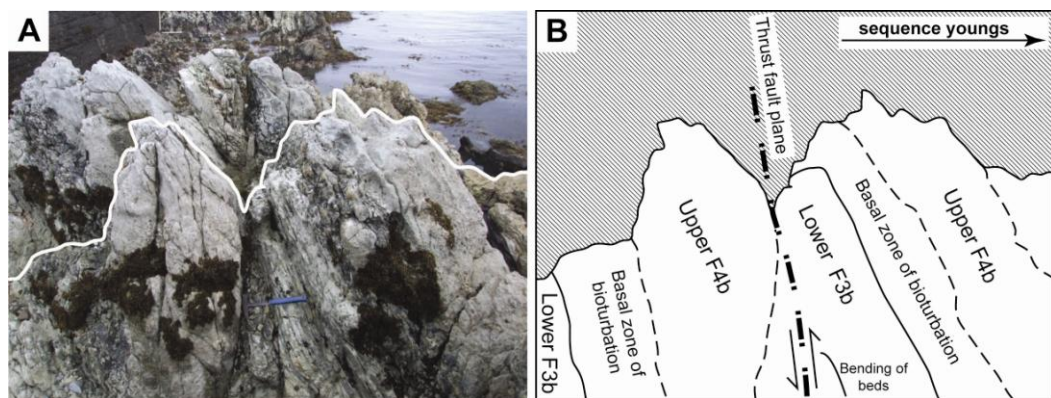


**Figure 4.26** Low angle to bedding thrust fault identified at the Kaikoura wharf (block 4, Figure 4.25), resulting in repetition of the lower micrite facies (F3b) unit and upper greensand facies (F4b) unit. (A) Interpretive sketch of (A), identifying repeated sequence. Direction of movement on this surface is inferred from possible fault drag structures in the overlying F3b unit.

The orientation of beds changes along the length of the section, from 040/50° SE in blocks at the southwestern end of the site, to 044/86° SW in blocks through the central part of the section, while the sedimentary

sequence at the northeastern end of the outcrop is overturned, with beds striking 062° and dipping between 45° and 82° to the northwest. Further to the northeast, inaccessible blocks return to dipping toward the southeast.

Numerous sedimentary dykes are also present within the Late Cretaceous-Early Eocene strata of the Kaikoura wharf section. Features such as lithologic similarities, deformation of bedding planes (Figure 4.27) and termination of dykes show that all sedimentary dykes observed in the Kaikoura wharf section, excluding one, are injected downward from the upper greensand unit. The upward intruded dyke is lithologically identical to the lower greensand unit and the dip and strike of this dyke differs significantly from others observed at this site.

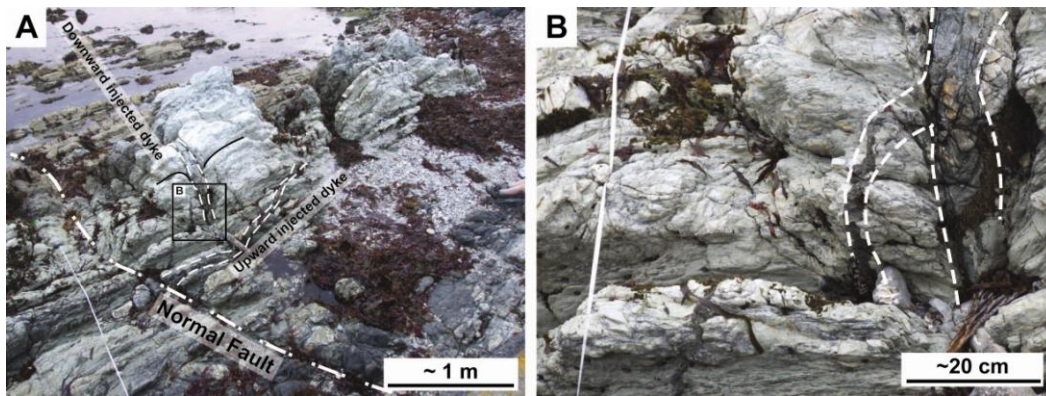


**Figure 4.27.** (A) Sedimentary dykes intersecting the Kaikoura wharf section. Note down-warping of beds adjacent to the downward injected dyke identifying the direction of injection. (B) Large clastic dyke (~10 cm wide) injected down from the upper greensand facies (F4b) unit at Kaikoura wharf which bifurcates away from source.

#### **4.5.2 Field Descriptions**

Morris (1987) identified three formations at the Kaikoura wharf section, which under the revised classification of Reay (1993) are the Mead Hill Formation and the Teredo Limestone Member and Lower Limestone lithotype of the Amuri Limestone (Figure 4.28). As part of this study, three lithofacies have been identified at Kaikoura wharf: siliceous micrite and chert facies (F1c); greensand facies (F4b); and micrite facies (F3b).

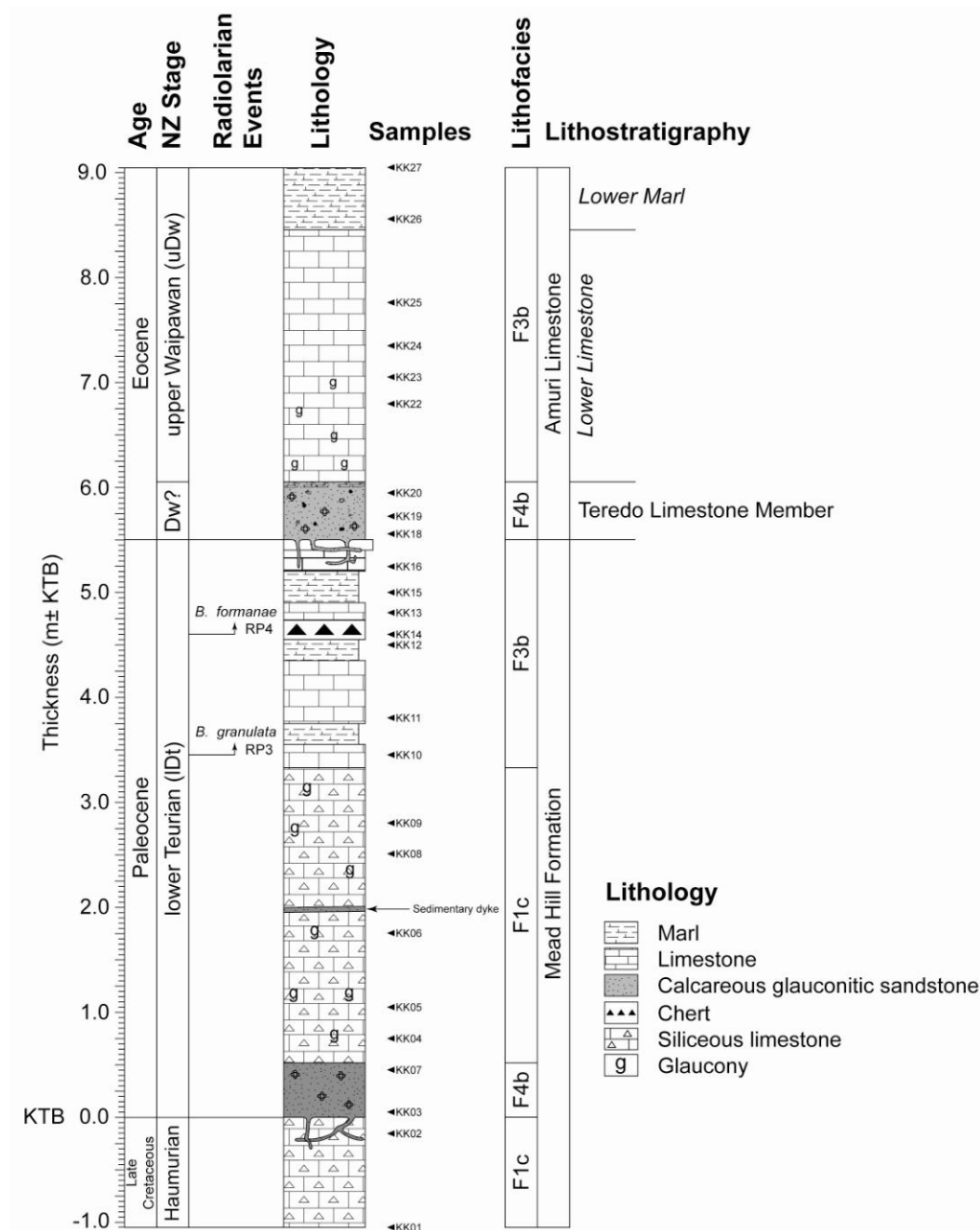


**Figure 4.28** Stratigraphic column of Late Cretaceous-Early Eocene strata at Kaikoura wharf. Age control and radiolarian events after Chris Hollis (pers. comm. 2010). Lithostratigraphy after Reay (1993) and Browne et al (2005a); italics denote informal lithotype. Lithology, lithofacies and samples (this study).

### *Siliceous micrite and chert facies (F1c)*

At the Kaikoura wharf the siliceous micrite and chert facies involves a lower and upper unit, separated by 0.5 m of greensand (Figure 4.29A). The lower unit of F1c, which corresponds with the Mead Hill Formation, consists of light brownish grey siliceous micrite. This unit is wavy bedded which results in a pinch-and-swell appearance, with beds reaching a



maximum thickness of ~10 cm. This unit is slightly weathered and hard to very hard, with the high silica content resulting in conchoidal fracture when fresh samples are broken from the outcrop.

Bioturbation is common in the lower unit of F1c at the Kaikoura wharf, with *Thalassinoides* burrows extending 30 cm into the unit from the overlying greensand facies. Other characteristic features of this facies include prominent calcite healed veins roughly perpendicular to bedding and pyrite nodules ranging in size from 1 to 10 cm. Pyrite nodules are easily identified in outcrop due to limonite staining as a result of weathering. When broken open, these nodules reveal brass yellow, very fine grained pyrite. Lawrence (1993, 1994) noted that pyrite is commonly associated with chert and dolomite in the Muzzle Group throughout southeastern Marlborough.

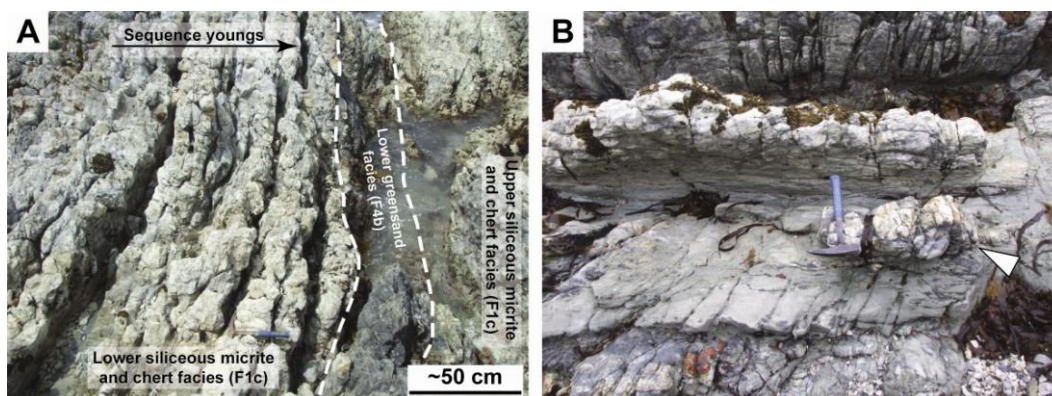


**Figure 4.29** (A) Upper and lower siliceous micrite and chert facies (F1c) units separated by the lower greensand facies (F4b) unit at Kaikoura wharf. Note the knobbly appearance of the lower F1c unit. (B) Prominent chert nodules (arrowed) in the upper siliceous micrite and chert facies (F1c) unit.

The F1c above the lower greensand consists of light greenish grey, glauconitic, fine sandy, siliceous micrite. This upper unit of F1c is coarsely bedded with a knobbly appearance. Beds are ~30 cm thick and contain elliptical concretionary shapes that are assumed to be chert nodules (Figure 4.29B). This unit is slightly weathered, with common limonite staining and is moderately hard to hard. Glaucony makes up 2-3% of the unit and consists of green to dark green, subangular to rounded, fine sand size grains. In the uppermost metre of this unit, the concentration of glaucony grains gives the facies a mm laminated appearance which is

more likely to be the result of concentration by bioturbation than primary sedimentary structures. The contact with the underlying greensand unit is abruptly gradational over 2 cm, suggesting that this contact is conformable.

#### *Greensand facies (F4b)*

The greensand facies consists of two separate units at the Kaikoura wharf section (Figure 4.28).

The lower F4b unit is characterised by ~50 cm of dark greenish grey, massive, calcareous, glauconitic sandstone. The unit is relatively hard and slightly to moderately weathered with limonite stained patches. Glaucony consists of green to dark green, subangular to rounded, fine sand sized grains making up ~5% of the total facies in hand sample. Fine scale bioturbation results in a mm laminated appearance of the unit due to unknown ichnotaxa, while large (~7 cm) elliptical and circular burrows observed in outcrop are tentatively identified as *Scolicia* (Figure 4.30). As stated above, the lower contact of F4b with underlying F1c is highly bioturbated, with *Thalassinoides* burrows infilled with calcareous glauconitic sandstone extending down ~30 cm into the underlying siliceous micrite.



**Figure 4.30** *Scolicia* burrows in the lower greensand facies units (F4b) at Kaikoura wharf.

It is suggested here that this lower F4b unit represents a significant unconformity, based on the identification of extensive *Thalassinoides* burrowing at the base of the unit, the presence of glaucony and the

thickness of the unit. This is supported by biostratigraphy (Figure 4.28) which shows that F1c below this greensand unit at the Kaikoura wharf section is upper Haumurian while F1c above the unit is lower Teurian (RP3-4) (Chris Hollis pers. comm. 2009).

The upper F4b unit at Kaikoura wharf has a very distinct appearance in comparison to lower greensand unit, with intense bioturbation, a lighter greenish grey colour and the presence of ubiquitous phosphatic clasts. It is a light greenish, grey speckled black, highly bioturbated, calcareous, glauconitic sandstone. This unit is slightly to moderately weathered and well indurated, resulting in the unit generally forming a prominent feature along the entirety of the outcrop (Figure 4.25). Black to dark brown, angular to subrounded phosphatic clasts ~1 cm in size are common throughout the unit (Figure 4.31A), along with less common shark teeth, ~1 cm in length. Glaucony in the unit consists of dark green to black, fine to medium sand sized grains and makes up ~10% of the facies.

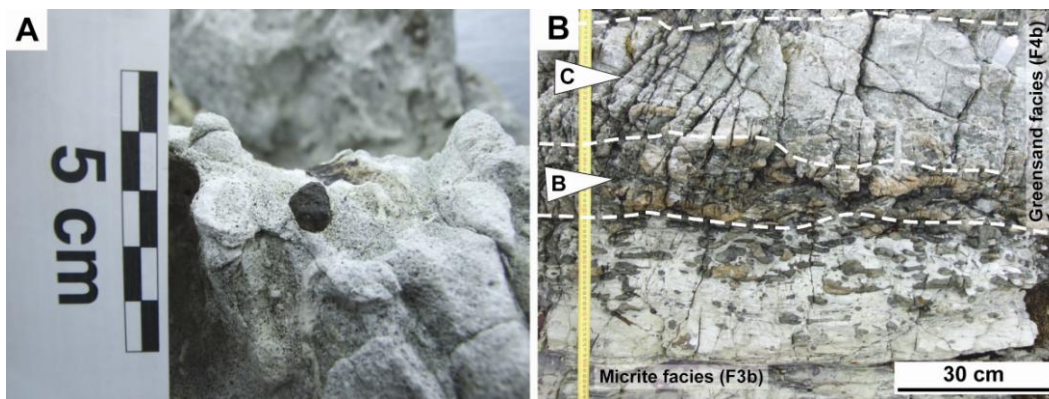


**Figure 4.31** (A) Distinctive subrounded phosphatic clast set in light greenish grey, highly bioturbated greensand of the upper F4b unit at Kaikoura wharf. (B) Extensive bioturbation at the base of the upper greensand facies (F4b) unit at Kaikoura wharf with *Thalassinoides* burrows extending down into the underlying micrite facies (F3b). B, Extensive *Thalassinoides* burrows at the base of the unit; C, Central area of F4b with indistinctive ichnotaxa, phosphatic clasts and shark teeth.

Bioturbation is extensive throughout the upper greensand facies unit and can be considered a characteristic feature identifying the unit along the length of the outcrop. *Thalassinoides* burrows are concentrated at the upper and lower contacts of the unit. The lower contact consists of a 10-20 cm zone of intense bioturbation with burrows extending a further 20-25

cm into the underlying micrite facies (Figure 4.31B). The upper contact consists of a 5-10 cm zone of intense bioturbation similar to the lower contact. Burrows range in size between ~1 and ~5 cm and are aligned roughly parallel to bedding. Within the centre of the unit, burrows are small and irregular, making identification difficult.

It is suggested here that the base of this unit represents a significant unconformity, based on the identification of extensive *Thalassinoides* burrowing, and that the top of the unit may be also unconformable. However, this intense bioturbation may just reflect the highly condensed nature of this unit as a whole. This is supported by biostratigraphy (Figure 4.28) which shows that F3b below this greensand unit at the Kaikoura wharf section is lower Teurian, probably early RP4, while upper F4b and F3b units are lower and upper Waipawan, respectively, based on foraminiferal evidence (Chris Hollis pers. comm. 2009).

#### *Micrite facies (F3b)*

The micrite facies consists of two separate units at the Kaikoura wharf section separated by the upper greensand deposit (Figure 4.28).

The lower micrite unit is characterised by dm bedded, light grey to cream, micrite interbedded with dm bedded, light grey, marl. One prominent, laterally continuous bed within this facies contains elliptical, light grey chert nodules that weather to an orange brown colour, suggesting that silica content is still high in portions of this lower micrite facies unit (Figure 4.32A). The chert nodules are very hard, show conchoidal fracture when a fresh sample is collected from the outcrop and tend to contain small (~5 cm in diameter), dark green to black, circular cores. Lawrence (1989) did not document any similar features within chert nodules from the Muzzle Group anywhere else in southeastern Marlborough. It is assumed here that this is a localised phenomenon and these black cores may represent the nucleus for the chert nodule as a whole.

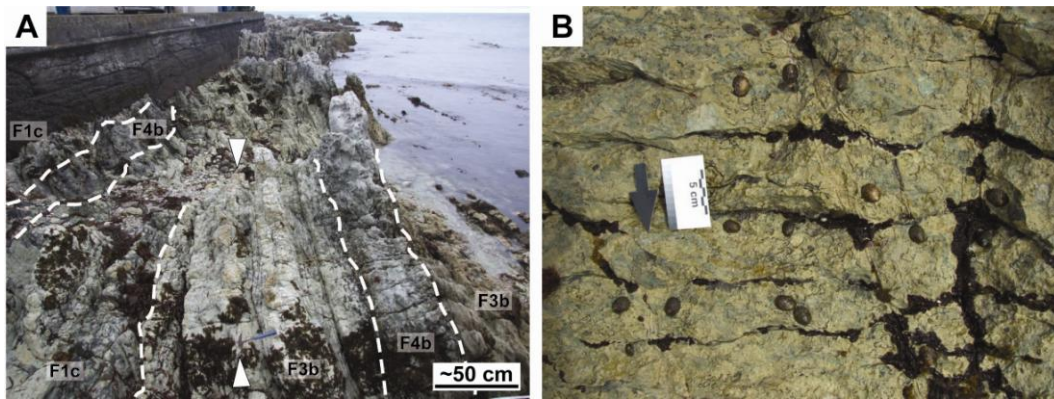


**Figure 4.32** (A) Upper and lower micrite facies (F3b) units separated by the upper greensand facies (F4b) unit at Kaikoura wharf. Note continuous bed of chert nodules (arrowed). (B) Flaggy appearance of the upper micrite facies (F3b) unit with thin glauconitic interbeds. Section youngs in direction of arrow.

The upper F3b unit consists of light grey to light blue grey micrite. Within 2.4 m of the contact with the underlying upper F4b unit, F3b has a flaggy appearance with maximum bed thicknesses reaching ~10 cm (Figure 4.32B). This portion of the upper micrite facies at the Kaikoura wharf is also glauconitic, with green to dark green, subangular to rounded, fine to medium sand sized glaucony grains disseminated throughout. Glaucony is also concentrated in discontinuous thin interbeds between limestone flags. 2.4 m above the contact, glaucony appears to be absent and bed thicknesses increase and generally show a more tabular geometry. This upper portion of the upper micrite facies unit at Kaikoura has a marly appearance and possibly shows closer lithologic association with the Lower Marl lithotype of the Amuri Limestone than the Lower Limestone.

### **4.5.3 Petrography and Mineralogy**

#### *Siliceous micrite and chert facies (F1c)*

The lower siliceous micrite and chert facies at Kaikoura wharf consists of light grey to brownish grey, clotted micrite. Siliciclastic grains, dominated by coarse silt sized, well sorted, angular to subangular detrital quartz and feldspars as well as rare muscovite, make up ~5% of samples in thin section and are concentrated up to 20% in burrows. Authigenic pyrite is ubiquitous throughout this unit, both as grains and infilling radiolarian and foraminiferal tests. Rare subangular to subrounded, bright green to dark green, microcrystalline pelletal glaucony grains tend to be concentrated in

burrows along with rare subangular to rounded, light brownish orange phosphatic grains.

In the upper F1c unit, well sorted, very fine sand sized, angular to subrounded, detrital grains of quartz, K feldspar, plagioclase and muscovite increase to ~10%. Glaucony grains are dominated by subrounded to rounded, microcrystalline pelletal forms but also include vermicular glauconitised biotite that exhibits faint, light green to dark green pleochroism and 3<sup>rd</sup> and 4<sup>th</sup> order interference colours under cross polarised light. This form of glaucony becomes less common upsection and is not observed at all in a thin section from sample KK08. Very fine grain authigenic pyrite is ubiquitous throughout the upper F1c unit. Rare shark teeth were also observed in thin sections of samples from this facies (Figure 4.33A)

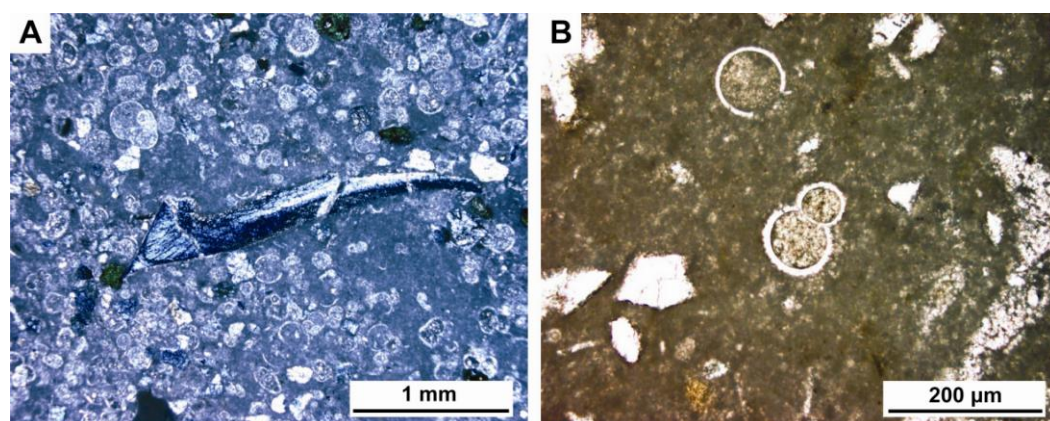


**Figure 4.33** (A) Shark tooth set in foraminiferal micrite from the upper siliceous micrite and chert facies (F1c) unit at Kaikoura wharf (XPL). (B) Thin walled, unornamented globigerinid planktic foraminifera infilled with light brown, isotropic silica from the lower siliceous micrite and chert facies (F1c) at Kaikoura wharf.

Below sample KK08, visible microfossils in F1c are dominated by thin walled, unornamented globigerinid planktic foraminifers (Figure 4.33B) and spumellarian radiolarians, making up ~5% of the total sample in thin section. Rare benthic foraminifera and siliceous sponge spicules are also present in F1c. The majority of microfossil tests tend to be recrystallised and infilled with light brown, isotropic silica or rarely light brownish grey micrite. In KK08, planktic foraminifera dominate (~25%), with subordinate spumellarian radiolarians making up 1% of the sample in thin section

(Figure 4.33A). Foraminiferal tests show recrystallised carbonate fabrics but retain evidence of pore structure and possible ornamentation and are infilled with microcrystalline carbonate cement.

Veins in F1c range in thickness up to ~1 mm and are generally oriented perpendicular to bedding. Vein infill is dominated by dusty calcite spar cement, though occasional veins have a thin lining of silica as well, suggesting multiple phases of vein infilling.

#### *Greensand facies (F4b)*

The lower greensand facies unit at Kaikoura wharf has a characteristic appearance in thin section that allows it to be differentiated from the upper greensand facies unit. Grain supported, angular to subangular, very fine sand sized quartz and less common K feldspar grains make up ~60% of the sample in thin section, with subordinate muscovite (3%) and rare plagioclase. Even though bioturbation is observed in hand samples of the lower F4b unit, the facies appears relatively homogenous in thin section, displaying grain supported fabrics set in adjacent zones of siliceous and calcareous matrix (Figure 4.34A, B). Glaucony makes up 7% of the lower F4b unit in thin section and is dominated by bright to dark green, microcrystalline pelletal glaucony grains with less common vermicular

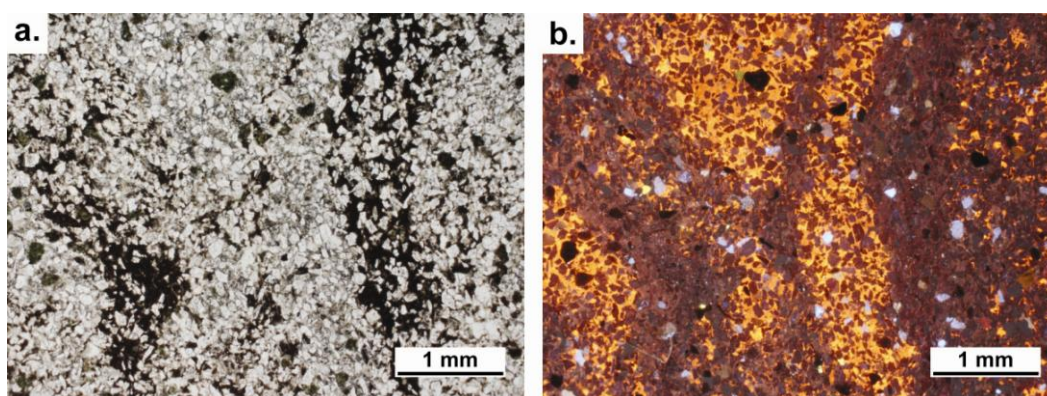


**Figure 4.34** Photomicrograph pairs under plane polarised light (a) and cathodoluminescence light (b) of the lower greensand facies (F4b) unit (KK03). Very fine sand sized detrital quartz and K feldspar grains identified by dull blue to reddish brown and bright blue luminescence, respectively, set in adjacent zones of siliceous and calcareous matrix. These differing zones are easily identified under CL light, with calcareous matrix showing bright orange luminescence and siliceous matrix showing dull reddish brown luminescence.

forms. Some grains exhibit hydration fractures and limonite staining of rims. Fine-grained authigenic pyrite is common throughout this lower F4b unit and appears to have an association with glaucony grains. The low percentage of glaucony in the lower greensand facies (F4b) unit at Kaikoura wharf means the unit should be classified as a glauconitic sandstone and makes it difficult to reconcile the dark green to black colour of the unit in outcrop. However it is chosen here to retain this unit in F4b due to genetic similarities between the two units at Kaikoura wharf (discussed in Chapter 5).

No microfossils, siliceous or calcareous, were observed in thin sections of samples collected from the lower F4b unit.

The upper greensand facies unit is characterised by a highly bioturbated fabric which preserves multiple phases of burrow infill (Figure 4.35A). Siliciclastic grains in this unit are dominated by moderately to well sorted, subangular to subrounded, fine sand sized detrital quartz grains (35%) and K feldspar (5%), as well as rare plagioclase and muscovite. Differentiation between quartz and K feldspar grains was made utilising CL light, with quartz grains exhibiting dull blue and brownish red luminescence, while K feldspars show characteristic bright blue luminescence under identical excitation conditions (Figure 4.35B, C). Glaucony consists mainly of bright green to brownish green, microcrystalline, subrounded to rounded pelletal grains, with less common vermicular, glauconitised biotite. Some grains exhibit limonitised rims and dehydration cracking.

Detrital, perigenic and bioclastic grains are all set in patches of siliceous and calcareous matrix, as in the lower F4b unit (Figure 4.34A, B), and exhibit grain supported fabrics.

Burrows tend to have sharp boundaries and are generally well defined by the proportion of siliciclastic and bioclastic grains. One phase of burrow infill is dominated by detrital quartz and feldspar grains, with no bioclasts observed. While in a second phase of burrow infill, planktic foraminifera



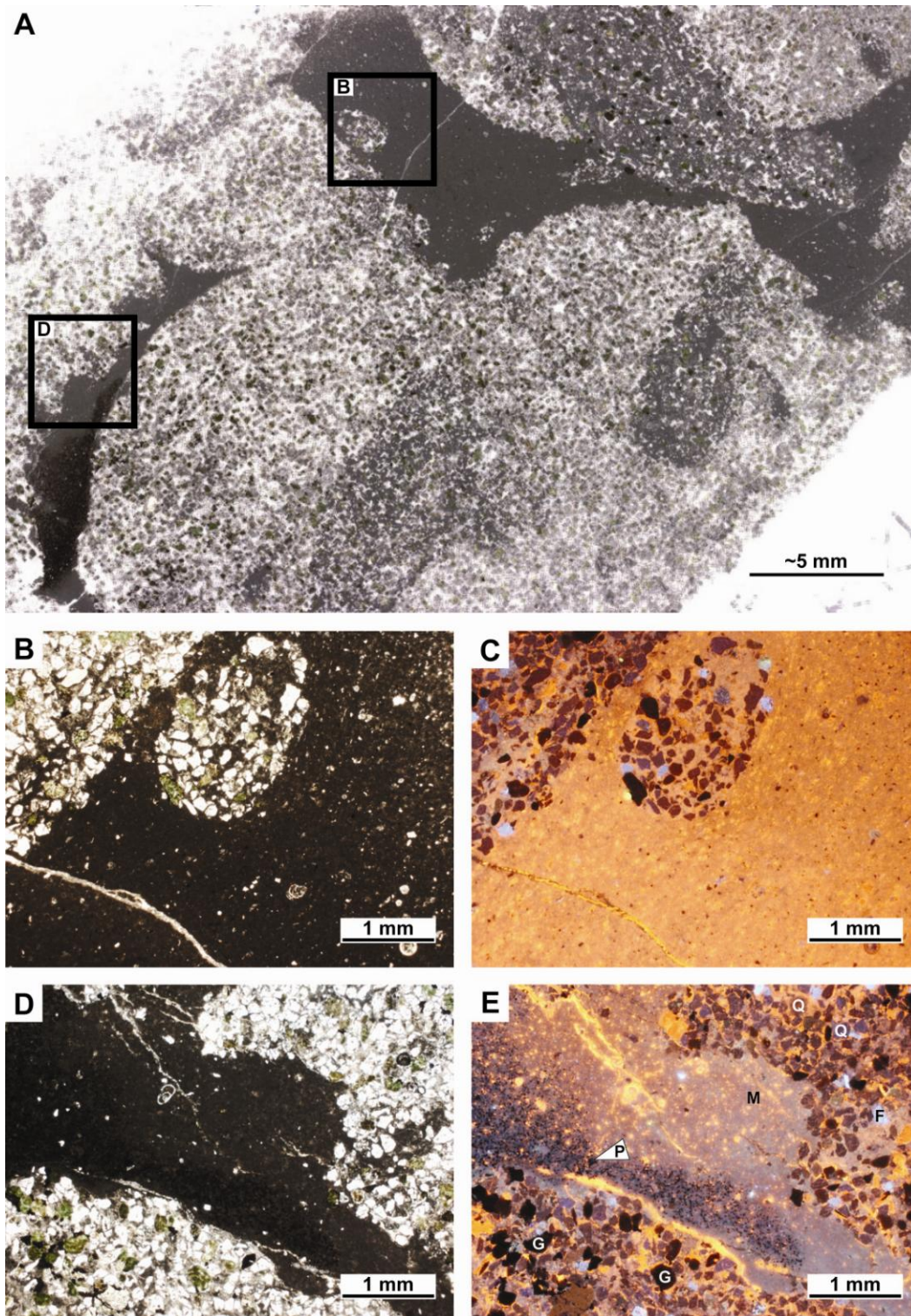


**Figure 4.35** (A) Scan of thin section (KK18) showing the location of (B) and (D). Photomicrograph pairs under plane polarised light (left) and cathodoluminescence light (right) of the upper greensand greensand facies (F4b) unit (KK18). (B) & (C) Siliciclastic rich burrows set in a micrite host. (D) & (E) Siliciclastic rich burrows set in a micrite host. F, bright blue luminescent detrital K feldspar grains; G, non-luminescent microcrystalline pelletal glaucony grains; M, micritic host sediment; Q, dull blue to reddish brown luminescent detrital quartz grains; P, abundant framboidal pyrite confined to micritic host.

make up to 25% of the clasts observed. Areas of relatively pure micrite, containing rare siliciclastics, planktic foraminifera and spumellarian radiolarians are inferred here to represent the remnants of the host sediment into which burrowing occurred. Some areas of micrite contain high concentrations of authigenic framboidal pyrite (Figure 4.35D, E), identified by its brassy yellow colour under reflected light.

#### *Micrite facies (F3b)*

In thin section, F3b at Kaikoura wharf has a similar appearance to F1c. F3b is generally characterised by light grey, clotted micrite containing up to 15% planktic foraminifera as well as varying concentrations of siliciclastic and perigenic grains. SEM analysis of F3b shows that this facies is dominated by detrital carbonate grains in the form of coccolith debris and recrystallised calcite spar. Grain size ranges from 0.5 to ~3  $\mu\text{m}$ .

Siliciclastic grains are dominated by angular to subrounded, coarse silt sized grains of quartz, with less common K feldspar and rare muscovite grains. The proportion of these grains in thin section decreases from ~7% in the lower F3b unit to 2% in the uppermost sample (KK27) collected from the Kaikoura wharf section. Perigenic grains in the form of bright green, microcrystalline pelletal glaucony and subangular to rounded, brownish orange phosphatic grains are observed in this facies but decrease to <1% 2.4 m above the contact with the upper F4b unit (Figure 4.36A)

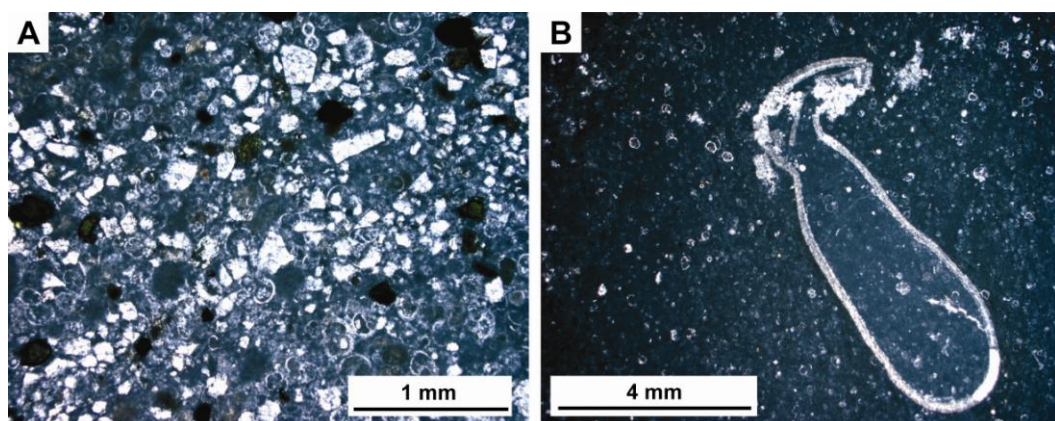


**Figure 4.36** (a) Sample of micrite facies (F3b) from Kaikoura wharf (KK23), with abundant very fine sand sized detrital siliciclastic grains, planktic foraminifera and microcrystalline, pelletal glaucony grains (PPL). (b) Possible compressed tiny echinoderm test from the upper micrite facies (F3b) unit at Kaikoura wharf (KK27) (PPL).

Microfossils identified in thin sections from F3b are dominated by planktic foraminifera, making up to 25% of samples. Much less common are benthic foraminifera, radiolarians and a large (~5 mm) unidentified, calcareous fossil, possibly a deformed echinoderm test (Figure 4.36B). Preservation of microfossil tests varies, though the majority of tests and shell fragments show significant recrystallisation; they are predominantly infilled with micrite, while rare tests are infilled with spary calcite cement or microcrystalline silica.

Sample KK14 was from a chert nodule collected from within the lower micrite facies unit at Kaikoura wharf. This sample consists of light brown, isotropic microcrystalline silica containing well preserved spumellarian and nassellarian radiolarians, oriented sponge spicules and very rare, silicified benthic foraminifera. Under CL light, this sample shows an orange luminescence more typical of calcite (Figure 4.37A), even though energy dispersive spectroscopy and bulk X-ray fluorescence analysis show the sample is ~100 wt% SiO<sub>2</sub>. This is also in stark contrast to the dull blue luminescence characteristic of silica (Figure 4.37B), exhibited in a thin section of a black 'core' from a chert nodule which has a similar SiO<sub>2</sub> content. This shows that CL colours are mainly dependent on included trace elements as opposed to the mineral itself.

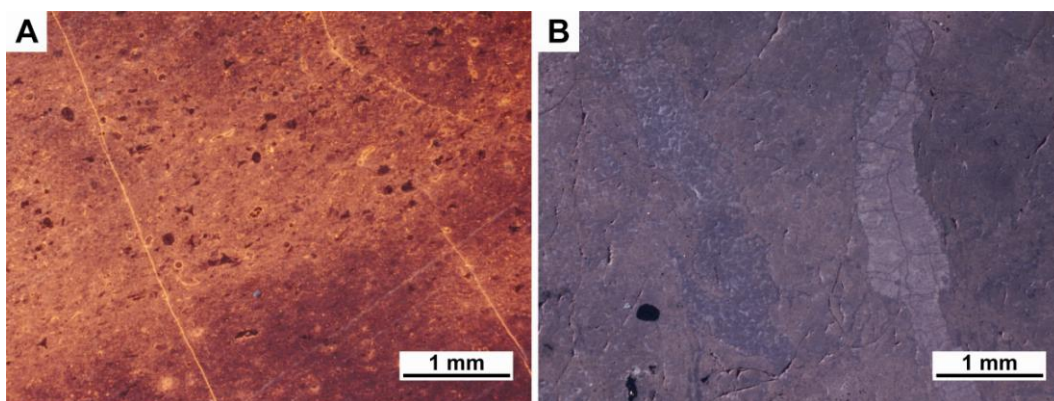


**Figure 4.37** (a) Dull orange luminescence of chert (KK14) from Kaikoura wharf. (b) Dull blue luminescence observed in the 'core' of a chert nodule (KK39) from Kaikoura wharf. Note the difference in CL colour even though the two images are almost identical.

## 4.5.4 Geochemistry

### *Inorganic Geochemistry*

The Al normalised elemental concentrations in samples of F1c, F4b and F3b are compared with average shale values of Wedepohl (1971) for both major and trace elemental concentrations to allow for comparison between sites. The bulk geochemical data are recorded in Appendix D.

### *Major Elements*

#### *Siliceous micrite and chert facies (F1c)*

Excluding  $\text{SiO}_2$ ,  $\text{CaO}$ ,  $\text{MgO}$  and  $\text{Na}_2\text{O}$ , Al normalised major elemental concentrations in samples collected from F1c at Kaikoura wharf are 'normal' when compared with average shale concentrations of Wedepohl (1971) (Figure 4.38A).

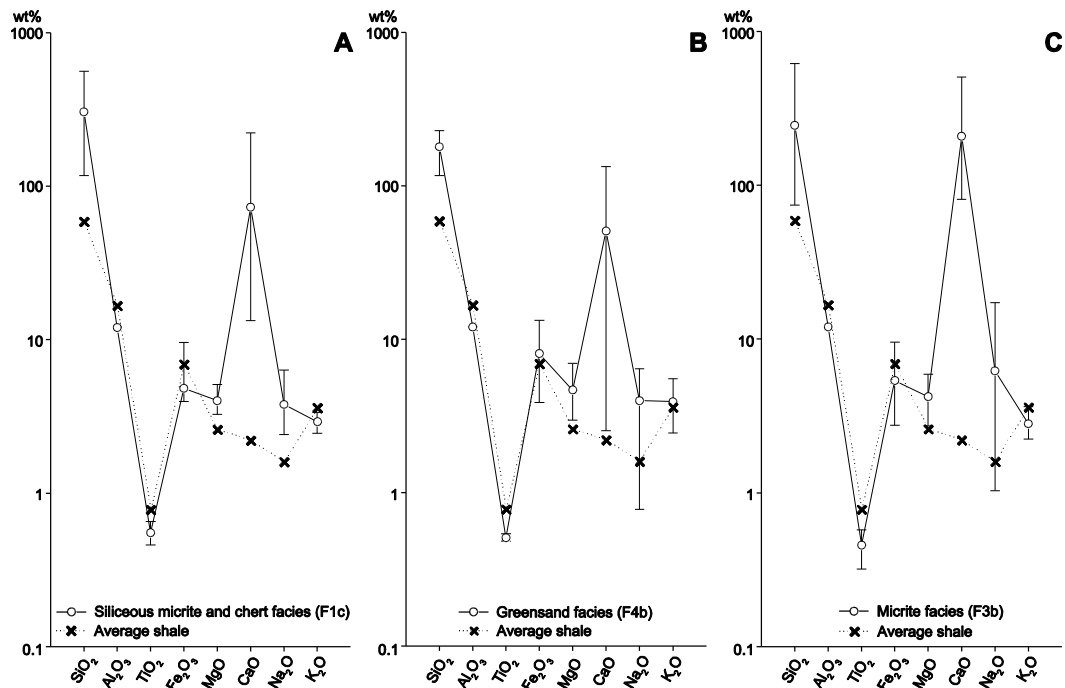


**Figure 4.38** Al normalised major element concentrations (range and mean values) for the three facies identified during field work at Kaikoura wharf compared against average shale (Wedepohl 1971). (a) Siliceous micrite and chert facies (F1c); (b) Greensand facies (F4b); (c) Micrite facies (F3b). Vertical bars indicate range of values.

#### *Greensand facies (F4b)*

As for F1c, all Al normalised major elemental concentrations excluding  $\text{SiO}_2$ ,  $\text{CaO}$  and  $\text{MgO}$  are 'normal' when compared with average shale values of Wedepohl (1971) (Figure 4.38B). While F4b contains, on

average, the lowest concentrations of SiO<sub>2</sub> and CaO of all the facies identified at the Kaikoura wharf section, it also contains the highest concentration of Fe<sub>2</sub>O<sub>3</sub> and K<sub>2</sub>O.

#### *Micrite facies (F3b)*

Samples from F3b show similar trends in Al normalised major element concentrations to both F1c and F4b (Figure 4.38C). SiO<sub>2</sub>, CaCO<sub>3</sub> and MgO concentrations in samples from this facies are all higher than concentrations in average shale of Wedepohl (1971), while other major element concentrations are 'normal'. Due to the extremely low concentration of Al<sub>2</sub>O<sub>3</sub> in the sample of chert (0.42 wt%), and the effect this had on average Al normalised elemental concentrations, this sample was not considered within geochemical plots of this facies.

#### *Discussion*

Consistently high Al normalised values for SiO<sub>2</sub> and CaO (>100 wt%) throughout all facies identified at Kaikoura wharf reflect the large biogenic component of the primary sediments. Fe<sub>2</sub>O<sub>3</sub> and K<sub>2</sub>O show a significant positive correlation with terrigenous supply (TRG) (Appendix D) and high concentrations of these elements in the greensand facies are inferred to be associated with the glaucony in this facies.

#### **Trace Elements**

##### *Siliceous micrite and chert facies (F1c)*

The siliceous micrite and chert facies at Kaikoura wharf is generally characterised by Al normalised trace elemental concentrations that are 'normal' with respect to average shale values (Figure 4.39A). U, Cr, Zn and Zr are enriched to the point where the range of measured values is higher than average shale values.

##### *Greensand facies (F4b)*

Samples from the greensand facies at Kaikoura wharf show significant enrichment in U and Co as well as the transition elements Cr, V and Zn, with the ranges of measured values falling above the elemental

concentration in the average shale (Figure 4.39B). Nb, Pb, Ni and Ce are depleted, with the range of measured values falling below elemental concentrations of average shale.

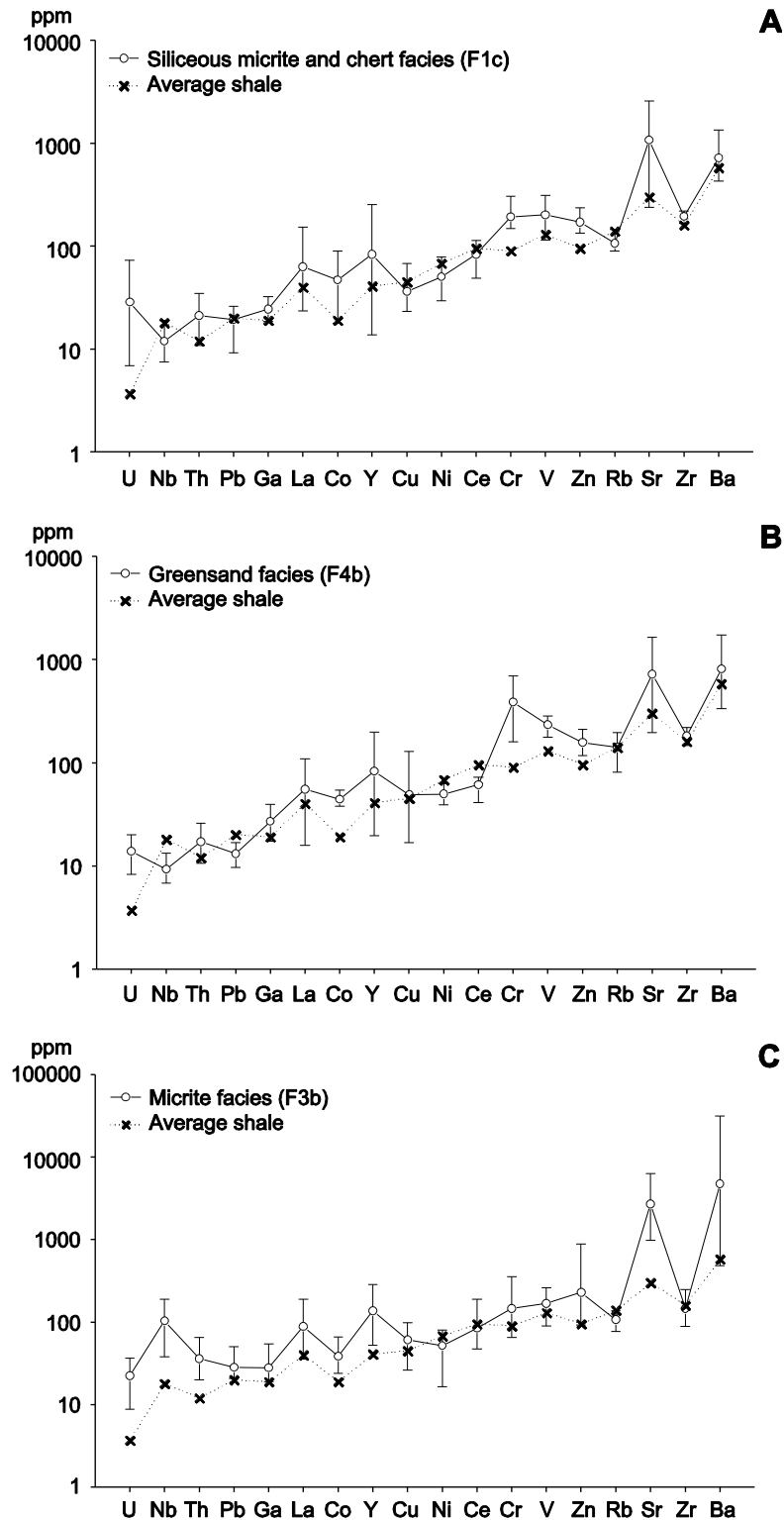


**Figure 4.39** Al normalised trace element concentrations (range and mean values) for the three facies identified during field work at Kaikoura wharf compared against average shale concentrations (Wedepohl 1971). (a) Siliceous micrite and chert facies (F1c); (b) Greensand facies (F4b); (c) Micrite facies (F3b). Vertical bars indicate range of values.

### *Micrite facies (F3b)*

Al normalised trace element concentrations of samples from the micrite facies at Kaikoura wharf show similar trends to F1c and F4b (Figure 4.39C). U, Nb, Th, Pb, Co, Y and Sr are all significantly enriched, while Rb is significantly depleted, with average shale concentrations falling outside the range of measured values for these elements.

### *Discussion*

Ernst (1970) stated that Co maybe concentrated in pyrite, which may explain the enrichment of Co in F4b and F3b. This explanation is considered plausible, based on the ubiquitous nature of pyrite in thin sections of samples from all facies at Kaikoura wharf and from the Muzzle Group as a whole (Lawrence 1989). Nb, Pb and Rb all show significant positive correlations with terrigenous supply through the measured section at Kaikoura wharf, suggesting these elements can be attributed to clays. Though this explains the depletion of Nb and Pb in F4b, it does not explain enrichment of these same elements in F3b, the facies with the lowest average terrigenous input (Figure 4.42B), suggesting Nb and Pb may be associated with an unidentified authigenic phase. Transition elements Cr, V and Zn are probably associated with glaucony, explaining their enrichment in the greensand facies. These elements have the ability to substitute for  $\text{Fe}^{3+}$ ,  $\text{Fe}^{2+}$  and  $\text{Mg}^{2+}$  at octahedral sites in the glaucony lattice due to similarities in ionic radius and charge (McConchie 1978) (Figure 3.14). Enrichment of Sr in the micrite facies is associated with  $\text{CaCO}_3$  in the facies as Sr tends to substitute for Ca in the crystal lattice.

### **Compositional Plots**

A strong correlation ( $R^2 = 0.9555$ ) between  $\text{TiO}_2$  and  $\text{Al}_2\text{O}_3$  in Figure 4.40 suggests that the majority of  $\text{TiO}_2$  is associated with clays, supporting the assumption that  $\text{TiO}_2$  can be used as a proxy for terrigenous supply. It can also be inferred from this graph that the source of terrigenous sediment appears to have remained constant through the Late Cretaceous to Early Eocene.

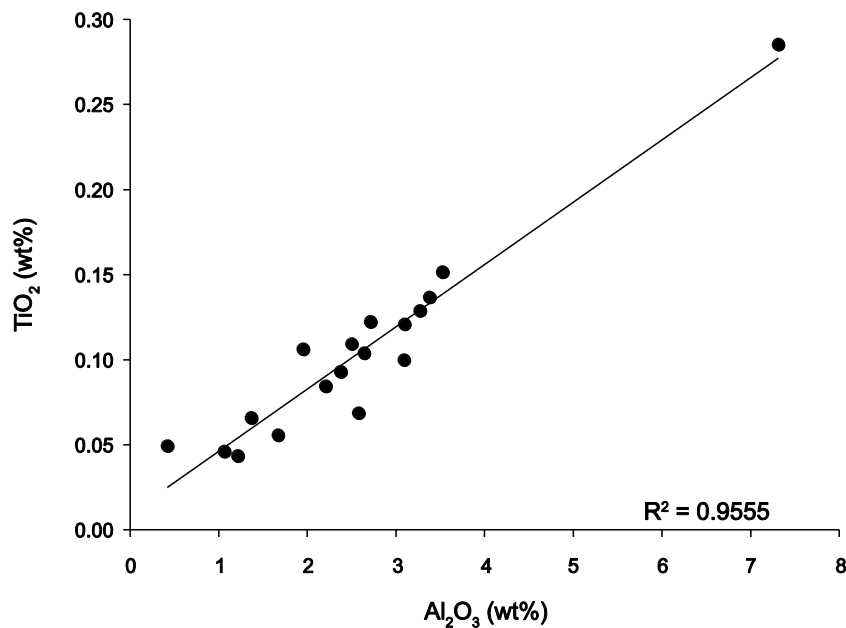


**Figure 4.40** Relationship between Al<sub>2</sub>O<sub>3</sub> and TiO<sub>2</sub> in Mead Hill Formation and Amuri Limestone at Kaikoura wharf.

On a ternary plot of the three major chemical components of sedimentary rocks, Al<sub>2</sub>O<sub>3</sub>, SiO<sub>2</sub> and CaCO<sub>3</sub>, representing clays, quartz and/or biogenic silica and calcium carbonate, it appears that the three lithofacies identified at Kaikoura wharf cannot be considered geochemically distinct (Figure 4.41). All three fields overlap within this plot, reflecting the complicated nature of the Kaikoura wharf section as a whole and issues with simplifications made when applying a broad facies model to this section.

Samples from F1c plot broadly near the SiO<sub>2</sub> pole of the ternary diagram, reflecting the siliceous nature of this facies. F4b plots near the axis between the SiO<sub>2</sub> and Al<sub>2</sub>O<sub>3</sub> poles, with only one sample having a high proportion of CaCO<sub>3</sub>. Samples from F3b plot in an arching trend along the axis between the SiO<sub>2</sub> and CaCO<sub>3</sub> poles, showing a distribution that is more characteristic of the siliceous micrite and chert facies at other sites (e.g. Mead Stream). All facies identified at Kaikoura wharf contain low proportions of clays in comparison to average shale, shown by low Al<sub>2</sub>O<sub>3</sub> values. This is a strong reflection of the biogenic nature of these sediments.



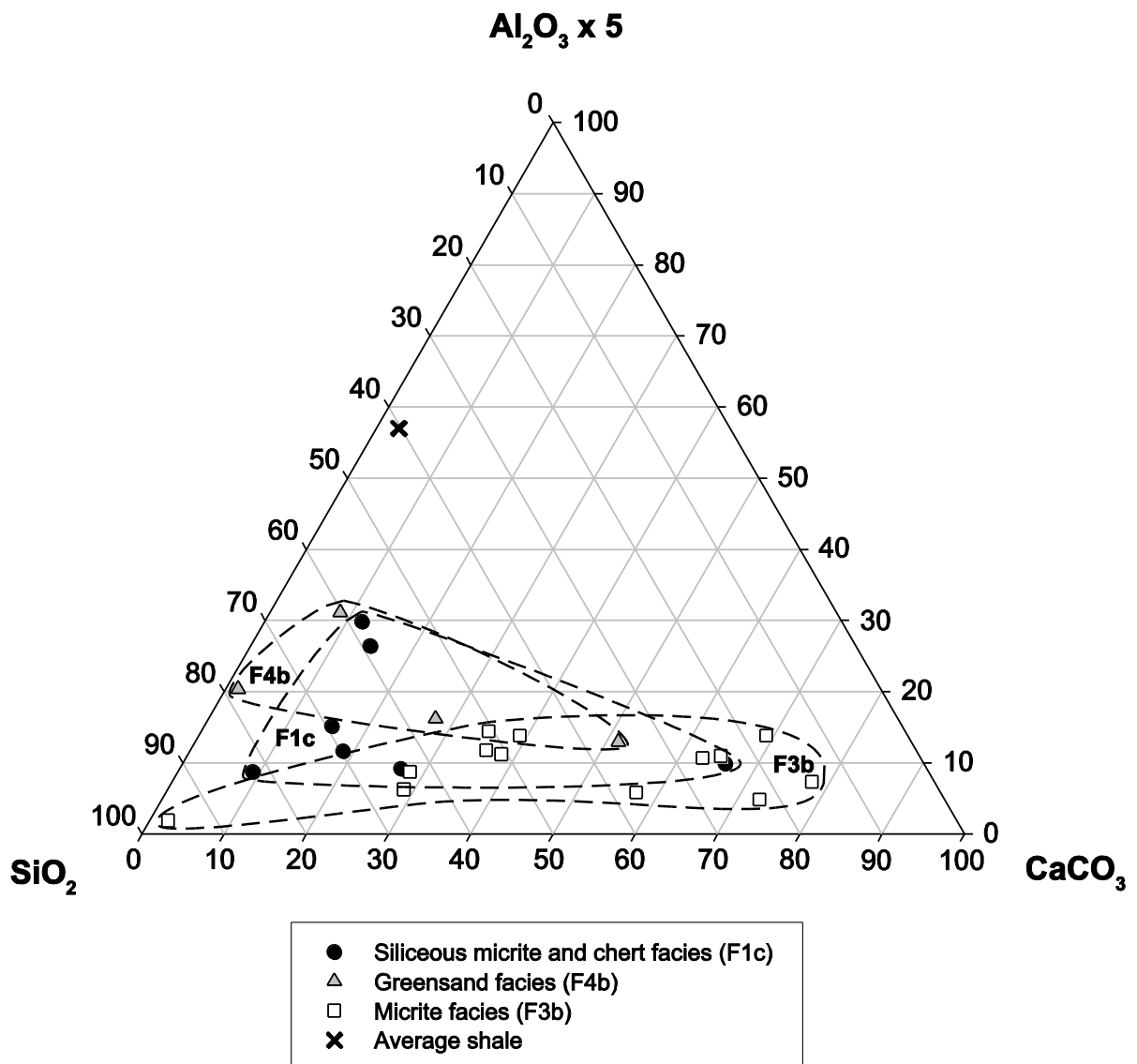


**Figure 4.41** Ternary diagram of relative proportions of Al<sub>2</sub>O<sub>3</sub> (x5), SiO<sub>2</sub> and CaCO<sub>3</sub> in the siliceous micrite and chert facies (F1c), greensand facies (F4b) and micrite facies (F3b) from Kaikoura wharf. An arbitrary multiplier of 5 is used for Al<sub>2</sub>O<sub>3</sub> in order to better distribute the data points within the graph (after Turgeon & Brumsack 2006). “Average shale” (AS) (Wedepohl 1971) is also shown.

### ***Proxies***

Terrigenous sediment input (TRG), a proxy for clay content of samples based on TiO<sub>2</sub> concentration, is relatively constant throughout the entire measured section with the largest increase occurring through the greensand unit directly above the Cretaceous-Tertiary boundary (Figure 4.42B). TRG increases from ~15 wt% in the Late Cretaceous Mead Hill Formation to a maximum of 46.0 wt% in the lower greensand unit before returning to ~15 wt% through the majority of the rest the section.

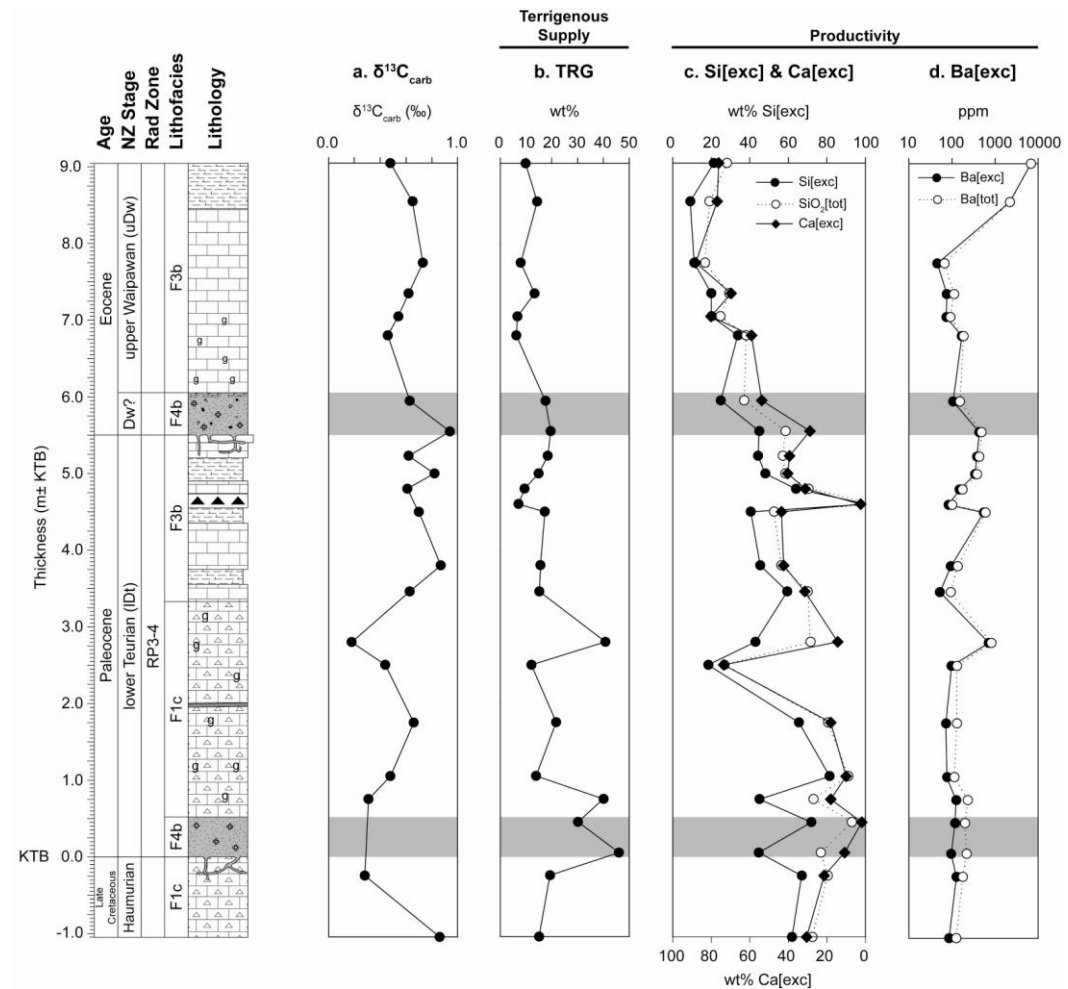


**Figure 4.42** Variations in (a)  $\delta^{13}\text{C}_{\text{carb}}$ , (b) terrigenous sediment (TRG), (c) excess silica and excess carbonate (Si[exc], Ca[exc]), and (d) barium (total and excess Ba, Ba[exc]) at Kaikoura wharf.

Paleoproductivity proxies, excess silica and excess calcium (Si[exc] and Ca[exc]), are variable throughout the measured section, but show a general trend from siliceous to calcareous productivity through the Late Cretaceous to Early Eocene at the Kaikoura wharf (Figure 4.42C). Si[exc] values decrease from ~60 wt% through F1c but remain relatively high (~40 wt%) through the lower micrite facies (F3b) unit, reaching a maximum of ~100 wt% in the bed of chert nodules within this facies. Si[exc] then decreases to an average of 19.3 wt% in the upper unit of F3b.

Ca[exc] shows the opposite trend to Si[exc], increasing from the Late Cretaceous to the Early Eocene (Figure 4.42C). Ca[exc] values are low, ~20 wt%, through the siliceous micrite and chert facies (F1c), reaching a minimum for the measured section of 1.8 wt% in the lower greensand

facies unit (F4b). Ca[exc] increases to ~35 wt% through the lower micrite facies unit (F3b), before increasing further to ~75 wt% in the upper micrite facies unit. Ca[exc] reaches a maximum for the measured section of 88 wt% approximately 1.7 m above the contact between the upper greensand and micrite facies units.

Total barium (Ba[tot]) and excess barium (Ba[exc]) are variable but low through the majority of the section (Figure 4.42D). Ba[exc] averages ~130 ppm, reaching 715 ppm and 552 ppm in the upper siliceous micrite and chert unit and lower micrite unit, respectively. Ba[exc] increases rapidly in the marly portion of the upper F3b unit, reaching a maximum of 6805 ppm in the uppermost sample collected from the top of micrite facies at the Kaikoura wharf.

### ***Stable Isotopes***

The  $\delta^{13}\text{C}$  of bulk carbonate varies little through the Kaikoura wharf section (Figure 4.42a). Values through the measured section only vary by 0.76‰, ranging between 0.18‰ and 0.94‰. The important fact that no discernible trends or carbon isotope excursions are detected at the Kaikoura wharf section will be discussed further in Chapter 5.

# **CHAPTER 5**

## **DISCUSSION**

---

This chapter is broken into four major sections that are considered to represent areas of significant interest and importance to this study. First, it discusses some aspects of the nomenclature for the Paleocene-Eocene stratigraphy in southeastern Marlborough and reinterprets the stratigraphic succession at Kaikoura wharf. Second, the key characteristics and paleoenvironmental significance of the lithofacies identified as part of this investigation are discussed. Third, a number of paleodistribution maps are presented to allow for discussion about the distribution of the Teredo Limestone and processes responsible for its deposition, as well as discussing the evolution of lithofacies in southeastern Marlborough through the Paleocene to Early Eocene. Finally, this chapter discusses possible ocean circulation patterns responsible for the development of lithofacies and unconformities identified in the Late Cretaceous to Early Eocene sections from southeastern Marlborough and Campbell Island.

### **5.1 REVISION OF EARLY PALEOGENE STRATIGRAPHIC NOMENCLATURE OF SOUTHEASTERN MARLBOROUGH**

During the Late Cretaceous to Early Eocene, strata now exposed onland in Marlborough were deposited on a broad terrigenous starved margin named the Marlborough paleo-platform which formed the eastern side of a large embayment referred to as the Marlborough paleo-embayment (Figure 5.1) (Crampton et al. 2003). The passive margin nature and high latitude position (~55°S; Lawver et al. 1992; King et al. 1999) of the region during this period mean that sedimentary sections provide some of the most complete onland records for studying climatic change through this period in the world (Field & Hollis 2003; Hollis 2003, 2006; Hollis et al. 2005b; Nicolo et al. 2007). Given this global significance, there is a need to ensure a robust stratigraphic nomenclature exists for the sedimentary sections that can be readily correlated throughout the region with little room for confusion. An extensive history of geological study, culminating with the study by Reay (1993), has led to the establishment of a generally

robust lithostratigraphic framework for the Late Cretaceous to Early Paleogene strata in southeastern Marlborough (Enclosure 1). However, it is suggested here that stratigraphic matters could benefit from some further refinement.

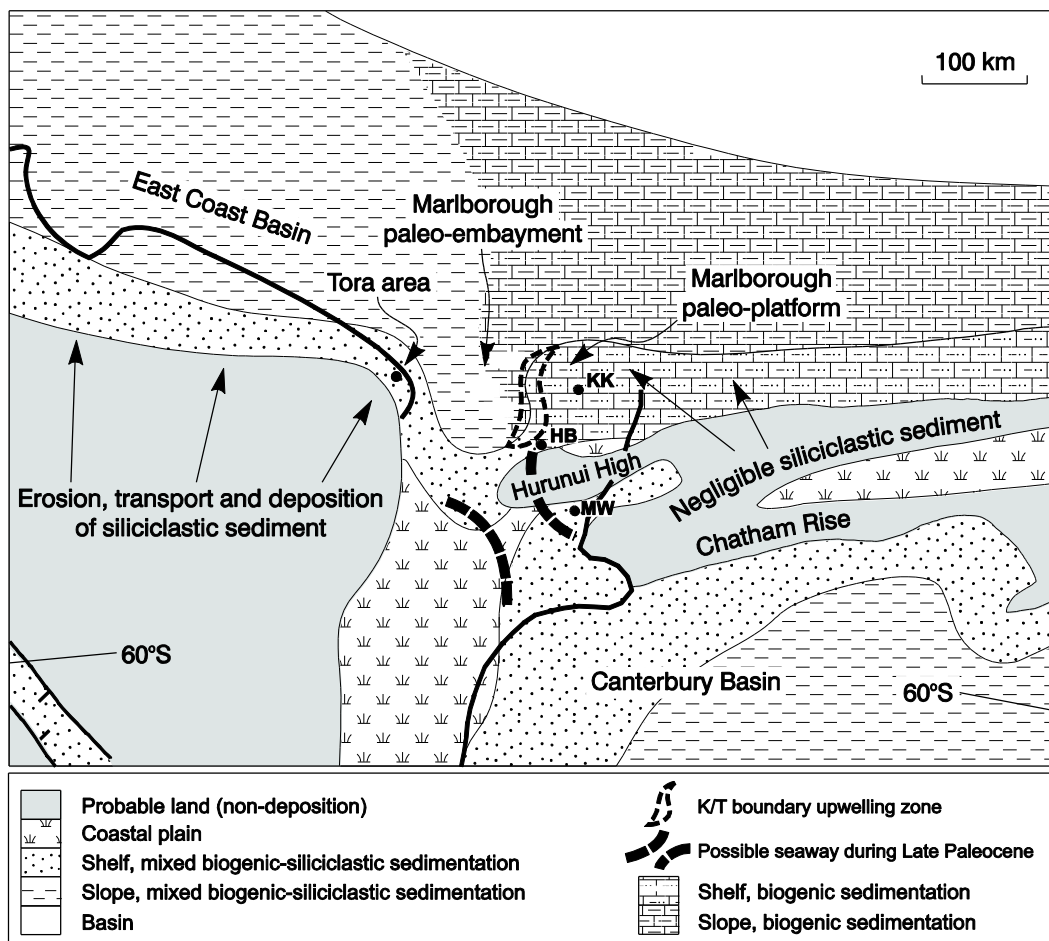


**Figure 5.1** Palinspastic reconstruction of central New Zealand at about the K/T boundary showing major features discussed in text (after Crampton et al. 2003; Hollis 2003). The generalised outlines of the modern coastline of eastern North Island and eastern South Island are shown as bold black lines for reference. HB: Haumuri Bluff; KK: Kaikoura wharf; MW: Mid-Waipara.

### **5.1.1 Reinterpretation of Lithostratigraphy at Kaikoura Wharf**

The Teredo Limestone at Kaikoura wharf was described by Morris (1987) as consisting of two greensand units separated by ~3 m of micritic limestone. Nowhere else in southeastern Marlborough is this couplet of greensand units described (Morris 1987; Reay 1993; Warren 1995), suggesting that the Kaikoura wharf section is unique within the region. Based on lithologic similarities between the Teredo Limestone at Muzzle Stream and the upper greensand unit at Kaikoura wharf, such as the

abundance of glaucony and grain size (Figure 4.20C, D and 4.35D, E), it is suggested here that only the upper greensand unit at the wharf site can be considered to be the Teredo Limestone (Figure 4.28 and Table 5.1). This is confirmed by micropaleontologic investigations carried out as part of this study which show that though the Kaikoura wharf section is greatly condensed, the two greensand units here were deposited as a result of completely separate oceanographic events. Consequently, combining both units into the Teredo Limestone based on lithology alone affects the production of isopach maps for the unit and their subsequent interpretations. Since the Teredo Limestone Member occupies the basal part of the Amuri Limestone, this means that the lower greensand unit and capping thin limestone at Kaikoura wharf are the uppermost units within the underlying Mead Hill Formation, whose top would then become the base of the upper greensand (or Teredo Limestone) unit (Table 5.1).

**Table 5.1** Comparison between previously published lithostratigraphy of Browne et al. (2005a) for Kaikoura wharf and the reinterpreted lithostratigraphy from this study.

<b>Browne et al. (2005a)</b>			<b>This study</b>		
<b>Stratigraphy</b>		<b>Lithology</b>	<b>Stratigraphy</b>		<b>Lithology</b>
<b>Formation</b>	<b>Member/Lithotype</b>		<b>Formation</b>	<b>Member/Lithotype</b>	
<b>Amuri Limestone</b>	<b>Lower Limestone lithotype</b>	<b>Limestone</b>	<b>Amuri Limestone</b>	<b>Lower Limestone lithotype</b>	<b>Limestone</b>
	<b>Teredo Limestone Member</b>	<b>Greensand</b>		<b>Teredo Limestone Member</b>	<b>Greensand</b>
		<b>Limestone</b>	<b>Mead Hill Formation</b>		<b>Limestone</b>
		<b>Greensand</b>			<b>Greensand</b>
<b>Mead Hill Formation</b>		<b>Siliceous micrite</b>			

### **5.1.2 Suggested Future Stratigraphic Nomenclature**

#### ***Amuri Limestone***

There have been few studies of the Muzzle Group outside the Clarence Valley following establishment of the name by Reay (1993), giving little opportunity to apply the new nomenclature in coastal areas such as Kaikoura Peninsula and Haumuri Bluff. Warren (1995) extended Reay's (1993) lithostratigraphic framework outside the Clarence Valley by

including the Amuri Limestone within the Muzzle Group around Haumuri Bluff. However, Rattenbury et al. (2006) confused the situation by stating that while the Amuri Limestone was assigned to the Muzzle Group in the north of the Kaikoura QMap area, this was not the case south of Kaikoura, where the formation was not assigned to a group at all (without making reference to Warren (1995)). Following Forsyth (2001), Rattenbury et al. (2006) assigned the Amuri Limestone to the Eyre Group.

Though assigning the Amuri Limestone to the Eyre Group may be applicable for the unit around Waipara in the Canterbury Basin, it is suggested here that this is not the case in the vicinity of Haumuri Bluff that lie to the north of the Hurunui High (Figure 5.1). The Hurunui High is a NW-SE trending structural high that was emergent through the latest Cretaceous-Paleocene and separated marine deposition of mudstone in the south from micritic limestone facies in the north (Figure 5.1) (Field et al. 1989). This high remained emergent through the early Paleocene and Field et al. (1989) inferred from seismic data that the high was overlapped in the Early Eocene, although King et al. (1999) suggest the area was submerged by the latest Paleocene. While its shape and size are poorly constrained, this structural high is inferred to have formed the southern boundary of the Marlborough paleo-embayment of Crampton et al. (2003) and therefore the boundary between the East Coast Basin and Canterbury Basin at this time (Figure 5.1). It is therefore suggested here that the Amuri Limestone in the Parnassus area be retained within the Muzzle Group, following convention from elsewhere in the East Coast Basin, and not based solely on present day geographic location within the north Canterbury region alone (Table 5.2).

### ***Teredo Limestone***

It appears that the name 'Teredo Limestone' is a misleading relic of early geological study in the area. The name 'Teredo' implies a relationship with the wood boring bivalve of the same name, even though wood and the bivalve *Teredo* are arguably not present in the unit at all (Warren & Speden 1978). Warren and Speden (1978) showed that calcitic tubes identified as *Teredo* by Hector (1874) at Haumuri Bluff, were probably

clavagellid bivalve tubes (Figure 5.2). Subsequently, Beu & Maxwell (1990) suggest that Warren & Speden (1978) may have also misidentified these fossils and that the tubes may actually be those of a sediment burrowing member of the Teredinidae. Nevertheless, similar tubes also occur in the overlying Lower Limestone (Morris 1987; Crampton 1988) and Lower Marl lithotypes of the Amuri Limestone (Reay 1993) and so are not a uniquely distinguishing feature of the Teredo Limestone. Moreover, the name *Teredo* does not follow stratigraphic convention because it is a fossil name rather than some appropriate geographical name. And finally, to compound this confusion further, the Teredo Limestone Member is, by definition, not a limestone, but rather a slightly to highly calcareous sandstone with varying quantities of glaucony (Reay 1993). For this reason, Field et al. (1997) referred to the unit simply as the Teredo Member.

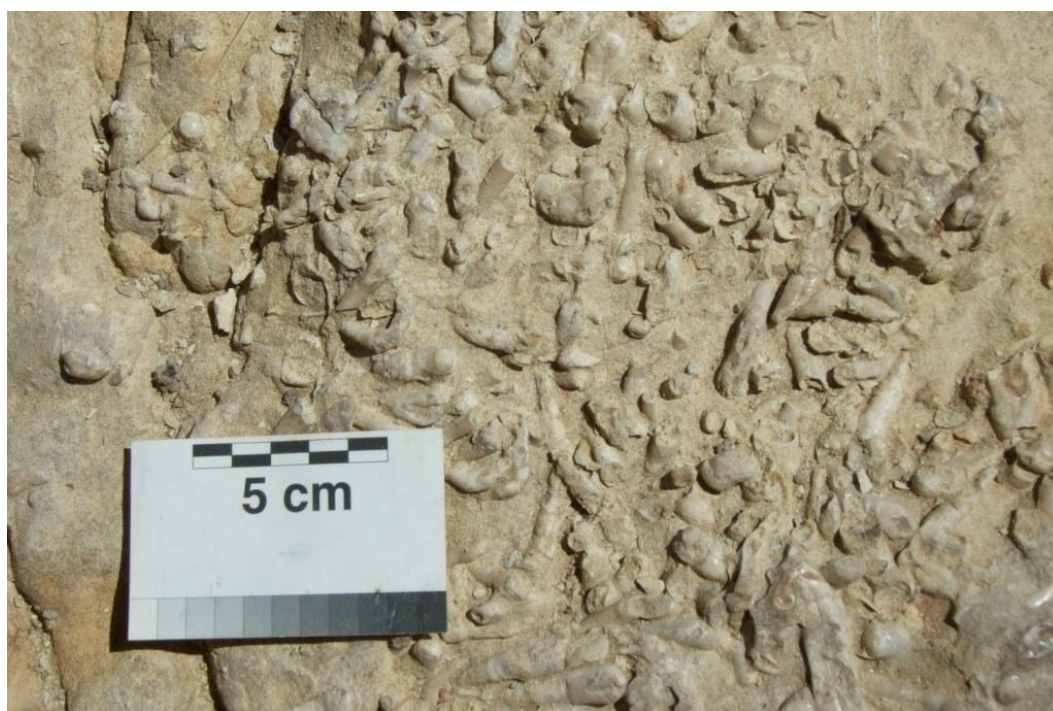


**Figure 5.2** Problematic calcitic bivalve tubes on the uppermost contact of the Teredo Limestone at Haumuri Bluff. Once identified as *Teredo* tubes by early geological workers, Warren & Speden (1978) suggested they were formed by another bivalve group, possibly the Clavagellidae. However, Beu & Maxwell (1990) subsequently suggested that, based on appearance, the tubes were probably a sediment burrowing member of the Teredinidae.

It is proposed here that the present Teredo unit be elevated to formation rank following the suggestion of Browne et al. (2005b) and that the name



'Teredo Limestone Member' be discontinued altogether (Table 5.2). Instead, in future work, it is suggested that the unit be renamed the '**South Bay Formation**' in recognition of the accessible outcrops of the unit at South Bay on the Kaikoura Peninsula (NZMS 260 O31 661646). Moreover, it is advocated here that the South Bay Formation be divided into two formal members based on the identification of two informal lithofacies within the Teredo Limestone by Reay (1993) (Table 5.2). The suggested name for the basal cream to grey, massive, slightly calcareous sandstone facies is the '**Hundalee Sandstone Member**', with reference to the easily accessible outcrop of this member in a railway cutting on Claverley Road near Hundalee (NZMS 260 O32 469444) (Enclosure 1). The upper green, glauconitic, highly calcareous sandstone name is suggested to be the '**Dart Greensand Member**', with reference to the northernmost outcrop of this unit in the Clarence Valley (NZMS 260 O30 674047). It is chosen here to retain the hypostratotype for the Teredo Limestone Member nominated by Reay (1993) at The Fell for the newly designated South Bay Formation, as this locality exposes both members and clearly shows their relationship.

**Table 5.2** Current Paleocene to Middle Eocene lithostratigraphic nomenclature in southeastern Marlborough (after Reay 1993; Hollis et al. 2005b) along with suggested future stratigraphic nomenclature for the region.

Reay (1993) & Hollis et al. (2005b)			Future recommendations from this study		
Group	Formation	Member or lithotype	Group	Formation	Member or lithotype
Muzzle Group	Amuri Limestone	Grasseed Volcanics	Muzzle Group	Amuri Limestone	Grasseed Volcanics
		Upper Marl			<i>Requires revision</i>
		Fells Greensand			Fells Greensand
		Upper Limestone			<i>Requires revision</i>
		Lower Marl			<i>Requires revision</i>
		Dee Marl Mbr			Dee Marl Mbr
		Lower Limestone			<i>Requires revision</i>
		Teredo Limestone Mbr			<b>Dart Greensand Member</b>
		<b>Hundalee Sandstone Member</b>			
		Waipawa Formation	Waipawa Formation		
	Mead Hill Formation	Mead Hill Formation			

### ***Amuri Limestone Lithotypes***

One further weakness of the lithostratigraphic nomenclature developed by Reay (1993) is the establishment of informal lithotypes within the Amuri Limestone. In studies following Reay (1993), the use of these units has required the establishment of conventions such as capitalising unit names to distinguish them from simple generic lithologies (Strong et al. 1995). However, this has not always been strictly adhered to (e.g. Field et al. 1997) and in some cases these units are not referred to at all (e.g. Rattenbury et al. 2006). Crampton et al. (2003) even used these unit names as formal members of the Amuri Limestone, which is contrary to guidelines for stratigraphic nomenclature that state that terms such as lower, middle and upper should not be used in formal subdivision of lithostratigraphic units (Hedberg 1976). As these changes in lithology are likely to reflect significant paleoclimatic events (Hollis et al. 2005a, b), and are therefore globally important, it is recommended that in an effort to avoid any further confusion that these units should be elevated to formal member rank within the Amuri Limestone in the future (Table 5.2). New names are not suggested here because of the limited scope of this study.

## **5.2 PALEOENVIRONMENTAL SIGNIFICANCE OF LITHOFACIES**

This section discusses the key characteristics of the six lithofacies identified as part of field work undertaken in southeastern Marlborough and on Campbell Island (Table 5.3). The inferred environment of deposition for each lithofacies is then discussed, utilising field, petrographic and geochemical data, before addressing the broad relationships between the identified lithofacies.

### **5.2.1 Siliceous Micrite and Chert Facies (F1)**

#### ***General Characteristics***

The siliceous micrite and chert facies (F1) is represented by the Late Cretaceous-Late Paleocene Mead Hill Formation and lower part of the Amuri Limestone at some locations in southeastern Marlborough. In outcrop, this facies is characterised by light grey to cream, highly indurated siliceous micrite with wavy bedding. Lawrence (1993, 1994) suggests that this pinch-and-swell morphology is results from differential

**Table 5.3** Key characteristics of the six lithofacies identified in southeastern Marlborough and at Campbell Island as part of this study.

Lithofacies	Location	NZ Stage <sup>1</sup>	Environment	Trace fossils	Siliciclastic grains	Glaucony	TRG <sup>2</sup>	Si[exc] <sup>3</sup>	Ca[exc] <sup>4</sup>	Ba[exc] <sup>5</sup>
<b>Siliceous micrite and chert facies (F1)</b>	Mead Stream Muzzle Stream Kaikoura wharf	Mh-uDt	Bathyal	<i>Zoophycus</i> <i>Chondrites</i> <i>Planolites</i>	No	No	Low	High	Low	Mod
<b>Organic mudstone facies (F2)</b>	Mead Stream	uDt	Bathyal	<i>Chondrites</i> <i>?Planolites</i>	No	Yes	High	High	Low	High
<b>Micrite facies (F3)</b>	Muzzle Stream Kaikoura wharf Campbell Island	uDt-Dm	Bathyal	<i>Zoophycus</i> <i>Chondrites</i> <i>Planolites</i>	No	No	Low	Low	High	Low
<b>Greensand facies (F4)</b>	Muzzle Stream Kaikoura wharf	IDt-Dw	Bathyal	<i>Thalassinoides</i> <i>Scolicia</i>	Yes	Yes	Mod-Low	Mod	Mod	Low
<b>Calcareous glauconitic mudstone (F5)</b>	Campbell Island	Dm	Bathyal	N/A	Yes	Yes	Mod	Mod	Mod	Mod
<b>Fine sandy mudstone facies (F6)</b>	Campbell Island	Mh-uDt	Inner Shelf	<i>?Zoophycus</i> <i>?Chondrites</i>	Yes	Yes	High	Mod	Low	Low

<sup>1</sup> New Zealand Stage abbreviations are defined in Appendix A; l: lower, u: upper.

<sup>2</sup> TRG – Terrigenous supply, a geochemical proxy for clays based on the elemental concentration of TiO<sub>2</sub> in samples

<sup>3</sup> Si[exc] – Silica excess, a geochemical proxy for biogenic silica based on the elemental concentration of SiO<sub>2</sub> in samples

<sup>4</sup> Ca[exc] – Calcium excess, a geochemical proxy for biogenic carbonate based on the elemental concentration of CaO in samples

<sup>5</sup> Ba[exc] – Barium excess, a geochemical proxy for productivity based on the elemental concentration of Ba in samples

compaction of relatively chert-free limestone around chert nodules. Petrographically, this facies consists of visible microfossils, especially radiolarians and silicified foraminifera. SEM reveals coccolith debris recrystallised microcrystalline spar and authigenic silica (Figure 4.11). Directly above and below any interbedded units of the greensand facies (F4), F1 contains both glaucony and fine to very fine sand sized quartz and feldspar grains. These are not considered to be characteristic of this facies as a whole but rather a result of vertical reworking of unlithified sediment through bioturbation. Most importantly, the siliceous micrite and chert facies is characterised by a low terrigenous component (otherwise dominantly clay minerals) and high concentrations of biogenic silica, evidenced by ternary plots from Mead Stream, Muzzle Stream and Kaikoura wharf (Figure 4.14, 4.23, 4.41) and geochemical proxies for terrigenous supply (TRG) and excess silica (Si[exc]), (Table 5.3 and Enclosure 1).

### ***Inferred Environment of Deposition***

As the siliceous micrite and chert facies (F1) corresponds to upper portions of the Mead Hill Formation and parts of the Lower Limestone lithotype of the Amuri Limestone, depositional environments suggested for these units by previous authors (e.g. Reay 1993; Field et al. 1997; Hollis et al. 2005b) are applicable for this facies. The siliceous micrite facies was deposited at bathyal depths (Strong et al. 1995), as a pelagic rain of sand to clay sized planktonic debris many kilometres from paleoshorelines in southeastern Marlborough during the Late Paleocene. Extensive bioturbation throughout F1 suggests that the upper few metres of this facies was deposited as soupy to soft sediment, under well oxygenated conditions (Ekdale et al. 1984). Both the geochemical and petrographic evidence from F1 are consistent with the suggestions of Hollis et al. (2005b) that the siliceous deposits formed during periods of relatively cool climate, with low precipitation and terrigenous input as well as increased bio-siliceous and -calcareous productivity in the southeastern Marlborough region through the Late Cretaceous to Paleogene.

## **5.2.2 Organic Mudstone Facies (F2)**

### ***General Characteristics***

The organic mudstone facies (F2) is only identified at Mead Stream and corresponds to the Waipawa Formation of Hollis et al. (2005b). This facies is characterised by a very distinctive 'rusty' dark brown, fissile appearance in outcrop (Figure 4.5). The organic mudstone facies has a reduced diversity of trace fossils in comparison to both the siliceous micrite and chert facies (F1) and micrite facies (F3). The very fine grained nature of F2 renders poor petrographic resolution apart from discernible increases in the abundance of radiolarians and sponge spicules (Figure 4.10E, F). Geochemically, the organic mudstone facies is characterised by high terrigenous supply (TRG), excess silica (Si[exc]) and excess barium (Ba[exc]), as well by significant depletion in manganese (Table 5.3 and Enclosure 1).

### ***Inferred Environment of Deposition***

At Mead Stream, the organic mudstone facies (F2) was deposited at bathyal depths (Strong et al. 1995) at a time of increased terrigenous supply as well as greatly enhanced productivity leading to the expansion or intensification of the Oxygen minimum zone (OMZ) during a period of invigorated ocean currents. This inferred environment of deposition is consistent with suggestions made elsewhere for the Waipawa Formation and lateral equivalents as a whole (Isaac et al. 1994; Strong et al. 1995; Field et al. 1997; Killops et al. 2000; Hollis et al. 2005b).

### ***Increased Terrigenous Supply***

The increase in terrigenous supply is evidenced firstly by the position the organic mudstone facies (F2) occupies when plotted on a ternary plot of the three major chemical components of sedimentary rocks (Figure 4.14A). The position along the axis between the SiO<sub>2</sub> and Al<sub>2</sub>O<sub>3</sub> poles infers that this facies is composed of a mixture of silica (mainly biogenic) and clays with negligible amounts of carbonate. The only other facies to plot near this position on the ternary plot is the fine sandy mudstone facies (F6) from Campbell Island (Figure 3.17) which was deposited in an inner shelf to brackish environment (Hollis et al. 1997). Second, the inorganic

geochemical proxy for terrigenous supply based on the concentration of  $\text{TiO}_2$  in the sample (TRG) is much higher through the organic mudstone facies (F2) when compared with the bounding siliceous micrite and chert facies (F1) at Mead Stream (Table 5.3 and Enclosure 1).

This observation of increased terrigenous supply is supported by an increase in the percentage of total phytoclasts (higher land plant tissue debris) and decrease in the ratio of black to brown phytoclasts in F2 at Mead Stream (Poul Schiøler pers. comm. 2009). High percentages of phytoclasts indicate proximal settings, while high ratios of black to brown phytoclasts generally indicate more distal depositional settings. Increases in these non-marine proxies through the Tartan Formation at distal sites in the Great South Basin and in the Waipawa Formation at Te Hoe Stream in northern Hawkes Bay are interpreted by Schiøler (2010) to represent a eustatically driven fall in sea-level. Taking into consideration the fact that Mead Stream lay at bathyal depths during the upper Teurian (Strong et al. 1995; Hollis et al. 2005b), it is suggested here that the palynofacies changes at this site are more a response to enhanced sediment transport conditions due to invigorated ocean currents than to simple eustatic sea-level fall.

#### *Enhanced Siliceous Productivity*

Ba, in the form of barite, is strongly correlated with biological productivity in modern day ocean surface waters (Dymond et al. 1992) and is widely used as a proxy for paleo-productivity on this basis (Schmitz 1987a; Schmitz et al. 1997; Schroeder et al. 1997; Thompson & Schmitz 1997). Large increases in Ba[exc] through the organic mudstone facies (F2) (Enclosure 1) are therefore interpreted here to reflect a sudden and rapid increase in productivity in the southeastern Marlborough sector of the Marlborough paleo-embayment. This is supported by the associated increase in Si[exc], an inorganic geochemical proxy for siliceous productivity, as well as the observed increase in abundance of radiolarians when compared with the bounding siliceous micrite and chert facies.

### *Reduced Oxygen Conditions*

Following Killips et al. (2000) and Hollis et al. (2005b), it is suggested here that this period of enhanced productivity resulted in the expansion or intensification of the OMZ due to degradation of large amounts of organic debris sinking through the water column. Indications of low oxygen provided by microfossil assemblages dominated by agglutinated foraminifera (Strong et al. 1995) are supported here by depletion of Mn through both Mudstone A and B (Enclosure 1), as well as increases in redox sensitive metals. Depletion of Mn in the organic mudstone facies (F2) is interpreted here to primarily reflect the redistribution of Mn within the water column and/or at the sediment-water interface because of oxygen deficiency. Reducing conditions above the Mead Stream site during the deposition of this facies would have dissolved soluble  $Mn^{2+}$  ions within the water column and at the sediment/water interface so that Mn flux was greatly reduced (Dickens & Owen 1994). Following this,  $Mn^{2+}$  would have been transported through the OMZ and deposited at sites below the redox boundary. If redirection of Mn has occurred during the deposition of the Waipawa Formation in the upper Teurian, this model could be confirmed by enrichment of Mn in sediments at deeper sites to the p-north during this period. This process only occurs when dissolved oxygen drops below 2.0 ml/l, placing an upper limit on dissolved concentrations at Mead Stream during this period. Given all this, diagenetic remobilisation of Mn within the sediment column and lowered carbonate accumulation rates (Dickens & Owen 1994) cannot be discounted as playing a part in the process of Mn depletion.

Mo is also a useful paleo-redox proxy as it forms stable oxyanions ( $MoO_4^{4-}$ ) under oxic conditions but is efficiently accumulated in sulphides under anoxic conditions or in sulphur-rich organic matter under high  $H_2S$  concentrations and reactive iron limited systems (Turgeon & Brumsack 2006, and references therein). Mo concentrations measured from the organic mudstone facies (F2) (Appendix D) are consistent with values from a range of dysoxic depositional environments reported by Lyons et al. (2009).

A reduction in the diversity of trace fossils further supports the inference of reduced oxygen conditions during the deposition of the organic mudstone facies (F2) at Mead Stream, while also suggesting that oxygen levels were not sufficiently low to entirely prevent colonisation or bioturbation. The possible identification of *Planolites* in thin sections of samples from this facies is questionable (Figure 4.10D), while the identification of *Chondrites* is consistent with poorly oxygenated conditions (Ekdale et al. 1984).

### **5.2.3 Micrite Facies (F3)**

#### ***General Characteristics***

The micrite facies (F3) corresponds to the uppermost beds of the Early Paleocene Mead Hill Formation and the Late Paleocene to Eocene Amuri Limestone in Marlborough, and also to the Eocene Tucker Cove Formation on Campbell Island. In outcrop, the micrite facies is characterised by light grey to cream, moderately hard to hard micrite, with varying bedding styles between regions. In southeastern Marlborough, F3 has a more tabular geometry, with 15-30 cm thick micrite beds interbedded with 2-10 mm thick marl beds, while on Campbell Island the facies comprises thinner (3-5 cm), strongly developed stylolitic beds. F3 is extensively bioturbated and includes *Zoophycus*, *Chondrites* and *Planolites* trace fossils. Like the siliceous micrite and chert facies (F1), the micrite facies is very fine grained, with SEM analysis showing a preponderance of recrystallised microcrystalline spar and carbonate detritus in the form of coccolith debris. Visible microfossils in thin section are dominated by planktic foraminifera with less common benthic foraminifera. Geochemically, the micrite facies (F3) can be viewed as a less siliceous, more calcareous equivalent of the siliceous micrite and chert facies (F1), as shown by the position of the micrite facies on ternary plots of the three major chemical components of sedimentary rocks and the geochemical proxies excess silica (Si[exc]) and excess calcium carbonate (Ca[exc]) (Table 5.3 and Enclosure 1).

#### ***Inferred Environment of Deposition***

The inferred environment of deposition of the micrite facies (F3) is identical to that suggested in previous studies of the Amuri Limestone (e.g. Nelson



1968; Morris 1987; Reay 1993; Field et al. 1997; Hollis et al. 2005b). It represents a nannofossil and foraminiferal ooze deposited in a low energy, bathyal, oceanic environment. Though this facies has only been described from a handful of sections covering a relatively short period of geological time as part of this study, it forms part of the very widely distributed Amuri carbonate megafacies (Hood & Nelson 1996). The Amuri carbonate megafacies was deposited throughout several of New Zealand's Cenozoic sedimentary basins from Northland to Campbell Island during the Paleocene to Oligocene in response to continued passive margin thermal subsidence. The widespread and long lived nature of the Amuri carbonate megafacies implies that processes responsible for the deposition of F3 was not confined to southeastern Marlborough and Campbell Island during the Late Paleocene to Early Eocene.

The limestone-marl bedding style of the micrite facies (F3) from southeastern Marlborough and Campbell Island is 'micro-rhythmic', a striking feature common to many carbonate occurrences in the sedimentary record (Einsele & Ricken 1991). Primarily, such limestone-marl alternations are developed in response to fluctuations of at least one component of the original deposit, either the carbonate fraction or non-carbonate fraction, or both (Westphal et al. 2004). For this reason, this style of bedding is regularly interpreted to reflect periodic variations in orbital parameters of the Earth leading to variations in carbonate production, terrigenous supply and/or periodic dissolution of carbonate (Einsele & Ricken 1991). Such an interpretation has been suggested for the Mead Hill Formation across the Cretaceous/Paleocene boundary (Field & Hollis 2003) and the Amuri Limestone across the Paleocene/Eocene boundary (Hollis et al. 2005b) in southeastern Marlborough.

However, it is widely recognised that diagenetic overprinting can lead to alteration and accentuation of original rhythms within these deposits (Ricken & Eder 1991). In a shallow marine burial environment, redistribution of calcium carbonate can occur through dissolution of

aragonite in marl interbeds and reprecipitation of calcite in limestone beds (Munnecke & Samtleben 1996; Munnecke et al. 2001), while in deeper burial environments there can be dissolution of calcite in marl beds and reprecipitation as cement in limestone beds (Ricken 1986, 1987). Given the deep burial history of the Amuri carbonate megafacies as a whole (Hood & Nelson 1996) and the discontinuous nature of beds in the micrite facies (F3) at Campbell Island, it could be suggested that this facies has been affected by diagenetic redistribution to some degree. Since Einsele & Ricken (1991) state that the chance of preserving primary limestone-marl alternations is greatly reduced by bioturbation when primary bed thickness drops below a critical thickness of 5-10 cm, the identification of marl interbeds thinner than 1 cm further supports a degree of diagenetic imprint for the beds in this facies. Consequently it is suggested that more investigation is needed before the significance of the bedding in the bathyal micrite facies (F3), and in the Amuri Limestone as a whole, is positively understood.

#### **5.2.4 Greensand Facies (F4)**

##### ***General Characteristics***

The greensand facies (F4) corresponds to the Late Paleocene to Early Eocene Teredo Limestone from southeastern Marlborough and the K/T boundary unconformity greensand unit at Kaikoura wharf. In outcrop this facies consists of light to dark greenish grey, moderately indurated, calcareous greensand. This facies is generally massive, with extensive bioturbation in the form of *Thalassinoides* and *Scolicia* trace fossils. One key feature of the upper greensand unit in outcrop at Kaikoura wharf is the presence of shark teeth and phosphatised micritic limestone clasts. In thin section the greensand facies is dominated by subangular to subrounded, moderately to well sorted, fine to very fine sand sized quartz and K feldspar, together with pelletal and vermicular glaucony, set in a predominantly (argillaceous) micritic matrix which appears siliceous in restricted zones. Geochemically, F4 is characterised by moderate to low abundance of clays as evidenced by the geochemical proxy for terrigenous supply (TRG), and by low excess silica (Si[exc]) and

intermediate concentrations of excess calcium carbonate (Ca[exc]) (Table 5.3 and Enclosure 1).

### ***Inferred Environment of Deposition***

The greensand facies (F4) was deposited during a period of reduced sedimentation and condensation, punctuated by phases of redistribution of siliciclastic and perigenic glaucony grains. During periods of low sedimentation, extensive infaunal bioturbation resulted in homogenisation of sediments and destruction of primary sedimentary structures.

As stated in Chapter 4, the low percentage of glaucony in the unit associated with the K/T boundary at Kaikoura wharf means the unit should be classified as a glauconitic sandstone. However, the retention of this unit within the greensand facies (F4) is based on the fact that both units appear to have been formed as a result of similar, if not identical, depositional processes during separate oceanographic events.

### ***Siliciclastic Sedimentation***

One of the key features of the greensand facies (F4) is the fine to very sand sized siliciclastic grains, otherwise rare to absent in previously discussed facies (F1, F2 and F3). The presence of this component in a bathyal deposit implies some it was significant sediment transport. This follows the suggestion of Hollis et al. (2005c) that the bathyal depth of sites in the middle Clarence Valley precludes sea-level fall as a driver for facies changes during the Late Paleocene to Eocene. Extensive bioturbation in the greensand facies (F4) has resulted in homogenisation of the facies and destruction of primary sedimentary structures at sites investigated as part of this study, making it difficult to determine the mechanism(s) of sediment transport. However, identification of low angle cross stratification in the Teredo Limestone at Seymour Stream and The Fell in the middle Clarence Valley by Reay (1993), strongly suggests that the transport of this sediment occurred as a result of invigorated ocean currents (discussed further in section 5.3).

The well sorted, subrounded to subangular nature of siliciclastic grains in F4, combined with the low percentage of clays represented by the inorganic geochemical proxy TRG (Enclosure 1), is consistent with Morris' (1987) interpretation that the siliciclastic components in the Teredo Limestone represent a texturally mature sediment. Morris (1987) inferred the textural maturity of siliciclastics in the Teredo Limestone to reflect recycling of the Late Cretaceous Claverley Sandstone provenance, with other extrabasinal sources playing an insignificant role (Figure 5.3). The observation of fine calcareous matrix making up 40-60% of the greensand facies (F4), however, is inconsistent with the Teredo Limestone as a whole, being a texturally mature sediment. However, Reid et al. (1990) noted that interpretations of depositional settings based on micrite content can be invalidated by the internal precipitation of micrite below the sediment/water interface, thereby seemingly altering the ratio of the mud (micrite)/grain ratio of deposits. It is possible that a combination of homogenisation by infaunal bioturbation and internal precipitation of fine carbonate could have resulted in the high proportion of micritic matrix in F4.

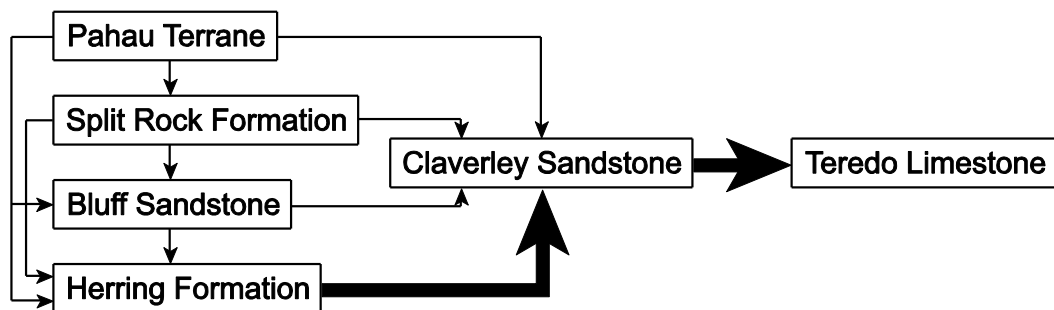


**Figure 5.3** Schematic diagram of inferred provenance relations for the siliciclastic fraction of the Teredo Limestone. Width of arrows indicates relative volumetric importance of each source (after Morris 1987).

### *Glauconitic Sediments*

Glaucony (glauconite) is a key characteristic of F4. Typically such green grains are regarded as authigenic, forming *in situ* by progressive alteration of carbonate particles, argillaceous faecal pellets and infilling foraminiferal tests through the growth of crystallites in pore spaces and the uptake of potassium and iron (Odin & Matter 1981). Optimal conditions for the

formation of glaucony require semi-confinement allowing for ionic exchange between the microenvironment and ambient open marine seawater (Odin & Matter 1981). However, glaucony can also be reworked (Amorosi 1997 and references therein), either through recycling from extrabasinal sources or through redistribution of grains formed contemporaneously within the basin. In the latter case, such grains are referred to as 'perigenic' in origin (Lewis 1964). While it is likely that at least some of the glaucony grains in the greensand facies (F4) are truly authigenic in origin, much of the glaucony from F4 in southeastern Marlborough displays features considered by Amorosi (1997) to be characteristic of transported glaucony. The dominance of well sorted, moderately to well rounded, pelletal glaucony is consistent with the transport of glaucony, and is consistent with the variable thickness of the Teredo Limestone across southeastern Marlborough as a whole. The most conclusive evidence does not come from sites investigated as part of this study, but from Seymour Stream and The Fell in the middle Clarence Valley, where glaucony is preferentially concentrated along foresets of low angle cross beds (Reay 1993). This is consistent with Morris' (1987) suggestion that not all glaucony of the Teredo Limestone should be considered first cycle, with at least some being recycled, along with siliciclastic grains, from the Claverley Sandstone. However, it is further suggested here that the majority, and possibly all, of the glaucony in F4 is perigenic rather than extrabasinal allogenic in origin, being contemporaneously developed on the Marlborough paleo-platform before transportation to deeper sites corresponding to the middle Clarence Valley area.

Phosphatic grains and phosphatised clasts of micritic limestone observed in the greensand facies (F4) are also considered to have a perigenic origin. These components represent rip-up clasts of mineralised and lithified, syndimentary cementation horizons (hardgrounds) associated with hiatal surfaces (Scholle & Ulmer-Scholle 2003). Hardgrounds and marine cementation surfaces in cool-water limestones generally form as a result of slow, arrested or negative sedimentation rates in relatively high energy environments (Kennedy & Garrison 1975; Nelson & James 2000;

Noe et al. 2006), so that the presence of these clasts in F4 is consistent with the above interpretations of this facies.

### **5.2.5 Calcareous Glauconitic Mudstone Facies (F5)**

#### ***General Characteristics***

The calcareous glauconitic mudstone facies (F5) corresponds to the base of the Early Eocene Tucker Cove Limestone on Campbell Island. One of the key characteristics of this facies in outcrop is its highly weathered nature, so that it is typically represented by a recessed zone wherever the boundary between the Garden Cove Formation and Tucker Cove Limestone is exposed. Another key characteristic of this facies that differentiates it from the overlying micrite facies (F3), is the abundance of glaucony which reaches ~10% directly above the lower contact with the Garden Cove Formation. The overall fine grained nature of this facies means the majority of components are indistinguishable in thin section, though some fine to medium sand sized, microcrystalline, pelletal glaucony and fine sand to coarse silt sized K-feldspar grains occur. Inorganic geochemical proxies show that this facies contains moderate quantities of terrigenous material (TRG), excess silica (Si[exc]) and excess calcium carbonate (Ca[exc]) (Table 5.3). On a ternary plot of the three major chemical components of sedimentary rocks, samples from F5 plot along a 'carbonate dilution line' between the underlying fine sandy mudstone facies (F6) and the overlying micrite facies (F3) (Figure 3.17). Interestingly, the calcareous glauconitic mudstone facies (F5) has high Al normalised concentrations of Zr (Enclosure 1) and rare earth elements (REEs) such as La, Nd and Y.

#### ***Inferred Environment of Deposition***

The calcareous glauconitic mudstone facies (F5) was deposited at bathyal depths (Hollis et al. 1997) and represents the initiation of deposition of the Amuri carbonate megafacies at Campbell Island in the form of the Tucker Cove Limestone following unconformity development through the Late Paleocene to Early Eocene. The high concentration of glaucony towards the base of this facies is consistent with the prolonged period of non-deposition represented by the unconformity between the Garden Cove

Formation and overlying Tucker Cove Limestone by Hollis et al. (1997). Increasing dilution by carbonate up through this facies into the overlying micrite facies (F3) at Campbell Island is evidence of increasing isolation of the site from the paleoshoreline, as well as continued drowning of sources of terrigenous sediment during passive margin thermal subsidence of the area through the early Cenozoic. Concomitant enrichment of Zr and REEs is consistent with the concentration of heavy minerals such as zircon, likely reflecting winnowing of sea-floor sediments by invigorated ocean currents responsible for the formation of the underlying unconformity.

### **5.2.6 Fine Sandy Mudstone Facies(F6)**

#### ***General Characteristics***

The fine sandy mudstone facies (F6) corresponds to the Late Cretaceous to Paleocene Camp Cove Formation on Campbell Island. In outcrop, this facies consists of brown, massive, highly bioturbated siliceous mudstone with varying amounts of fine sand. One important characteristic of F6 is the presence of quartz pebbles 'floating' within the uppermost 30 cm of the unit. In thin section this facies is dominated by a siliceous/argillaceous and carbonaceous matrix containing abundant fine to very fine sand sized quartz and feldspar as well as microcrystalline pelletal glaucony and vermicular glauconitised biotite. Geochemically, the fine sandy mudstone facies (F6) is characterised by high quantities of terrigenous material, evidenced by its position on a ternary plot of the three major chemical components of sedimentary rocks (Figure 3.17) and by the inorganic geochemical proxy for terrigenous supply (TRG) (Table 5.3 and Enclosure 1). F6 also has moderate concentrations of excess silica, and low excess calcium carbonate (Ca[exc]) (Enclosure 1).

#### ***Inferred Environment of Deposition***

High TRG and low Ca[exc] values in the fine sandy mudstone facies (F6) (Enclosure 1) are consistent with an inner shelf depositional environment as suggested by Hollis et al. (1997). The observation of glaucony in the upper 1.4 m of this facies suggests probably reduced sedimentation rates at Campbell Island during the Paleocene.

Based on the fact that the underlying basement rock of the Complex Point Group at Campbell Island is characterised by an absence of feldspar (Beggs 1976; Beggs et al. 1990), the occurrence of K feldspar detected under cathodoluminescent light supports Beggs' (1976) suggestion that the source area for the Garden Cove Formation contained granitic rocks. This implies that Cretaceous silicic and intermediate plutonic rocks constituting basement rocks in areas like Auckland Island and the Great South Basin (Beggs et al. 1990) were exposed and actively supplying sediment in the form of quartz, feldspar and kaolinite (Beggs 1976) to the Campbell Island site during the Late Cretaceous to Paleocene.

Given the relatively fine grained nature of the fine sandy mudstone facies (F6), the observation of quartz pebbles appears to be highly anomalous. However, similar pebbles have been described from time-equivalent formations: the Abbotsford Formation at Fairfield Quarry, Otago (Pont Lurcock pers. comm. 2009) and from the Whangai Formation at Angora Stream near Tawanui and Riversdale in southeastern North Island (Leckie et al. 1995) (Enclosure 1). Based on the lack of evidence of high energy bed load transport mechanisms, and micropaleontologic and organic geochemistry, Leckie et al. (1995) interpreted lone stones from the east coast of the North Island to represent ice rafted debris transported by ice bergs or seasonal ice calving from glaciers, probably originating from Antarctica. Given the paleogeographic location of Campbell Island during the Paleocene, and a similar lack of evidence of high energy bed load transport mechanisms, it is suggested that the floating quartz pebbles in F6 on Campbell Island are related to the same ice rafting event described by Leckie et al. (1995).

### **5.2.7 Lithofacies Relationships**

A key to interpreting the paleoenvironmental importance of the lithofacies changes identified in this research relates to appreciating their spatial distribution across the study sites (Figure 5.4). The siliceous micrite and chert facies (F1), micrite facies (F3) and fine sandy mudstone facies (F6) are considered here to represent the general 'background' sedimentation



that occurred during continued passive margin thermal subsidence of the eastern margin of Zealandia. As part of formal lithostratigraphic units, the facies were developed over a prolonged period from the Late Cretaceous to Late Oligocene (Enclosure 1). Similarities in trace elemental concentrations of samples from F1 and F3 in southeastern Marlborough and F6 and F3 from Campbell Island suggest that the source of terrigenous material remained constant through the deposition of these facies. This supports the suggestion of Reay (1993) that the Mead Hill Formation is essentially a chert rich facies of the Amuri Limestone

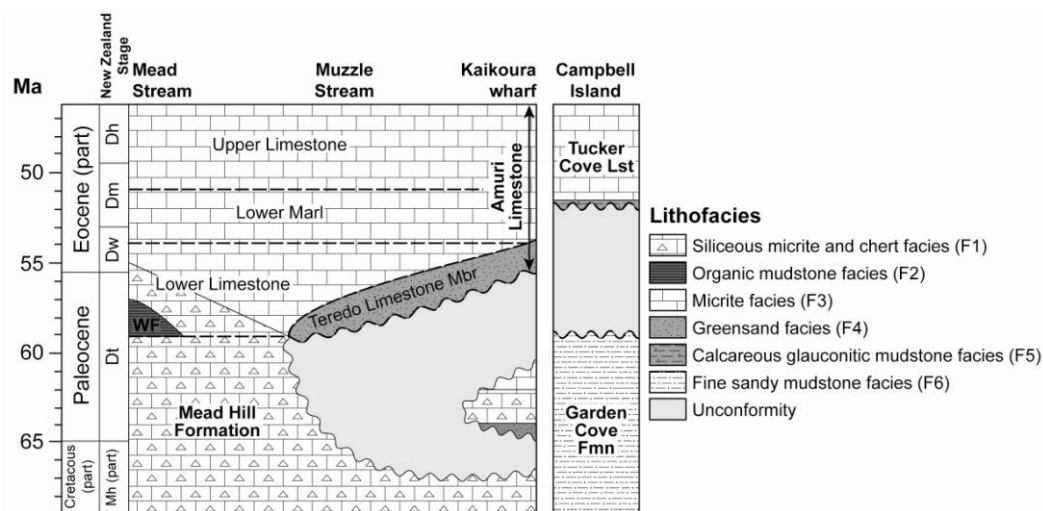


**Figure 5.4** Relationship between lithofacies in the study sites of this investigation at Mead Stream, Muzzle Stream and Kaikoura wharf, southeastern Marlborough, and on Campbell Island along with formal stratigraphic units of Reay (1993) and Hollis et al. (2005b) (Table 5.2). Solid lines denote boundaries of lithofacies; dashed lines denote boundaries of formal stratigraphic units. WF: Waipawa Formation.

However, during the upper Teurian to Mangaorapan, ‘normal’ background sedimentation was sufficiently affected by changes in oceanographic conditions to result in formation of a regionally extensive unconformity and the deposition in different places of the organic mudstone facies (F2), greensand facies (F4) and calcareous glauconitic mudstone facies (F5) (Figure 5.4). In southeastern Marlborough, deposition of the organic mudstone facies (F2) reflects a temporary increase but sudden increase in terrigenous supply and siliceous productivity which resulted in expansion of the oxygen minimum zone at the distal Mead Stream site. In more proximal sites, at Muzzle Stream and Kaikoura wharf, the greensand facies (F4) is underlain by a significant unconformity. This facies was

deposited as a result of continuing reduced sedimentation rates, associated with previous unconformity development, punctuated by the periodic supply of detrital siliciclastic and perigenic glaucony and phosphatic grains. The greensand facies (F4) and organic mudstone facies (F2) are considered to be equivalent (Strong et al. 1995), based on the fact that at Mead Stream and Muzzle Stream the two lithofacies were deposited contemporaneously (Hollis et al. 2005c). However, both the basal and top contact of F4 is time-transgressive, younging towards the southwest (Figure 5.4). On Campbell Island the calcareous glauconitic mudstone facies (F5) directly overlies a major unconformity and shows that winnowing of sea-floor sediments and reduced sedimentation rates, probably as a result of invigorated ocean currents, prevailed during its deposition.

### 5.3 PALEODISTRIBUTION MAPS

Attempts to construct paleogeographic and isopach maps for the Cretaceous to Paleogene strata of southeastern Marlborough have been hampered by pervasive Neogene tectonic deformation that has resulted from the propagation and subsequent development of the Pacific/Australian plate boundary through New Zealand (Crampton et al. 2003). Until the study of Crampton et al. (2003) previous reconstructions of basin morphology and facies relationships had simply used present day geographic configurations and no attempt at palinspastic maps had been made.

**Table 5.4** Deformations and adopted retro-deformations used in the retro-deformation models, listed in order of processing (from Crampton et al. 2003).

Deformation	Magnitude	Adopted retro-deformation
1 NW-SE shortening across Awatere block	2-6 km immediately N of Tapuae-o-Uenuku	4 km extension at Tapuae-o-Uenuku
2 Shortening across Flag Creeks Thrust	5 km	5 km extension
3 Dextral strike-slip across Clarence Fault	25 ± 10 km	25 km sinistral
4 NW-SE shortening across Clarence Fault	2-3 km	2.5 km extension
5 Dextral strike-slip on Fidget Fault	1 km	0 km
6 NW-SE shortening across Clarence block	17 km in NE, 10 km in centre and S	Extension: 17 km in NE; 10 km in centre and S
7 NW-SE shortening across London Hill Fault	1.3 km	1.3 km extension
8 Dextral strike-slip on Jordan Stream Thrust/Kekerengu Fault	5-15 km	5 km sinistral strike-slip on Kekerengu Fault segment
9 NW-SE shortening across Kekerengu block	7 km in southern half	7 km extension
10 Dextral strike-slip on Hope Fault	20 km	20 km sinistral
11 NW-SE shortening across Kaikoura block	2 km at Kaikoura; 4 km at Haumuri Bluff; 5 km in S	Extension: 2 km at Kaikoura; 4 km at Haumuri Bluff; 5 km in S
12 Clockwise, vertical-axis rotation of all blocks	100°	100° anticlockwise

Retro-deformations carried out by Crampton et al. (2003) shown in Table 5.4 were applied to the five major structural blocks identified in southeastern Marlborough (Figure 5.5). Using the Awatere Fault as the northwestern boundary, retro-deformations were performed from northwest to southeast in the order shown in Table 5.4, resulting in the configuration shown in Figure 5.6. This process is described in full in Crampton et al. (2003).

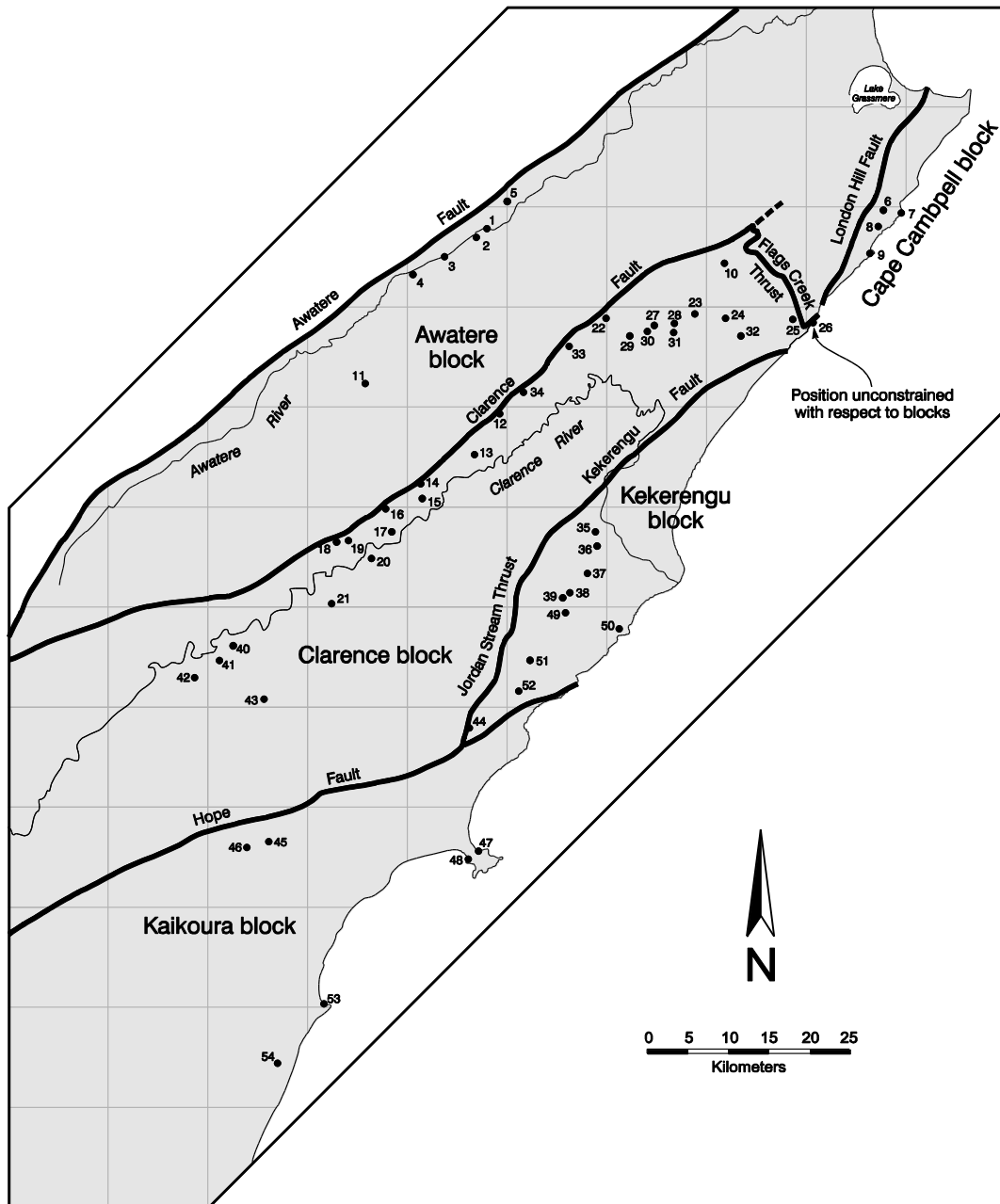


**Figure 5.5** The major structural boundaries and blocks used in the retro-deformation of southeastern Marlborough to establish late Early Cretaceous to Early Eocene configurations (from Crampton et al. 2003). Also shown are the stratigraphic data localities (Table 5.5) and the 10 km New Zealand map grid.

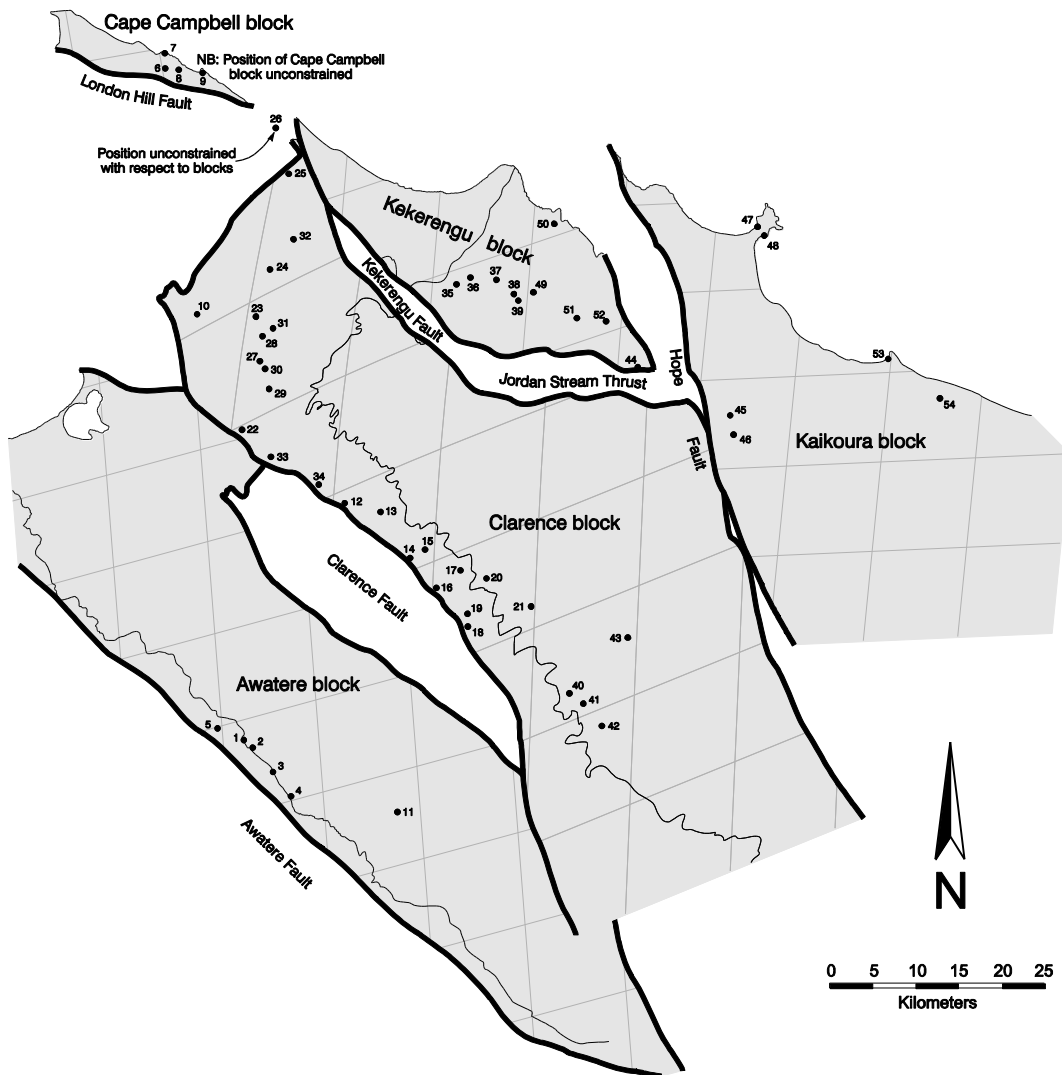


**Figure 5.6** Retro-deformed configuration of southeastern Marlborough, showing the stratigraphic data localities and 10 km New Zealand grid retained for reference. This map is used for all the Cretaceous and Paleogene palinspastic maps of Crampton et al. (2003) and for the Teredo Limestone palinspastic map (this study). White areas between blocks represent areas uplifted and eroded since the Oligocene (from Crampton et al. 2003).

Stratigraphic data localities shown in Figure 5.5 are summarised in Table 5.5, while thickness data used in the creation of the palinspastic maps in Figures 5.7 to 5.9. is summarised in digital appendices, along with electronic copies of retro-deformed base maps. Following Crampton et al. (2003), the same base map has been used for the Teredo Limestone as for all other Cretaceous and Paleogene reconstructions and assumes negligible deformation in the area during this period. All compass bearings cited in the following text that refer to retro-deformed maps are prefixed by “p-”, indicating that they are paleo-bearings. As the retro-deformation performed by Crampton et al. (2003) involved 100°

anticlockwise rotation, p-north is approximately equivalent to a bearing of 100° in present-day co-ordinates.

**Table 5.5** Stratigraphic data localities used for the late Early Cretaceous to Early Eocene palinspastic reconstructions. The localities are numbered from northwest to southeast according to the present-day map NZMS 260 map of southeastern Marlborough. Note that grid references are approximate and may span greater stratigraphic intervals than those of interest here; original sources should be consulted for full details. The data sources are as follows: logs held in the stratigraphic measured section file at GNS, Lower Hutt, are prefixed by CCP and given a map sheet and unique column (“C”) number; other sources can be found in the reference list or are self explanatory.

Locality no.	Locality	Map sheet	Grid ref. base	Grid ref. top	Data sources
1	Isis R. – Awatere R.	O29	678277	673280	Crampton et al. 2003
2	Cam R. – Awatere R.	O29	667266	663273	Crampton et al. 2003
3	Hodder R. – Clyde Stm	O29	634242	640255	Crampton et al. 2003
4	Limestone Stm	O29	603233	603233	Crampton et al. 2003
5	Penk Stream	P29	705304	O29/693310	CCP P29/c20
6	Flaxbourne R.	P29	*	*	Crampton et al. 2003
7	Chancet Rocks	P29	086286	094295	Morris 1987
8	Butt Stm	P29	055292	057290	Crampton et al. 2003
9	Needles Point	P29	065255	065255	Crampton et al. 2003
10	Isolation Ck	P29	916226	916228	CCP P29/c21
11	Winterton R.	O30	581139	506104	CCP O30/c16
12	Branch Stm, middle branch	O30	693093	691094	O30/c7
13	Dart Stm	O30	674047	659059	O30/c2
14	Muzzle Stm, W branch	O30	614024	612026	This study
15	Muzzle Stm – Dead Horse Gully	O30	620011	605013	CCP O30/c9
16	Bluff Stm upper	O30	576998	576002	O30/c3
17	Bluff Stm	O30	590973	585975	O30/c1
18	Gentle Annie Stm	O30	529963	529963	O30/c13
19	Bluff R.	O30	540957	541975	O30/c5
20	Dubious Stm	O30	566950	563954	CCP O30/c18
21	Limestone Hill	O30	521902	522900	O30/c14
22	Swale Stm	P30	*	*	C. Hollis (unpubl. data)
23	Kekerengu R., upper reaches	P30	890192	884195	Crampton et al. 2000
24	Ben More Stm, upper reaches	P30	920186	922190	CCP P30/c14
25	Woodside Ck	P30	975188	992191	CCP P30/c5
26	Wharanui Point	P30	*	*	Crampton et al. 2003
27	Cover Stm	P30	842180	845181	Crampton et al. 2003
28	Southern flanks Whernside	P30	864183	864183	CCP P30/c7
29	Ouse Gorge – Sawpit Gully	P30	808147	828180	Crampton et al. 2003
30	Coverham track above Wharf Stm	P30	840174	840174	Crampton et al. 2003
31	Burnt Saddle	P30	867171	866174	Crampton et al. 2003
32	S-flow tributary Ben More Stm	P30	931166	932169	Crampton et al. 2000
33	Mead Stm	P30	762160	753164	Strong et al. 1995, Hollis et al. 2005, this study
34	Dee Stm	P30	706117	704119	Hancock et al. 2003
35	Farm track N Miller Stm	P30	794977	788977	Crampton et al. 2003
36	Miller Stm	P30	790966	783963	Crampton et al. 2003
37	Wharekiri Stm, lower gorge	P30	783942	774932	Crampton et al. 2003
38	Wharekiri Stm, main section	P30	768920	748913	CCP P30/c10
39	Wharekiri Stm, W limb	P30	747913	748912	Crampton et al. 2003
40	Seymour Stm	O31	424859	423859	O31/c8, J. Crampton (unpubl. data)
41	The Fell	O31	414844	415846	O31/c3, J. Crampton (unpubl. data)
42	Wallow Stm	O31	384831	387829	O31/c5, J. Crampton (unpubl. data)
43	Bluff Dump	O31	463807	458806	Crampton et al. 2003
44	Hapuku R.	O31	663794	662795	Crampton et al. 2003
45	Monkey Face 1	O31	c. 465670	c. 465670	Crampton 1988
46	Monkey Face 2	O31	c. 440660	c. 440660	Crampton 1988
47	Kaikoura Peninsula, N side	O31	674656	674656	This study
48	Kaikoura Peninsula, S side	O31	661646	674656	O31/c1
49	Limestone Stm headwaters	P31	766895	761896	P31/c3
50	Mororimu Stm	P31	808880	813886	Morris 1987
51	Jordan Stm – Puhī Puhī R	P31	724849	723846	P31/c4
52	Puhī Puhī R. at Clinton confluence	P31	711814	711814	P31/c5
53	Haumuri Bluff	O32	514507	525503	J. Crampton (unpubl. data)
54	Conway R. mouth	O32	469444	475442	O32/c3

### **5.3.1 Spatial Distribution of Late Cretaceous to Early Eocene Units, With Emphasis on the Teredo Limestone**

#### ***Urutawan-Motuan Sediments***

The initial phase of deposition in southeastern Marlborough is recorded by Urutawan to Motuan (late Early Cretaceous) sediments (Figure 5.7). These sediments directly overlie Torlesse basement rocks of the Pahau Terrane and thicken to the p-southwest, showing substantial local variation in thickness. This distribution is inferred to result from pre-existing erosional topography and syndepositional tectonic activity along p-NE-SW trending normal faults on the Awatere block and p-NW-SW trending normal faults on the Clarence block during this period. This largely extensional tectonic activity is related to the initial stages of crustal extension prior to opening of the Tasman Sea and predates the major phase of extension in other basins (King et al. 1999; Crampton et al. 2003). Paleocurrent data from these strata show that these faults greatly influenced gravity flows responsible for the deposits mapped by Crampton et al. (2003).

#### ***Herring Formation***

Crampton et al. (2003) state that the Piripauan (mid-Late Cretaceous) signifies the cessation of rifting and onset or pronounced acceleration of thermal subsidence in southeastern Marlborough, resulting in a major p-north to p-south marine transgression (Figure 5.8). Palinspastic maps for the Piripauan Stage and Herring Formation show a general thickening of isopachs toward the p-northwest and identify a trough-shaped depocentre named the Kaikoura Trough by Crampton et al. (2003) (Figure 5.8). This feature opened to the p-northeast and ran parallel to the paleoshoreline from the centre of the Clarence block. The trough was separated from thicker deposits in the p-northwest by the Wharekiri Swell, the combined isopachs from the Piripauan Stage and Herring Formation showing significant thickness variations between the axes of these two features (Crampton et al. 2003). These structures run roughly parallel to Motuan normal faults on the Awatere block (Figure 5.7) and are inferred by Crampton et al. (2003) to represent a graben (or grabens) related to earlier extension. The persistence of this feature for ~10 My from the

Piripauan through to the lower Haumurian suggests that minor faulting continued throughout this period.

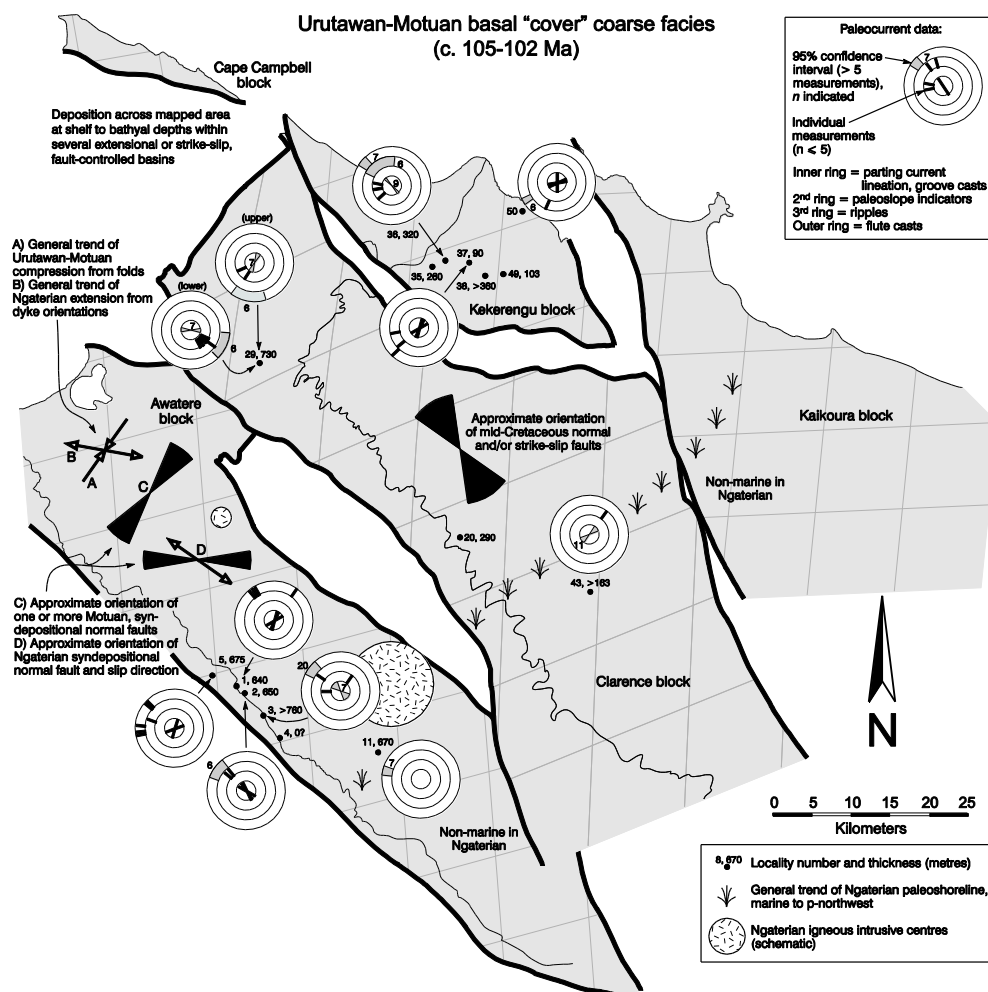


**Figure 5.7** Palinspastic map for the Urutawan-Motuan (late Early Cretaceous) basal 'cover' coarse facies, showing thickness and facies data (from Crampton et al. 2003). Locality numbers refer to localities in Table 5.5.

### **Mead Hill Formation**

The palinspastic map for the Mead Hill Formation shows very little evidence for any inherited topographic or structural features by upper Haumurian time, suggesting that they had been buried by deposits of the earlier Herring Formation (Figure 5.9A). Isopachs identify a broad shelf or platform, named the Marlborough paleo-platform (Crampton et al. 2003), centred on the Kekerengu block in the p-northeast of the Marlborough paleo-embayment (Figure 5.1). Isopachs show relatively uniform thickness trends across the Marlborough paleo-platform, with a steeper gradient in the p-south. This change in gradient is interpreted by Crampton et al. (2003) to represent steeper topographic gradients and

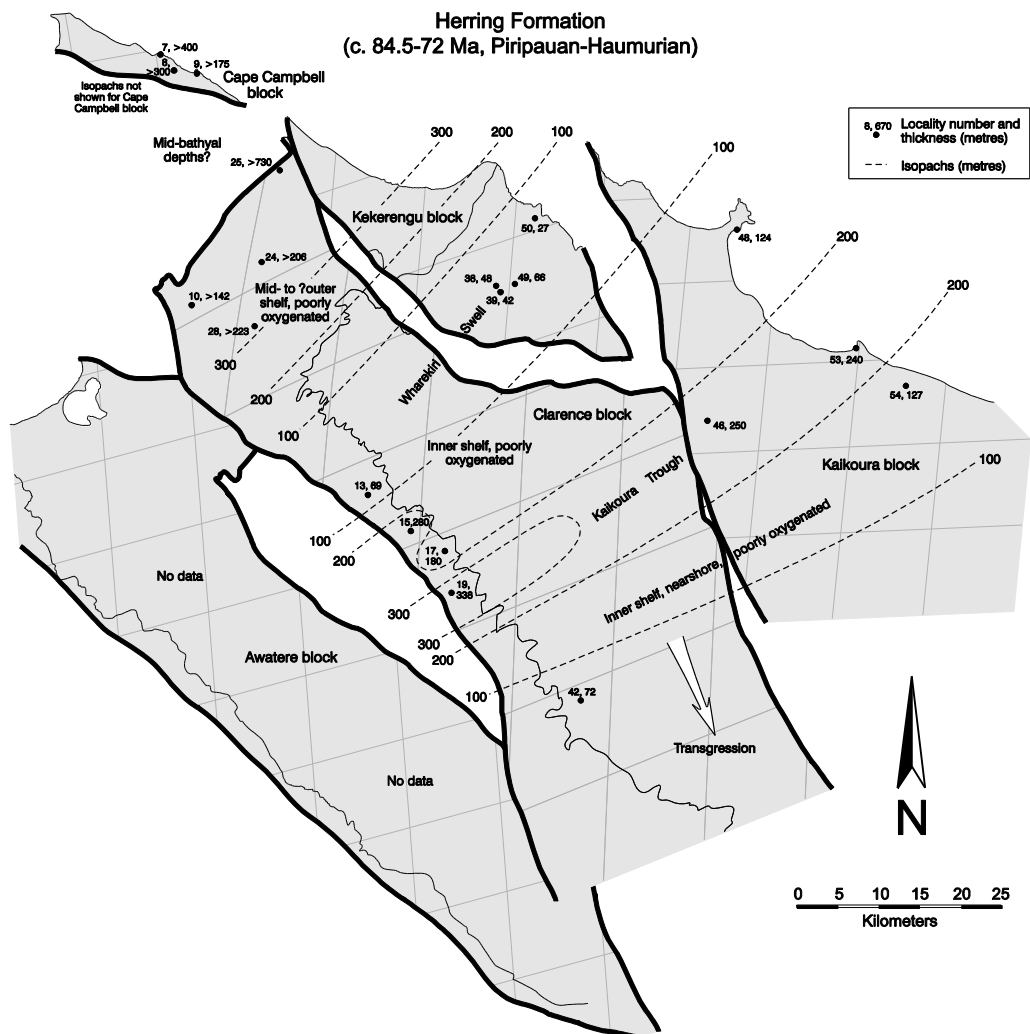


**Figure 5.8** Palinspastic map for the Herring Formation, showing thickness and facies data (from Crampton et al. 2003). Locality numbers refer to localities in Table 5.5.

possible constriction of the platform in this region, though no data are available for the Awatere block to constrain such interpretations. Through the upper Haumurian (latest Cretaceous), the Mead Hill Formation was predominantly deposited in inner to mid-shelf depths, deepening to upper to mid-bathyal depths in the p-northwest. Mead Hill Formation of Paleocene age was mainly deposited in upper bathyal depths and is only preserved in the p-northwest due to Paleocene erosion or non-deposition elsewhere.

### ***Amuri Limestone***

Crampton et al. (2003) chose to map only the distribution of the Lower Marl lithotype of the Amuri Limestone in an attempt to minimise the effects of truncation by unconformities bounding the formation (Figure 5.9B). The



palinspastic map for this lithotype shows almost identical trends in isopachs to the underlying Mead Hill Formation, confirming the presence of a broad, low gradient platform to the p-north which is more constricted to the p-south. Isopachs thicken from 0 m in the p-southeast to >100 m in the p-northwest.

### ***Teredo Limestone***

The Teredo Limestone lies between the two units mapped in Figure 5.9A & B and isopachs for this unit are relatively thin in comparison to the lithostratigraphic units and chronostratigraphic intervals mapped by Crampton et al. (2003). The palinspastic map for the Teredo Limestone (Figure 5.9C) shows some consistencies with those for the Mead Hill Formation and Lower Limestone lithotype of the Amuri Limestone, but overall different trends are evident. The Teredo Limestone was not widely deposited across the broad Marlborough paleo-platform during the Late Paleocene to Early Eocene. Unlike the Mead Hill Formation and Lower Limestone, thicknesses for the Teredo reduce quickly from the p-south towards the p-northwest and the unit is not recorded to the p-north of Dart Stream in the Clarence Valley or p-west of Kaikoura Peninsula. The distribution of isopachs is significantly affected by the absence of Teredo Limestone at Monkey Face (locality 46) and the Kekerengu block in general, resulting in the separation of two areas of comparatively thick deposits centred on Haumuri Bluff (locality 53) and Seymour Stream (locality 40).

At Monkey Face, a lithology similar to the Teredo Limestone is only preserved in *Thalassinoides* burrows which extend down into the Late Cretaceous Conway Formation, a correlative of the Herring Formation, which is unconformably overlain by the Lower Limestone lithotype of the Amuri Limestone (Morris 1987; Crampton 1988). In the Puhī Puhī River at the confluence with the Jordan Stream (locality 52), Morris (1987) assigned 4.6 m of 10-50 cm bedded, light to medium pinkish grey, glauconitic wackestone (limestone) interbedded with 1 cm thick light grey marl partings to the Teredo Limestone. The thickness of this unit is anomalously large in comparison to surrounding sites and it also does not

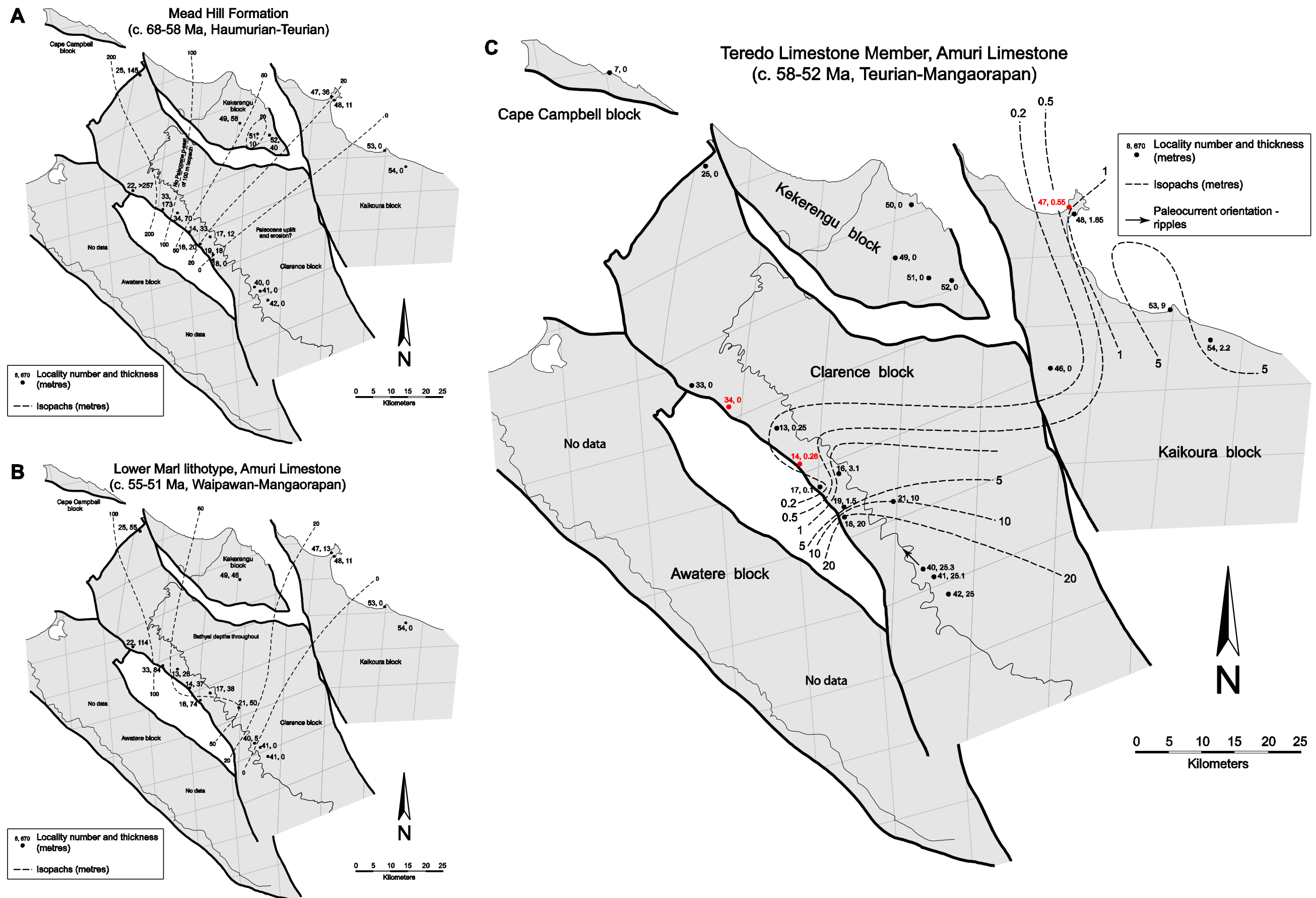


**Figure 5.9** Palinspastic recreation of southeastern Marlborough during deposition of the (A) Mead Hill Formation, (B) Lower Marl lithotype of the Amuri Limestone and (C) Teredo Limestone Member, showing thickness and facies data. (A & B from Crampton et al. 2003). Locality numbers refer to localities in Table 5.5. Localities in red are those investigated as part of this study.



fit the definition for the Teredo Limestone *sensu stricto* of Reay (1993). It appears that this unit at Puhi Puhi River shows a closer lithologic affinity with the basal portion of the Lower Limestone lithotype observed overlying the Teredo Limestone at Kaikoura wharf and it is therefore attributed to this lithotype in this study.

Major differences in the distribution of the Teredo Limestone (Figure 5.9C), when compared with bounding units (Figure 5.9A, B), suggest that the processes responsible for the formation of the Teredo unit were quite different from those that dominated throughout the majority of the Late Cretaceous to Middle Eocene.

Even though the deposition of the Waipawa Formation and lateral equivalents (e.g. Tartan Formation, Great South Basin) has been inferred to have occurred in response to a eustatically driven sea-level fall in the Late Paleocene (Schjøler et al. 2010), Hollis et al. (2005c) note that the bathyal water depth of sites in the middle Clarence Valley precluded sea-level change alone as being the principal driver for unconformity formation and lithofacies changes observed in Late Paleocene to Middle Eocene strata. It is therefore suggested that sedimentation and erosion patterns in the Marlborough paleo-embayment during this period were more likely caused by variations in current intensity and sediment pathways which were possibly more directly linked to climate changes driving eustatic changes (Hollis et al. 2005c).

### ***The Clarence Drift***

Based on this interpretation, combined with the isopach trends observed in Figure 5.9C, it is inferred here that the Teredo Limestone was deposited as a skin drift across the p-south to p-southeast of the Marlborough paleo-platform under the influence of significant seafloor currents. Isopachs identify two lobes of sediment, one in the p-east centred on Haumuri Bluff and another in the p-south centred on Seymour Stream. The latter occurrence is of particular interest and is here named the Clarence Drift. Despite the distribution of this drift being poorly constrained to the p-west and p-south due to a lack of data, it appears that the Clarence Drift has an

elongated shape, ~15-20 km long and ~10 km wide, and reaches ~25 m thick. This fossil drift is much smaller in comparison to major present day drifts documented from the Eastern New Zealand Oceanic Sedimentary System (ENZOSS) (Figure 5.10), such as the Rekohu Drift (ODP Site 1124) which extends ~250 km towards the Kermadec Trench from the northern slope of the Chatham Rise (Joseph et al. 2004). However, these drifts represent deep water sediment drifts, deposited in water depths in excess of ~3500 m, under semi-permanent oceanic currents, the Antarctic Circumpolar Current (ACC) and Pacific Deep Western Boundary Current (DWBC) (Carter, L. et al. 2004). Accumulation of these ‘modern’ drifts has

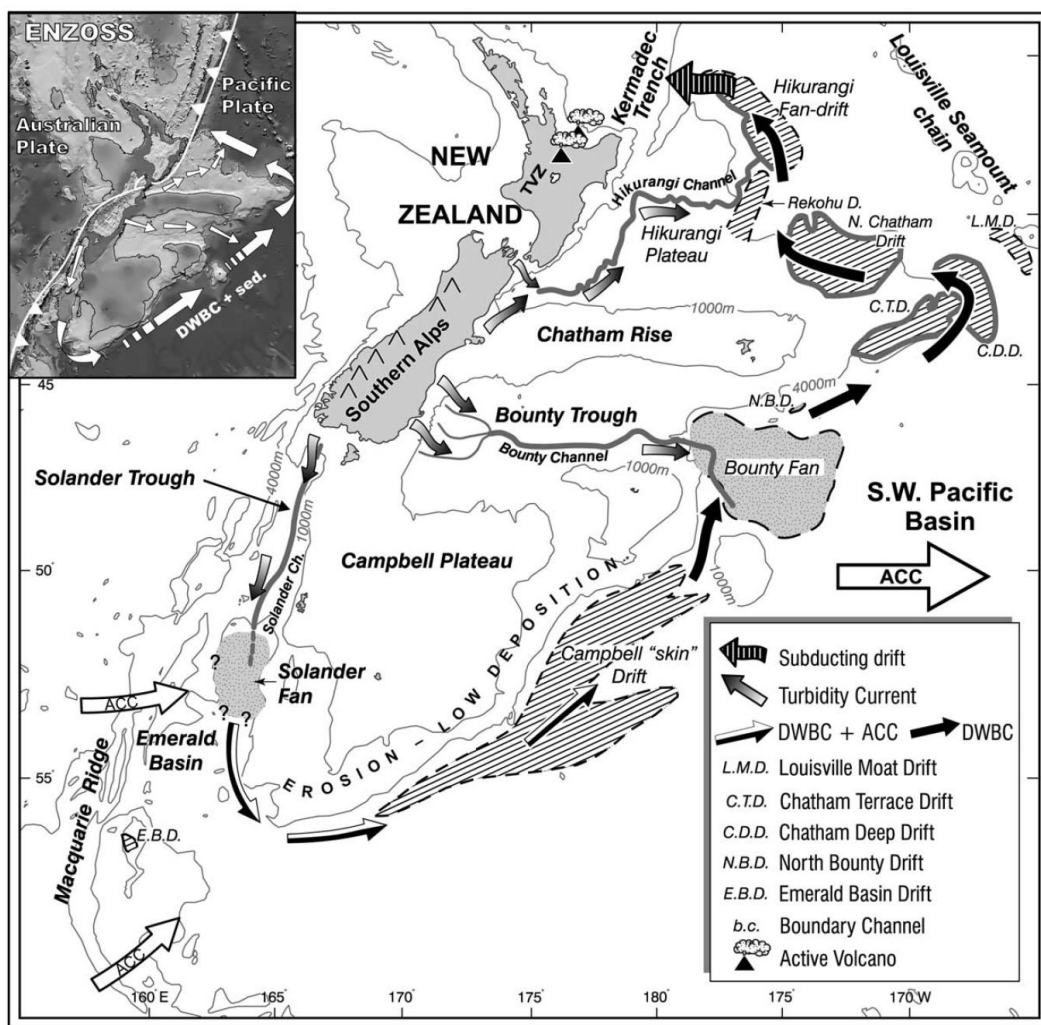


**Figure 5.10** Outline of the Solander, Bounty and Hikurangi channels as well as the main drift deposits beneath the Deep Western Boundary Current (DWBC) off southern and eastern New Zealand at the present day. (Inset) The Eastern New Zealand Oceanic Sedimentary System (ENZOSS) described by Carter L. et al. (2004) showing the main sediment delivery channels (small arrows) and abyssal transport directions (large arrows) (from Carter L. et al. 2004).

occurred over a much longer time period in comparison to the Clarence Drift, with the North Chatham Drift (ODP Site 1123) developing between the Early Miocene and the present day (Carter, R. M. et al. 2004b) and initiation of the Campbell 'Skin' Drift (see Figure 5.10) (ODP Site 1121) being at least as far back as the Middle Miocene (Graham et al. 2004).

The size and depth of deposition of the Clarence Drift would suggest that it is more comparable to Pliocene initiated drifts identified beneath the present day Canterbury slope at the head of the Bounty Trough (ODP Site 1119) (Lu et al. 2003; Carter, R. M. et al. 2004a). These Canterbury Drifts reach a maximum size of 50 km long, 20 km wide and 1 km thick, while smaller drifts, termed sediment waves by Lu et al. (2003), are mostly no bigger than 10 km long, 3 km wide and 0.1 km thick (Carter, R. M. et al. 2004a). These drifts were deposited along the mid-slope, in 400-800 m water depth, as a result of northeastward-flowing currents analogous to the modern day Southland Current which consists of Subantarctic Mode Water (SAMW) and Antarctic Intermediate Water (AAIW). Sediment was transported under inferred current speeds of ~5-15 cm/s. These drifts aggraded to the west (upslope) under the influence of the Coriolis affect (Lu et al. 2003; Carter, R. M. et al. 2004a).

The alignment of the axis of the Clarence Drift, as well as paleocurrent data from Seymour Stream and The Fell (Reay 1993), indicate that this drift moved from the p-southeast towards the p-northwest, running approximately parallel to the paleo-slope in this region of the Marlborough paleo-embayment (Figure 5.1). Extensive bioturbation in the Teredo Limestone means that primary sedimentary structures are not preserved in any other sections, making identification of paleocurrent directions difficult outside the Seymour Stream area. However, the direction of transport towards the p-northwest is supported by decreases both in grain size (Morris 1987) and the abundance of sand sized siliciclastic grains down the Clarence Valley (Figure 5.11). The concomitant increase in abundance of glaucony in the Teredo Limestone could be explained by a number of mechanisms. First, the decreasing abundance of siliciclastic sand could lead to an observed increase in the abundance of glaucony as

a result of decreased 'dilution'. Second, greater condensation of the unit as a consequence of decreased sedimentation in more distal sites (e.g. Muzzle Stream) could result in an increasing abundance of glaucony. Third, hydraulic sorting could have led to concentration of glaucony towards the p-northwest. As the hydrodynamic behaviour of glaucony is similar to that of lighter grains (McRae 1972; Amorosi 1997) it could have been transported greater distances than other comparably sized siliciclastics as current speeds decreased, resulting in the bimodal grain size distribution observed in the Teredo Limestone. This is supported by the observation of glaucony grains within the Waipawa Formation at Mead Stream. As glaucony generally forms at average water depths between about 50 m and 500 m (Amorosi 1997 and references therein), it is suggested here that these grains are entirely perigenic in origin (see section 5.2.4). It is inferred here that a combination of all these mechanisms is responsible for the observed changes in the abundance of glaucony, supporting significant sediment transport from the p-southeast.

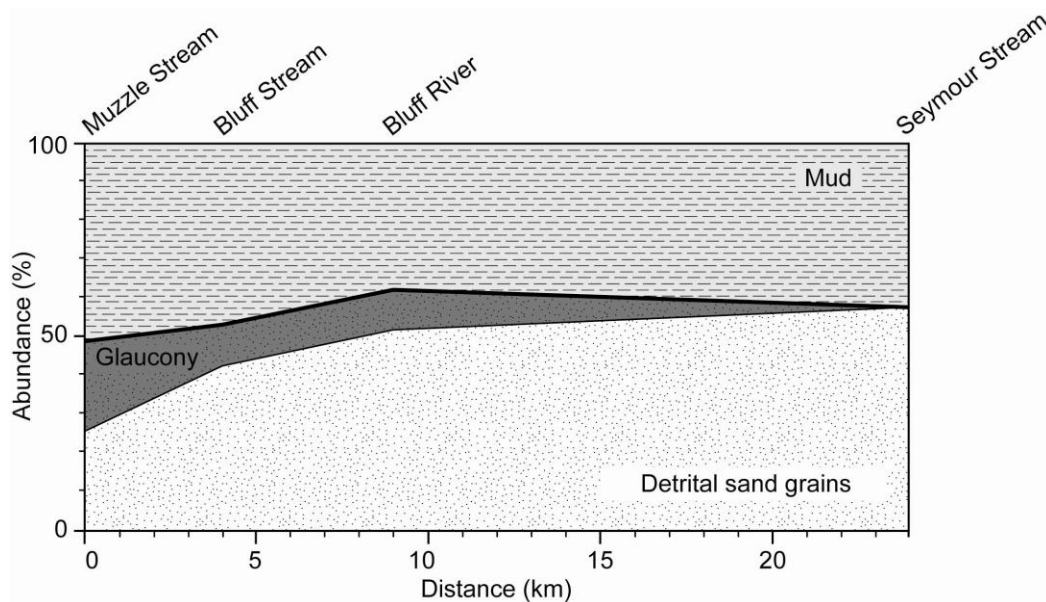


**Figure 5.11** Transect through the middle Clarence Valley showing the changing abundance of the major components within the Teredo Limestone (after Morris 1987, and this study).

It is therefore inferred here, taking into consideration issues outlined in Stow et al. (1998), that the postulated Clarence Drift may represent a fossil contourite deposit. Contourites are defined by Faugères & Stow

(1993) as sediments in relatively deepwater (>300 m) that have been deposited or significantly reworked by a stable geostrophic current.

Descriptions of the Teredo Limestone from southeastern Marlborough as a whole are consistent with descriptions of the sandy contourite facies by Stow et al. (1998), though descriptions from Seymour Stream (locality 40), The Fell (locality 41) and Wallow Stream (locality 42) are of particular relevance. Extensive bioturbation through the Teredo Limestone is considered to primarily reflect the condensed nature of the unit as a result of greatly reduced sedimentation rates during its deposition, a feature characteristic of many sandy contourite facies. Stow et al. (1998) state that preservation of primary horizontal and cross-lamination may occur in rare cases where sedimentation rates are relatively high and food supply for burrowing benthos is limited. This appears to have been the case at Seymour Stream and The Fell, where the Teredo Limestone reaches its maximum thickness (~25 m) and cross-lamination is evidenced by concentrations of glaucony and preferential weathering along foresets at these sites (Reay 1993). Of particular importance is the identification of occasional thin horizons of well rounded quartz and greywacke grains and angular phosphatised micrite and sandstone granules at sites in the p-south. These horizons are interpreted to represent minor disconformities within the Teredo Limestone and are consistent with the description of irregular erosional contacts and coarser concentrations or lags in beds from sandy contourite facies (Stow et al. 1998; Viana et al. 1998).

### **5.3.2 Temporal Lithofacies Changes**

This section records the broad distribution in southeastern Marlborough of the main lithofacies for four periods during the Paleocene-Early Eocene, namely lower Teurian (~64 Ma), upper Teurian (~58 Ma), Waipawan (~55 Ma) and Mangaorapan (~52 Ma). The paleo-lithofacies maps are necessarily highly generalised because of the scattered and sparse nature of control data points and lack of high resolution biostratigraphic information at sites other than Mead, Dee, Muzzle and Branch streams. Nevertheless, the ages from these sites have been extrapolated to the



wider region to allow interpretation of the timing of lithofacies changes and paleoclimate events.

### ***Lower Teurian***

During the lower Teurian, siliceous micrite and chert of the Mead Hill Formation was deposited throughout the p-northwest of the Marlborough paleo-platform (Figure 5.12). During the same period a greensand unit was deposited at the more proximal, Kaikoura wharf site (locality 47) on the north side of the peninsula (Figure 5.4). These lower Teurian deposits reach a maximum thickness of ~108 m at Mead Stream (locality 33) (Hollis et al. 2005b), while the thickness at Kaikoura wharf is highly condensed, up to 5.5 m. No rocks of Early Paleocene age are recorded from the p-southwest of the Marlborough paleo-platform. Following Morris (1987) and Reay (1993), it is suggested here that sedimentation either did not occur in this region during the lower Teurian or was subsequently removed during a period of erosion in the upper Teurian.

Though the majority of the lower Teurian is characterised by the lithofacies shown in Figure 5.12, the base of the Teurian (K/T boundary) is represented by an unconformity contained within the Mead Hill Formation. Around the K/T boundary, a portion of the Marlborough paleo-platform lay under a zone of nutrient upwelling and high bio-siliceous productivity (Figure 5.1) (Hollis et al. 2003b, c). Hollis et al. (2003b, c) investigated four sites representing an outer shelf to mid-bathyal depth transect through this zone, of which Branch Stream (locality 12) was the shallowest, and Flaxbourne River (locality 6) the deepest and considered to be the most stratigraphically complete. This suggestion was based on the identification of a K/T boundary fallout layer within claystone at the Flaxbourne River, as shown by a large geochemical anomaly of elements considered to be mainly or partly of meteorite origin (e.g. Ir, Ni, Cr, and Zn), and the most complete earliest Paleocene foraminiferal succession in the South Pacific (Hollis et al. 2003c). Woodside Creek contains a well documented K/T boundary fallout layer (Alvarez et al. 1980). However, this is directly overlain by Zone P $\alpha$ -P1a foraminifera (see Appendix A), suggesting a hiatus of >30 000 yr within the boundary clay at this site

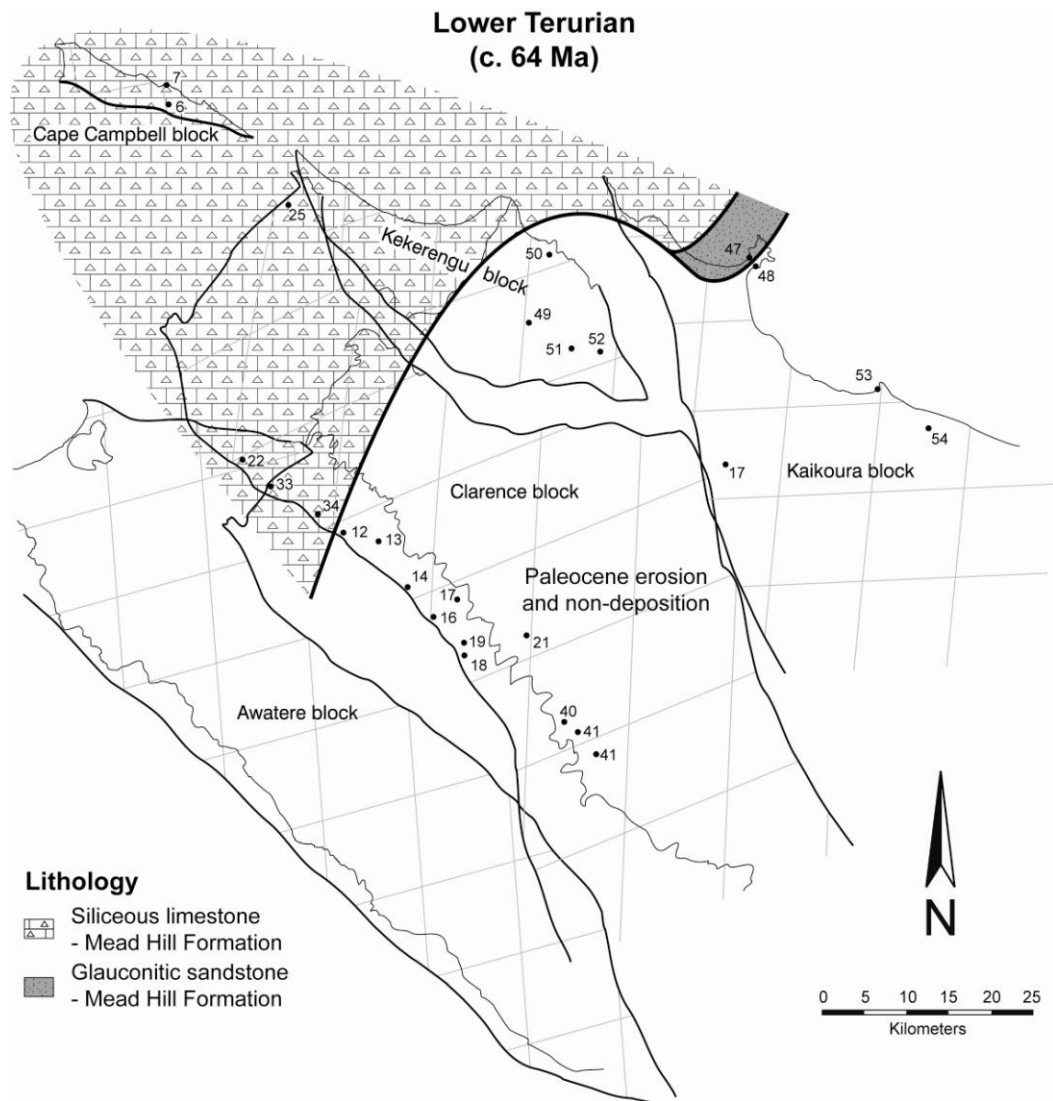


**Figure 5.12** Lithofacies map of southeastern Marlborough during the lower Teurian stage (c. 64 Ma). See text for references and discussion. Locality numbers refer to localities in Table 5.5.

(Hollis et al. 2003c). At Mead and Branch streams in the northern Clarence Valley, an unconformity of similar duration is inferred by Hollis et al. (2003b), based on the absence of a well defined fallout layer and definitive Zone P0 foraminiferal assemblages.

The unconformity described by Hollis et al. (2003b, c) from Branch Stream, Mead Stream and Woodside Creek is correlated here with the greensand unit and underlying unconformity contained within the top part of the Meade Hill Formation at Kaikoura wharf (Figure 4.28). Though sedimentation rates were greatly reduced during this period, evidenced by the presence of glaucony in the unit, there is also evidence for a shift from

microbioclastic sedimentation to siliciclastic sedimentation. This is shown by an increase in the abundance of detrital coarse silt sized quartz and feldspar grains observed in thin section, along with increases in terrigenous supply (TRG; Enclosure 1), and implies significant transport of terrigenous sediment during this period. Consistently low excess barium (Ba<sub>exc</sub>) values throughout the Late Cretaceous to Early Paleocene strata at Kaikoura wharf suggest the site lay outside the zone of upwelling centred on the region between Branch Stream to Flaxbourne River (Figure 5.1). Based on the occurrence of Zone RP3 radiolarians from samples of the siliceous micrite and chert facies (F1c), the return to deposition of late Cretaceous type lithofacies probably occurred within ~2 m.y. of the K/T boundary at Kaikoura wharf (Chris Hollis pers. comm. 2010). This is consistent with trends described by Hollis (2003), which showed that deeper sites (Woodside Creek and Flaxbourne River) returned to background sedimentation within 600 000 yr of the K/T boundary, while at Branch Stream the resumption of Cretaceous type facies occurred after ~1.5 m.y.

Hollis et al. (2003c) suggested that two relative sea-level falls at 64.9 Ma and 64.6 Ma resulted in basinward facies shifts and corresponded with increases in biogenic silica. The depositional hiatus described from Woodside Creek, as well as Mead and Branch streams, is also attributed to the initial sea-level fall (Hollis 2003, Hollis et al. 2003b, c). However, Hollis (2003) suggested that the magnitude of sea-level changes required to produce the facies shifts observed at the bathyal Flaxbourne site would be >200 m, but that sea-level changes of such magnitude would have resulted in much greater lithofacies changes in shallower sites such as at Branch Stream, Tora (Laird et al. 2003) and mid-Waipara (Hollis & Strong 2003) than are actually observed. It was therefore suggested by Hollis et al. (2003a) that Antarctic sourced deep water supplying nutrients to the coastal upwelling zone could have also played a role in unconformity formation during this period.

## Upper Teurian

The upper Teurian signifies a significant shift in the ocean circulation pattern in the Marlborough paleo-embayment when compared to the majority of the lower Teurian. Though 'normal' sedimentation continued with the deposition of siliceous micrite and chert through many sites in the p-northwest, this was disrupted at sites in the Clarence Valley (Figure 5.13). At Mead Stream (locality 33), organic mudstone of the Waipawa Formation was deposited during this period, while towards the p-southeast at Branch Stream (locality 13) and Muzzle Stream (Locality 14), greensand of the Teredo Limestone was deposited contemporaneously. During this period, erosion or non-deposition continued in the p-southwest of the Marlborough paleo-platform (Figure 5.13).

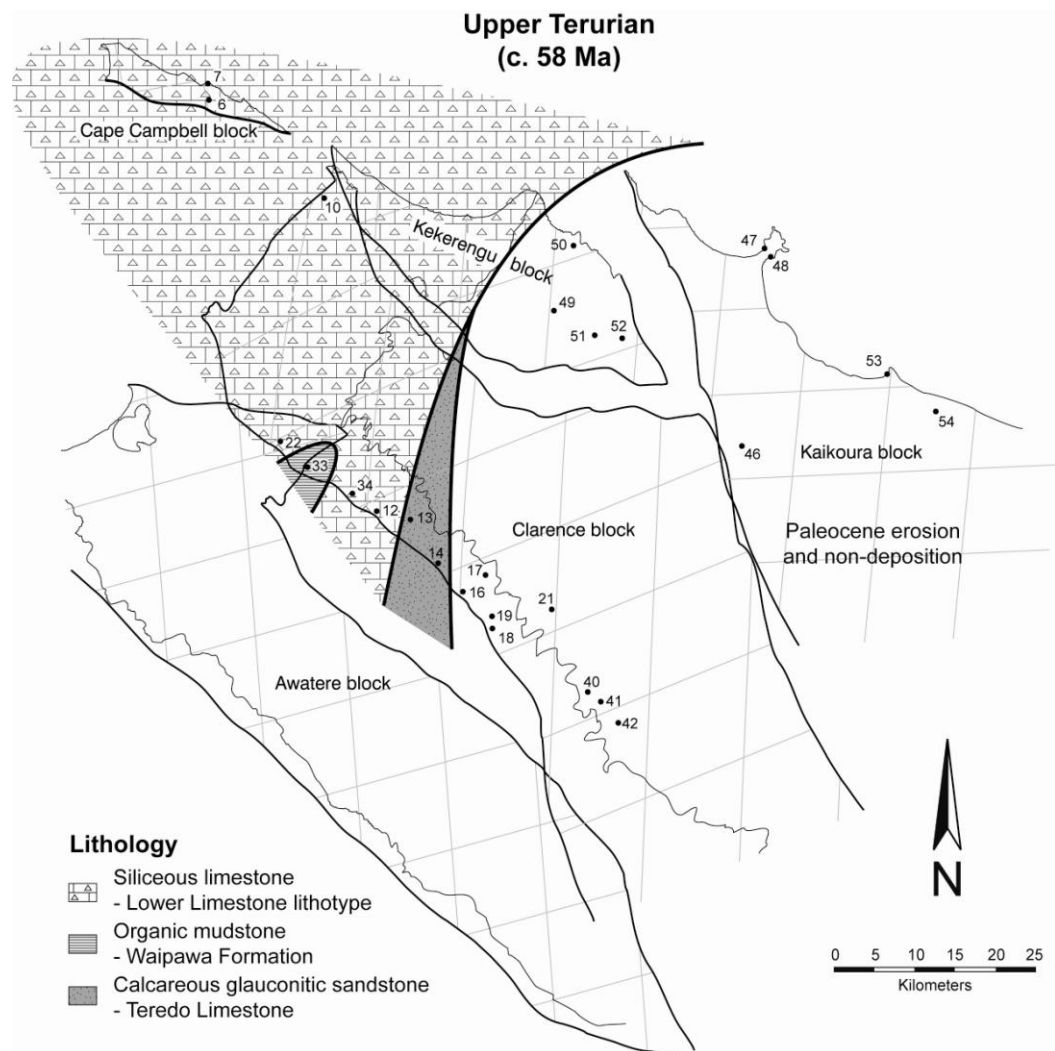


**Figure 5.13** Lithofacies map of southeastern Marlborough during the upper Teurian stage (c. 58 Ma). See text for references and discussion. Locality numbers refer to localities in Table 5.5.

At Mead Stream, the organic mudstone of the Waipawa Formation was deposited as two separate units, Mudstone A and B (Figure 4.6), as a result of increased terrigenous supply and siliceous productivity, as discussed in section 5.2. Fluctuations in terrigenous supply (TRG, Enclosure 1) in the Waipawa Formation correspond to stratal bedding observed in the field, with siliceous mudstone beds representing periods of lower terrigenous input, and argillaceous mudstone interbeds having higher concentrations of clays (Figure 4.9). These fluctuations in terrigenous supply would suggest cyclic variations in processes affecting sedimentation at this site (Mead Stream), such as bottom water energy, oxygenation, or detrital flux and composition (Arthur & Dean 1991). Based on a sedimentation rate of 0.7 cm/kyr (Hollis et al. 2005b), Mudstone A was deposited over 189 000 yr, while Mudstone B was deposited over 21 000 yr. These units contain ~20 and 4 peaks respectively of increased terrigenous supply represented by interbedded argillaceous mudstone units, respectively, which corresponds to intervals of ~9 000 and ~4 500 yr between peaks for Mudstone A and B. While such bedding couplets were emplaced in too short a time frame to directly record precession (19 000 and 23 000 yr), they are consistent with the range of depositional time periods for the latest Paleocene to Early Eocene for the Lower Limestone lithotype at Mead Stream reported by Hollis et al. (2005b). It is inferred by Hollis et al. (2005b) that groups of beds record Milankovitch scale cyclicity and it is suggested here that this may also be the case for the Waipawa Formation. Further investigation of this high frequency cyclicity may help identify processes responsible for the deposition of this unit.

Similar fluctuations are observed in excess silica (Si[exc]) and excess barium (Ba[exc]) (Enclosure 1) and are interpreted here to reflect changes in recycling and supply of nutrients during the upper Teurian. Si[exc] shows a significant negative correlation with TRG, suggesting periods of high siliceous productivity occurred during periods of reduced terrigenous input (Figure 5.14). However, the interpretation requires caution because components of percentage data are not free to vary independently, so that decreases in one component will force an increase in another (Rollinson

1993). Therefore, while increases in Si[exc] broadly reflect an increase in productivity during the deposition of both Mudstone A and B, variations in this proxy cannot be used for reliable estimates of actual changes. Ba, in the form of barite, is strongly correlated with biological productivity in modern day ocean surface waters (Dymond et al. 1992) and is widely used as a proxy for paleo-productivity on this basis (Schmitz 1987a; Schmitz et al. 1997; Schroeder et al. 1997; Thompson & Schmitz 1997). Ba[exc] does not correlate with TRG (Figure 5.14), and is therefore considered to be a better representation of variation in nutrients resulting in periodic increases in productivity.

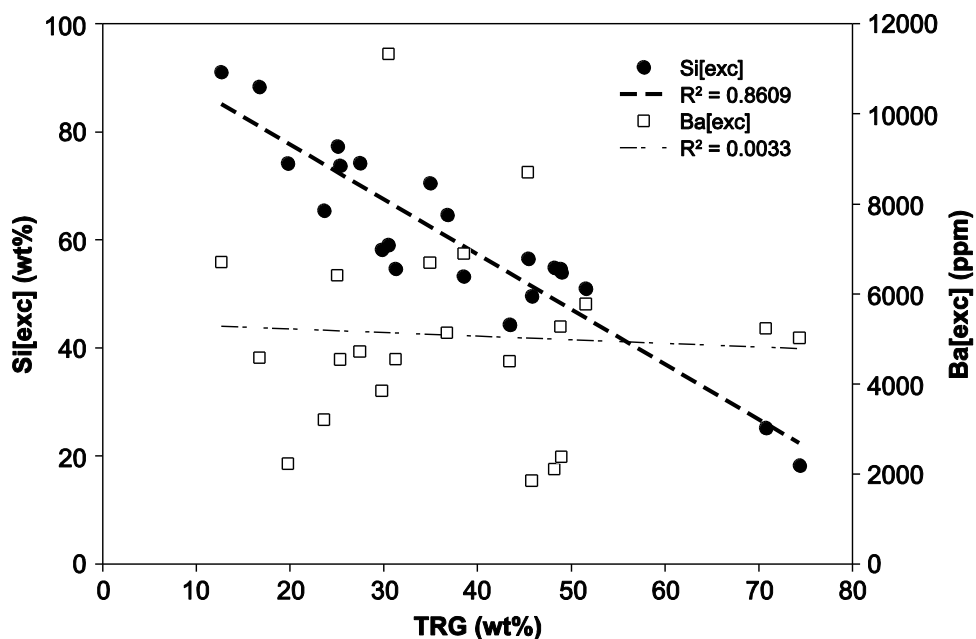


**Figure 5.14** Graph showing the relationship between Si[exc], Ba[exc] and TRG at Mead Stream.

Fluctuating currents responsible for the transportation of terrigenous material to the distal Mead Stream site during the upper Teurian were of sufficient velocity to cause erosion at proximal sites in the p-south to p-southeast, as well as to transport and deposit fine to very fine sand sized quartz and feldspar grains at Dart and Muzzle Streams during the same period. Based on the modal size of these siliciclastic grains, current speeds would have had to reach in excess of 20 cm/s to cause erosion in the p-southeast during the upper Teurian (Figure 5.15). As current velocities dropped below ~5 cm/s at Muzzle and Dart streams, deposition of the glauconitic, sandy Teredo Limestone would have occurred. This

range of values is consistent with current speeds suggested to be responsible for the formation of the Canterbury Drifts during Pliocene to Recent times (Carter, R. M. et al. 2004a) and corresponds to the mid-range of velocities for the modern day Southland Current (Sutton 2003).

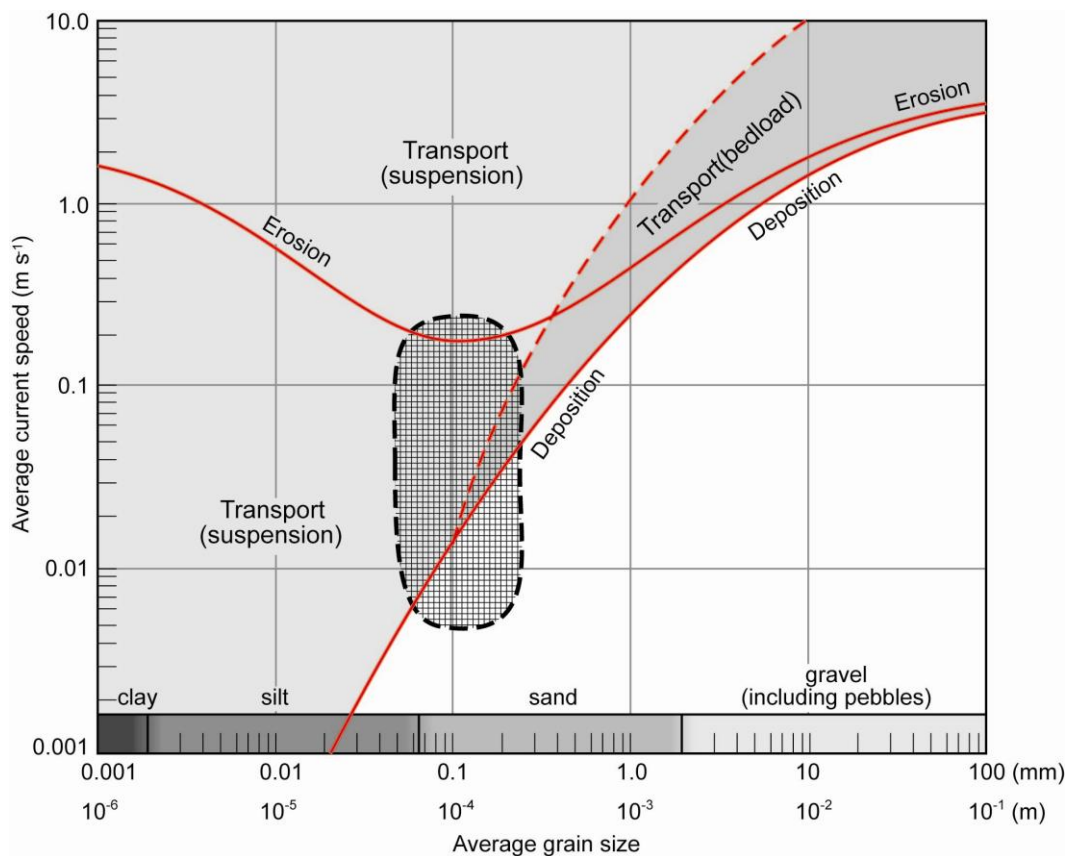


**Figure 5.15** Schematic diagram showing the range of average current speeds at which sediment particles of different sizes are eroded, transported, and deposited (after Bearman 1989). Hatched zone shows area occupied by sediments of the Teredo Limestone.

These velocities are also comparable to those of the modern DWBC (Figure 5.10) reported by McCave & Carter (1997), which range between 1 and 30 cm/s at sites from south of the Chatham Rise to the Kermadec Trench. They record that seafloor topography can significantly affect the current speed of the DWBC, with greatly increased current speeds observed in areas of constriction or steep topography (McCave & Carter 1997).

The unconformity at the base of the Teredo Limestone is described by Morris (1987) and Reay (1993) as being mildly angular over large distances, ~2° between Dart and Branch streams (Reay 1993), and

suggested that the unconformity formed as a result of differential erosion. Morris (1987) invoked local tectonic activity to account for the differential erosion. This would suggest that even though the eastern margin of Zealandia is considered to be a passive one and tectonically relatively quiescent during this period (Ballance 1993; King et al. 1999; Crampton et al. 2003), local tectonic activity did occur. If this is the case, timing of this tectonic episode on the Marlborough paleo-platform can only be loosely constrained between upper Teurian and Waipawan.

### ***Waipawan***

During the Waipawan, the distribution of lithofacies can generally be divided into three broad zones (Figure 5.16). In the p-northwest of the Marlborough paleo-embayment, sedimentation is dominated by siliceous micrite and chert of the Lower Limestone lithotype. Towards the p-southeast, micritic limestone of the Lower Limestone lithotype was deposited in a p-southwest to p-northeast trend across the centre of the Clarence block and the southeastern end of the Kekerengu block. Throughout the p-southwest of the Marlborough paleo-embayment, greensand of the Teredo Limestone was deposited widely in proximal settings.

Though the lithofacies distribution shown in Figure 5.16 is characteristic of the Waipawan, the base of this stage is represented by the Dee Marl at sites where the Paleocene-Eocene boundary is not truncated by the unconformity underlying the Teredo Limestone (Enclosure 1) (Hancock et al. 2003; Hollis et al. 2005b, c). This recessive unit, with lower carbonate concentrations in comparison to surrounding lithologies, was deposited during the Paleocene-Eocene Thermal Maximum (PETM). Hollis et al. (2005b) suggested that as the lithologic expression of this climatic event, the Dee Marl was deposited as a result of increased precipitation, high terrigenous discharge and overall decreased biological productivity. In the cooling phase that directly followed the PETM (Zachos et al. 2001), deposition of siliceous micrite and chert resumed once again at Mead Stream (Hollis et al. 2005b) (Figure 5.16). Based on similarities in lithofacies and abundance of radiolarians, Hollis et al. (2005b) inferred this



period of siliceous micrite and chert deposition represented the return to cooler (but still warm) oceanographic conditions that characterised the majority of the Paleocene.

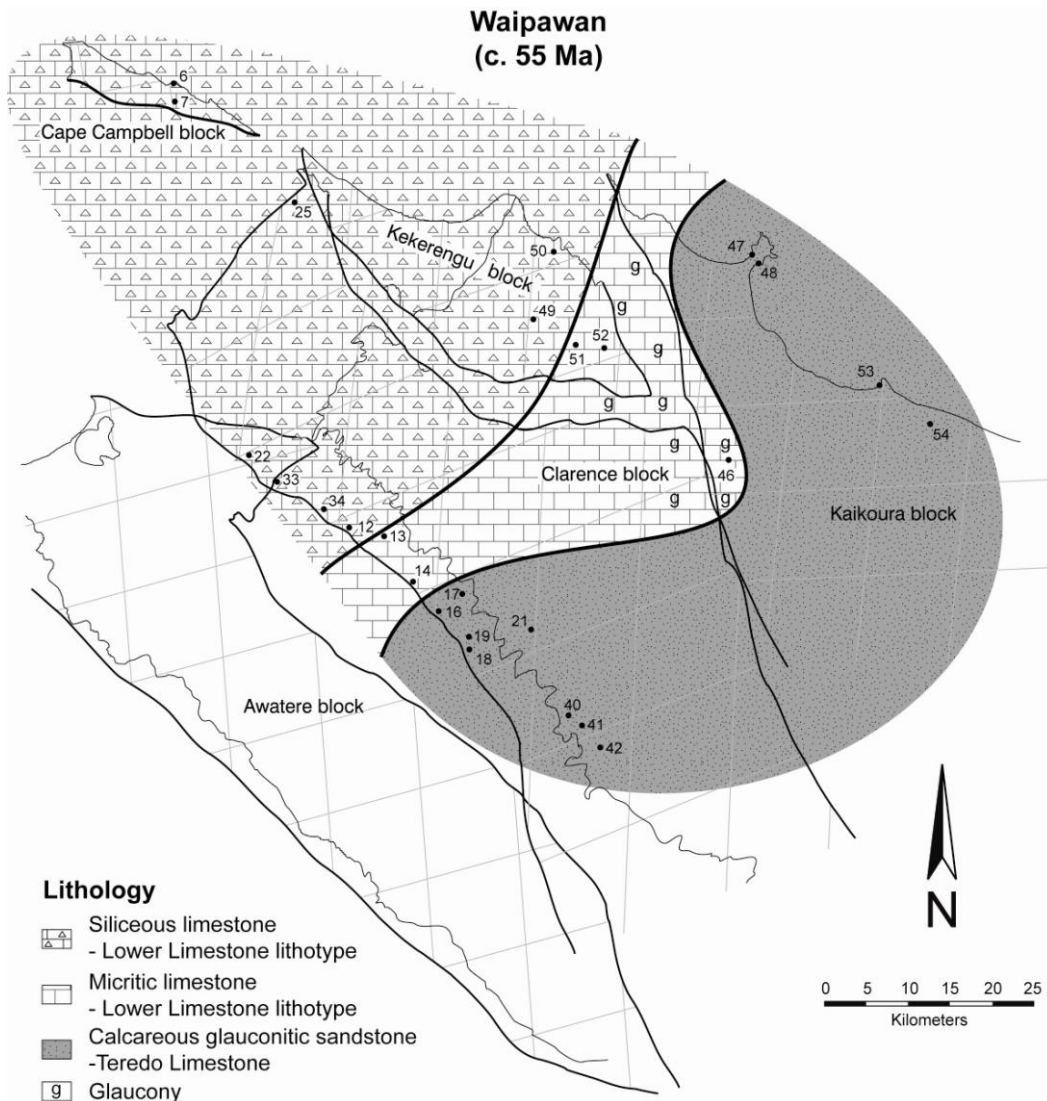


**Figure 5.16** Lithofacies map of southeastern Marlborough during the Waipawan stage (c. 55 Ma). See text for references and discussion. Locality numbers refer to localities in Table 5.5.

During the Waipawan, the currents that resulted in erosion in proximal sites in the p-east to p-southeast through the upper Teurian waned, resulting in widespread deposition of the Teredo Limestone (Figure 5.16). The observation of phosphatised clasts of micritic limestone in the Teredo Limestone at Kaikoura wharf, as well as descriptions of similar clasts from other sections (Morris 1987), would suggest that at least one hardground formed during the period of reduced sedimentation.

Contemporaneous tectonic activity is evidenced by low-angle thrust faulting at the Kaikoura wharf section (Figure 4.25 and 4.26), which is interpreted here to represent intraformational slumping. It is suggested that this period of tectonic activity resulted in overpressuring, mainly of the Teredo Limestone and to a lesser degree the underlying greensand associated with the K/T boundary at Kaikoura wharf, which led to the forced emplacement of clastic dykes (Figure 4.25, 4.26, 4.47).

### ***Mangaorapan***

During the Mangaorapan, sedimentation across the Marlborough paleo-platform was almost entirely dominated by deposition of the Lower Marl lithotype of the Amuri Limestone (Figure 5.17). By the Mangaorapan, deposition of the Teredo Limestone was confined to a relatively small area in the p-south of the Marlborough paleo-platform around Seymour Stream (locality 40).

Deposition of the micrite facies (F3) as part of the Lower Marl lithotype of the Amuri Limestone represents a return to 'background' sedimentation throughout much of the Marlborough paleo-platform during this period. Hollis et al. (2005b) showed that deposition of this unit occurred during the early Eocene climatic optimum (EECO), a peak that occurred between 52 and 50 Ma during a prolonged period of global warming (Zachos et al. 2001). Hollis et al. (2005b) suggest that processes responsible for the deposition of the Dee Marl at the Paleocene/Eocene boundary were also responsible for the deposition of the Lower Marl during the EECO. Increased precipitation and high terrigenous discharge coupled with decreased biological accumulation in warm oligotrophic waters resulted in the deposition of this marly lithology.

Waning currents that resulted in the deposition of the Teredo Limestone through the upper Teurian and Waipawan, continued to affect sites in the p-south of the Marlborough paleo-platform prior to cessation represented by the onset of deposition of the Lower Marl lithotype at these sites. Deposition of the Lower Marl directly upon the Teredo Limestone at Seymour Stream was initiated by the Mangaorapan and is probably

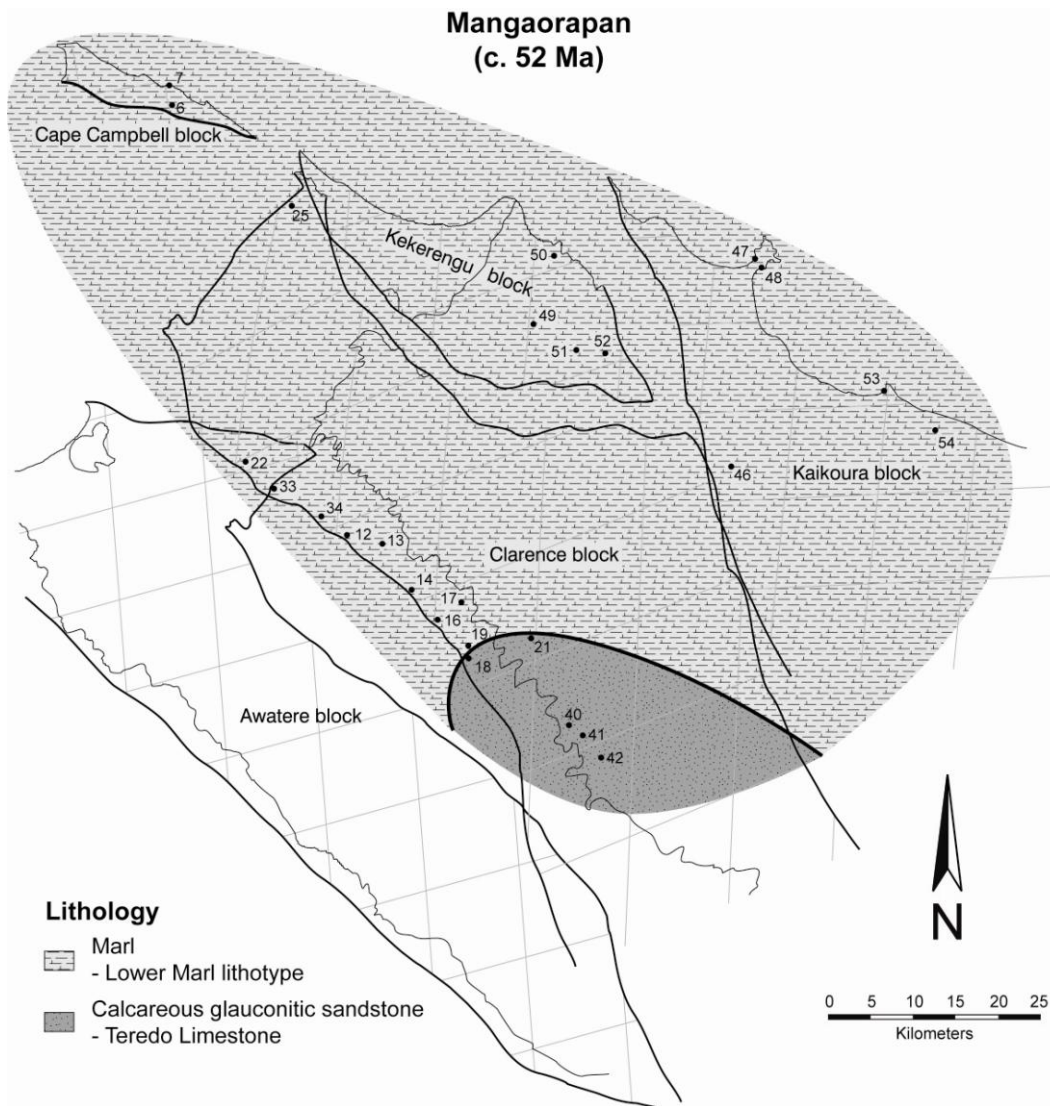


**Figure 5.17** Lithofacies map of southeastern Marlborough during the Mangaorapan stage (c. 52 Ma). See text for references and discussion. Locality numbers refer to localities in Table 5.5.

Heretaungan in age ~1.5 m above the base of the Lower Marl (Chris Hollis pers. comm. 2010). The Teredo Limestone exposed in The Fell is probably of similar age based on microfossil assemblages.

The initiation of deposition of the Lower Marl at these sites signifies the end of oceanographic conditions that resulted in the deposition of the Teredo Limestone and its lateral equivalent, the Waipawa Formation, in southeastern Marlborough.

#### **5.4 PALEOCENE-EOCENE OCEAN CIRCULATION PATTERNS**

Based on the correlation of the Waipawa Formation and Teredo Limestone Member of the Amuri Limestone (Figure 5.4), along with the

fact that these two units were deposited contemporaneously across the Marlborough paleo-platform in the upper Teurian, it is necessary for any depositional model for the Waipawa Formation to take these matters into consideration. This point is further supported by the identification of similar relationships between the Waipawa Formation and upper Te Uri Member of the Whangai Formation from sections within the East Coast Basin on the east coast of the North Island (Rogers et al. 2001).

Based on evidence that suggested the Waipawa Formation was deposited under dysoxic conditions during a period of global warming that was initiated in the mid-Paleocene and climaxed in the PETM, Killops et al. (2000) inferred the formation to be deposited as a result of upwelling of oxygen depleted warm saline deep water (WSDW) at a front between converging water masses. The source of WSDW during this period is suggested to have been the tropical Pacific (originally Tethyan) (Killops et al. 2000), as low-latitude areas where high temperatures and high evaporation rates dominate played a significant role in deep water formation through the Late Cretaceous to Early Eocene (Kennett & Stott 1990; Corfield & Cartlidge 1992; Thomas 1992; D'Hondt & Arthur 2002).

However, contrary to Killops et al. (2000) suggestion that the Waipawa Formation was deposited during a period of warming, biostratigraphic investigations (Hollis et al. 2000; Hollis et al. 2005b; Schiøler et al. 2010) show that deposition of this unit occurred between 58 and 57.5 Ma and is not associated with the PETM. This period actually corresponds to some of the coolest temperatures recorded from the Paleocene, comparable to those reported across the K/T boundary (Zachos et al. 2001). This is supported by temperature records from the East Tasman Plateau which show that sea surface temperatures in the Tasman Sea reached as low as ~18°C during the Late Paleocene, ~17°C less than temperatures recorded for the EECO (Bijl et al. 2009). On a broader scale, the deposition of bio-siliceous sediments during this period of cooling is consistent with observations in modern day oceans where these deposits are found beneath relatively cool and productive surface waters (Hollis et al. 2005b). Waters need not be inherently oxygen depleted; for example, Kender et al.

(2009) documented significant expansion of the OMZ overlying the Congo Fan, East Africa, during the Middle Miocene as a result of increased upwelling of cool nutrient rich water.

It is suggested here that processes responsible for increased productivity, unconformity formation and greensand deposition in southeastern Marlborough across the K/T boundary (Hollis 2003; Hollis et al. 2003b, c) are similar to those responsible for an identical event during the Late Paleocene to Early Eocene. This comparison is based firstly on the fact that both oceanographic events resulted in upwelling of nutrient rich water and increased productivity. Secondly, this comparison between these separate oceanographic events is based on the similarities of lithofacies observed at Kaikoura wharf. At this site, similar unconformities and greensand units were developed at the K/T boundary and during the upper Teurian to Waipawan (Figure 4.28). It was the similarities between the two units at Kaikoura that in the past was responsible for lumping both units into the Teredo Limestone (Morris 1987; Browne et al. 2005a), a situation not followed in the present study (see section 5.1.1).

Based on the paleo-circulation models of Huber & Sloan (2001) and Bice & Marotzke (2002), Hollis et al. (2003b) suggested that the nutrient-rich cool waters responsible for increased siliceous productivity in southeastern Marlborough over the K/T boundary originated from downwelling at the Antarctic margin. These currents were considered to be analogous to the modern Deep Western Boundary Current (DWBC). However, based on the inner shelf to mid bathyal paleodepths of sites investigated as part of this study, it is suggested here that unlike the model of Hollis et al. (2003b), currents that affected these sites during the Late Paleocene to Early Eocene cannot be considered true deep ocean currents. Given the present day structure of oceanic fronts and water masses in the New Zealand sector of the Southern Ocean (Figure 5.18), where the DWBC is no shallower than ~2000 m (McCave & Carter 1997), the water mass responsible for increased siliceous productivity and unconformity formation is more consistent with an intermediate water mass, such as Antarctic Intermediate Water (AAIW). AAIW forms as a

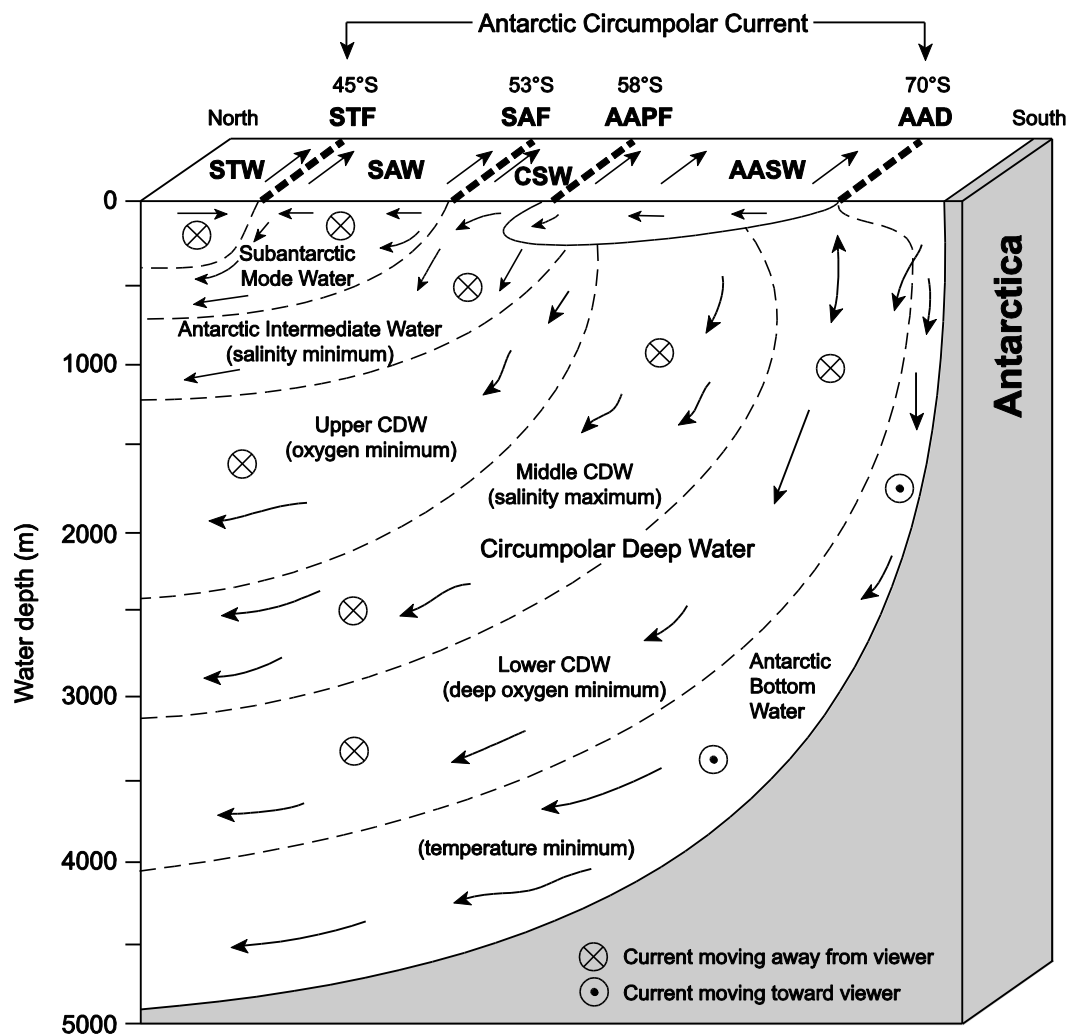


**Figure 5.18** Water masses, fronts, and circulation patterns that characterise the present day New Zealand sector of the Southern Ocean (after Carter, R. M. et al. 2004b). STF = Subtropical Front, SAF = Subantarctic Front, AAPF = Antarctic Polar Front, AAD = Antarctic Divergence, CDW = Circumpolar Deep Water, STW = Subtropical Water, SAW = Subantarctic Water, CSW = Circumpolar Surface Water, AASW = Antarctic Surface Water.

result of cold water sinking at the Antarctic Polar Front (McCave & Carter 1997). However, the present day configuration of oceanic fronts and water masses in the New Zealand sector of the Southern Ocean was not established until the late Early to Late Miocene, Nelson & Cooke (2001) state that no oceanic fronts are positively identifiable during the Paleocene. Given this, Nelson & Cooke's (2001) interpretation of oceanic front development was based on the assumption of ice free conditions during the Paleocene and it is possible that brief Antarctic glaciation could have resulted in periodic development of an Antarctic Polar Front on timescales below the resolution of that study. Conversely, if there was no

Antarctic Polar Front for AAIW to sink along, it would appear that the source of intermediate water during the Late Paleocene could be similar to that suggested for the Late Eocene by Lazarus & Caulet (1993). Based on the mixing of cool and warm water radiolarians away from the Antarctic continent during this period, Lazarus & Caulet (1993) inferred a northward-moving cool intermediate water was developed in, and sinking from, surface water near Antarctica.

Applying this model to the paleogeographic map for the upper Teurian (Figure 5.19), calving Antarctic glaciers responsible for downwelling and invigoration of ocean currents initially delivered ice rafted debris to Campbell Island on the southern margin of the Campbell Plateau in the upper Teurian. During the same period, invigorated currents moving along the eastern margin of Zealandia would have eventually resulted in non-deposition at this site, where large increases in Zr at the boundary between the Garden Cove Formation and Tucker Cove Limestone reflected winnowing of sea-floor sediments and concentration of heavy minerals (Enclosure 1). Further north, these nutrient-rich currents were forced to rise, either as a result of prevailing westerly winds, as suggested by Killips et al. (2000), or topographic features, resulting in the formation of widespread upwelling zones and deposition of bio-siliceous sediments. The widespread nature of this upper Teurian upwelling event is evidenced by descriptions of bio-siliceous deposits of this age at ODP Site 1121 (Figure 5.19) where Hollis (2002) suggests the rate of compacted accumulation doubled from 15 to 30 mm/ka due in large part to a sudden and pronounced increase in all siliceous microfossils during this period. In shallower sites near the shelf/slope break, such as at Mead Stream, this increased productivity resulted in the expansion or intensification of the OMZ responsible for influencing the deposition of the Waipawa Formation. The identification here of fossil contourite deposits, the Clarence Drift (see section 5.3.1) supports this model by showing that the Teredo Limestone formed under the influence of currents moving parallel to the paleo-slope.

It is interesting to note that while the Waipawa Formation was deposited over a 500 000 yr period during the upper Teurian, the invigorated

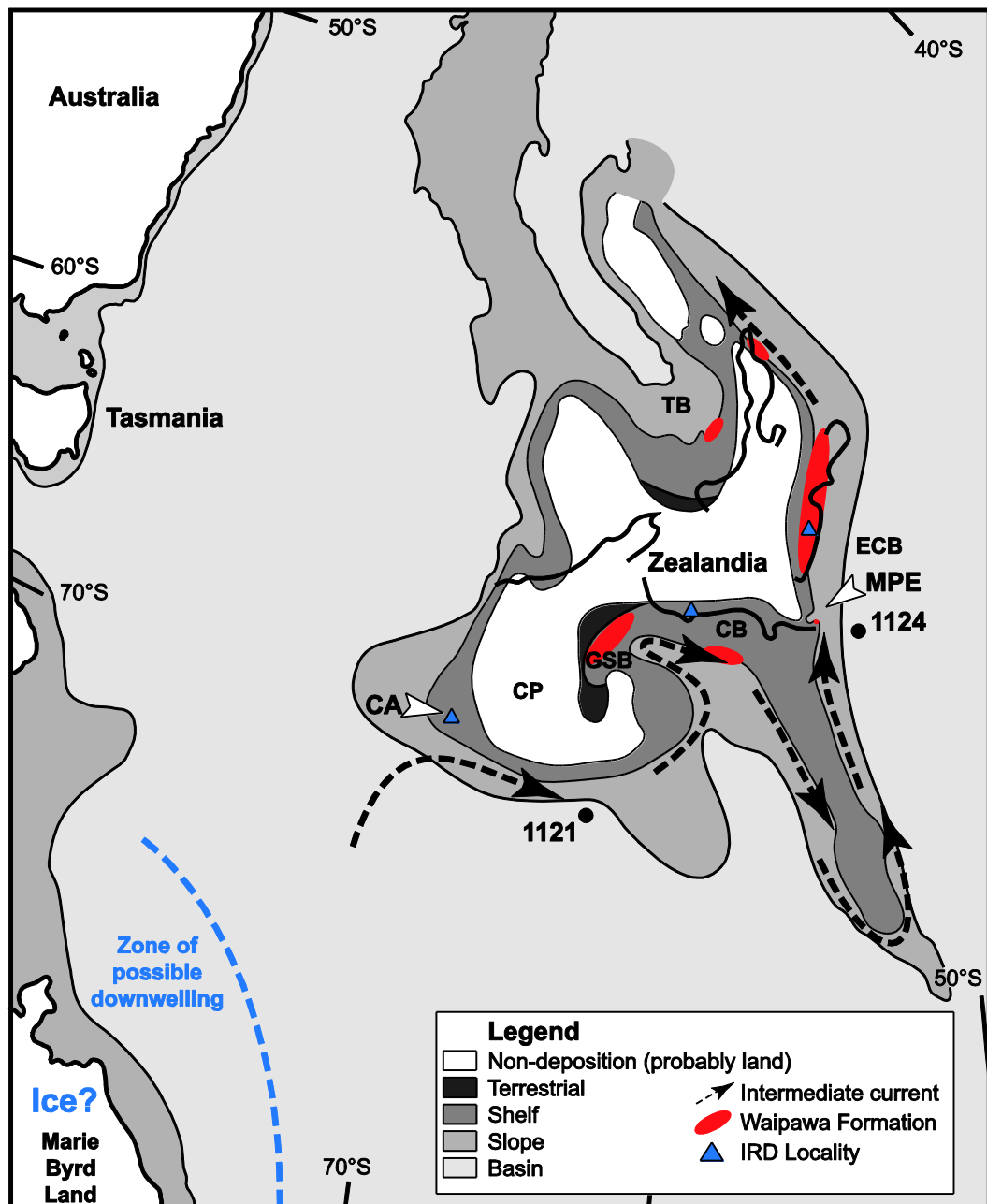


**Figure 5.19** Paleogeographic reconstruction for New Zealand during the Late Paleocene (56 Ma) (after Kamp 1986; King et al. 1999) showing the distribution of the Waipawa Formation (after Killops et al. 2000) and paleo-circulation directions of postulated intermediate depth ocean currents (following Hollis et al. (2003a) (after Huber & Sloan 2001; Bice & Marotzke 2002)). IRD localities denote locations of documented Late Paleocene ice rafted debris. CA: Campbell Island; MPE: Marlborough Paleo-embayment; TB: Taranaki Basin; ECB: East Coast Basin; CB: Canterbury Basin; GSB: Great South Basin; CP: Campbell Plateau.

currents responsible for unconformity formation at Campbell Island and the condensed sections in southeastern Marlborough were much longer lived. At both locations, unconformity formation and reduced



sedimentation conditions lasted from the upper Teurian to Mangaorapan (Hollis et al. 1997, Chris Hollis pers. comm. 2010), suggesting aberrant climatic events such as the PETM had little effect on this circulation pattern.

Sites where this upper Teurian to Mangaorapan oceanographic event is recorded share no characteristics that are common to all. For example, the Waipawa Formation at Mead Stream was deposited at bathyal water depths (Strong et al. 1995) while the Tartan Formation, the lateral equivalent of the Waipawa Formation in the Great South Basin, was deposited in an inner shelf environment (0-20 m) (Schjøler et al. 2010). This event is also not only recorded in eastern basins, but also in the Taranaki Basin on the western margin of Zealandia (Figure 5.19). It is therefore suggested that one mechanism alone cannot be invoked to account for deposition of the lithofacies related to this event and that local factors, such as topography and the effect of eustatically driven sea-level, must be important. In southeastern Marlborough, features such as the Marlborough paleo-platform and a possible seaway linking the Marlborough paleo-embayment with the Canterbury Basin (Figure 5.1) (Field et al. 1989; Crampton et al. 2003) likely influenced depositional processes within this region. However, the extent to which such morphologic structures played a role is difficult to quantify because of the limited nature of appropriate outcrop.

# CHAPTER 6

## SUMMARY AND CONCLUSIONS

---

The eastern margin of the micro-continent of Zealandia contains unique, high latitude, southwest Pacific rock records of climatic change through the Late Cretaceous to Paleogene. This study has focused on some selected key sites from this margin, investigating some sections in southeastern Marlborough and on Campbell Island to document and better understand sedimentary responses to climatic variation during the Late Paleocene to Early Eocene (early Paleogene), thereby satisfying the aims outlined in Chapter 1.

### 6.1 REVISED PALEOCENE-EOCENE LITHOSTRATIGRAPHY OF SOUTHEASTERN MARLBOROUGH

As part of this study, a revision of the early Paleogene stratigraphy of southeastern Marlborough was considered. This involved a reinterpretation of the lithostratigraphy at the key Kaikoura wharf section as well as suggesting future stratigraphic nomenclature for specific units in the region. Sedimentologic and micropaleontologic studies of the sedimentary succession at Kaikoura wharf have shown that the *Teredo* Limestone is confined to the upper greensand unit only at this site (Table 5.1). The lower greensand bed at the site, previously considered to represent the base of the *Teredo* Limestone (Table 5.1), is here considered to be the uppermost part of the underlying Mead Hill Formation. This study has shown that the name 'Teredo Limestone' is an inappropriate one for this stratigraphic unit based on the premises that the identification of *Teredo* tubes is problematic, the unit is actually a glauconitic, calcareous sandstone, not a limestone, and the name does not utilise a local geographic locality. For these reasons it is suggested that in future studies the *Teredo* Limestone Member of the Amuri Limestone be elevated to formation rank and be renamed the South Bay Formation, containing the Hundalee Sandstone Member (a basal, cream to grey, massive, slightly calcareous sandstone) overlain by the Dart Greensand Member (a highly calcareous, glauconitic sandstone). It is

also suggested that in future work the present informal lithotypes of the Amuri Limestone be raised to formal member status with appropriate stratigraphic names.

## **6.2 LITHOFACIES CHANGES IN SOUTHEASTERN MARLBOROUGH AND CAMPBELL ISLAND**

As part of the first two aims of this study (Chapter 1), sedimentologic investigations, including both detailed field descriptions and petrographic studies, have shown that some significant changes in depositional processes occurred locally in southeastern Marlborough and on Campbell Island during the Late Paleocene to Early Eocene. In southeastern Marlborough, normal 'background' sedimentation represented by micro-bioclastic sediments of the Mead Hill Formation and Amuri Limestone was periodically interrupted by the deposition of siliceous mudstone of the Waipawa Formation at the distal Mead Stream site during this period. Petrographic study of the Waipawa Formation shows rapid increases in the abundance of radiolarian microfossils and sponge spicules in comparison to the underlying Mead Hill Formation and overlying Lower Limestone lithotype of the Amuri Limestone. Thin sections of samples from the Waipawa unit also show extensive bioturbation and rare pelletal and vermicular glaucony. In more proximal sites, at Muzzle Stream and Kaikoura wharf, formation of a regionally extensive unconformity was followed by deposition of quartz and glaucony rich sediments of the upper Teurian to Mangaorapan (Late Paleocene to Early Eocene) Teredo Limestone. Thin sections of samples from this unit show it consists of well sorted, fine to very fine sand sized siliciclastic grains and fine sand sized pelletal and vermicular glaucony, set in a calcareous matrix that shows evidence of secondary silicification. Even though this unit is a lateral equivalent of the Waipawa Formation, both the base and top of the Teredo Limestone are time-transgressive, meaning the unit is upper Teurian at Muzzle Stream, while to the southwest at Seymour Stream the unit is Waipawan to Mangaorapan in age. On Campbell Island, the time period of interest is represented by an unconformity between the Garden Cove Formation and Tucker Cove Limestone.

The suggestion that lithofacies changes observed in southeastern Marlborough and on Campbell Island represent a significant change in depositional processes is supported by inorganic geochemical proxies (Enclosure 1). At Mead Stream, in southeastern Marlborough, increases in excess silica (Si[exc]), excess barium (Ba[exc]) and total organic carbon reaching as high as ~5% in the Waipawa Formation reflect abrupt enhancement of productivity through this unit. This is associated with reduced oxygen conditions at the site as a result of degradation of large amounts of organic debris sinking through the water column throughout the period of increased productivity. An inorganic geochemical proxy for terrigenous supply (TRG) also shows a significant increase during the deposition of the Waipawa Formation, implying an increased supply of clays to this distal site during the upper Teurian. Though geochemical records from Muzzle Stream and Kaikoura wharf in southeastern Marlborough do not show such abrupt changes as are recorded at Mead Stream, they do show a general shift from bio-siliceous to bio-calcareous dominated deposition from the Late Cretaceous to Early Eocene. On Campbell Island, inorganic geochemical proxies show similar trends to those observed at Muzzle Stream and Kaikoura wharf. Increases in Zr, associated with contemporaneous increases in rare earth elements across the unconformable boundary between the Garden Cove Formation and Tucker Cove Limestone, are interpreted to result from the winnowing of sea-floor sediments and concentration of heavy minerals under invigorated current action responsible for the unconformity formation at the site.

Palinspastic mapping of the Teredo Limestone (Figure 5.9C) further implies that the unit was deposited as a result of processes starkly disparate to those responsible for deposition of the bounding Mead Hill Formation and Amuri Limestone in southeastern Marlborough. In contrast to other Late Cretaceous to Early Eocene units from the region, the Teredo Limestone increases in thickness to the p-southeast (Figure 5.9A, B, C) and is not recorded in distal sites towards the p-northwest of Dart Stream in the Clarence Valley and Kaikoura wharf on Kaikoura Peninsula. Furthermore, along with sedimentologic descriptions from key sites in

southeastern Marlborough, Figure 5.9C suggests that the Teredo Limestone was deposited as a 'skin drift' on the Marlborough paleo-platform. One 'lobe' of this deposit, centred on the present day middle Clarence Valley, and here named the Clarence Drift, appears to have been deposited under the influence of intermediate depth contour currents that affected the Marlborough paleo-embayment during the Late Paleocene to Early Eocene.

### **6.3 ICE IN THE GREENHOUSE**

Evidence for a period of enhanced siliceous productivity, invigorated ocean currents and possible episodes of ice rafting is consistent with a brief period of Antarctic ice sheet growth during a phase of global cooling in the Late Paleocene. Calving Antarctic ice sheets responsible for the transport of quartz pebbles to Campbell Island would have also cooled waters adjacent to the Antarctic continent resulting in downwelling and invigoration of intermediate depth ocean currents. These currents subsequently impinged upon the eastern margin of the micro-continent of Zealandia where they reworked fine to very fine sand sized siliciclastic grains and perigenic glaucony across the Marlborough paleo-platform and supplied nutrient rich water to sites such as ODP Site 1121 and the Marlborough paleo-platform where pronounced upwelling resulted in the deposition of bio-siliceous sediments during the Late Paleocene (Figure 5.19).

The possible identification of Antarctic ice sheets, ephemeral though they may have been, not only challenges long held beliefs that the Antarctic continent remained ice free during the early Paleogene greenhouse world but also questions the suggested mechanisms responsible for Antarctic ice sheet growth. The lack of ocean gateways in the Southern Ocean during this time effectively rules out thermal isolation of the Antarctic continent as a driver. Given that this period of ice sheet growth is contemporaneous with a documented period of enhanced global ocean productivity and terrestrial carbon accumulation and related draw down in atmospheric CO<sub>2</sub>, it is suggested this may represent the driver responsible

for brief Antarctic glaciation during this period, though the postulated link requires further investigation.

However, it may not be entirely correct to invoke one mechanism to account for both enhanced siliceous productivity and invigorated ocean currents during the early Paleogene. The period of enhanced siliceous productivity was relatively short lived, only occurring between about 58 and 57.5 Ma, and while coinciding with the above postulated period of global cooling, nevertheless ocean currents remained invigorated across the Paleocene-Eocene boundary and into the Maastrichtian. It remains difficult to envisage Antarctic ice surviving to drive invigorated ocean currents in the southwest Pacific during the period of aberrant warming at the Paleocene-Eocene boundary into the prolonged warm period of the early Eocene climatic optimum.

#### **6.4 SUGGESTIONS FOR FUTURE STUDY**

Though southeastern Marlborough contains important records of Late Cretaceous to early Paleogene climatic events, the sedimentary facies developed in this region are markedly different from those developed in the East Coast Basin (North Island) proper to the northeast and in the adjacent Canterbury Basin (South Island) to the southwest. It is therefore suggested that future work focus broadly on linking records from southeastern Marlborough to well studied successions in Hawke's Bay around Tawanui and Te Hoe Stream and the mid-Waipara region in Canterbury Basin. For the former, this could be achieved through investigation of sites around Tora, southern Wairarapa, which lay on the western side of the Marlborough paleo-embayment during the Late Cretaceous to Early Eocene (Figure 5.1). While for the latter, investigation of key sections in the area of the Hurunui High in North Canterbury between Haumuri Bluff and mid-Waipara (Figure 5.1) is desired.

On a much finer scale, it is suggested that investigation of the origin of limestone-marl alternations in the Amuri Limestone is required to determine the extent to which diagenetic redistribution of calcite has played a role in the formation of this style of bedding. This appears to be

crucial in establishing whether or not the limestone-marl alternations in this unit formed as a result of changes in primary sedimentary processes, which might then have been formed in response to early Paleogene climate change in the southwest Pacific.

It is suggested that further investigation of glaucony from the Late Paleocene-Early Eocene Teredo Limestone Member of the Amuri Limestone in southeastern Marlborough also be carried out. This should initially involve the characterisation of these grains, including the morphology, mineralogy and geochemistry, to determine if they are suitable for isotopic type studies. If this is the case, isotopic studies including Rb/Sr and K/Ar dating of glaucony grains should be carried out to date sections where biostratigraphic control is poor or lacking and to differentiate authigenic or perigenic grains from those derived by recycling of glaucony from the underlying Claverley Sandstone, thereby quantifying the amount of reworking of glaucony in this unit. Following this, investigation of neodymium and hafnium isotopic ratios in glaucony grains could aid firstly in constraining the source of intermediate water affecting southeastern Marlborough by broadly discriminating between warm deep saline water from the tropical Pacific (originally Tethyan) versus intermediate water from Southern Ocean sources. Secondly, these isotopic records could record fluctuations in mechanical weathering on the Antarctic continent as a result of periodic glaciation during this period of otherwise greenhouse conditions during the early Paleogene.

# REFERENCES

---

- Adams CJ 1962. Thickness of the Earth's crust beneath the Campbell Plateau. *New Zealand Journal of Geology and Geophysics* 5(1): 74-85.
- Adams CJ, Morris PA, Beggs JM 1979. Age and correlation of volcanic rocks of Campbell Island and metamorphic basement of the Campbell Plateau, South-west Pacific. *New Zealand Journal of Geology and Geophysics* 22(6): 679-691.
- Alvarez LW, Alvarez W, Asaro F, Michel HV 1980. Extraterrestrial Cause for the Cretaceous-Tertiary Extinction. *Science* 208(4448): 1095-1108.
- Amorosi A 1997. Detecting compositional, spatial, and temporal attributes of glaucony: A tool for provenance research. *Sedimentary Geology* 109(1-2): 135-153.
- Andrews PB 1982. Revised guide to recording field observations in sedimentary sequences. Report NZGS 102. Lower Hutt, New Zealand, New Zealand Geological Survey.
- Arthur MA, Dean WE 1991. A holistic geochemical approach to cyclomania: examples from Cretaceous pelagic limestone sequences. In: Einsele G, Ricken W, Seilacher A eds. *Cycles and events in stratigraphy*. Berlin, Springer-Verlag. Pp 126-166.
- Ballance PF 1993. The paleo-Pacific, post-subduction, passive margin thermal relaxation sequence (Late Cretaceous-Paleogene) of the drifting New Zealand continent. In: Ballance PF ed. *South Pacific sedimentary basins*. Elsevier. Pp 93-110.
- Barber C 1974. Major and trace element associations in limestones and dolomites. *Chemical Geology* 14: 273-280.
- Barrett P 2003. Palaeoclimatology - Cooling a continent. *Nature* 421(6920): 221-223.
- Bearman G ed. 1989. *Waves, tides and shallow-water processes*. Oxford, Butterworth-Heinemann.
- Beggs JM 1976. Sedimentary and metamorphic geology of Campbell Island, South West Pacific Ocean. Unpublished Dip. Sci. thesis, University of Otago.
- Beggs JM 1978. Geology of the metamorphic basement and Late Cretaceous to Oligocene sedimentary sequence of Campbell Island, southwest Pacific Ocean. *Journal of the Royal Society of New Zealand* 8: 161-177.



- Beggs JM, Challis GA, Cook RA 1990. Basement geology of the Campbell Plateau - implications for correlation of the Campbell Magnetic Anomaly system. *New Zealand Journal of Geology and Geophysics* 33(3): 401-404.
- Beu AG, Maxwell PA 1990. Cenozoic Mollusca of New Zealand. *New Zealand Geological Survey Paleontological Bulletin* 58. Lower Hutt, New Zealand.
- Bice KL, Marotzke J 2002. Could changing ocean circulation have destabilized methane hydrate at the Paleocene/Eocene boundary? *Paleoceanography* 17:10.1029/2001PA000678
- Bijl PK, Schouten S, Sluijs A, Reichert GJ, Zachos JC, Brinkhuis H 2009. Early Palaeogene temperature evolution of the southwest Pacific Ocean. *Nature* 461(7265): 776-779.
- Bradshaw JD 1989. Cretaceous geotectonic patterns in the New-Zealand region. *Tectonics* 8(4): 803-820.
- Brenstrum E 2004. Campbell Island weather. In: Dingwall P, Gregory G eds. *A musterer's sojourn on Campbell Island: the diary of Alfred Austin, 1919–1921*. Department of Conservation. 135 pp.
- Browne GH 1987. In situ and intrusive sandstone in Amuri facies limestone at Te Kaukau Point, Southeast Wairarapa, New Zealand. *New Zealand Journal of Geology and Geophysics* 30(4): 363-374.
- Browne GH 1995. Sedimentation patterns during the Neogene in Marlborough, New Zealand. *Journal of the Royal Society of New Zealand* 25(4): 459-483.
- Browne GH, Laird MG, Field BD 2005a. Stratigraphic and sedimentological teasers, Kaikoura Peninsula, Marlborough. Field Trip 5B. In: Pettinga JR, Wandres AM eds. *Field trip guides. Geological Society of New Zealand 50 Annual Conference, Kaikoura, New Zealand. Geological Society of New Zealand Miscellaneous Publication 119B: Pp 129–140.*
- Browne GH, Speden IG, Field BD 2005b. Following in McKay's Footsteps - Iconic Cretaceous to Neogene successions, Haumuri Bluff, Marlborough. In: Pettinga JR, Wandres AM eds. *Field trip guides. Geological Society of New Zealand 50 Annual Conference, Kaikoura, New Zealand. Geological Society of New Zealand Miscellaneous Publication 119B: Pp 179–195.*
- Carter L, Carter RM, McCave IN 2004. Evolution of the sedimentary system beneath the deep Pacific inflow of eastern New Zealand. *Marine Geology* 205: 9-27.
- Carter RM, Fulthorpe CS, Lu H 2004a. Canterbury Drifts at Ocean Drilling Program Site 1119, New Zealand: Climatic modulation of southwest

Pacific intermediate water flows since 3.9 Ma. *Geology* 32(11): 1005-1008.

- Carter RM, McCave IN, Carter L 2004b. Leg 181 synthesis: fronts, flows, drifts, volcanoes, and the evolution of the southwestern gateway to the Pacific Ocean, eastern New Zealand. In: Richter C ed. *Proc. ODP, Sci. Results, 181: College Station, TX (Ocean Drilling Program)*. Pp 1-111.
- Cook R, Sutherland R, Zhu H, Funnell R, Killips SD 1999. *Cretaceous-Cenozoic geology and petroleum systems of the Great South Basin, New Zealand*. Institute of Geological and Nuclear Sciences monograph 20. 188 p. + 2 sheets. Lower Hutt, New Zealand, Institute of Geological and Nuclear Sciences Ltd.
- Coplen TB 1988. Normalization of oxygen and hydrogen isotope data. *Chemical Geology* 72: 293-297.
- Coplen TB 1994. Reporting of stable hydrogen, carbon, and oxygen isotopic abundances. *Pure and applied chemistry* 66: 273-276.
- Corfield RM, Cartlidge JE 1992. Oceanographic and climatic implications of the Palaeocene carbon isotope maximum. *Terra Nova* 4(4): 443-455.
- Coxhall HK, Pearson PN 2007. The Eocene-Oligocene transition. In: Williams M, Haywood AM, Gregory FJ, Schmidt DN eds. *Deep-time perspectives on climate change: marrying the signal from computer models and biological proxies*. The Micropaleontological Society, Special Publication. The Geological Society, London. Pp 351-387.
- Crampton JS 1988. Stratigraphy and structure of the Monkey Face area, Marlborough, New Zealand, with special reference to shallow marine Cretaceous strata. *New Zealand Journal of Geology and Geophysics* 31(4): 447-470.
- Crampton JS, Laird M, Nicol A, Townsend D, Van Dissen R 2003. Palinspastic reconstructions of southeastern Marlborough, New Zealand, for mid-Cretaceous-Eocene times. *New Zealand Journal of Geology and Geophysics* 46(2): 153-175.
- Crouch EM, Hollis CJ, Huber M, Strong CP 2009. Climatic and biotic events of the Paleocene - CBEP 2009: Preface. In: Crouch EM, Hollis CJ, Strong CP eds. *Climatic and Biotic Events of the Paleogene (CBEP 2009)*, extended abstracts from an international conference in Wellington, New Zealand, 12-15 January 2009. *GNS Science Miscellaneous Series* 18. Pp 3-4.
- D'Hondt S, Arthur MA 2002. Deep water in the late Maastrichtian ocean. *Paleoceanography* 17(1): 11.
- DeConto RM, Pollard D 2003. Rapid Cenozoic glaciation of Antarctica induced by declining atmospheric CO<sub>2</sub>. *Nature* 421(6920): 245-249.

- DeConto RM, Pollard D, Wilson PA, Palike H, Lear CH, Pagani M 2008. Thresholds for Cenozoic bipolar glaciation. *Nature* 455(7213): 652-U52.
- Dickens GR, Owen RM 1994. Late Miocene-early Pliocene manganese redirection in the central Indian Ocean - Expansion of the intermediate water oxygen minimum zone. *Paleoceanography* 9(1): 169-181.
- Dingwall P, Gregory G 2004. A musterer's sojourn on Campbell Island: The diary of Alfred Austin, 1919–1921. Department of Conservation. 135 pp.
- Dymond J, Suess E, Lyle M 1992. Barium in Deep-Sea Sediment: A Geochemical Proxy for Paleoproductivity. *Paleoceanography* 7(2): 163-181.
- Einsele G, Ricken W 1991. Limestone-marl alternation - an overview. In: Einsele G, Ricken W, Seilacher A eds. *Cycles and events in stratigraphy*. Berlin, Springer-Verlag. Pp 23-47.
- Ekdale AA, Bromley RG, Pemberton SG 1984. Ichnology: the use of trace fossils in sedimentology and stratigraphy. Society of Economic Palaeontologists and Mineralogists, Short Course Notes no. 15. 317 pp.
- Ernst W 1970. *Geochemical facies analysis*. Elsevier Publishing Co. 155 pp.
- Faugères J-C, Stow DAV 1993. Bottom-current-controlled sedimentation: a synthesis of the contourite problem. *Sedimentary Geology* 82(1-4): 287-297.
- Fell D 2002. *Campbell Island: Land of the blue sunflower*. Auckland, New Zealand, David Bateman.
- Field BD, Hollis CJ 2003. Orbitally controlled cyclicity around the Cretaceous/Tertiary boundary, northern South Island, New Zealand. *New Zealand Journal of Geology and Geophysics* 46(2): 235-241.
- Field BD, Browne GH, Davy B, Herzer RH, Hoskins RH, Raine JI, Wilson GJ, Sewell RJ, Smale D, Watters WA 1989. Cretaceous and Cenozoic sedimentary basins and geological evolution of the Canterbury region, South Island, New Zealand. *New Zealand Geological Survey Basin Studies* 2. Lower Hutt, New Zealand Geological Survey.
- Field BD, Uruski CI, Beu A, Browne GH, Crampton J, Funnell R, Killips SD, Laird M, Mazengarb C, Morgans HEG, Rait G, Smale D, Strong CP 1997. Cretaceous-Cenozoic geology and petroleum systems of the East Coast Region, New Zealand. Institute of Geological and

Nuclear Sciences monograph 19. 301 p. + 7 sheets. Lower Hutt, New Zealand, Institute of Geological and Nuclear Sciences Ltd.

- Fischer AG 1984. The two Phanerozoic supercycles. Princeton, N. J. Pp 129-150.
- Flügel ER 2004. Microfacies of carbonate rocks: Analysis, interpretation and application. Berlin, Springer-Verlag.
- Forsyth PJ 2001. Geology of the Waitaki Area. Institute of Geological & Nuclear Sciences 1:250 000 geological map 19. 1 sheet + 64p. Lower Hutt, New Zealand, GNS Science.
- Furlong KP, Kamp PJJ 2009. The lithospheric geodynamics of plate boundary transpression in New Zealand: Initiating and emplacing subduction along the Hikurangi margin, and the tectonic evolution of the Alpine Fault system. *Tectonophysics* 474(3-4): 449-462.
- Graham IJ, Carter RM, Ditchburn RG, Zondervan A 2004. Chronostratigraphy of ODP 181, Site 1121 sediment core (Southwest Pacific Ocean), using  $^{10}\text{Be}/^{9}\text{Be}$  dating of entrapped ferromanganese nodules. *Marine Geology* 205(1-4): 227-247.
- Hancock HJL, Dickens GR, Strong CP, Hollis CJ, Field BD 2003. Foraminiferal and carbon isotope stratigraphy through the Paleocene-Eocene transition at Dee Stream, Marlborough, New Zealand. *New Zealand Journal of Geology and Geophysics* 46(1): 1-19.
- Hector J 1874. On fossil reptilia of New Zealand. *Transactions of the New Zealand Institute* 6: 333–358.
- Hedberg H ed. 1976. International stratigraphic guide: A guide to stratigraphic classification, terminology, and procedure. New York, John Wiley and Sons.
- Hesse R 1990. Origin of chert: diagenesis of biogenic siliceous sediments. In: McIlreath IA, Morrow DW eds. *Diagenesis*. Geological Association of Canada. 338 pp.
- Hoernle K, White JDL, van den Bogaard P, Hauff F, Coombs DS, Werner R, Timm C, Garbe-Schonberg D, Reay A, Cooper AF 2006. Cenozoic intraplate volcanism on New Zealand: Upwelling induced by lithospheric removal. *Earth and Planetary Science Letters* 248(1-2): 350-367.
- Hollis CJ 2002. Biostratigraphy and paleoceanographic significance of Paleocene radiolarians from offshore eastern New Zealand. *Marine Micropaleontology* 46(3-4): 265-316.
- Hollis CJ 2003. The Cretaceous/Tertiary boundary event in New Zealand: profiling mass extinction. *New Zealand Journal of Geology and Geophysics* 46(2): 307-321.

- Hollis CJ 2006. Radiolarian faunal turnover through the Paleocene-Eocene transition, Mead Stream, New Zealand. *Eclogae Geologicae Helvetiae* 99(0): S79-S99.
- Hollis CJ, Strong CP 2003. Biostratigraphic review of the Cretaceous/Tertiary boundary transition, mid-Waipara River section, North Canterbury, New Zealand. *New Zealand Journal of Geology and Geophysics* 46(2): 243-253.
- Hollis CJ, Beu AG, Raine JI, Strong CP, Turnbull IM, Waghorn DB, Wilson GJ 1997. Integrated biostratigraphy of Cretaceous-Paleogene strata on Campbell Island, southwest Pacific. Institute of Geological and Nuclear Sciences science report 97/92. 56 pp.
- Hollis CJ, Jones CM, Dickens GR, Field BD, Strong CP 2000. Age and origin of the Waipawa (Black Shale) Formation. *Geological Society of New Zealand Miscellaneous Publication* 108A, 77.
- Hollis CJ, Field BD, Rodgers KM, Strong CP 2003a. Stratigraphic, paleontological, and geochemical data from Upper Cretaceous and lower Paleocene strata in southeastern Marlborough, New Zealand. *Institute of Geological & Nuclear Sciences Report* 2003/9. 64 pp.
- Hollis CJ, Rodgers KA, Strong CP, Field BD, Rogers KM 2003b. Paleoenvironmental changes across the Cretaceous/Tertiary boundary in the northern Clarence valley, southeastern Marlborough, New Zealand. *New Zealand Journal of Geology and Geophysics* 46(2): 209-234.
- Hollis CJ, Strong CP, Rodgers KA, Rogers KM 2003c. Paleoenvironmental changes across the Cretaceous/Tertiary boundary at Flaxbourne River and Woodside Creek, eastern Marlborough, New Zealand. *New Zealand Journal of Geology and Geophysics* 46(2): 177-197.
- Hollis CJ, Strong P, Laird MG, Crampton J 2005a. Cretaceous-Paleogene stratigraphy of eastern Marlborough: Opening a South Pacific window on a greenhouse earth. In: Pettinga JR, Wandres AM eds. *Field trip guides. Geological Society of New Zealand 50 Annual Conference, Kaikoura, New Zealand. Geological Society of New Zealand Miscellaneous Publication* 119B: Pp 1–35.
- Hollis CJ, Dickens GR, Field BD, Jones CM, Strong CP 2005b. The Paleocene-Eocene transition at Mead Stream, New Zealand: a southern Pacific record of early Cenozoic global change. *Palaeogeography Palaeoclimatology Palaeoecology* 215(3-4): 313-343.
- Hollis CJ, Field BD, Jones CM, Strong CP, Wilson GJ, Dickens GR 2005c. Biostratigraphy and carbon isotope stratigraphy of uppermost Cretaceous-lower Cenozoic Muzzle Group in middle Clarence valley, New Zealand. *Journal of the Royal Society of New Zealand* 35(3): 345-383.

- Hollis CJ, Handley L, Crouch EM, Morgans HEG, Baker JA, Creech J, Collins KS, Gibbs SJ, Huber M, Schouten S, Zachos JC, Pancost RD 2009a. Tropical sea temperatures in the high-latitude South Pacific during the Eocene. *Geology* 37(2): 99-102.
- Hollis CJ, Huber M, Handley L, Taylor K, Pancost RD, Creech J, Baker JA, Schouten S, Crouch EM, Schiøler P 2009b. Climate see-saws in Paleogene New Zealand. In: Crouch EM, Hollis CJ, Strong CP eds. *Climatic and Biotic Events of the Paleogene (CBEP 2009)*, extended abstracts from an international conference in Wellington, New Zealand, 12-15 January 2009. GNS Science Miscellaneous Series 18. Pp 76-77.
- Hood SD, Nelson CS 1996. Cementation scenarios for New Zealand Cenozoic nontropical limestones. *New Zealand Journal of Geology and Geophysics* 39(1): 109-122.
- Huber M 2008. A hotter greenhouse? *Science* 321(5887): 353-354.
- Huber M, Sloan LC 2001. Heat transport, deep waters, and thermal gradients: Coupled simulation of an Eocene Greenhouse Climate. *Geophysical Research Letters* 28(18): 3481-3484.
- Hume TM, Nelson CS 1982. X-ray diffraction analytical procedures and some mineralogical characteristics for South Auckland region sediments and sedimentary rocks, with special reference to their clay fraction. Occasional Report No. 10. University of Waikato, Department of Earth Sciences. 33 pp.
- Hutton FW 1874. Report on the geology of the north-east portion of the South Island, from Cook Straits to Rakaia. Pp. 39-40. In: Reports of geological explorations during 1873-74, with maps and sections. Geological Survey of New Zealand. Wellington, Government Printer. 164 pp.
- Isaac MJ, Herzer R, Brook FJ, Hayward BW 1994. Cetaceous-Cenozoic sedimentary basins of Northland, New Zealand. Institute of Geological and Nuclear Sciences monograph 8. 203 p. + 4 sheets. Lower Hutt, New Zealand, Institute of Geological and Nuclear Sciences Ltd.
- JCPDS ed. 1980. Mineral powder diffraction file: Data book. Pennsylvania, USA, International Centre for Diffraction Data.
- John CM, Bohaty SM, Zachos JC, Sluijs A, Gibbs S, Brinkhuis H, Bralower TJ 2008. North American continental margin records of the Paleocene-Eocene thermal maximum: Implications for global carbon and hydrological cycling. *Paleoceanography* 23(2): 20.
- Joseph LH, Rea DK, van der Pluijm BA 2004. Neogene history of the Deep Western Boundary Current at Rekohu sediment drift, Southwest Pacific (ODP Site 1124). *Marine Geology* 205(1-4): 185-206.

- Kamp PJJ 1986. Late Cretaceous-Cenozoic tectonic development of the southwest Pacific region. *Tectonophysics* 121(2-4): 225-251.
- Kender S, Peck VL, Jones RW, Kaminski MA 2009. Middle Miocene oxygen minimum zone expansion offshore West Africa: Evidence for global cooling precursor events. *Geology* 37(8): 699-702.
- Kennedy WJ, Garrison RE 1975. Morphology and genesis of nodular chalks and hardgrounds in the Upper Cretaceous of southern England. *Sedimentology* 22(3): 311-386.
- Kennett JP 1982. *Marine Geology*. Englewood Cliffs, NJ, Prentice-Hall. 813 pp.
- Kennett JP, Stott LD 1990. Proteus and proto-Oceanus: Ancestral Paleogene oceans as revealed from Antarctic stable isotopic results; ODP Leg 113. In: Barker PF, Kennett JP eds. *Proc. ODP, Sci. Results, 113*: College Station, TX (Ocean Drilling Program). Pp 865-880.
- Kerr IS 1976. *Campbell Island: A history*. Wellington, New Zealand, A. H. & A. W. Reed Ltd. 182 pp.
- Killops SD, Hollis CJ, Morgans HEG, Sutherland R, Field BD, Leckie DA 2000. Paleooceanographic significance of Late Paleocene dysaerobia at the shelf/slope break around New Zealand. *Palaeogeography Palaeoclimatology Palaeoecology* 156(1-2): 51-70.
- King PR, Naish TR, Browne GH, Field BD, Edbrooke SW 1999. *Cretaceous to Recent sedimentary patterns in New Zealand*. Institute of Geological & Nuclear Sciences Folio Series 1. Lower Hutt, New Zealand, Institute of Geological & Nuclear Science Limited.
- Kingma JT 1960. Outline of the Cretaceous-Tertiary sedimentation in eastern basin of New Zealand. *New Zealand Journal of Geology and Geophysics* 3: 222-234.
- Kurtz A, Kump LR, Arthur MA, Zachos JC, Paytan A 2003. Early Cenozoic decoupling of the global carbon and sulphur cycles. *Paleoceanography* 18(4):10.1029/2003PA000908
- Laird MG, Bassett KN, Schioler P, Morgans HEG, Bradshaw JD, Weaver SD 2003. Paleoenvironmental and tectonic changes across the Cretaceous/Tertiary boundary at Tora, southeast Wairarapa, New Zealand: a link between Marlborough and Hawke's Bay. *New Zealand Journal of Geology and Geophysics* 46(2): 275-293.
- Laird MG, Bradshaw JD 2004. The Break-up of a Long-term Relationship: the Cretaceous Separation of New Zealand from Gondwana. *Gondwana Research* 7(1): 273-286.

- Landis CA, Campbell HJ, Begg JG, Mildenhall DC, Paterson AM, Trewick SA 2008. The Waipounamu Erosion Surface: questioning the antiquity of the New Zealand land surface and terrestrial fauna and flora. *Geological Magazine* 145(2): 173-197.
- Lawrence MJF 1989. Chert and dolomite in the Amuri Limestone Group and Woolshed Formation, Eastern Marlborough, New Zealand. Unpublished thesis, University of Canterbury, New Zealand.
- Lawrence MJF 1993. Sedimentology and petrography of early diagenetic chert and dolomite in the Late Cretaceous Early Tertiary Amuri Limestone Group, eastern Marlborough, New Zealand. *New Zealand Journal of Geology and Geophysics* 36(1): 9-25.
- Lawrence MJF 1994. Conceptual-model for early diagenetic chert and dolomite, Amuri Limestone Group, north-eastern South Island, New Zealand. *Sedimentology* 41(3): 479-498.
- Lawver LA, Gahagan LM, Coffin MF 1992. The development of paleoseaways around Antarctica. In: Kennett JP, Warnke DA eds. *The Antarctic paleoenvironment: A perspective on global change, Part One*. American Geophysical Union Antarctic Research Series Volume 56. Pp 7-30.
- Lazarus D, Caulet JP 1993. Cenozoic Southern Ocean reconstructions from sedimentologic, radiolarian and other microfossil data. In: *The Antarctic paleoenvironment: A perspective on global change, Part Two*. American Geophysical Union Antarctic Research Series Volume 60. Pp 145-174.
- Leckie DA, Morgans H, Wilson GJ, Edwards AR 1995. Mid-Paleocene dropstones in the Whangai Formation, New Zealand - evidence of mid-Paleocene cold climate? *Sedimentary Geology* 97(3-4): 119-129.
- Lewis DW 1964. 'Perigenic'; a new term. *Journal of Sedimentary Research* 34(4): 875-876.
- Lu H, Fulthorpe CS, Mann P 2003. Three-dimensional architecture of shelf-building sediment drifts in the offshore Canterbury Basin, New Zealand. *Marine Geology* 193(1-2): 19-47.
- Luyendyk BP 1995. Hypothesis for Cretaceous rifting of east Gondwana caused by subducted slab capture. *Geology* 23(4): 373-376.
- Lyons TW, Anbar AD, Severmann S, Scott C, Gill BC 2009. Tracking Euxinia in the Ancient Ocean: A Multiproxy Perspective and Proterozoic Case Study. *Annual Review of Earth and Planetary Sciences* 37: 507-534.
- MacPherson EO 1948. The upper Senonian transgression in New Zealand. *New Zealand Journal of Science and Technology* B29(6): 280-296 (table).



- Marshall DJ 1988. Cathodoluminescence of geological materials. Wellington, New Zealand., Allen and Unwin (New Zealand) Ltd.
- McCave IN, Carter L 1997. Recent sedimentation beneath the Deep Western Boundary Current off northern New Zealand. *Deep-Sea Research Part I-Oceanographic Research Papers* 44(7): 1203-1237.
- McConchie DM 1978. Cretaceous and Lower Tertiary glauconite in the South Island of New Zealand. Unpublished thesis, University of Canterbury, New Zealand.
- McKay A 1886. On the geology of the eastern part of Marlborough provincial district. Pp. 27-136. In: No 17: Reports of geological explorations during 1885, with maps and sections. Colonial Museum and Geological Survey of New Zealand. Wellington, Government Printer. 202 pp.
- McRae SG 1972. Glauconite. *Earth-Science Reviews* 8(4): 397-440.
- Miller KG, Fairbanks RG, Mountain GS 1987. Tertiary Oxygen Isotope Synthesis, Sea Level History, and Continental Margin Erosion. *Paleoceanography* 2(1): 1-19.
- Miller KG, Mountain GS, Browning JV, Kominz M, Sugarman PJ, Christie-Blick N, Katz ME, Wright JD 1998. Cenozoic global sea level, sequences, and the New Jersey transect: Results from coastal plain and continental slope drilling. *Reviews of Geophysics* 36(4): 569-601.
- Miller KG, Wright JD, Browning JV 2005. Visions of ice sheets in a greenhouse world. *Marine Geology* 217(3-4): 215-231.
- Moore PR 1988. Stratigraphy, composition and environmental deposition of the Whangai Formation and associated Late Cretaceous-Paleocene rocks, eastern North Island, New Zealand. *New Zealand Geological Survey Bulletin* 100.
- Moore P 2004. Wildlife of Campbell Island. In: Dingwall P, Gregory G eds. *A musterer's sojourn on Campbell Island: the diary of Alfred Austin, 1919-1921*. Department of Conservation. 135 pp.
- Morris JC 1987. The stratigraphy of the Amuri Limestone Group, east Marlborough, New Zealand. Unpublished thesis, University of Canterbury, New Zealand.
- Mortimer N 2004. New Zealand's Geological Foundations. *Gondwana Research* 7(1): 261-272.
- Mountain GS, Burger RL, Delius H, Fulthorpe CS, Austin JA, Goldberg DS, Steckler MS, McHugh CM, Miller KG, Monteverde DH, Orange DL, Pratson LF 2007. The long-term stratigraphic record on continental margins. In: Nittroer CA, Austin JA, Field ME, Kravitz

- JH, Syvitski JP, Wiberg PL eds. Continental margin sedimentation: From sediment transport to sequence stratigraphy. International Association of Sedimentologists Volume 37. Malden, Massachusetts, Blackwell Publishing. Pp 381-458.
- Muller RA, MacDonald GJ eds. 2000. Ice ages and astronomical causes: Data, spectral analysis and mechanisms. London, Springer-Verlag.
- Munnecke A, Samtleben C 1996. The formation of micritic limestones and the development of limestone-marl alternations in the Silurian of Gotland, Sweden. *Facies* 34(1): 159-176.
- Munnecke A, Westphal H, Elrick M, Reijmer J 2001. The mineralogical composition of precursor sediments of calcareous rhythmites: a new approach. *International Journal of Earth Sciences* 90(4): 795-812.
- Nelson CS 1968. Sedimentology of redeposited calcareous and glauconitic beds at Pahaoa, South-east Wellington. *Transactions of the Royal Society of New Zealand* 6(5): 45-62.
- Nelson CS 1978. Temperate shelf carbonate sediments in the Cenozoic of New Zealand. *Sedimentology* 25(6): 737-771.
- Nelson CS, James NP 2000. Marine cements in mid-Tertiary cool-water shelf limestones of New Zealand and southern Australia. *Sedimentology* 47(3): 609-629.
- Nelson CS, Cooke PJ 2001. History of oceanic front development in the New Zealand sector of the Southern Ocean during the Cenozoic—a synthesis. *New Zealand Journal of Geology and Geophysics* 44: 535–553.
- Nelson CS, Smith AM 1996. Stable oxygen and carbon isotope compositional fields for skeletal and diagenetic components in New Zealand Cenozoic nontropical carbonate sediments and limestones: A synthesis and review. *New Zealand Journal of Geology and Geophysics* 39(1): 93-107.
- Nesbitt HW 1979. Mobility and fractionation of rare earth elements during weathering of a granodiorite. *Nature* 279: 206-210.
- New Zealand - A regional profile: Marlborough. 1999. Wellington, New Zealand, Statistics New Zealand.
- New Zealand - A regional report: Canterbury. 1999. Wellington, New Zealand, Statistics New Zealand.
- Nicolo MJ, Dickens GR, Hollis CJ, Zachos JC 2007. Multiple early Eocene hyperthermals: Their sedimentary expression on the New Zealand continental margin and in the deep sea. *Geology* 35(8): 699-702.

- Noe S, Titschack J, Freiwald A, Dullo WC 2006. From sediment to rock: diagenetic processes of hardground formation in deep-water carbonate mounds of the NE Atlantic. *Facies* 52(2): 183-208.
- Odin GS, Matter A 1981. De glauconiarum origine. *Sedimentology* 28(5): 611-641.
- Oliver RL, Finlay HJ, Fleming CA 1950. The geology of Campbell Island, vol. Cape Expedition Series, Bulletin No. 3. Wellington, DSIR. 1 map + 62 p.
- Ota Y, Pillans B, Berryman K, Beu A, Fujimori T, Miyauchi T, Berger G 1996. Pleistocene coastal terraces of Kaikoura peninsula and the Marlborough coast, South Island, New Zealand. *New Zealand Journal of Geology and Geophysics* 39(1): 51-72.
- Pagani M, Zachos JC, Freeman KH, Tipple B, Bohaty S 2005. Marked decline in atmospheric carbon dioxide concentrations during the Paleogene. *Science* 309(5734): 600-603.
- Parson B, Sclater JG 1977. An analysis of the variation of ocean floor bathymetry and heat flow with age. *Journal of Geophysical Research - Solid Earth* 82(5): 803-827.
- Pearson PN, Palmer MR 2000. Atmospheric carbon dioxide concentrations over the past 60 million years. *Nature* 406(6797): 695-699.
- Pearson PN, van Dongen BE, Nicholas CJ, Pancost RD, Schouten S, Singano JM, Wade BS 2007. Stable warm tropical climate through the Eocene Epoch. *Geology* 35(3): 211-214.
- Pratson LF & 21 others 2007. Seascapes evolution on clastic shelves and slopes. In: Nittrouer CA, Austin JA, Field ME, Kravitz JH, Syvitski JP, Wiberg PL eds. *Continental margin sedimentation: From sediment transport to sequence stratigraphy*. International Association of Sedimentologists Volume 37. Malden, Massachusetts, Blackwell Publishing. Pp 339–380.
- Rattenbury MS, Townsend DB, Johnston MR 2006. Geology of the Kaikoura Area. Institute of Geological & Nuclear Sciences 1:250 000 geological map 13. 1 sheet + 70p. Lower Hutt, New Zealand, GNS Science.
- Reay MB 1993. Geology of the middle Clarence valley. Scale 1:50 000. Institute of Geological and Nuclear Sciences geological map 10. 1 sheet + 144p. Lower Hutt, New Zealand, Institute of Geological and Nuclear Sciences Limited.
- Reid RP, Macintyre IG, James NP 1990. Internal precipitation of microcrystalline carbonate - a fundamental problem for sedimentologists. *Sedimentary Geology* 68(3): 163-170.

- Ricken W 1986. Diagenetic bedding: a model for limestone-marl alternations. Berlin, Springer Verlag.
- Ricken W 1987. The carbonate compaction law: a new tool. *Sedimentology* 34(4): 571-584.
- Ricken W, Eder W 1991. Diagenetic modification of calcareous beds - an overview. In: Einsele G, Ricken W, Seilacher A eds. *Cycles and events in stratigraphy*. Berlin, Springer-Verlag. Pp 430-449.
- Rogers KM, Morgans HEG, Wilson GS 2001. Identification of a Waipawa Formation equivalent in the upper Te Uri Member of the Whangai Formation - implications for depositional history and age. *New Zealand Journal of Geology and Geophysics* 44(2): 347-354.
- Rollinson HR 1993. *Using geochemical data: Evaluation, presentation, interpretation*. Longman, Harlow. 352 pp.
- Roser BP, Cooper RA, Nathan S, Tulloch AJ 1996. Reconnaissance sandstone geochemistry, provenance, and tectonic setting of the lower Paleozoic terranes of the West Coast and Nelson, New Zealand. *New Zealand Journal of Geology and Geophysics* 39(1): 1-16.
- Schiøler P, Rogers K, Sykes R, Hollis CJ, Ilg B, Meadows D, Roncaglia L, Uruski C 2010. Palynofacies, organic geochemistry and depositional environment of the Tartan Formation (Late Paleocene), a potential source rock in the Great South Basin, New Zealand. *Marine and Petroleum Geology* 27(2): 351-369.
- Schmitz B 1987a. Barium, Equatorial High Productivity, and the Northward Wandering of the Indian Continent. *Paleoceanography* 2(1):63-77.
- Schmitz B 1987b. The  $TiO_2/Al_2O_3$  ratio in the Cenozoic Bengal Abyssal Fan sediments and its use as a paleostream energy indicator. *Marine Geology* 76: 195-206.
- Schmitz B, Asaro F, Michel HV, Thierstein HR, Huber BT 1991. Element stratigraphy across the Cretaceous/Tertiary boundary in Hole 738C. *Proc. ODP, Sci. Results*, 119: College Station, TX (Ocean Drilling Program). Pp 719-730.
- Schmitz B, Charisi SD, Thompson EI, Speijer RP 1997. Barium,  $SiO_2$  (excess), and  $P_2O_5$  as proxies of biological productivity in the Middle East during the Palaeocene and the latest Palaeocene benthic extinction event. *Terra Nova* 9(2): 95-99.
- Scholle PA, Ulmer-Scholle DS 2003. *A colour guide to the petrography of carbonate rocks: grains, textures, porosity, diagenesis*. AAPG Mem 77:1-474.
- Schroeder JO, Murray RW, Leinen M, Pflaum RC, Janecek TR 1997. Barium in Equatorial Pacific Carbonate Sediment: Terrigenous,

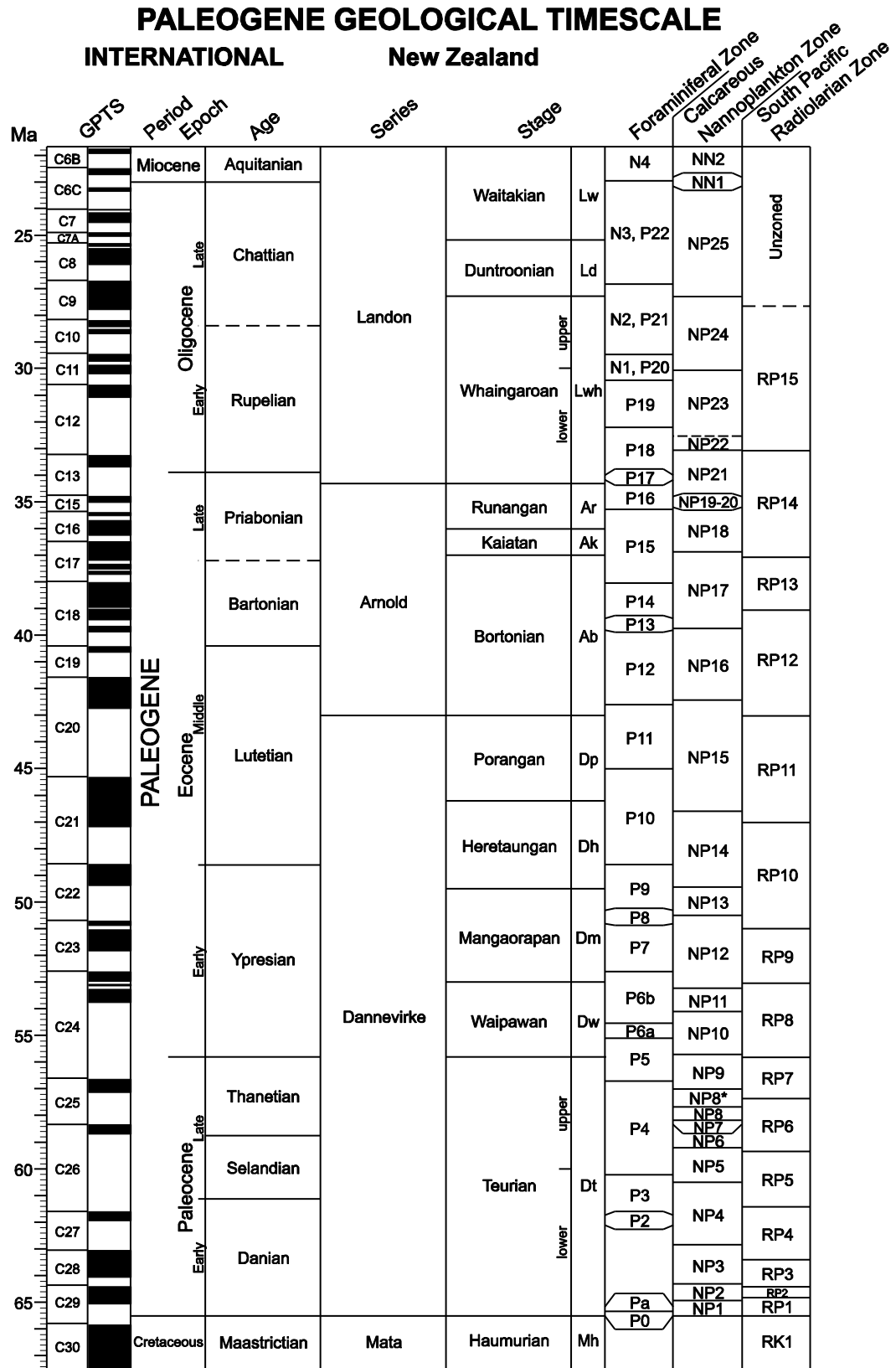
- Oxide, and Biogenic Associations. *Paleoceanography* 12(1): 125-146.
- Shackleton NJ, Backman J, Zimmerman H, Kent DV, Hall MA, Roberts DG, Schnitker D, Baldauf JG, Desprairies A, Homrighausen R, Huddlestun P, Keene JB, Kaltenback AJ, Krumsiek KAO, Morton AC, Murray JW, Westberg-Smith J 1984. Oxygen isotope calibration of the onset of ice-rafting and history of glaciation in the North Atlantic region. *Nature* 307(5952): 620-623.
- Spielhagen RF, Tripathi A 2009. Evidence from Svalbard for near-freezing temperatures and climate oscillations in the Arctic during the Paleocene and Eocene. *Palaeogeography, Palaeoclimatology, Palaeoecology* 278(1-4): 48-56.
- Spörli KB 1980. New Zealand and oblique slip margins: tectonic development up to and during the Cainozoic. In: Ballance PF, Reading HG eds. *Sedimentation in oblique-slip mobile zones*. International Association of Sedimentologists special publication 4.
- Stow DAV, Faugères J-C, Viana A, Gonthier E 1998. Fossil contourites: a critical review. *Sedimentary Geology* 115(1-4): 3-31.
- Strong CP, Hollis CJ, Wilson GJ 1995. Foraminiferal, radiolarian, and dinoflagellate biostratigraphy of Late Cretaceous to Middle Eocene pelagic sediments (Muzzle Group), Mead Stream, Marlborough, New Zealand. *New Zealand Journal of Geology and Geophysics* 38(2): 171-209.
- Sutton PJH 2003. The Southland Current: a subantarctic current. *New Zealand Journal of Marine and Freshwater Research* 37(3): 645-652.
- Taylor SR, McLennan SM 1988. The significance of the rare earths in geochemistry and cosmochemistry In: Gschmeidner KA, Eyring L eds. *Handbook of the physics and chemistry of rare earths*. Elsevier Science Publishers. Pp 486-578.
- Terry RD, Chilingar GV 1955. Summary of "Concerning some additional aids in studying sedimentary formations," by M. S. Shvetsov. *Journal of Sedimentary Research* 25(3): 229-234.
- Thomas E 1992. Cenozoic deep-sea circulation: Evidence from deep-sea benthic foraminifera. In: Kennett JP, Warnke DA eds. *The Antarctic paleoenvironment: A perspective on global change, Part One*. American Geophysical Union Antarctic Research Series Volume 56. Pp 141-156.
- Thompson EI, Schmitz B 1997. Barium and the late Paleocene delta C-13 maximum: Evidence of increased marine surface productivity. *Paleoceanography* 12(2): 239-254.

- Turgeon S, Brumsack HJ 2006. Anoxic vs dysoxic events reflected in sediment geochemistry during the Cenomanian-Turonian Boundary Event (Cretaceous) in the Umbria-Marche Basin of central Italy. *Chemical Geology* 234(3-4): 321-339.
- Van Dissen R, Yeats RS 1991. Hope fault, Jordan thrust, and uplift of the Seaward Kaikoura Range, New Zealand. *Geology* 19(4): 393-396.
- Van Sickel WA, Kominz MA, Miller KG, Browning JV 2004. Late Cretaceous and Cenozoic sea-level estimates: backstripping analysis of borehole data, onshore New Jersey. *Basin Research* 16(4): 451-465.
- Viana AR, Faugères JC, Stow DAV 1998. Bottom-current-controlled sand deposits: a review of modern shallow- to deep-water environments. *Sedimentary Geology* 115(1-4): 53-80.
- Warren G 1995. Geology of the Parnassus area, Scale 1:50 000. Institute of Geological and Nuclear Sciences geological map 18. 1 sheet + 36p. Lower Hutt, New Zealand, Institute of Geological and Nuclear Sciences Limited.
- Warren G, Speden IG 1978. The Piripauan and Haumurian stratotypes (Mata Series, Upper Cretaceous) and correlative sequences in the Haumuri Bluff district, south Marlborough. *New Zealand Geological Survey bulletin*. Wellington, Department of Scientific and Industrial Research. 60 pp.
- Webb PN 1966. New Zealand Late Cretaceous foraminifera and stratigraphy. Unpublished Ph.D. thesis lodged in the Library, State University of Utrecht. 320 pp.
- Wedepohl KH 1971. Environmental influences on the chemical composition of shales and clays. *Physics and Chemistry of The Earth* 8: 305-333.
- Westphal H, Munnecke A, Pross J, Herrle JO 2004. Multiproxy approach to understanding the origin of Cretaceous pelagic limestone-marl alternations (DSDP site 391, Blake-Bahama Basin). *Sedimentology* 51(1): 109-126.
- Williams M, Haywood AM, Gregory FJ, Schmidt DN 2007. Deep-time perspective climate change: an introduction. In: Williams M, Haywood AM, Gregory FJ, Schmidt DN eds. *Deep-time perspectives on climate change: marrying the signal from computer models and biological proxies*. The Micropaleontological Society, Special Publication. The Geological Society, London. Pp 1-3.
- Wing SL, Gingerich P, Schmitz B, Thomas E 2003. Preface. In: Wing SL, Gingerich P, Schmitz B, Thomas E eds. *Causes and Consequences of Globally Warm Climates in the Early Paleogene*, Special Paper. Geological Society of America. Pp vii –x.

- Zachos JC, Breza JR, Wise SW 1992. Early Oligocene ice-sheet expansion on Antarctica: Stable isotope and sedimentological evidence from Kerguelen Plateau, southern Indian Ocean. *Geology* 20(6): 569-573.
- Zachos JC, Pagani M, Sloan L, Thomas E, Billups K 2001. Trends, rhythms, and aberrations in global climate 65 Ma to present. *Science* 292(5517): 686-693.
- Zachos JC, Dickens GR, Zeebe RE 2008. An early Cenozoic perspective on greenhouse warming and carbon-cycle dynamics. *Nature* 451(7176): 279-283.

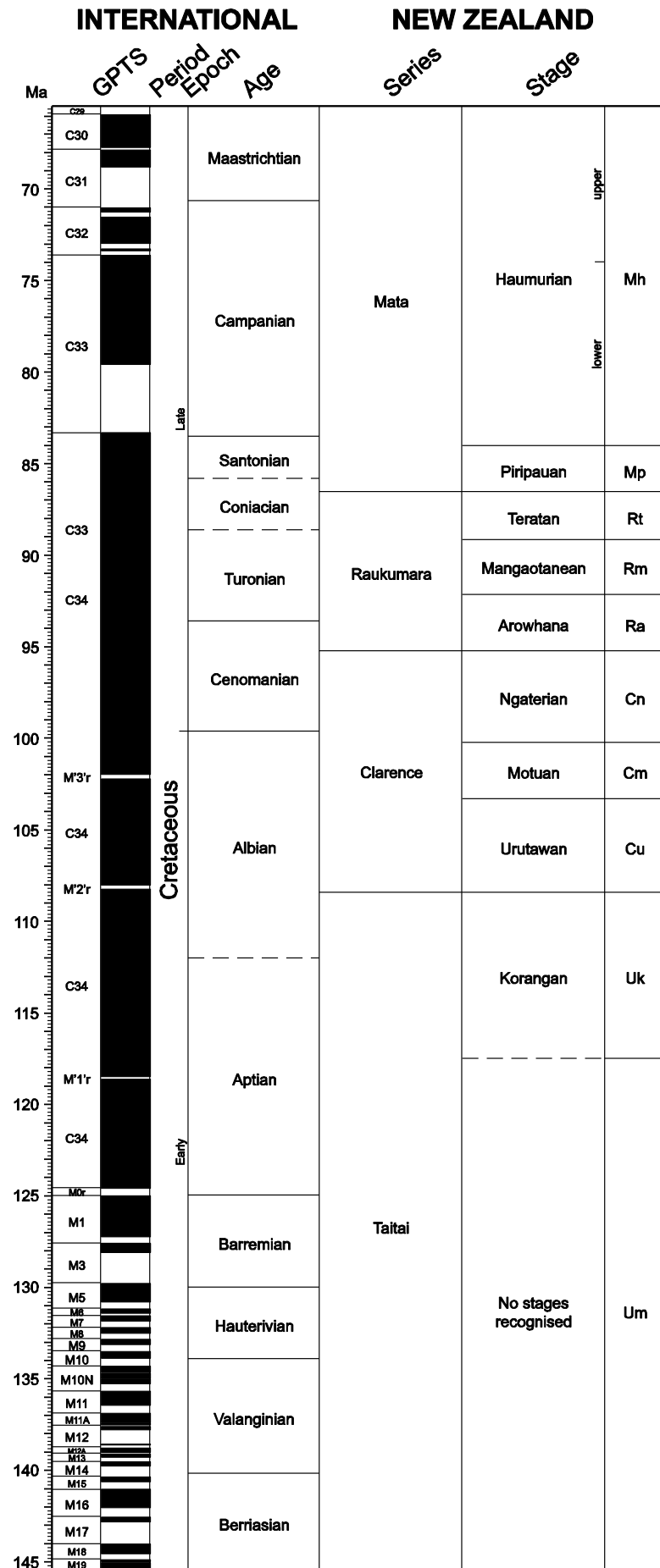
# APPENDIX A

## GEOLOGICAL TIMESCALES





# CRETACEOUS GEOLOGICAL TIMESCALE



# APPENDIX B

## SAMPLE CATALOGUE

Location: Limestone Point, Campbell Island - S 52°33'02.5", E 169°05'30.1" (Figure 3.4)						
Field Number	Waikato Number	Thickness*	Unit	Description	Bulk Sample	Thin Section
LP01	20100500	3.00	Tucker Cove Limestone	Light grey cream micrite		
LP02	20100501	1.40	Tucker Cove Limestone	Light grey cream micrite		
LP03	20100502	0.08	Tucker Cove Limestone	Light grey cream, glauconic micrite		
LP07	20100503	0.72	Tucker Cove Limestone	Light grey cream, glauconic micrite		
*Thickness with respect to boundary between Garden Cove Formation and Tucker Cove Limestone						
Location: Camp Cove, Campbell Island - S 52°33'02.5", E 169°05'30.1" (Figure 3.4)						
Field Number	Waikato Number	Thickness*	Unit	Description	Bulk Sample	Thin Section
CC01	20100504	0.95	Tucker Cove Limestone	Light grey cream micrite		
CC02	20100505	0.55	Tucker Cove Limestone	Light grey cream micrite		
CC03	20100506	0.10	Tucker Cove Limestone	Light grey cream micrite		
CC04	20100507	0.05	Tucker Cove Limestone	Light grey cream, glauconic micrite		
CC05	20100508	0.02	Tucker Cove Limestone	Light grey cream, glauconic micrite		
CC06	20100509	0.02	Tucker Cove Limestone	Dark brown very fine sandy mudstone		
CC07	20100510		Garden Cove Formation	Dark brown muddy fine sandstone		
CC08	20100511		Garden Cove Formation	Dark brown muddy fine sandstone		
CC09	20100512		Garden Cove Formation	Dark brown muddy fine sandstone		
CCB0	20100583	-0.10		Dark brown very fine sandy mudstone		
CCB01	20100513	-0.50	Garden Cove Formation	Dark brown muddy fine sandstone		
CCB02	20100514	-0.80	Garden Cove Formation	Dark brown muddy fine sandstone		
CCB03	20100515	-2.00	Garden Cove Formation	Dark brown very fine sandy mudstone		
CCB04	20100516	-3.30	Garden Cove Formation	Dark brown very fine sandy mudstone		
CCB05	20100517	-4.70	Garden Cove Formation	Dark brown very fine sandy mudstone		
CCB06	20100578	-13.90	Garden Cove Formation	Dark brown very fine sandy mudstone		
CCB07	20100579	-17.60	Garden Cove Formation	Dark brown very fine sandy mudstone		
CCB08	20100580	-20.50	Garden Cove Formation	Dark brown, laminated very fine sandy mudstone		
CCB09	20100581	-23.10	Garden Cove Formation	Dark brown, laminated very fine sandy mudstone		
CCB10	20100582	-25.80	Garden Cove Formation	Dark brown, laminated very fine sandy mudstone		
*Thickness with respect to boundary between Garden Cove Formation and Tucker Cove Limestone						

Location: Mead Stream, southeastern Marlborough -NZMS 260 P30 758160 (Figure 4.6)

Field Number	Waikato Number	Thickness*	Unit	Description	Bulk Sample	Bulk Powder	Thin Section
MD0	20100518	107.10	Mead Hill Formation	Light grey siliceous micrite			
MD01	20100519	107.30	Mead Hill Formation	Dark grey to black chert nodule			
MD02	20100520	107.38	Mead Hill Formation	Light grey siliceous micrite			
MD03	20100521	107.63	Mead Hill Formation	Light grey siliceous micrite			
MD05	20100522	108.29	Waipawa Formation	Dark brown organic mudstone			
MD06	20100523	108.44	Waipawa Formation	Dark brown organic mudstone			
MD07	20100524	108.58	Waipawa Formation	Dark brown organic mudstone			
MD08	20100525	108.76	Waipawa Formation	Dark brown organic mudstone			
MD09	20100526	109.02	Waipawa Formation	Dark brown organic mudstone			
MD10	20100527	109.14	Waipawa Formation	Dark brown organic mudstone			
MD11	20100528	108.66	Waipawa Formation	Dark brown organic mudstone			
MD12	20100529	109.54	Waipawa Formation	Dark brown organic mudstone			
MD13	20100530	110.20	Waipawa Formation	Dark brown organic mudstone			
MD14	20100531	110.38	Waipawa Formation	Dark brown organic mudstone			
MD15	20100532	110.78	Waipawa Formation	Dark brown organic mudstone			
MD16	20100533	110.84	Waipawa Formation	Dark brown organic mudstone			
MD17	20100534	110.97	Waipawa Formation	Dark brown organic mudstone			
MD18	20100535	111.48	Waipawa Formation	Light grey siliceous micrite and chert nodule			
MD19	20100536	111.58	Waipawa Formation	Light grey siliceous micrite			
MD20	20100537	115.28	Waipawa Formation	Light grey siliceous micrite			
MD21	20100538	115.80	Waipawa Formation	Dark grey organic mudstone			
MD22	20100539	115.92	Waipawa Formation	Dark grey organic mudstone			
MD23	20100540	116.02	Waipawa Formation	Dark grey organic mudstone			
MD24	20100541	117.04	Lower Limestone	Light grey siliceous micrite			
MD25	20100542	118.62	Lower Limestone	Light grey siliceous micrite			
MD26	20100543	121.04	Lower Limestone	Light grey siliceous micrite			

\*Thickness with respect to the Cretaceous/Tertiary boundary

**Location: Muzzle Stream, southeastern Marlborough - NZMS 260 O30 613025 (Figure 4.17)**

Field Number	Waikato Number	Thickness* Unit	Description	Bulk Sample	Bulk Powder	Thin Section
MZ01	20100544	-1.00	Mead Hill Formation Light grey siliceous micrite			
MZ02	20100545	-0.30	Mead Hill Formation Light grey siliceous micrite			
MZ03	20100546	-0.05	Mead Hill Formation Light grey siliceous micrite with <i>Thalassinoides</i> burrows			
MZ04	20100547	0.08	Teredo Limestone Mbr Greenish grey calcareous greensand			
MZ05	20100548	0.25	Teredo Limestone Mbr Greenish grey calcareous greensand			
MZ06	20100549	0.34	Lower Limestone Light grey to cream, glauconitic micrite			
MZ07	20100550	0.78	Lower Limestone Light grey to cream micrite			
MZ08	20100551	0.98	Lower Limestone Light grey to cream micrite			

\*Thickness with respect to boundary between Mead hill Formation and Teredo Limestone Member

**Location: Kaikoura wharf, southeastern Marlborough - NZMS 260 O30 678657 (Figure 4.28)**

Field Number	Waikato Number	Thickness* Unit	Description	Bulk Sample	Bulk Powder	Thin Section
KK01	20100552	-1.05	Mead Hill Formation Light grey siliceous micrite			
KK02	20100553	-0.25	Mead Hill Formation Light grey, glauconitic siliceous micrite			
KK03	20100554	0.05	Mead Hill Formation Dark greenish grey calcareous greensand			
KK04	20100555	0.75	Mead Hill Formation Light greenish grey, glauconitic siliceous micrite			
KK05	20100556	1.05	Mead Hill Formation Light greenish grey, glauconitic siliceous micrite			
KK06	20100557	1.75	Mead Hill Formation Light greenish grey, glauconitic siliceous micrite			
KK07	20100558	0.45	Mead Hill Formation Dark greenish grey calcareous greensand			
KK08	20100559	2.50	Mead Hill Formation Light greenish grey, glauconitic siliceous micrite			
KK09	20100560	2.80	Mead Hill Formation Light greenish grey, glauconitic siliceous micrite			
KK10	20100561	3.46	Mead Hill Formation Light grey to cream micrite			
KK11	20100562	3.80	Mead Hill Formation Light grey to cream micrite			
KK12	20100563	4.50	Mead Hill Formation Light grey to cream micrite			
KK13	20100564	4.80	Mead Hill Formation Light grey to cream micrite			
KK14	20100565	4.60	Mead Hill Formation Light grey chert nodule			
KK15	20100566	5.00	Mead Hill Formation Light grey to cream micrite			
KK16	20100567	5.23	Mead Hill Formation Light grey to cream micrite			
KK17	20100584	5.40	Mead Hill Formation <i>Thalassinoides</i> burrows			
KK18	20100568	5.55	Teredo Limestone Mbr Greenish grey calcareous greensand			
KK19	20100569	5.70	Teredo Limestone Mbr Phosphatised micritic limestone clast			
KK20	20100570	5.95	Teredo Limestone Mbr Greenish grey calcareous greensand			

KK22	20100571	6.80	Lower Limestone	Light grey to cream, glauconitic micrite	
KK23	20100572	7.05	Lower Limestone	Light grey to cream, glauconitic micrite	
KK24	20100573	7.35	Lower Limestone	Light grey to cream, glauconitic micrite	
KK25	20100574	7.75	Lower Limestone	Light grey to cream micrite	
KK26	20100575	8.55	Lower Marl	Light grey to cream micrite	
KK27	20100576	9.05	Lower Marl	Light grey to cream micrite	
KK39	20100577	4.60	Mead Hill Formation	Black chert nodule core	

\*Thickness with respect to the Cretaceous/Tertiary boundary

# APPENDIX C-1

## PETROGRAPHIC DATA

Semi-quantitative abundance limits used during petrographic analysis.

Abbreviation	Term	% Abundance
VA	Very abundant	>75
A	Abundant	50-75
VC	Very common	25-50
C	Common	15-25
M	Many	5-15
S	Some	1-5
R	Rare	<1
-	Absent	0

A: angular; a: subangular; r: subrounded; R: rounded.

PS: poorly sorted; MS: moderately sorted; WS: well sorted.

Petrographic Data Sheet

Thin section number	MZ01	MZ03.1A	MZ03.1B	MZ04	MZ05	MZ06.2	MZ07.3	MZ08.1B	MZ08.1A	MZ09	M10
<b>Siliciclasts &amp; Authigenic Grains</b>											
<b>Siliclastic %</b>	5	50	40	70	40	5	<1	<1	<1	<1	<1
Quartz	S	VC	VC	VC	C	S	R	R	R	R	-
Feldspar	R	S	S	S	S	R	-	-	-	-	-
IRFs	-	-	-	-	-	-	-	-	-	-	-
SRFs	-	-	-	-	R	-	-	-	-	-	-
Micas	R	-	-	R	R	-	-	-	-	-	-
Pyrite grains	R	R	R	S	R	R	-	-	-	-	-
Pyrite infills	-	-	-	-	R	R	-	-	-	-	-
Phosphatic Grains	-	S	S	S	R	R	-	-	-	-	-
Glaucony	-	C	C	C	C	S	R	R	R	-	-
Other	-	-	-	-	-	-	R	R	R	-	R
Modal size 1 (mm)	0.05	0.15	0.20	0.13	0.13	0.13	0.05	0.13	0.08	-	0.05
Modal size 2 (mm)	-	0.25	0.10	-	-	0.00	-	-	-	-	-
Shape/abrasion	ar	ar	ar	ar	ar	ar	ar	r	ar	-	A
Sorting	WS	MS	MS	WS	MS	MS	WS	-	PS	-	PS
<b>Bioclasts</b>											
<b>Total bioclast %</b>	5	10	7	<1	<1	10	12	15	15	5	3
Benthic foraminifera	R	S	R	-	-	R	R	-	R	-	-
Planktic foraminifera	S	S	S	R	R	M	M	M	M	S	-
Bryozoans	-	-	-	-	-	-	-	-	-	-	-
Bivalves	-	-	-	-	-	-	-	-	-	-	-
Echinoderms	-	-	-	-	-	-	-	-	-	-	-
Gastropods	-	-	-	-	-	-	-	-	-	-	-
Calcareous algae	-	-	-	-	-	-	-	-	-	-	-
Barnacles	-	-	-	-	-	-	-	-	-	-	-
Spicules & spines	-	M	M	-	-	-	-	-	-	-	-
Radiolarians	R	R	R	R	R	R	R	S	R	-	S
Modal size 1 (mm)	0.13	0.10	0.13	0.05	0.05	0.13	0.15	0.18	-	-	-
Modal size 2 (mm)	-	0.15	-	-	-	-	-	-	-	-	-
Shape/abrasion	-	B	-	B	B	Wb	Wb	Wb	-	-	-

**Petrographic Data Sheet**

Thin section number		MD13	MD18	MD24.1	MD25	MD26.1	KK01.1B	KK02.1A	KK03.2A	KK03.2B	KK04.1	KK08.1
<b>Siliclasts &amp; Authigenic Grains</b>	<b>Siliclastic %</b>	5	<1	-	-	-	25	23	75	60	50	15
	Quartz	S	-	-	-	-	C	C	A	VC	VC	M
	Feldspar	-	-	-	-	-	R	R	-	-	-	-
	IRFs	-	-	-	-	-	-	-	-	-	-	-
	SRFs	-	-	-	-	-	-	-	-	-	-	-
	Micas	-	-	-	-	-	S	S	S	S	S	R
	Pyrite grains	S	-	-	-	-	R	R	R	R	S	R
	Pyrite infills	-	-	-	-	-	R	R	-	-	-	-
	Phosphahtic grains						R	R	R	R	R	R
	Glaucony	R	-	-	-	-	S	S	M	M	M	S
	Other	R	R	-	-	-	-	-	-	-	-	-
	Modal size 1 (mm)	0.05	-	-	-	-	0.08	0.08	0.05	0.05	0.05	0.13
	Modal size 2 (mm)		-	-	-	-	-	0.18	0.25	0.25	0.25	-
	Shape/abrasion	ar	-	-	-	-	Aa	Aa	Ar	Ar	Ar	ar
Sorting	MS	-	-	-	-	WS	PS	PS	PS	PS	PS	
<b>Bioclasts</b>	<b>Total bioclast %</b>	15	<1	2	10	10	3	7	-	-	<1	40
	Benthic foraminifera	-	-	R	R	S	R	R	-	-	-	R
	Planktic foraminifera	-	-	R	M	M	S	S	-	-	-	VC
	Bryozoans	-	-	-	-	-	-	-	-	-	-	-
	Bivalves	-	-	-	-	-	-	-	-	-	-	-
	Echinoderms	-	-	-	-	-	-	-	-	-	-	-
	Gastropods	-	-	-	-	-	-	-	-	-	-	-
	Calcareous algae	-	-	-	-	-	-	-	-	-	-	-
	Barnacles	-	-	-	-	-	-	-	-	-	-	-
	Spicules & spines	-	-	-	-	-	-	-	-	-	-	-
	Radiolarians	C	-	R	S	S	S	S	-	-	R	R
	Modal size 1 (mm)	0.15	-	-	0.13	0.13	0.13	0.13	-	-	-	0.13
	Modal size 2 (mm)	-	-	-	0.20	-	-	-	-	-	-	-
Shape/abrasion	WB	-	-	WB	WB	Bw	Bw	-	-	-	Wb	

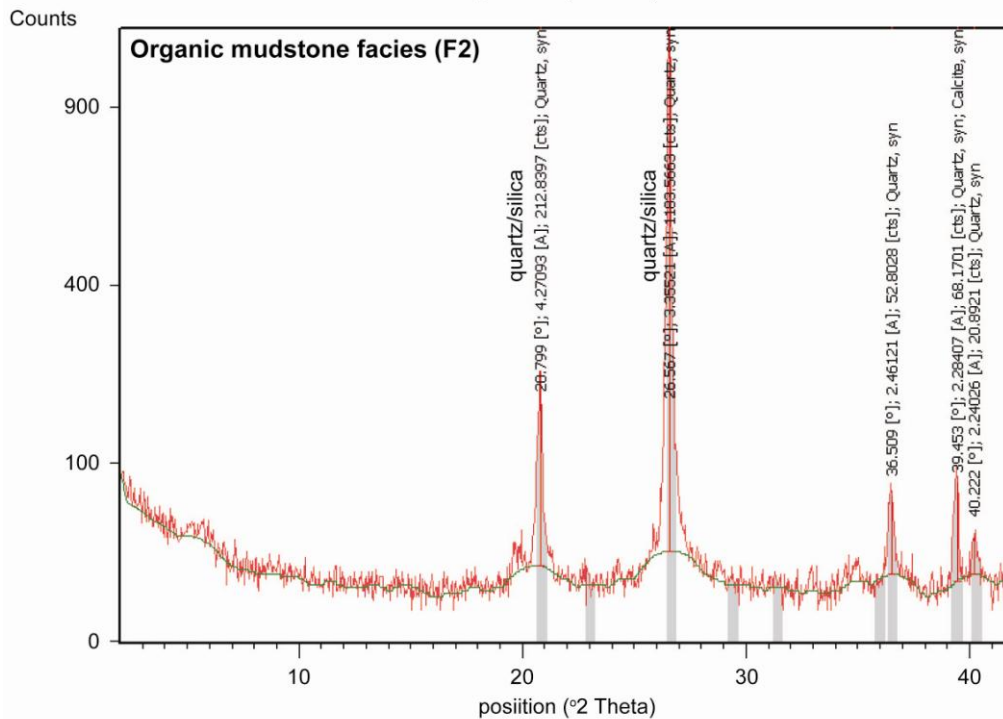
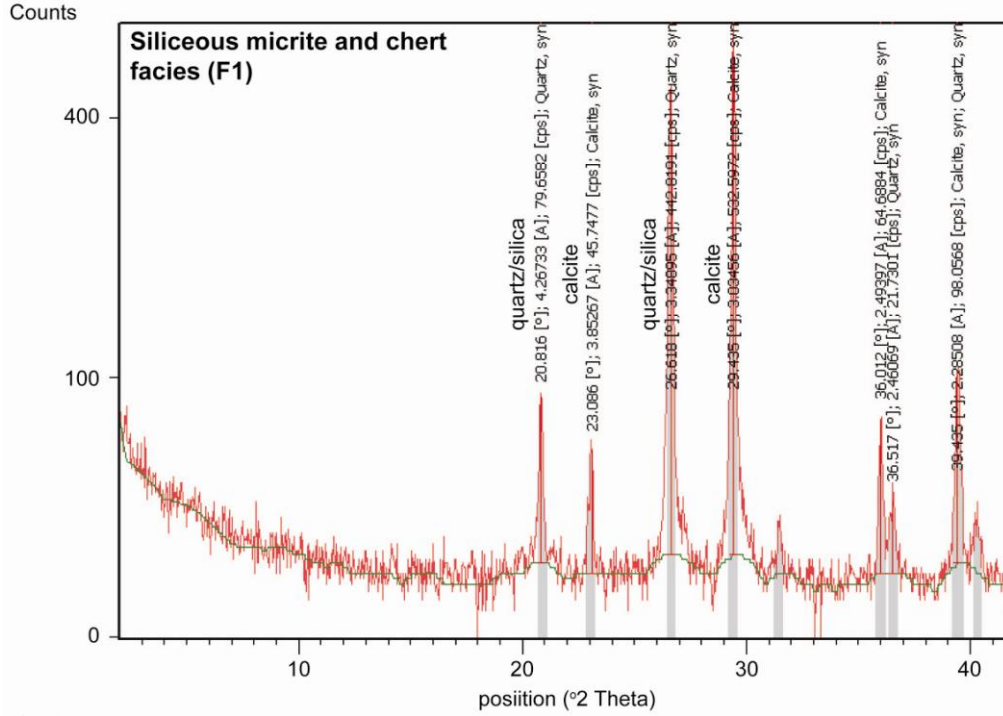
Petrographic Data Sheet

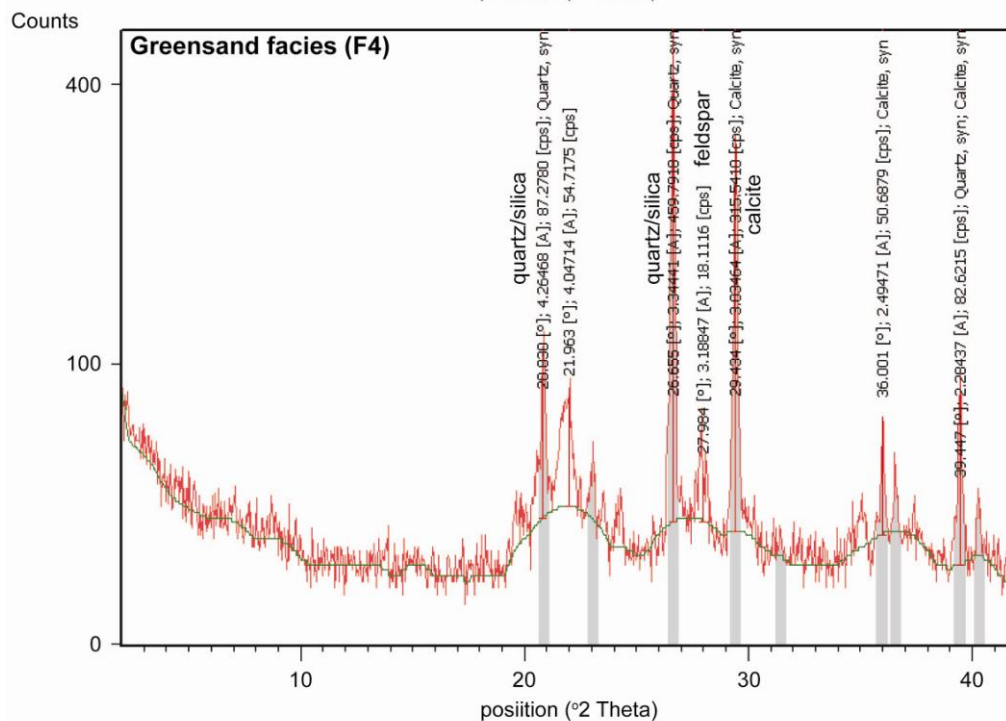
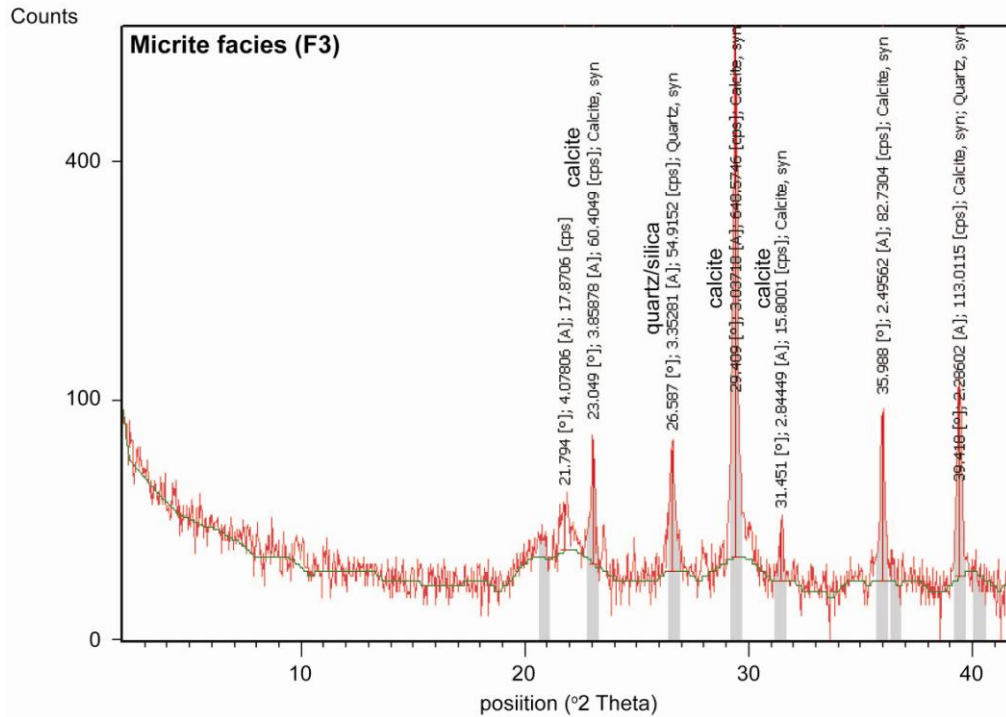
Thin section number	KK17.1	KK18.1A	KK23.1	KK24.2	KK27.2	KK28.2B	CC01	CC07	CC08	CC08.2	CC09.1	LP01	LP03	
<b>Siliclasts &amp; Authigenic Grains</b>	<b>Siliclastic %</b>	50	40	7	10	2	15	6	40	50	45	35	1	12
	Quartz	VC	VC	M	M	S	M	S	VC	VC	VC	VC	-	S
	Feldspar	-	-	-	-	-	-	-	R	R	R	R	-	-
	IRFs	-	-	-	-	-	-	-	-	-	-	-	-	-
	SRFs	-	-	-	-	-	-	-	-	-	-	-	-	-
	Micas	R	R	R	R	-	R	R	S	S	S	S	-	R
	Pyrite grains	S	S	R	R	R	R	-	S	R	-	S	-	R
	Pyrite infills	-	-	R	-	-	-	-	-	-	-	-	R	-
	Phosphatic grains	R	R	S	S	R	R	-	S	S	-	R	-	R
	Glaucony	M	M	S	S	R	S	M	M	M	M	M	R	M
	Other	-	-	-	-	-	-	-	-	R	R	-	-	-
	Modal size 1 (mm)	0.18	0.15	0.10	0.13	0.10	0.08	0.05	0.10	0.08	0.08	0.08	-	0.10
	Modal size 2 (mm)	-	-	-	-	-	-	-	-	-	-	-	-	-
	Shape/abrasion	Ar	Ar	Ar	AR	ar	ar	Ar	Aa	Aa	Aa	Aa	-	rR
	Sorting	W	W	W	VP	M	W	M	M/W	M	M	M/P	-	W
<b>Bioclasts</b>	<b>Total bioclast %</b>	2	3	30	30	25	2	25	1	1	-	-	20	<1
	Benthic foraminifera	-	R	S	R	R	-	R	-	-	-	-	R	-
	Planktic foraminifera	S	S	VC	VC	VC	-	C	-	-	-	-	C	R
	Bryozoans	-	-	-	-	-	-	-	-	-	-	-	-	-
	Bivalves	-	-	-	-	-	-	-	-	-	-	-	R	-
	Echinoderms	-	-	-	-	-	-	-	-	-	-	-	-	-
	Gastropods	-	-	-	-	-	-	-	-	-	-	-	-	-
	Calcareous algae	-	-	-	-	-	-	-	-	-	-	-	-	-
	Barnacles	-	-	-	-	-	-	-	-	-	-	-	-	-
	Spicules & spines	-	-	-	-	-	-	-	-	-	-	-	-	-
	Radiolarians	S	S	S	S	M	S	S	R	R	-	-	-	-
	Modal size 1 (mm)	-	-	0.10	0.10	0.13	-	-	-	-	-	-	-	-
	Modal size 2 (mm)	-	-	-	-	-	-	-	-	-	-	-	-	-
Shape/abrasion	-	-	-	-	-	-	-	-	-	-	-	-	-	

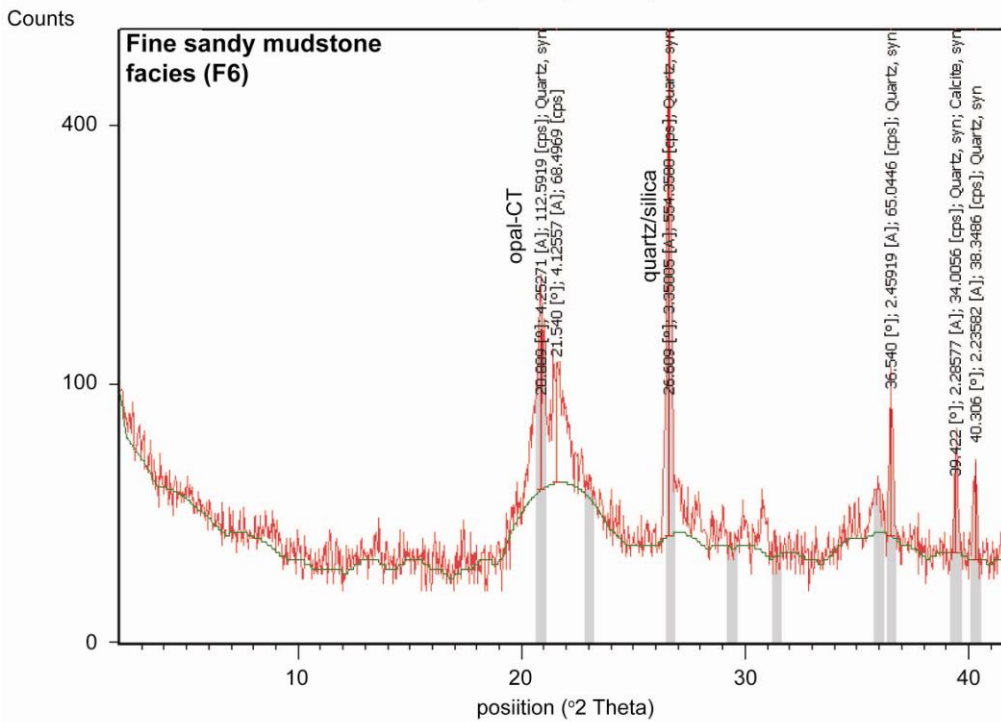
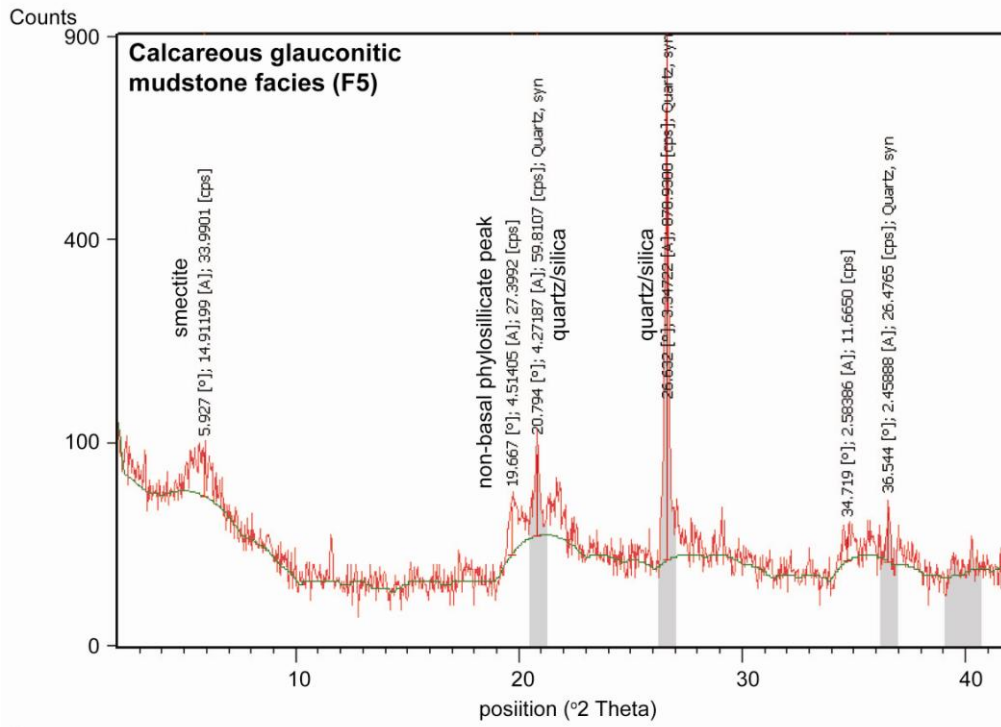


# APPENDIX C-2

## REPRESENTATIVE BULK UNORIENTED XRD TRACES







# APPENDIX D-1

## CAMPBELL ISLAND BULK GEOCHEMICAL DATA

Sample No.	Thickness*	XRF (major elements)										XRF (trace elements)										XRF (trace elements)					Lithofacies components				Barium		Other proxies			Stable isotopes				
		SiO <sub>2</sub>	CaO	Al <sub>2</sub> O <sub>3</sub>	Fe <sub>2</sub> O <sub>3</sub>	MnO	MgO	Na <sub>2</sub> O	K <sub>2</sub> O	TiO <sub>2</sub>	P <sub>2</sub> O <sub>5</sub>	V	Cr	Co	Ni	Cu	Zn	Ga	Rb	Sr	Y	Zr	Nb	Ba	La	Ce	Pb	Th	U	TRG	Si[exc]	Ca[exc]	Sum	Ba[exc]	Ba/Al	U/Th	Zr/Ti	La/U	δ <sup>13</sup> C <sub>org</sub>	δ <sup>13</sup> C <sub>carb</sub>
		wt%										ppm										ppm					wt%				wt%		ratio			‰				
LP01	3.00	23.36	44.28	3.01	0.56	0.05	0.56	0.27	0.42	0.09	0.15	bd	23	bd	bd	6.3	19.4	5.1	20.5	1055	20.5	21.8	4	107.8	15.1	4.8	15.9	8	2.6	10.03	15.80	79.05	105	92	67.54	0.33	412	5.81	0.73	-3.89
LP02	1.40	24.17	43.23	2.40	0.62	0.06	0.47	1.87	0.37	0.06	0.15	bd	20	bd	5.3	4.5	39.2	3.5	17.8	920.4	22.1	23.1	3.8	1013	12.1	4.9	12.5	7.7	2.1	6.98	18.91	77.18	103	1002	795.76	0.27	628	5.76	0.62	-4.47
CC01	0.95	21.33	45.57	1.69	0.93	0.06	0.36	0.89	0.26	0.04	0.16	11	29	bd	2	6.8	12.4	3.6	14.8	1229	19.1	25.9	3.5	595.1	10.4	3.6	11.3	6.3	2.5	5.01	17.55	81.36	104	587	663.66	0.40	980	4.16	1.15	-2.33
LP07	0.72	28.02	42.05	2.88	1.01	0.06	0.70	bd	0.40	0.08	0.23	22	39	bd	7.4	7.5	26.1	4.7	20.7	860.2	26	34.9	3.2	961.2	18	5.5	15.3	7	5.1	9.27	21.03	75.08	105	946	629.88	0.73	714	3.53	0.69	-4.64
CC02	0.55	24.98	43.77	2.16	1.43	0.06	0.61	bd	0.41	0.09	0.24	28	61	bd	12.9	4.8	28.8	5.4	26.9	1150	32.9	87.7	4.2	655.8	16.4	4.8	23.2	5.9	2.2	9.91	17.51	78.15	106	640	574.76	0.37	1677	7.45	1.33	-2.35
CC03	0.10	24.17	43.13	2.21	1.50	0.06	0.60	bd	0.39	0.09	0.24	38	57	bd	8.4	5.9	32.7	4.8	29.9	1145	34	65.6	4.1	123.6	15.3	4.9	24.3	8.6	4.1	10.08	16.57	77.00	104	108	105.82	0.48	1234	3.73	1.33	-2.12
LP03	0.08	55.76	18.83	6.86	4.99	0.03	2.16	bd	1.91	0.26	0.94	149	338	27.3	71.3	30	162	19.5	115.8	469.8	85.6	135.1	6.6	1779	51.8	10.1	61.9	11.6	13	29.93	33.19	33.57	97	1731	489.95	1.12	856	3.98	0.45	-4.21
CC04	0.05	54.37	14.45	9.04	5.25	0.02	2.57	bd	2.03	0.45	0.82	173	267	27.4	39.9	30.3	164.3	16.9	128.2	792.3	109	308.7	11.7	206.6	57.1	12.6	79.2	14.9	16.7	51.31	15.68	25.70	93	125	43.17	1.12	1140	3.42	1.46	-1.55
CC05	0.02	74.54	1.91	11.32	7.31	0.00	3.34	0.07	2.59	0.53	0.83	259	356	40	89	22.1	612	23.7	165.8	1181	134.3	261.6	11.9	581.1	65.5	14.3	100	15.1	26.7	59.73	29.50	3.29	93	486	97.01	1.77	830	2.45		
CC06	0.02	59.76	13.66	6.93	5.47	0.02	2.00	bd	1.92	0.37	1.05	149	272	33	31.8	23.3	143.8	15.4	109	1480	124.4	374.6	9.5	205.2	68.2	11.8	100	14.4	25.2	42.00	28.09	24.32	94	138	55.94	1.75	1690	2.71	1.31	-2.00
CCB00	-0.10	97.92	0.62	5.06	2.30	0.00	1.18	0.24	1.42	0.36	0.55	86	119	39.1	11.8	9.7	48.5	8.5	80.6	1292	16.7	312.2	9.1	423.5	29.7	10.2	52.1	13.9	14	40.81	67.15	1.03	109	359	158.08	1.01	1450	2.12	-25.41	
CCB01	-0.50	87.76	0.17	9.92	2.65	0.00	1.57	0.22	1.97	0.64	0.22	96	95	32	13.8	8.3	103.6	13.7	122.1	580.2	16.9	198.6	12.8	336.4	34.8	16.9	63.8	11.7	4.9	72.37	33.19	0.16	106	221	64.08	0.42	520	7.10	-26.84	
CCB02	-0.80	88.17	0.18	10.30	2.47	0.01	1.68	0.22	1.81	0.61	0.11	80	87	26.3	28.1	18.5	89.6	14.6	111.8	393.1	18.5	137.6	12.4	477	29.9	19.1	57.4	13.5	9.5	68.82	36.27	0.19	105	368	87.49	0.70	379	3.15	-27.10	
CCB03	-2.00	90.27	0.18	10.11	2.76	0.01	1.81	0.10	1.78	0.60	0.14	82	84	19.9	23.9	18.4	56.3	13.4	111.7	355.2	20.4	144.7	12.1	243.9	34.7	19.2	61.6	14.5	8.2	67.63	39.27	0.18	107	136	45.56	0.57	406	4.23	-27.32	
CCB04	-3.30	87.87	0.29	10.27	2.99	0.01	2.21	0.06	1.83	0.59	0.11	74	84	24.8	34.2	13.5	99	13.5	110.4	320.9	18.8	122.8	12.2	297.7	35	20.4	61.2	13.2	9.5	66.85	37.46	0.38	105	191	54.77	0.72	348	3.68	-27.21	
CCB05	-4.70	91.57	0.37	8.92	2.46	0.01	1.98	0.43	1.69	0.52	0.15	68	75	16.3	24.1	11.9	50.4	12.7	95.8	378.2	13	128.1	11.1	289.4	23	18.4	46.4	13.4	5.4	59.35	46.82	0.54	107	195	61.26	0.40	409	4.26	-27.04	
CCB06	-13.90	75.04	0.14	13.61	3.21	0.01	1.67	0.27	2.47	0.87	0.16	72	112	22.4	25.6	19.8	34	16.4	118	133.5	24.3	337.2	18	326.6	37.2	23.7	71.5	21.8	11	99.34	0.12	0.05	100	169	45.32	0.50	643	3.38	-26.00	
CCB07	-17.60	68.30	0.21	13.10	3.30	0.01	2.82	2.83	3.49	0.76	0.15	70	148	92.7	34.9	7.9	97	15.2	143.7	105.9	23	479.6	15	353	40.8	19.3	87.2	17.3	7.6	86.21	3.29	0.21	90	216	50.91	0.44	1055	5.37	-24.86	
CCB08	-20.50	69.65	0.12	14.69	2.20	0.01	1.76	2.26	4.00	0.80	0.08	46	78	158.7	39.4	14.6	123.1	14.7	162.9	65.1	21.1	441	15.2	411.5	45.7	20.6	78.6	16.4	9.3	90.66	1.28	0.04	92	267	52.90	0.57	922	4.91	-26.03	
CCB09	-23.10	70.50	0.13	14.36	2.09	0.01	1.26	1.85	3.86	0.77	0.10	69	76	166.7	32.2	12.2	60.4	13.7	148.6	145.8	23.1	519.7	15	407.2	49.4	21.2	93.1	19.6	9.1	87.10	4.82	0.05	92	269	53.57	0.46	1131	5.43	-26.41	
CCB10	-25.80	77.73	0.11	11.66	1.92	0.01	0.85	1.47	3.40	0.68	0.18	41	69	183.4	70.9	19.4	24.4	12.4	119.2	246.6	25.4	609.6	14.8	391.5	40.1	19.4	75.8	19.4	5.4	77.35	19.40	0.05	97	269	63.45	0.28	1494	7.43	-26.62	

**Correlation Coefficient**

TRG	0.80	-0.92	0.98	0.35	-0.86	0.58	0.18	0.89	1.00	-0.17	0.16	0.16	0.51	0.41	0.38	0.19	0.70	0.88	-0.77	-0.08	0.74	0.99	-0.34	0.56	0.98	0.79	0.91	0.29		-0.15	-0.92		-0.45	-0.72	0.01	-0.15	0.01	
Si[exc]	0.47	-0.23	-0.23	0.14	-0.32	0.11	-0.63	-0.28	-0.15	0.26	0.21	0.14	-0.54	-0.04	0.08	0.09	0.04	-0.05	0.30	0.01	-0.28	-0.16	0.07	-0.05	-0.07	-0.08	-0.18	0.20	-0.15		-0.23		0.09	-0.04	0.30	-0.13	-0.37	
Ca[exc]	-0.96	1.00	-0.89	-0.48	0.98	-0.68	0.07	-0.81	-0.92	-0.03	-0.35	-0.32	-0.29	-0.48	-0.47	-0.30	-0.76	-0.89	0.61	-0.03	-0.67	-0.92	0.27	-0.62	-0.92	-0.81	-0.85	-0.44	-0.92	-0.23			0.37	0.73	-0.22	0.14	0.17	
Ba[exc]	-0.34	0.37	-0.36	0.02	0.36	-0.13	0.25	-0.27	-0.45	0.28	0.08	0.24	-0.11	0.14	0.10	0.08	-0.06	-0.25	0.11	0.15	-0.34	-0.47	0.99	-0.09	-0.42	-0.30	-0.40	-0.07	-0.45	0.09	0.37			0.77	0.77	0.11	-0.01	0.01
Ba/Al	-0.67	0.73	-0.69	-0.38	0.74	-0.53	0.20	-0.62	-0.72	-0.02	-0.33	-0.21	-0.19	-0.36	-0.35	-0.20	-0.57	-0.68	0.38	-0.09	-0.56	-0.74	0.71	-0.51	-0.71	-0.68	-0.71	-0.38	-0.72	-0.04	0.73			0.77		-0.17	0.08	0.15
N =	21	21	21	21	21	21	15	21	21	21	19	21	15	20	21	21	21	21	21	21	21	21	21	21	21	21	21	21	21	21	21	21	21	21	21	21	21	21
P = 0.01	0.55	0.55	0.55	0.55	0.55	0.55	0.64	0.55	0.55	0.55	0.58	0.55	0.64	0.55	0.55	0.55	0.55	0.55	0.55	0.55	0.55	0.55	0.55	0.55	0.55	0.55	0.55	0.55	0.55	0.55	0.55	0.55	0.55	0.55	0.55	0.55	0.55	0.55

\*Thickness with respect to the boundary between the Garden Cove Formation and Tucker Cove Limestone







# APPENDIX D-3

## MUZZLE STREAM BULK GEOCHEMICAL DATA

Sample No.	Thickness*	XRF (major elements)									XRF (trace elements)										Lithofacies components				Barium		Other proxies			Stable isotopes									
		SiO <sub>2</sub>	CaO	Al <sub>2</sub> O <sub>3</sub>	Fe <sub>2</sub> O <sub>3</sub>	MnO	MgO	K <sub>2</sub> O	TiO <sub>2</sub>	P <sub>2</sub> O <sub>5</sub>	V	Cr	Co	Ni	Cu	Zn	Ga	Rb	Sr	Y	Zr	Nb	Ba	La	Ce	Pb	Th	U	TRG	Si[exc]	Ca[exc]	Sum	Ba[exc]	Ba/Al	U/Th	Zr/Ti	La/U	δ <sup>13</sup> C <sub>carb</sub>	δ <sup>18</sup> O <sub>carb</sub>
		wt%									ppm										wt%				wt%		ratio			‰									
MZ08	0.98	22.78	47.90	0.96	0.39	0.04	0.14	0.19	0.01	0.19	bd	18	bd	2.4	7.0	18.4	3.4	5.8	733.2	17.9	12.1	2.5	389	10.3	5.8	2.9	5.6	3.2	1.25	21.91	85.54	108.69	386	765.90	0.57	2314	3.22	2.39	-3.14
MZ07	0.78	23.79	46.13	1.06	0.40	0.04	0.19	0.19	0.02	0.17	bd	17	bd	4.5	25.7	2.7	5.9	720.2	16.6	13.6	2.3	490.7	5.4	<5.8	3.4	5.4	3.7	2.29	22.18	82.36	106.83	485	873.60	0.69	1417	1.46	2.39	-3.14	
MZ06	0.34	33.63	41.17	1.38	0.87	0.04	0.36	0.40	0.04	0.25	10	69	bd	6.8	8.0	29.9	4.3	14.1	638.9	21.4	15.9	2.6	437.8	8.6	14.7	4.4	5.8	4.7	6.39	29.15	73.51	109.05	421	599.23	0.81	593	1.83	2.39	-2.9
MZ05	0.25	44.36	23.46	4.53	4.38	0.02	1.49	1.71	0.19	0.72	111	334	15.8	34.6	18.1	84.4	15.3	69.5	349	47.3	54.5	3.9	359	27.2	37.6	5.8	6.9	5.3	27.47	25.13	41.84	94.45	285	149.77	0.77	473	5.13	1.78	-3.87
MZ04	0.08	51.49	16.54	5.22	4.39	0.01	1.93	2.00	0.21	0.67	142	399	12.3	26.3	8.4	98.5	15.7	71.8	269.7	37.9	46.5	3.1	394.8	24.4	36.8	3.9	6.1	4.9	30.19	30.35	29.47	90.01	313	142.84	0.80	367	4.98	1.08	-4.74
MZ03H	-0.05	93.24	8.92	0.80	0.27	0.01	0.27	0.27	0.06	0.08	14	29	19.6	5.5	4.3	13.6	3.2	10.4	193	7.2	12.3	1.6	715.3	10.5	11.9	0.9	2.6	2.5	8.50	87.29	15.90	111.69	692	1693.42	0.96	345	4.20	1.58	-4.67
MZ03B	-0.05	72.92	14.84	3.10	2.52	0.01	1.08	1.30	0.13	0.52	151	236	36.4	19.7	8.8	77	12.1	49	308.6	30.3	40.3	2.6	544.1	18.3	27.5	3.8	5.3	4.0	19.27	59.43	26.47	105.17	492	331.77	0.75	498	4.58	1.71	-4.08
MZ02	-0.30	75.81	16.90	2.68	0.84	0.01	0.70	0.60	0.14	0.16	23	32	bd	13.6	9.6	57.8	5.6	24.4	306.4	18.6	26.3	3.0	744.4	10.5	11.7	4.3	5.6	5.7	19.68	62.03	30.14	111.85	691	523.86	1.02	318	1.84	1.46	-3.51
MZ01	-1.00	69.28	20.19	2.16	0.69	0.02	0.56	0.45	0.11	0.08	24	33	bd	9.8	8.3	44.6	4.2	19.4	357.1	14.8	24.1	2.5	768.7	8.2	11.4	3.6	5.0	3.1	15.65	58.33	36.02	109.99	727	671.94	0.62	367	2.65	1.5	-3.97

### Correlation Coefficient

TRG	0.36	-0.68	0.96	0.87	-0.70	0.95	0.91	1.00	0.76	0.77	0.84	-0.39	0.92	0.67	0.94	0.89	0.93	-0.73	0.76	0.93	0.71	-0.07	0.84	0.86	0.53	0.42	0.61		0.07	-0.68	-0.23	-0.67	0.30	-0.67	0.64	
Si[exc]	0.96	-0.77	-0.20	-0.31	-0.75	-0.15	-0.19	0.07	-0.39	-0.39	-0.27	0.43	-0.30	-0.28	-0.15	-0.21	-0.17	-0.72	-0.49	-0.16	-0.51	0.85	-0.19	-0.33	-0.56	-0.79	-0.34	0.07		-0.77	0.81	0.54	0.57	-0.56	0.11	
Ca[exc]	-0.92	1.00	-0.46	-0.35	1.00	-0.51	-0.46	-0.68	-0.23	-0.26	-0.38	-0.27	-0.38	-0.18	-0.48	-0.43	-0.49	0.99	-0.13	-0.47	-0.03	-0.53	-0.43	-0.35	0.14	0.36	-0.08	-0.68	-0.77		-0.40	-0.02	-0.60	0.82	-0.55	
Ba[exc]	0.69	-0.40	-0.48	-0.67	-0.40	-0.50	-0.57	-0.23	-0.77	-0.67	-0.67	0.39	-0.54	-0.45	-0.43	-0.61	-0.54	-0.33	-0.77	-0.49	-0.59	0.99	-0.63	-0.64	-0.51	-0.70	-0.39	-0.23	0.81	-0.40		0.59	0.33	-0.32	-0.42	
Ba/Al	0.31	-0.02	-0.80	-0.75	0.00	-0.74	-0.74	-0.67	-0.76	-0.66	-0.70	0.03	-0.72	-0.69	-0.84	-0.75	-0.74	0.02	-0.84	-0.78	-0.87	0.49	-0.64	-0.67	-0.88	-0.91	-0.75	-0.67	0.54	-0.02	0.59		0.20	0.15	-0.26	
n=	9	9	9	9	9	9	9	9	9	7	9	4	8	9	9	9	9	9	9	9	9	9	9	8	9	9	9	9	9	9	9	9	9	9	9	
P=0.01	0.80	0.80	0.80	0.80	0.80	0.80	0.80	0.80	0.80	0.85	0.80	0.99	0.83	0.80	0.80	0.80	0.80	0.80	0.80	0.80	0.80	0.80	0.80	0.80	0.80	0.80	0.80	0.80	0.80	0.80	0.80	0.80	0.80	0.80	0.80	0.80

\*Thickness with respect to the boundary between the Mead Hill Formation and Teredo Limestone Member





# APPENDIX D-4

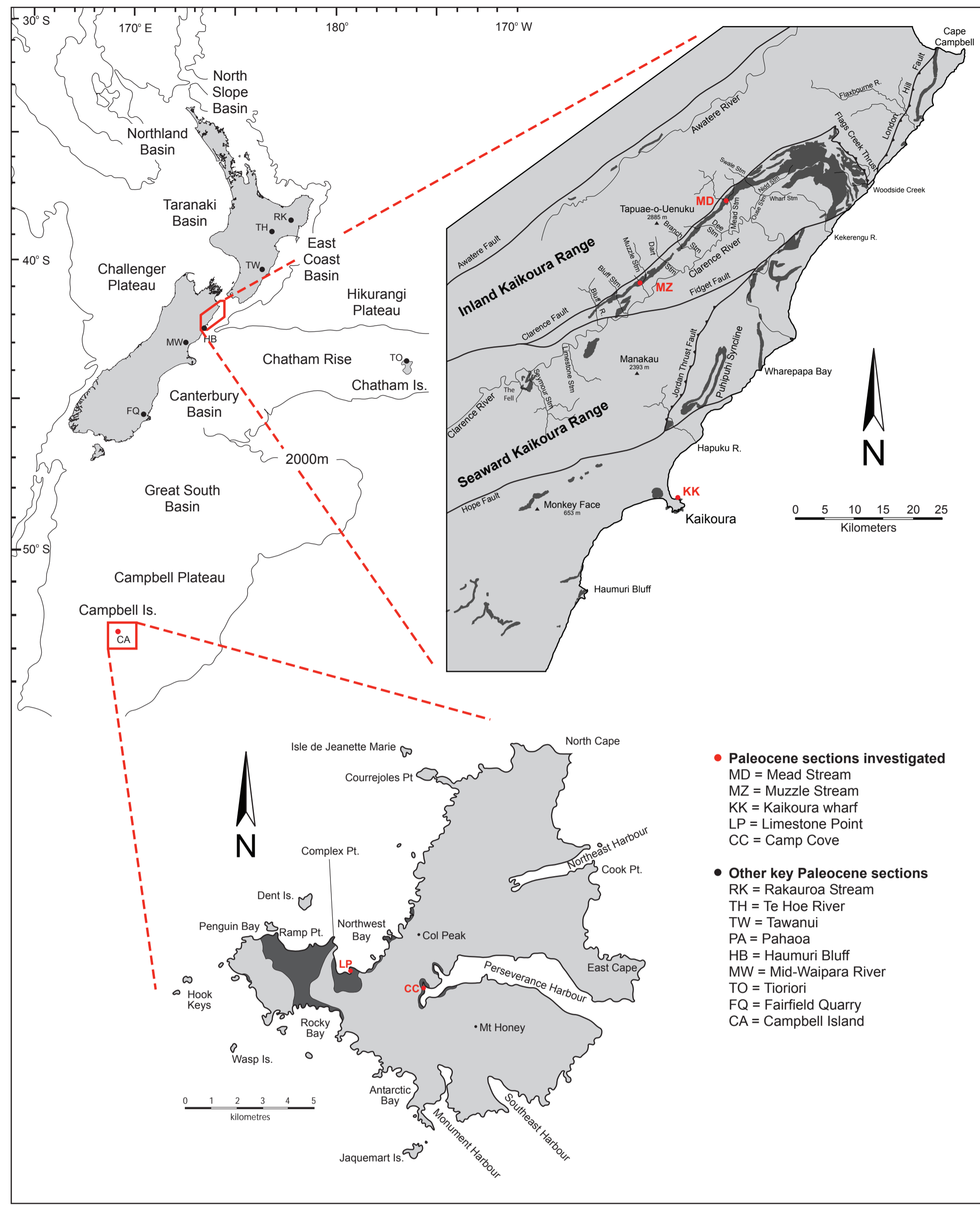
## KAIKOURA WHARF BULK GEOCHEMICAL DATA

Sample No.	Thickness*	XRF (major elements)									XRF (trace elements)										XRF (trace elements)				Lithofacies components				Barium		Other proxies			Stable isotopes						
		SiO <sub>2</sub>	CaO	Al <sub>2</sub> O <sub>3</sub>	Fe <sub>2</sub> O <sub>3</sub>	MnO	MgO	K <sub>2</sub> O	TiO <sub>2</sub>	P <sub>2</sub> O <sub>5</sub>	V	Cr	Co	Ni	Cu	Zn	Ga	Rb	Sr	Y	Zr	Nb	Ba	La	Ce	Nd	Pb	Th	U	TRG	Si[exc]	Ca[exc]	Sum	Ba[exc]	Ba/Al	U/Th	Zr/Ti	La/U	δ <sup>13</sup> C <sub>carb</sub>	δ <sup>18</sup> O <sub>carb</sub>
		wt%									ppm										wt%				wt%		ratio			‰										
KK01	-1.05	72.49	17.11	2.09	0.71	0.02	0.71	0.52	0.11	0.24	20	27	bd	9.5	6.6	41.1	4.2	18	274.4	14.3	31.8	2.4	126.7	10.4	11.1	10.4	3.6	4.8	7.2	15.02	61.97	30.52	107.52	86	114.76	1.50	504	1.44	0.86	-2.37
KK02	-0.25	80.45	12.05	2.68	0.88	0.02	0.92	0.68	0.13	0.71	70	37	13.9	17.6	5.2	31.3	4.6	25.3	275.8	25.4	45	2.8	179.4	16.7	25.5	12.9	5.8	4.8	16.3	19.26	66.97	21.47	107.70	127	126.43	3.40	557	1.02	0.28	-3.92
KK03	0.05	76.94	6.11	7.95	2.57	0.01	1.96	1.62	0.32	0.31	144	105	25.1	35.7	11.1	77.6	11.5	53.8	134.3	13.1	113	4.5	220.5	10.4	27	14.7	7.7	7.0	5.5	46.04	44.71	10.81	101.56	96	52.39	0.79	585	1.89		
KK07	0.45	93.05	1.03	4.87	1.73	0.01	1.64	1.21	0.21	0.19	114	72	21.9	25.3	7.4	47.3	7.7	39.4	79.7	7.9	88.3	2.9	199.8	15.3	29.1	20.9	3.9	5.4	4.2	30.14	71.95	1.77	103.86	119	77.53	0.78	698	3.64		
KK04	0.75	73.03	10.07	6.53	2.25	0.02	1.87	1.36	0.28	0.48	125	94	9.7	26.9	15.3	105.3	10.3	49.9	168.6	21.6	108.2	4.4	233.5	23.7	56	36.8	7.0	7.2	11.1	39.98	45.04	17.91	102.93	126	67.51	1.54	645	2.14	0.31	-3.06
KK05	1.05	91.19	5.66	1.95	0.69	0.01	0.60	0.53	0.10	0.12	35	36	14.6	7.8	5.4	22.8	4.5	16.5	103.2	6.8	33.3	1.6	114.3	11.7	16.9	13.8	4.2	2.4	3.7	13.82	81.51	10.08	105.41	77	110.86	1.54	574	3.16	0.48	-2.2
KK06	1.75	80.68	10.13	3.52	1.26	0.01	1.23	0.84	0.15	0.25	62	60	12.6	12.7	13.1	62.3	7.1	29.3	161.1	14.4	64.5	2.8	131.1	11.9	24.5	16.2	4.5	4.7	5.9	21.63	65.54	18.05	105.23	73	70.26	1.26	711	2.02	0.66	-2.83
KK08	2.50	26.93	41.17	2.21	1.77	0.03	0.76	0.62	0.08	0.72	21	57	<8.0	6.2	12.6	25.8	6.0	26.7	474	46.7	35.1	3.5	131.2	28.1	13.9	22.1	4.0	6.4	4.5	12.04	18.50	73.50	104.04	99	112.14	0.70	695	6.24	0.44	-3.2
KK09	2.80	71.49	8.13	7.31	2.40	0.02	1.99	1.49	0.29	0.11	113	103	13.4	18	14.3	81.6	11.3	54.3	145.8	8.4	117.9	4.6	825.2	14.3	29.6	17.2	5.6	6.6	4.2	40.75	42.96	14.43	98.14	715	213.17	0.64	689	3.40	0.18	-3.63
KK10	3.46	70.14	17.57	1.96	0.68	0.02	0.83	0.48	0.11	0.11	36	24	7.6	10.7	5.1	27.2	4.6	18.2	237.5	11.8	27	2.5	93.7	5.9	11.8	9.5	3.8	5.0	3.3	15.15	59.53	31.35	106.03	53	90.53	0.66	425	1.79	0.63	-2.19
KK11	3.80	56.38	23.73	2.50	0.90	0.03	0.96	0.57	0.11	0.28	32	31	5.4	14	5.5	41.3	5.2	21.5	305.8	18	37.8	2.8	137.1	9.5	17	17.6	4.7	6.2	4.6	15.60	45.46	42.34	103.40	95	103.55	0.74	577	2.07	0.87	-1.75
KK12	4.50	52.64	24.40	3.10	1.02	0.03	1.22	0.65	0.12	0.14	16.9	35	bd	20.8	18.8	42.2	4.9	25.8	307.1	18.2	30.1	2.8	598.7	11.7	14.1	9.8	6.3	6.0	3.2	17.27	40.55	43.53	101.36	552	365.28	0.53	415	3.66	0.7	-1.77
KK14	4.60	105.79	1.39	0.42	0.19	0.00	0.42	0.28	0.05	0.08	6.3	9.3	56.9	33.5	11.2	7.5	3.1	10	55.5	7.6	8.5	1.1	102.4	16.9	21.3	25.9	2.3	2.3	3.7	7.03	100.87	2.47	110.37	83	457.76	1.61	288	4.57		
KK13	4.80	70.54	17.47	1.37	0.45	0.02	0.62	0.41	0.07	0.10	21.7	24	bd	7.5	11.2	26.3	4.0	15.7	219.6	10.9	14	2.1	176.4	6.5	9.7	10.5	4.1	4.8	4.2	9.38	63.98	31.18	104.54	151	243.55	0.88	356	1.55	0.61	-1.7
KK15	5.00	58.46	22.55	2.64	0.80	0.03	0.97	0.61	0.10	0.15	22.5	31	bd	17.7	19	52.4	4.7	23.9	300	15.7	22.1	3.3	385.4	9.9	13	13.3	6.2	7.6	5.0	14.85	48.07	40.24	103.15	345	275.48	0.66	355	1.98	0.82	-1.61
KK16	5.23	57.15	22.08	3.27	1.07	0.03	1.12	0.65	0.13	0.13	21.0	37	6.5	13.9	20	37	6	26.3	267.1	14.3	36.1	2.9	431.6	11.3	17.6	bd	5.9	5.5	2.4	18.39	44.28	39.39	102.06	382	249.34	0.44	468	4.71	0.62	-2.04
KK18	5.55	58.61	16.13	3.38	3.04	0.02	1.96	1.56	0.14	0.61	73	194	11.5	12.2	36.1	59.1	11.1	55.1	239.8	26.5	41.3	2.8	483.7	16.3	19.3	16.7	4.0	5.3	4.7	19.50	44.96	28.77	93.23	431	270.37	0.89	505	3.47	0.94	-2.53
KK20	5.95	37.20	30.16	2.71	3.01	0.02	1.06	1.05	0.12	0.87	40	117	bd	8.8	7.2	41.3	7.3	43.2	366.6	44.5	43.1	3.0	153.9	24.7	14.2	21.6	3.8	5.8	4.5	17.45	24.98	53.83	96.26	107	107.17	0.78	588	5.49	0.63	-2.59
KK22	6.80	38.16	33.06	1.22	0.97	0.03	0.60	0.36	0.04	0.34	6.7	27	6.7	7.1	4.5	15.2	5.5	13.1	489.3	27.7	25	2.4	187.1	12.6	10.9	13.4	5.1	5.1	3.0	6.20	33.82	59.02	99.04	170	290.71	0.59	962	4.20	0.46	-3.42
KK23	7.05	24.81	44.85	1.06	0.79	0.04	0.24	0.30	0.05	0.28	31.4	22	bd	2.6	4.2	17.3	2.8	10.9	556.9	25.2	18.7	2.8	92	15	9.2	10.1	3.3	5.8	3.0	6.57	20.21	80.08	106.86	74	163.58	0.52	678	5.00	0.54	-2.93
KK24	7.35	29.37	39.06	2.38	1.44	0.04	0.80	0.55	0.09	0.54	21.1	41	bd	9.2	7.0	25.1	6.2	23.4	455.3	42.9	34.2	3.3	111.5	26.2	16.1	29.4	4.2	6.8	4.1	13.25	20.09	69.72	103.07	76	88.56	0.60	615	6.39	0.62	-2.91
KK25	7.75	16.82	49.31	1.67	0.88	0.05	0.53	0.35	0.06	0.24	28.1	26	bd	2.3	9.6	16.9	3.7	13.7	618	22.7	19.4	2.6	67.7	12.9	8.4	11	3.2	5.6	3.5	7.94	11.26	88.05	107.25	46	76.38	0.63	582	3.69	0.73	-2.73
KK26	8.55	19.16	43.03	3.09	1.19	0.07	0.89	0.58	0.10	0.15	bd	23	bd	11.2	11.8	23.6	5.3	22.9	559.8	23.9	23.1	3.3	2237	9.2	12.2	25.2	5.4	8.0	3.7	14.25	9.19	76.82	100.25	2199	1367.36	0.46	386	2.49	0.65	-2.61
KK27	9.05	28.28	42.67	2.58	0.59	0.07	0.69	0.54	0.07	0.19	bd	21	bd	4.8	14.9	190.4	4.7	16.7	625.4	22.7	20.3	3.4	6831	40.7	40.8	41.1	5.7	5.6	4.4	9.79	21.42	76.18	107.39	6805	5004.40	0.79	494	9.25	0.48	-2.77

### Correlation Coefficient

TRG	0.41	-0.57	0.98	0.66	-0.39	0.90	0.89	1.00	0.06	0.93	0.59	-0.08	0.66	0.20	0.41	0.86	0.86	-0.55	-0.26	0.97	0.73	-0.12	-0.05	0.64	0.14	0.62	0.37	0.33		0.12	-0.57		-0.14	-0.21	0.09	0.20	-0.33	
Si[exc]	0.95	-0.88	-0.04	-0.28	-0.79	0.06	0.02	0.12	-0.32	0.08	-0.07	0.73	0.51	-0.07	-0.15	-0.07	-0.05	-0.85	-0.68	0.09	-0.51	-0.32	-0.36	0.15	-0.21	-0.17	-0.71	0.23	0.12		-0.88		-0.32	-0.27	0.55	-0.26	-0.45	
Ca[exc]	-0.97	1.00	-0.43	-0.14	0.86	-0.51	-0.48	-0.57	0.21	-0.53	-0.30	-0.65	-0.72	-0.10	-0.04	-0.39	-0.41	0.98	0.66	-0.53	0.08	0.34	0.34	-0.39	0.12	-0.14	0.41	-0.31	-0.57	-0.88			0.35	0.35	-0.46	0.11	0.53	
Ba[exc]	-0.33	0.35	0.00	-0.15	0.69	-0.09	-0.08	-0.14	-0.17	0.15	-0.15	-0.20	-0.21	0.18	0.75	-0.08	-0.12	0.45	0.04	-0.16	0.19	1.00	0.58	0.36	0.59	0.23	0.14	-0.09	-0.14	-0.32	0.35			0.99	0.99	-0.13	-0.17	0.57
Ba/Al	-0.31	0.35	-0.08	-0.22	0.67	-0.17	-0.15	-0.21	-0.17	-0.44	-0.20	0.52	-0.21	0.14	0.73	-0.15	-0.19	0.45	0.04	-0.23	0.10	0.99	0.60	0.34	0.60	0.17	0.06	-0.09	-0.21	-0.27	0.35			0.99	0.99	-0.10	-0.19	0.59
n=	24	24	24	24	24	24	24	24	24	22	24	13	24	24	24	24	24	24	24	24	24	24	24	24	24	23	24	24	24	24	24	24	24	24	24	24	24	24
P=0.01	0.52	0.52	0.52	0.52	0.52	0.52	0.52	0.52	0.52	0.54	0.52	0.68	0.52	0.52	0.52	0.52	0.52	0.52	0.52	0.52	0.52	0.52	0.52	0.52	0.52	0.52	0.52	0.52	0.52	0.52	0.52	0.52	0.52	0.52	0.52	0.52	0.52	0.52

\*Thickness with respect to the Cretaceous/Tertiary boundary



- Paleocene sections investigated  
MD = Mead Stream  
MZ = Muzzle Stream  
KK = Kaikoura wharf  
LP = Limestone Point  
CC = Camp Cove
- Other key Paleocene sections  
RK = Rakaroa Stream  
TH = Te Hoe River  
TW = Tawanui  
PA = Pahaoa  
HB = Haumuri Bluff  
MW = Mid-Waipara River  
TO = Tioriori  
FQ = Fairfield Quarry  
CA = Campbell Island

